

Cell Signaling Pathways in Experimental Kidney Diseases

Thesis submitted to Faculty of Medicine,
Monash University in fulfillment of the requirements
For the Degree of Doctor of Philosophy

Yingjie Han

Department of Nephrology,
Monash Medical Centre,
Clayton, Victoria
Australia

Department of Medicine,
Monash University,
Clayton, Victoria
Australia

Contents	Page
Declaration	9
Thesis Summary	10
Acknowledgements	12
Abstracts presented at National and International Conferences	14
Publications arising from this Thesis	14
Abbreviations	15
Chapter 1. Literature Review and Introduction	22
1.1 Introduction to kidney disease	22
1.2 Animal models	23
1.2.1 Introduction	23
1.2.2 Passive accelerated anti-GBM glomerulonephritis	23
1.2.3 Anti-Thy-1 mesangioproliferative glomerulonephritis	25
1.2.4 Unilateral ureteral obstruction	26
1.3 Pathogenesis of renal disease	26
1.3.1 Immune-cell mediated renal injury	27
1.3.1.1 Macrophages	27
1.3.1.1.1 Cells of the macrophage lineage	27
Macrophage activation	28
Recruitment of macrophages	30
Proliferation of macrophages/Apoptosis of macrophages	32
1.3.1.1.2 Macrophages in kidney disease	33
Macrophages in human glomerulonephritis	33
Macrophage induced glomerular damage	34

	Macrophages in crescent formation	36
	Macrophages in tubulointerstitial damage	38
1.3.1.2	Dendritic cells	40
1.3.1.3	Neutrophils	41
1.3.1.4	T cells	42
1.3.1.4.1	T cells in adaptive immunity	42
1.3.1.4.2	CD4 ⁺ helper T cells	43
1.3.1.4.3	CD8 ⁺ cytotoxic T cells	45
1.3.1.4.4	Regulatory T cells	45
1.3.1.5	B cells	46
1.3.1.6	Mast cells	47
1.3.2	Renal fibrosis	49
1.3.2.1	Mesangial cells	49
1.3.2.2	Podocytes	51
1.3.2.3	Myofibroblasts	52
1.3.3	Cell Proliferation – a feature in progressive renal disease	53
1.3.4	Apoptosis	54
1.3.4.1	Introduction	54
1.3.4.2	Apoptosis cascades	55
1.3.4.3	Apoptosis in kidney disease	56
1.4	M-CSF/c-fms kinase signaling pathway	56
1.4.1	M-CSF and monocyte/macrophage lineage	57
1.4.2	M-CSF and its receptor	57
1.4.3	Functions of M-CSF	57

1.4.4	M-CSF in human kidney diseases	58
1.4.5	M-CSF in experimental kidney diseases	58
1.5	Extracellular signaling-regulated kinase signaling pathway	60
1.5.1	Introduction	60
1.5.2	ERK signaling pathways involved in cell proliferation	60
1.5.3	ERK in human and experimental kidney disease	60
1.6	c-Jun N-terminal kinase signaling pathway	61
1.6.1	Introduction	61
1.6.2	JNK signaling pathway involved in apoptosis and cell proliferation	62
1.6.3	JNK in human and experimental kidney disease	63
1.7	Hypotheses and aims	64
Chapter 2. Materials and Methods		66
2.1	Animals	66
2.2	Kinase inhibitors	66
2.2.1	MEK1/2 kinase inhibitor	66
2.2.2	68JNK kinase inhibitor	66
2.2.3	c-fms kinase inhibitor	67
2.3	Antibodies	68
2.3.1	Primary antibodies	68
2.3.2	Secondary antibodies	68
2.4	General reagents	68
2.4.1	Tissue fixatives	68

2.4.2	General solutions	68
2.4.3	Periodic acid – Schiff reaction reagents	69
2.4.4	Immunohistochemistry materials	69
2.4.4.1	Sera	69
2.4.4.2	Other blocking agents	69
2.4.4.3	Avidin DH: biotinylated horseradish peroxidase H complex	70
2.4.4.4	Substrates for enzyme reactions to detect antigens by immunohistochemistry	70
2.4.4.5	Mounting media for tissue sections	71
2.4.4.6	Antigen retrieval buffer	71
2.4.5	Coomassie protein assay reagent	71
2.4.6	Anaesthetic agents for animal experiments	71
2.5	Animal models	72
2.5.1	Unilateral ureteric obstruction	72
2.5.2	Anti-Thy1 mesangioproliferative glomerulonephritis	73
2.5.3	Passive accelerated anti-GBM disease	73
2.5.3.1	Preparation of anti-GBM serum	73
2.5.3.2	Immunization with sheep IgG	74
2.5.3.3	Passive accelerated anti-GBM glomerulonephritis	74
2.6	Biochemistry analysis	75
2.6.1	White blood cell counts	75
2.6.2	Serum and urinary creatinine	75
2.6.3	Serum CC401 levels	76
2.7	Periodic acid – Schiff staining	76

2.8	Immunohistochemistry	77
2.8.1	Tissue fixation	77
2.8.2	Tissue embedding	77
2.8.3	Tissue sectioning	78
2.8.4	Deparaffinization of paraffin embedded tissue section	78
2.8.5	Antigen retrieval using microwave heating	79
2.8.6	Antigen retrieval using high pressure cooker	79
2.8.7	Peroxidase anti-peroxidase (PAP) method	80
2.8.8	ABC method	81
2.8.9	Haematoxylin or Periodic acid – Schiff count staining	82
2.8.10	Direct immunofluorescence staining	82
2.9	Renal histology and quantification of immunohistochemistry	83
2.9.1	Renal histology	83
2.9.2	Analysis of direct immunofluorescence staining	85
2.9.3	Quantification of immunostaining	85
2.10	Western blotting	88
2.11	Flow cytometry	88
2.12	Coomassie protein assay	89
2.13	Isolation of rat glomeruli	90
2.14	RNA extraction and reverse transcription	90
2.15	Probes and primers	91
2.16	Real time RT-PCR	91
2.17	Statistical analysis	92

Chapter 3. Extracellular signal-regulated kinase-dependent interstitial cell proliferation in the obstructed mouse kidney	94
3.1 Introduction	94
3.2 U0126 inhibits ERK activation <i>in vivo</i>	96
3.3 Effect of U0126 treatment on cell proliferation and apoptosis in the obstructed kidney	97
3.4 Effect of ERK blockade on fibrosis in the obstructed kidney	98
3.5 Effect of ERK blockade on JNK activation in the obstructed kidney	98
3.6 Discussion	99
Chapter 4. JNK signaling in mesangial proliferative nephritis	102
4.1 Introduction	102
4.2 JNK activation in rat anti-Thy-1 mesangioproliferative nephritis	102
4.3 The JNK inhibitor, CC401, did not prevent mesangial cell loss on day 3 of anti-Thy-1 nephritis	104
4.4 CC401 treatment over day 3 to 8 did not affect mesangial cell accumulation and activation on day 8 of anti-Thy-1 nephritis	105
4.5 Serum level of CC401 in treated rat anti-Thy-1 nephritis	106
4.6 Discussion	106
Chapter 5. Inhibition of c-fms kinase activity reverses glomerular macrophage infiltration and halts development of crescentic anti-GBM glomerulonephritis in the rat	111

5.1	Introduction	111
5.2	fms-I reverses glomerular macrophage infiltration	113
5.3	fms-I ameliorates renal pathology and renal dysfunction	116
5.4	fms-I does not modulate proteinuria	118
5.5	fms-I suppresses renal inflammation	118
5.6	fms-I suppresses T cell and dendritic cell infiltration	119
5.7	fms-I does not modify glomerular deposition of rat IgG and C3	121
5.8	Discussion	121

Chapter 6. c-fms kinase inhibition in the established rat crescentic

	glomerulonephritis	125
6.1	Introduction	125
6.2	fms-I treatment starting on day 14 depletes the renal macrophage infiltration	126
6.3	Effect of fms-I on renal pathology and renal dysfunction	127
6.4	Effect of fms-I on interstitial fibrosis	128
6.5	Effect of fms-I on renal inflammation and glomerular T cells	129
6.6	Discussion	129

Chapter 7. Discussion

7.1	ERK blockade in mouse obstructed kidney	131
7.2	c-fms blockade in rat progressive crescentic glomerulonephritis	135
7.2.1	fms-I treatment and macrophage infiltration	135
7.2.2	fms-I treatment and glomerular lesion and crescent formation	139

7.2.3	fms-I treatment and renal function and proteinuria	142
7.2.4	fms-I treatment and tubulointerstitial damage	143
7.2.5	fms-I treatment and pro-inflammatory factors	148
7.2.6	fms-I treatment and T cell and dendritic cell infiltration	150
7.3	Further studies	152
7.4	Conclusion	154
Chapter 8. Bibliography		156

Declaration

This thesis contains no material which has been accepted for the award of any other degree or diploma in any other university or institution, and to the best of my knowledge and belief contains no material previously published or written by another person except when due reference is made in the text of the thesis. All experimental work was performed myself except where due acknowledgement is given.

Notice 1

Under the Copyright Act 1968, this thesis must be used only under the normal conditions of scholarly fair dealing. In particular no results or conclusions should be extracted from it, nor should it be copied or closely paraphrased in whole or in part without the written consent of the author. Proper written acknowledgment should be made for any assistance obtained from this thesis.

Notice 2

I certify that I have made all reasonable efforts to secure copyright permissions for third-party content included in this thesis and have not knowingly added copyright content to my work without the owner's permission.

Yingjie Han

Department of Nephrology

Monash Medical Centre

Department of Medicine

Monash University

Thesis Summary

Renal inflammation and fibrosis are common features in progressive forms of kidney disease. The infiltration of immune cells, such as macrophages, invariably accompanies renal inflammation and fibrosis. Inflammatory cytokines and reactive oxygen species produced by infiltrating leukocytes and damaged renal cells can activate cellular signaling pathways such as the c-Jun N-terminal kinase (JNK) pathway, extracellular signaling-regulated kinase (ERK) pathway and M-CSF/c-fms pathway. These activated signaling pathways can induce a wide range of cellular responses, including cell proliferation, survival, apoptosis and inflammation. These inflammatory events cause damage that promotes renal fibrosis, characterized by glomerulosclerosis and tubulointerstitial fibrosis, and progressive loss of renal function.

In order to investigate the pathological role of these signaling pathways in renal inflammation and fibrosis and to assess the therapeutic potential of their blockade, three individual studies were undertaken. First, the functional role of the ERK signaling pathway in the development of renal interstitial fibrosis was examined using a small molecule MEK1/2 kinase inhibitor, U0126. In the mouse unilateral ureteric obstruction model, ERK phosphorylation was inhibited by U0126 treatment, and the proliferation and accumulation of interstitial F4/80⁺ macrophages were significantly reduced. However, ERK blockade had no effect upon renal interstitial fibrosis. Thus, interstitial accumulation of macrophages but not tubulointerstitial fibrosis in the obstructed kidney is, in part, dependent upon the MEK-ERK signaling pathway. Second, activation of the JNK signaling

was identified in a rat model of mesangial proliferative nephritis (Thy-1 disease). However, administration of CC401, a well characterized JNK inhibitor, failed to modify mesangial cell apoptosis in the early phase (Day 0-3) of Thy-1 disease or to affect mesangial cell proliferation and matrix deposition in the late phase (Day 3-8) of Thy-1 disease, although target serum CC401 levels were achieved.

Third, the role of macrophages in the pathogenesis of rat crescentic glomerulonephritis was examined in a rat model of rapidly progressive crescentic glomerulonephritis (anti-GBM disease) using a novel inhibitor of the M-CSF/c-fms signaling pathway termed fms-I. In the first experiment, fms-I treatment was given during the induction phase of disease (days 0 to 14). This treatment reversed an early glomerular macrophage infiltration, and prevented glomerular and tubulointerstitial damage and loss of renal function. This was associated with prevention of the upregulation of pro-inflammatory factors and dendritic cell infiltration. In the second experiment, fms-I treatment was given during established crescentic disease (day 14 to 35). fms-I treatment reversed the renal macrophage infiltrate, improved renal function, had a minor beneficial effect upon crescent formation and reduced interstitial fibrosis in terms of the deposition of collagen IV. Thus, while fms-I treatment was highly effective when given early in the disease process, it still had beneficial effects when given late in the disease. In conclusion, this thesis has identified important mechanisms by which ERK and M-CSF/c-fms signaling promote renal inflammation and fibrosis. Furthermore, blockade of M-CSF/c-fms signaling pathway may be a potential therapeutic strategy in the treatment of human rapidly progressive glomerulonephritis.

Acknowledgements

This study was made possible thanks to the co-operative effort and expertise of several colleagues and friends. I therefore thank the following people for their important contributions:

Associate Professor David J. Nikolic-Paterson (principal supervisor), for his guidance, advice, support, introduction to experimental nephrology and immunopathology and help with manuscript preparation.

Dr Greg Tesch, for his guidance and advice with pathology and animal work and helpful discussions on the design of my experimental work.

Dr Frank Ma, for his expert assistance in performing real time RT-PCR and animal experiment.

Ms Lois Jones (Laboratory manager), for her continuous motivation and kind support in financial assistance.

Ms Tara Robertson (Laboratory manager), for her continuous support in obtaining reagents, laboratory equipment.

Ms Elyce Ozols, for her instruction and assistance in animal techniques.

Ms Lyn Hurst, for her instruction and assistance in cell culture technique.

Mr Pete Frost, for his assistance for immunohistochemistry, tissue embedding and sectioning.

I also thank to my family for understanding and support, most of all, my wife,

Xinya Ma, for her unfaltering love, support and encouragement during my PhD candidateship.

In addition, I wish to acknowledge the support of a National Health & Medical Research Council PhD scholarship.

Abstracts Presented at National and International Conferences

Han Y, Ma F, Manthey C, Nikolic-Paterson DJ: Inhibition of c-fms kinase activity suppresses rat crescentic glomerulonephritis

43rd Annual Meeting of the Australian and New Zealand Society of Nephrology, Newcastle NSW, 2007

Young Investigator Award Finalist

Han Y, Ma F, Manthey C, Nikolic-Paterson DJ: Inhibition of c-fms kinase activity suppresses rat crescentic glomerulonephritis

41st Annual Meeting of the American Society of Nephrology, Philadelphia, Nov, 2008.

J Am Soc Nephrol 19:64A, 2008

Publications Arising from This Thesis

Han Y, Masaki T, Hurst LA, Ikezumi Y, Trzaskos JM, Atkins RC, Nikolic-Paterson DJ. Extracellular signal-regulated kinase-dependent interstitial macrophage proliferation in the obstructed mouse kidney. *Nephrology* 13:411-418, 2008

Han Y, Ma FY, Tesch GH, Manthey CL, Nikolic-Paterson DJ: c-fms blockade reverses glomerular macrophage infiltration and halts development of anti-GBM crescentic glomerulonephritis in the rat. *Lab Invest* 91:978-991, 2011

Abbreviations

AP-1	activator protein-1 complex
ABC	biotinylated horseradish peroxidase H
AIF	apoptosis inducing factor
APC	antigen presenting cell
ACE	angiotensin converting-enzyme
α -SMA	α -smooth muscle actin
ANCA	anti-neutrophil cytoplasmic antibody
ASK1	apoptosis signal-regulating kinase 1
ATN	acute tubular necrosis
ATRA	angiotensin II type I receptor antagonist
BrdU	bromodeoxyuridine
BSA	bovine serum albumin
C3	complement 3
CD4 ⁺	helper T cell
CD8 ⁺	cytotoxic T cell
CD11c	integrin, alpha X
CD20	non-glycosylated phosphoprotein
CD25	alpha chain of the IL-2 receptor
CD28	receptor for B7.1 (CD80) and B7.2 (CD86)
CD40	TNF receptor superfamily member 5
CD80	activation B7-1 antigen
CD86	activation B7-2 antigen
c-fms	proto-oncogene codes for the M-CSF receptor

CKD	chronic kidney disease
CrCl	creatinine clearance
CSF-1	colony stimulating factor-1
CSF-1R	colony stimulating factor-1 receptor
CTGF	connective tissue growth factor
Coll IV	collagen IV
DAB	3,3-diaminobenzidine tetrahydrochloride
DMSO	dimethyl sulphoxide
DT	diphtheria toxin
DTH	delayed type hypersensitivity
DC	dendritic cell
EC	endothelial cell
ECM	extracellular matrix
EGF	epidermal growth factor
EMT	epithelial-mesenchymal transition
ERK	extracellular signal regulated kinase
ESRD	end stage renal disease
ELISA	enzyme-linked immunosorbent assay
FADD	Fas-Associated protein with Death Domain
FCS	foetal calf serum
FGF-2	Basic fibroblast growth factor-2
FITC	fluorescein isothiocyanate
FSGS	focal and segmental glomerulosclerosis
GBM	glomerular basement membrane

gcs	glomerular cross-section
Glu	glutamine
Gly	glycine
GN	glomerulonephritis
GPCR	G protein-coupled receptor
HLA-DR	a major histocompatibility complex
hpf	high power field
HRP	horseradish peroxidase
ip	intraperitoneal
iNOS (NOS2)	inducible nitric oxide synthase
ICAM-1	intracellular adhesion molecule-1
IC ₅₀	The concentration of an inhibitor that is required for 50% inhibition of an enzyme <i>in vitro</i> .
IL-1	interleukin-1
IL-4	interleukin-4
IL-10	interleukin-10
IL-12	interleukin-12
IL-13	interleukin-13
IL-17	interleukin-17
IFN-γ	interferon-γ
IF	immunofluorescence
I/R	ischemia-reperfusion
JNK	c-Jun amino terminal kinase
JIP	JNK-interacting protein

JNK1	<i>Jnk1</i> gene product
JNK2	<i>Jnk2</i> gene product
JNK3	<i>Jnk3</i> gene product
kDa	kilodalton
LFA-1	leukocyte function antigen-1
LPS	lipopolysaccharide
MAPK	mitogen activated protein kinase
MAPKK	mitogen activated protein kinase kinase
MAPKKK	mitogen activated protein kinase kinase kinase
MC	mesangial cell
MCNS	minimal change nephritic syndrome
MCP-1/CCL2	monocyte chemoattractant protein-1
M-CSF	macrophage-colony-stimulating factor
M-CSF-R	macrophage-colony-stimulating factor receptor
MEK1	mitogen activated protein /ERK1 kinase
MEK2	mitogen activated protein /ERK2 kinase
MEKK	mitogen activated protein /ERK kinase kinase
MHC	major histocompatibility complex
MKK3	mitogen activated protein kinase kinase 3
MKK4	mitogen activated protein kinase kinase 4
MKK6	mitogen activated protein kinase kinase 6
MKK7	mitogen activated protein kinase kinase 7
MLK	mixed-lineage kinase
MKP	mitogen activated protein kinase phosphatase

MIF	macrophage migratory inhibitory factor
Methylcarn	methyl Carnoy's tissue fixative
MMPs	matrix metalloproteinases
MMP12	matrix metalloproteinase 12
MPGN	membranoproliferative glomerulonephritis
NTN	nephrotoxic nephritis
NGF	nerve growth factor
No Tx	no treatment group
NMS	normal mouse serum
NRS	normal rat serum
NRabS	normal rabbit serum
NS	not significant
NShS	normal sheep serum
OD	optical density
PAS	period acid and Schiff reagent
PAI-1	plasminogen activator inhibitor-1
PAP	peroxidase anti peroxidase
PCNA	proliferating cell nuclear antigen
PDGF	platelet derived growth factor
p-ERK	phosphorylation of ERK at Tyr204 and Thr202 residues
p-JNK	phosphorylation of JNK at Tyr185 and Thr183 residues
p-c-Jun (Ser63)	phosphorylation of c-Jun at the serine 63 residue

p-c-Jun (Ser73)	phosphorylation of c-Jun at the serine 73 residue
p-JunD (Ser100)	phosphorylation of JunD at the serine 100 residue
PLP	paraformaldehyde-lysine-periodate
p38	38kDa protein
p-p38	phosphorylation of p38 at Tyr182 and Thr180 residues
Pro	proline
RANTES/CCL5	normal T cell expressed and secreted
RPGN	rapidly progressive glomerulonephritis
RTK	receptor tyrosine kinase
RT-PCR	real time reverse transcriptase polymerase chain reaction
SAPK	stress activated protein kinase
SD	Sprague-Dawley rats
Ser	serine
SLE	systemic lupus erythematosus
Stat1/3	signal transducer and activator of transcription
TAK1	transforming growth factor β -activated kinase 1
Th1	type 1 helper T cell
Th2	type 2 helper T cell
Th17	T helper 17 cells
TGF- β	transforming growth factor- β
TPA	tissue plasminogen activator
Treg	regulatory T cell

TLR	Toll-like receptor
TIMPS	tissue inhibitor of metalloproteinases
TLOs	tertiary lymphoid organs
TNF- α	tumour necrosis factor- α
TNF- β	lymphotoxin
TNF-R	tumour necrosis factor receptor
UUO	unilateral ureteric obstruction
VCAM-1	vascular cell adhesion molecule-1
Veh	vehicle treatment group
VLA-4	very late activation antigen-4
WKY	Wistar Kyoto rat

Chapter 1. Literature review and introduction

1.1 Introduction to renal disease

Increasing numbers of patients are affected by chronic kidney disease (CKD) worldwide. The progressive nature of chronic kidney diseases and the ensuing chronic kidney failure erode the quality and quantity of the patient's life (*Lysaght, 2002*). As a consequence, increasing numbers of patients are reaching end stage renal diseases (ESRD) resulting in an increased demand for renal replacement therapies of dialysis and transplantation.

The leading cause of ESRD in the developed world, as well as in many emerging countries, is diabetic nephropathy. The other common causes include glomerulonephritis and renal vascular disease (e.g. hypertensive nephrosclerosis). Kidney disease is relatively common in our community, which can be relatively benign, or can progress rapidly or slowly to ESRD. Table 1.1 lists the most common types of chronic kidney disease. Population-based studies have shown that glomerulonephritis is the second most common cause of ESRD in patients in Australia and New Zealand (*ANZDATA annual report, 2009*). Within the many types of glomerulonephritis, rapidly progressive forms of glomerulonephritis demand urgent diagnosis and treatment to prevent end stage renal failure.

Kidney disease is assessed from clinical and pathological perspectives. Clinical indices of worsening renal function include an elevated serum creatinine and diminishing creatinine clearance (CrCl). Another important marker of renal injury

is proteinuria. Elevated proteinuria not only suggests glomerular injury, but is a major risk marker for progressive tubulointerstitial damage in most types of GN (*D'Amico et al., 1995*). Renal biopsy is the gold standard both diagnostically and prognostically. The pathological description addresses glomerular involvement, cell involvement, changes in noncellular components of the glomerulus, and tubulointerstitial injury.

1.2 Animal models

1.2.1 Introduction

Rodent models have provided many insights into the pathogenesis of renal diseases. The reproducibility of such animal models has permitted a step-by-step dissection of many of the mechanisms involved. The three disease models used in this thesis are described below and include anti-glomerular basement membrane (GBM) glomerulonephritis (GN), anti-Thy-1 mesangioproliferative glomerulonephritis and unilateral ureteric obstruction (UUO). These are widely used models of rapidly progressive crescentic glomerulonephritis (anti-GBM GN), mesangial proliferative nephritis (anti-Thy-1 nephritis) and interstitial fibrosis (UUO).

1.2.2 Passive accelerated anti-GBM glomerulonephritis

This is a model of human anti-GBM glomerulonephritis that is defined by the presence of autoantibodies directed at specific antigenic targets within the glomerular basement membrane and features rapid deterioration of renal function with prominent leukocyte infiltration and crescent formation. To model

this disease, animals are injected with a heterologous antibody raised against the glomerular basement membrane (GBM), which deposits in the kidney and causes transient injury (the heterologous phase). The animal then mounts its own immune response to the foreign immunoglobulin, which acts as a planted antigen on the GBM (the autologous phase) and can develop crescentic glomerulonephritis. This model can be accelerated by pre-immunizing the animal with immunoglobulin from the species in which the anti-GBM antibodies are raised, such that the autologous phase occurs together with heterologous injury. This type of anti-GBM glomerulonephritis is also known as nephrotoxic serum nephritis.

Although these models have been developed in various species, most recent studies have used either mice or rats. Anti-GBM disease in mice can be difficult to induce and is highly strain-dependent. Anti-GBM disease induced in Th1 dominant strains (e.g. C57BL/6J), develop crescentic glomerulonephritis, while Th2 dominant strains (e.g. BALB/c) develop a humoral mediated injury (*Tipping et al., 2005*). Anti-GBM disease in rats is also strain-dependent. In the WKY rat, a single injection of nephrotoxic serum leads rapidly to severe crescentic glomerulonephritis, whereas Lewis rats are completely resistant. The susceptibility of WKY rats to anti-GBM glomerulonephritis has recently been shown to be due to a polymorphism of the *fcg3* gene which affects macrophage responsiveness (*Aitman et al., 2006*). In some other strains, such as Sprague-Dawley rats, crescentic nephritis can be achieved using an accelerated model.

Nephrotoxic serum nephritis in the rat has been widely used to test anti-inflammatory therapies.

1.2.3 Anti-Thy-1 mesangioproliferative glomerulonephritis

Anti-Thy-1 nephritis is a rat model of mesangioproliferative glomerulonephritis. However, while the mesangial proliferative lesions in this model resemble those seen in IgA nephropathy, the anti-Thy-1 disease model is transient and undergoes spontaneous resolution. Following injection of an antibody recognizing the Thy-1 antigen on the mesangial cell surface, an acute complement-dependent loss of mesangial cells (mesangiolysis) occurs associated with an influx of platelets, neutrophils and macrophages which peak at 24 hours (*Bagchus et al., 1986*). A marked proliferation of mesangial cells and an alteration in mesangial cell phenotype follow, associated with increased synthesis and deposition of extracellular matrix (ECM). In the resolution phase mesangial cell and macrophage cell numbers return to normal, excess extracellular matrix is removed, and normal glomerular architecture is largely restored.

The significance of this model is not that the disease closely parallels the course of human IgA nephropathy, but that it allows investigation of the pathological processes underlying the mesangial response to injury over a short time period. Therefore, the model is ideal to study the responses of mesangial cells to injury, such as mesangial apoptosis and proliferation. A chronic version

of this model can be induced by repeated episodes of anti-Thy-1 antibody induced mesangiolysis, but this option was not examined in this thesis.

1.2.4 Unilateral ureteral obstruction

Unilateral ureteral obstruction (UUO) is a commonly used animal model, which can be performed either in rats or mice. The surgical UUO causes complete obstruction of the ureter, which has the advantage that it mimics, in an accelerated manner, the different stages of human obstructive nephropathy resulting in tubulointerstitial fibrosis.

The main use of this model is to examine the mechanisms of interstitial fibrosis – an important component in the progression of all types of kidney disease. The main advantage of this model is that severe interstitial fibrosis with myofibroblast accumulation and extracellular matrix deposition occurs within 7 days of UUO surgery. This model also features tubular atrophy and apoptosis, and macrophage accumulation.

1.3 Pathogenesis of renal disease

Glomerulonephritis includes a range of immune-mediated disorders that cause inflammation within the glomerulus and secondary development of tubulointerstitial damage. Although the pathogenesis of glomerulonephritis is complex and still to be fully elucidated, studies with animal models have shown the interaction between infiltrated immune cells and renal intrinsic cells is crucial to the pathogenesis of glomerulonephritis (*Chadban et al., 2005*). A variety of

cellular stresses, such as inflammatory cytokines and reactive oxygen species produced by infiltrating leukocytes and damaged renal cells, can activate cellular signaling pathways such as JNK and ERK. These events are able to induce a wide range of cellular responses, including cell proliferation, apoptosis and inflammation (*Ma et al., 2009b; Tian et al., 2000*).

1.3.1 Immune-cell mediated renal damage

This section considers the different type of immune cells that have been implicated in promoting renal injury, or providing protection from injury, in different forms of glomerulonephritis.

1.3.1.1 Macrophages

1.3.1.1.1 Cells of the macrophage lineage

Macrophages are distributed throughout the body. They are large, motile, highly differentiated cells of the mononuclear phagocytic lineage. Circulating blood monocytes are continuously derived from hematopoietic progenitor cells in the bone marrow and migrate into tissues and differentiate into tissue macrophages under the influence of several hematopoietic growth factors, such as macrophage colony-stimulating factor (M-CSF), also named colony stimulating factor-1 (CSF-1) (*Staney et al., 2001*).

Macrophages are important participants in many cellular functions, including immune defense and normal tissue homeostasis. They play critical roles in immune-mediated tissue damage, as well as in the resolution of inflammation

with tissue remodeling and repair depending upon the local microenvironment (Gordon, 2007).

Macrophage activation

Due to a lack of phagocytic capacity and expression of various cell surface receptor/ligands, blood monocytes as the precursor of macrophages remain relatively inactive in the circulation. Circulating monocytes can be rapidly recruited into the site of inflammation and differentiate into macrophages as defined by their capacity to phagocytose. At the inflamed site, there is a range of signals waiting for transmission to the naïve macrophages. Endothelial, epithelial and mesenchymal cells at sites of tissue injury can release chemokines and cytokines to recruit and activate monocytes. Binding of immune complexes or phagocytosis of opsonized particles and debris can trigger monocyte/macrophage activation through receptor signaling. Activating signals are also received from lymphocytes and molecules released by invading organisms which potently stimulate monocyte activation through specific receptor/ligand interactions (Aliberti *et al.*, 1999; Jun *et al.*, 1995).

Depending upon the nature of signals received by cell surface receptor binding in the local microenvironment, macrophages can develop a wide range of potential functions. Some factors induce macrophages into a “classically activated” pattern of differentiation. The classically activated macrophages are also known as M1 type macrophages, which overall generate large amounts pro-inflammatory cytokines, nitric oxide and reactive oxygen radicals. The Th1

cytokine interferon γ (IFN- γ) augments the classical M1 type activation of macrophages in response to bacterial products, such as lipopolysaccharide (LPS), and to pro-inflammatory cytokines, including tumor necrosis factor - α (TNF- α) and interleukin-1 (IL-1) (*Erwig et al., 1998*). Macrophages that have been exposed to IFN- γ combined with one of those activating stimuli release substantially increased levels of cytokines and nitrogen radicals compared to those macrophages without IFN- γ stimulation. Macrophages stimulated with IFN- γ also increase the expression of the receptors essential for effective antigen presentation to T cells. Macrophages can also be activated by immune complexes by signaling via Fc- γ receptors (Fc- γ Rs), but, rather than nitric oxide production, toxic oxygen radicals prevail. Compared to the level of IL-2 released when macrophages are treated with LPS, Fc- γ R1 activation results in the release of low levels of this cytokine (*Lake et al., 1994; Gerber et al., 2001*). However, not all cytokines cause macrophages to develop into “classically activated”. Exposure of naïve macrophages to Th2 cytokines, such as IL-4, or transforming growth factor - β (TGF- β), prevents differentiation into a pro-inflammatory state, even when such macrophages are challenged with pro-inflammatory cytokines later on. These cytokines induce so called “alternatively activated” macrophages (also called M2 type macrophages) which produce anti-inflammatory cytokines and suppress the synthesis of pro-inflammatory cytokines. They are resistant to reactivation (*Stein et al., 1992; Goerdts et al., 1999*). In fact, several other cytokines (IL-10 and IL-13) and glucocorticoids can also induce alternative macrophage activation. Macrophages exposed to these

“non-inflammatory” cytokines do not remain naïve or inactive; instead, they show enhanced capacity for antigen presentation and enhanced phagocytosis of debris and particles. It also needs to be remembered that the so-called M1/M2 phenotypes represent the extremes of macrophage polarization and many intermediate phenotypes exist.

Recruitment of macrophages

Macrophages accumulate at sites of inflammation via recruitment of blood monocytes and, to a lesser degree, by local proliferation of recruited macrophages. Endothelial cells (EC) and the sub-endothelial environment at sites of inflammation show up-regulation and *de novo* expression of a number of molecules that direct blood monocyte recruitment. There are several steps in this process, each of which is directed by specific families of adhesion molecules and chemokines.

Following their initial contact with the luminal surface of endothelial cells, the monocytes roll through rapid association and dissociation between counter ligands on the monocytes and selectins including P-, E- and L-selectin expressed on the endothelial cells. These interactions are strong enough to resist shear stress, thereby slowing the cells sufficiently to permit sampling of the microenvironment on the EC surface. The rolling monocytes then firmly adhere to the EC through interactions between the β 1 integrin, very late activation antigen-4 (VLA-4), and the β 2 integrin, leukocyte functional antigen-1 (LFA-1), and their respective counter-receptors, vascular cell adhesion

molecule-1 (VCAM) and intercellular adhesion molecule-1 (ICAM-1). These molecules are expressed by endothelial cells at low levels under normal conditions, and markedly upregulated by pro-inflammatory cytokines such as IL-1 β , interferon- γ (IFN- γ), and TNF- α (*Brady., 1994*). There is up-regulation of the adhesion molecule ICAM-1 on endothelial cells, as seen in rat anti-GBM glomerulonephritis (*Hill et al., 1994*). After firm adherence to EC, the monocyte crawls along gradients of chemokines and adhesion molecules to intercellular junctions, where there is diapedesis to the subendothelial space. Whilst VLA-4 preferentially mediates lateral migration along the endothelium to the intercellular junction, LFA-1 primarily mediates diapedesis (*Weber et al., 1998*). It has been shown that antibody-based blocking of ICAM-1 and LFA-1 significantly inhibits leukocyte recruitment and ameliorates rat crescentic glomerulonephritis (*Kawasaki et al., 1992*).

Chemokines are small chemotactic cytokines that direct leukocyte recruitment in inflammation. The rolling of monocytes on endothelial cells may allow them exposure to inflammatory chemokines produced by intrinsic renal or inflammatory cells. Monocyte chemoattractant protein-1 (MCP-1/CCL2) mediates monocyte shape change, spreading, and subsequent transendothelial migration. Regulated upon activation, normal T cell expressed and secreted (RANTES/CCL5) promotes integrin-mediated adhesion and then supports monocyte spreading and shape change, and subsequent transendothelial migration. Studies in human biopsies and animal models consistently indicate a role for MCP-1/CCL2 and RANTES/CCL5 in macrophage recruitment and renal

injury in progressive kidney disease (*Eardley et al., 2006*).

M-CSF is also a potent macrophage chemoattractant. *De novo* expression of M-CSF protein correlates with local macrophage infiltration, proliferation, and activation in human glomerulonephritis (*Isbel et al., 2001a*). By using mice deficient of M-CSF or treated with an M-CSF receptor-blocking antibody, interstitial macrophage infiltration and proliferation and tubular injury were significantly reduced in the unilateral ureteric obstruction model of interstitial fibrosis (*Le Meur et al., 2002; Lenda et al., 2003*).

Macrophage proliferation and apoptosis

A second mechanism contributing to macrophage infiltration in the inflamed glomeruli and interstitium is local macrophage proliferation. High levels of local macrophage proliferation, identified by the presence of mitotic figures, incorporation of bromodeoxyuridine (BrdU) and expression of the proliferating cell nuclear antigen (PCNA), have been demonstrated in models of severe renal injury and aggressive forms of human glomerulonephritis (*Lan et al., 1997a; Yang et al., 1998*).

There is evidence to support a role for macrophage-colony stimulating factor (M-CSF), a well-characterized macrophage growth factor, in this process. Studies of murine lupus nephritis and rat crescentic glomerulonephritis have shown increased glomerular and tubular M-CSF mRNA and protein expression that correlates with macrophage proliferation and accumulation (*Isbel et al.,*

2001b; Lenda *et al.*, 2004). In addition, a study of human glomerulonephritis found an increase in glomerular M-CSF protein expression in cases of IgA nephropathy and lupus nephritis that correlated with glomerular macrophage proliferation and accumulation (*Isbel et al.*, 2001a).

Macrophage apoptosis appears to be an important mechanism for counterbalancing macrophage proliferation to limit the extent of tissue damage during the inflammatory response (*Lan et al.*, 1997b). However, apoptosis is not the only mechanism by which macrophages can be removed from the site of inflammation. Trafficking of macrophages from the site of inflammation to the local draining lymph nodes has been described in the models of kidney inflammation (*Lan et al.*, 1993).

1.3.1.1.2 Macrophages in kidney disease

Macrophages in human glomerulonephritis

There are small numbers of resident glomerular and interstitial macrophages in the normal human kidney. However, elevated macrophage accumulation can be observed in most types of human glomerulonephritis. Atkins *et al* in 1976 first reported large numbers of highly motile cells that phagocytosed latex and yeast, and had ultrastructural characteristics of macrophages, and were observed in the outgrowth from cultured glomeruli that had been isolated from patients with rapidly progressive crescentic glomerulonephritis. Subsequent studies with antibody-labeling demonstrated that glomerular and interstitial macrophage infiltration occurs in most forms of primary and secondary glomerulonephritis

(Hooke et al., 1984; Hooke et al., 1987; Yang et al., 1998; Rastaldi et al., 2000).

The density of interstitial macrophage infiltrates correlates with renal function at the time of biopsy (Hooke et al., 1987; Yang et al., 1998; Markovic-Lipkovski et al., 1990). The degree of interstitial macrophage accumulation predicts disease progression in lupus nephritis and IgA nephropathy (Alexopoulos et al., 1989; Stachura et al., 1984). It is well established that the number of interstitial macrophages correlates with the degree of renal dysfunction at the time of biopsy. However, although glomerular macrophage accumulation has been confirmed in many studies of human glomerulonephritis, the relationship between macrophage numbers and the degree of renal dysfunction and proteinuria is still unclear with some studies demonstrating correlations but other studies finding none (Nikolic-Paterson et al, 2001).

Macrophage induction of glomerular damage

Time-course studies have shown a close association between macrophage accumulation and the development of renal injury in many animal kidney disease models, including focal and segmental glomerulosclerosis and anti-GBM crescentic glomerulonephritis. Descriptive data in human biopsies also suggest a role for macrophages in causing renal injury, although this is not conclusive.

Depletion of macrophage in animal models of glomerulonephritis has provided direct evidence. Systemic irradiation with kidney shielding prevented glomerular

macrophage infiltration and abolished proteinuria in rat accelerated anti-GBM disease (*Schreiner et al., 1978*). Glomerular macrophage infiltration and proteinuria have also been blocked by administration of polyclonal anti-macrophage sera in models of anti-GBM disease, serum sickness and Heymann's nephritis (*Holdsworth et al., 1981; Matsumoto et al., 1990; Hara et al., 1991*). A genetic approach to this question is the transgenic mouse (CD11b-DTR), in which tissue macrophages can be specifically and selectively ablated by injections of minute doses of diphtheria toxin (DT). Renal inflammatory macrophages were depleted in progressive crescentic glomerulonephritis. This resulted in a reduction in the number of glomerular crescents, improved renal function, and reduced proteinuria (*Duffield et al., 2005*). Dichloromethylene diphosphonate is a micro-encapsulated toxic drug, which is taken up preferentially by phagocytic cells. In spite of an efficient means to kill macrophages, such preparations can also deplete circulating C3 and neutrophils. This method has been used to inhibit glomerular macrophage accumulation and proteinuria in anti-GBM glomerulonephritis (*Huang et al., 1997*). The same approach can inhibit glomerular macrophage accumulation with a consequent reduction in mesangial matrix expansion in anti-Thy-1 mesangioproliferative nephritis (*Westerhuis et al., 2000*).

Blocking blood monocyte recruitment into inflamed kidneys had been attempted and approved effective in inhibiting renal macrophage infiltration,. Inhibition of macrophage accumulation and consequent renal injury glomerulonephritis both in the induction phase and progressive phase in models of anti-GBM via

blockade of chemokines (MCP-1/CCL2, RANTES/CCL5) or leukocyte adhesion molecules (ICAM-1, osteopontin) was established. (*Nishikawa et al., 1993; Tang et al., 1996; Lloyd et al., 1997; Yu et al., 1998; Tesch et al., 1999*). The results strongly support a role for macrophages in causing renal injury in both the induction and progressive phases of experimental kidney disease. However, caution ought to be taken in this interpretation, because blockade of chemokines and adhesion molecules also suppresses T-cell infiltration, and as we know, that renal injury in the commonly studied models (anti-GBM disease and lupus nephritis) is T-cell dependent.

Macrophages in crescent formation

The extent of crescent formation is an indicator of the severity of glomerular inflammation, and is associated with a poor prognosis (*Kerr et al., 1996*).

Cellular crescents are defined as the presence of two or more layers of cells within Bowman's space (*Atkins et al., 1996*). Some studies have identified parietal epithelial cells as the main component (*Morita et al., 1973; Magil et al., 1985*), whereas other investigations have demonstrated that macrophages are a major cell type within cellular crescents (*Atkins et al., 1976; Hancock et al., 1984*). Moreover, recent studies of human biopsies and mouse glomerulonephritis show that podocytes can be detected as an integral cellular component of glomerular crescents (*Moeller et al., 2004; Thorner et al., 2008*).

A prominent feature in the development of advanced cellular crescents is the accumulation of macrophages within Bowman's space. One mechanism of

macrophage accumulation within Bowman's space is recruitment of macrophages from the glomerular tuft, a process that is likely to involve chemokines and cell-matrix and cell-cell adhesion interactions. Fibrin is the chemotactic molecule directly implicated in macrophage accumulation in Bowman's space (*Tippling et al., 1986*). Macrophages express a variety of adhesion molecules, such as VLA-4 and Mac- 1 of the integrin family, that facilitate adhesion to fibronectin and fibrinogen. These two molecules are often present in Bowman's space at the start of crescent formation. However, several other molecules may be involved, such as MCP-1/CCL2, M-CSF and macrophage migration inhibitory factor (MIF) (*Rovin et al., 1994; Bloom et al., 1993; Lan et al., 1996*).

A second way by which macrophages accumulate in crescents is via local proliferation within Bowman's space. Macrophage proliferation within cellular crescents in rat anti-GBM glomerulonephritis has been shown by the presence of mitotic figures, bromodeoxyurine (BrdU) incorporation, and expression of the proliferating cell nuclear antigen (PCNA) by ED1⁺ macrophages. Moreover, the number of proliferating macrophages within Bowman's space has a significant positive correlation with the total number of macrophages within Bowman's space. A third way of macrophage accumulation in crescents is migration through rupture of Bowman's capsule from periglomerular region, which also is important for the entry of periglomerular myofibroblasts and progression to fibro-cellular crescents (*Lan et al., 1997*).

Macrophages in tubulointerstitial damage

It is well known that macrophages are closely associated with progressive interstitial damage and renal impairment. Human biopsy studies and animal models of kidney disease show a strong association between prominent interstitial macrophage infiltration and tubulointerstitial damage. Further evidence that macrophages cause progressive renal damage comes from macrophage depletion studies in which interstitial damage and renal function have been improved significantly (*Duffield et al., 2005*).

Macrophages have the potential to cause direct damage to intrinsic renal cells through the generation of radical oxygen species (ROS), nitric oxide (NO), complement factors, and pro-inflammatory cytokines (*Rodriguez-Iturbe et al., 2001; Henderson et al., 2008*). Macrophages can also affect supporting matrix and vasculature through the production/secretion of metalloproteinases and vasoactive peptides. Resident interstitial fibroblasts and myofibroblasts can proliferate in response to macrophage-derived proliferative growth factors, and their increased cell number contributes to the subsequent renal scarring and decline in renal function. Interstitial myofibroblasts are the primary source of the extracellular matrix (ECM) proteins that accumulate during interstitial fibrosis (*Lin et al., 2008*). They may be derived from local proliferation and/or transdifferentiated tubular epithelial cells, a process promoted by profibrogenic cytokines, including transforming growth factor- β expressed by macrophages and tubular epithelial cells as a consequence of macrophage-mediated tubular cell injury (*Lan, 2003*). TGF- β promotes the production of all the major matrix

proteins by fibroblasts, and upregulates expression of plasminogen-activator inhibitor-1 (PAI-1).

1.3.1.2 Dendritic cells

Renal dendritic cells were recognized in 1981 on the basis of MHC class II⁺ cells with stellate and mononuclear phagocyte morphology in the interstitium and mesangium of rat kidney (*Hart et al., 1981a; Hart et al., 1981b*). This discovery was further confirmed by electron microscopy (*Schreiner et al., 1981; Kaissling et al., 1994*). Of note, although dendritic cells can be derived from mononuclear phagocyte cell lineage, they are often considered as having a separate lineage from macrophages.

Dendritic cells exist in renal tissue in close communication with the entire renal parenchyma, constantly surveying for and responding to local environmental signals. As sentinels of the immune system, they are positioned to integrate into the local microenvironment and influence innate immune responses anywhere within the kidney (*Soos et al., 2006*). The rapid integration of external stimuli by renal dendritic cells and their subsequent proinflammatory activation can prime and amplify innate immune responses. This occurs mainly through the secretion of cytokines (e.g. TNF- α , IFN- α , IL-1,) and chemokines by dendritic cells that act on adjacent renal parenchymal cells and other innate immune cells (*Munz et al., 2005; Foti et al., 2004*).

Dendritic cells are well-equipped antigen-presenting cells of the adaptive

immune system. In normal kidney, resident dendritic cells express MHC class I and class II molecules but only low levels of co-stimulatory molecules (e.g., CD80, CD86, CD40) (*Austyn et al., 1994*). Resident dendritic cells search their immediate environment and capture self and non-self molecules, whether derived from within or outside the kidney, via phagocytosis, pinocytosis, and receptor-mediated endocytosis. In response to the same stimuli that invoke innate immune responses, dendritic cells up-regulate the expression of co-stimulatory molecules and, migrate to secondary lymphoid tissues bearing any molecules captured within the kidney to present to adaptive immune cells. They stimulate T lymphocyte proliferation and, depending upon the nature of stimuli, secrete cytokines that promote the differentiation of naïve T lymphocytes toward specific T helper (Th) effectors such as Th1 or Th2 (*Dong et al., 2005; Soos et al., 2006*). Moreover, Coates and colleagues demonstrated that immature renal dendritic cells can induce the expansion of T regulatory lymphocytes in mixed leukocyte reactions and suppress allorecognition *in vivo* (*Coates et al., 2004*). These findings suggest that renal dendritic cells may be tolerogenic if engaged by T lymphocytes that have escaped thymic selection and are reactive to self-antigens within the kidney.

While human biopsy studies suggest a positive correlation between the inflammatory intrarenal dendritic cells and renal injury, studies in animal models provide conflicting evidence for the role of dendritic cells (DC) in renal inflammation. Sequential ablation of inflammatory CD11c⁺ DCs and all other intrarenal and extrarenal CD11c⁺ DC subsets in mice with experimental

nephrotoxic nephritis, aggravated tubulointerstitial and glomerular injury (*Scholz et al., 2008*). In contrast with these potential anti-inflammatory mechanisms is the recent finding that renal dendritic cells facilitate the recruitment of detrimental CD4⁺ T lymphocytes secreting IL-17 following experimental acute urinary obstruction (*Dong et al., 2008*). Further studies are required to clarify the pathogenic roles of dendritic cells in renal injury.

1.3.1.3 Neutrophils

Neutrophils are peripheral blood polymorphonuclear leukocytes derived from the myeloid lineage, which is the major component of the circulating phagocytes. They swiftly respond to injury and can be rapidly mobilized to the sites of inflammation.

Neutrophils are a major protective effector of the innate immune response. They respond to invading pathogens either by phagocytosis or releasing granules containing proteases and other enzymes, and generate reactive oxygen species. Antibody and complement deposition can trigger neutrophil influx to the glomerular capillary tuft. The underlying mechanism of leukocyte accumulation and transmigration across vascular endothelium involve multiple molecular events, which include adhesion molecules, chemokines, cytokines and platelets. A significant neutrophil presence is seen in many different forms of glomerulonephritis, particularly in proliferative crescentic lupus nephritis (*Camussi et al., 1980*), vasculitis-associated glomerulonephritis (*Brouwer et al., 1994*), and other forms of rapidly progressive nephritis (*Saeki et al., 1995*).

Among animal models the most closely associated with neutrophil-mediated injury is the acute phase of glomerular injury induced by passive administration of heterologous anti-GBM antibody, where neutrophils appear to be an essential component of injury. The glomerular influx of neutrophils occur within 2 to 4 hours but their transient accumulation only lasts a few hours after the administration of anti-GBM serum (*Lan et al., 1992; Takazoe et al., 2000*). Depletion of neutrophils in a rat of nephrotoxic nephritis and adoptive transfer studies have confirmed the capacity of neutrophils to induce renal injury (*Cochrane et al., 1965; Henson et al., 1972; Naish et al., 1975; Takazoe et al., 2000*).

1.3.1.4 T cells

1.3.1.4.1 T cells in adaptive immunity

Glomerular and periglomerular T cells infiltrates are regularly observed in human kidney biopsies in many types of glomerulonephritis, such as in diffuse proliferative and crescentic lupus nephritis, IgA nephropathy or ANCA-associated glomerulonephritis (*Kurts et al., 2007*). Extensive T cell infiltrates are also observed within the tubulointerstitium in both acute and chronic renal transplant rejection (*Valujskikh et al., 2007*). Furthermore, work in animal models provides formal experimental proof that T cells have a crucial role in mediating kidney damage. Antibody-based depletion studies in the autologous phase of anti-GBM glomerulonephritis in rats demonstrated that acute glomerular injury is dependent upon both CD4⁺ and CD8⁺ T cells (*Huang et al.,*

1997). Also, CD4⁺ T cells are required for the development of a mouse model of anti-GBM glomerulonephritis (*Tipping et al., 1998*). More recently, it was shown that crescentic anti-GBM glomerulonephritis could be transferred by CD4⁺ T cells (*Wu et al., 2002*).

Different T cell subsets are involved in the regulation of the adaptive immune responses, including cellular (Th1), humoral (Th2), Th17 and T regulatory (Treg) immune responses (*Strom et al., 2009*). The cellular immune response involves the recruitment and activation of macrophages and effector T cells into inflammatory sites. T cell immunity is also important in antibody production. Furthermore, the T cell response is negatively regulated by a subset of T regulatory cells (CD4⁺CD25⁺Treg) which maintain T cell tolerance and thereby regulate effector T cell responses (*Wolf et al., 2005*).

1.3.1.4.2 Th1 and Th2 T cells

CD4⁺T cells differentiate into functionally distinct subsets termed Th1, Th2 and Th17 from naïve T cells, which requires T cell receptor recognition of specific antigen in association with MHC I or II complexes on the surface of antigen presenting cells (APC). In addition, the interaction of the costimulatory molecule CD28 on the T cell and B7 on the APC is required for full T cell differentiation as a second signal.

Th1 and Th2 subsets produce distinct immune responses associated with distinct patterns of cytokine secretion and cause different patterns of renal

injury. The Th1 subset is characterized by the production of interferon- γ (IFN- γ), interleukin (IL)-2, and lymphotoxin- α . Th1 responses induce macrophage and cytotoxic T-lymphocyte activation and immunoglobulin IgG subclass switching to favour complement fixation and opsonization. Experimental models of anti-GBM glomerulonephritis in Th1-prone strains exhibit prominent delayed type hypersensitivity (DTH) response within glomeruli. Glomerular T cells promote injury, and manipulation of Th1 and Th2 cytokines confirms the Th1 predominance. The administration of Th1 cytokines exacerbates injury, whereas Th2 cytokines (IL-4 and IL-10) attenuate the nephritogenic immune responses and the severity of Th1-mediated glomerulonephritis (*Holdsworth et al., 1999*). In contrast, Th2 cells, defined by their propensity to secrete interleukin (IL)-4, IL-5, IL-13 and IL-10, are important in allergy, mast cell/IgE-mediate immediate type hypersensitivity responses. In addition, cytokines produced by Th2 cells act as regulators of the immune response. IL-4, IL-13, and particularly IL-10 negatively regulate Th1 responses, especially in the context of the activation by Th1 cytokines such as IFN- γ (*Fiorentino et al., 1991; Zurawski et al., 1994*). Animal models of glomerulonephritis associated with polyclonal B cell activation and autoimmunity have Th2-predominant immune responses. They develop glomerulonephritis with similar immunopathological features to human membranous glomerulonephritis. The inhibition of Th2 cytokines and administration of Th1 cytokines in these experimental models attenuated both the nephritogenic immune response and the associated glomerulonephritis (*Holdsworth et al., 1999*).

1.3.1.4.3 CD8⁺ Cytotoxic T cells

CD8⁺ cytotoxic T cells recognize antigens presented on MHC I and induce injury by secretory molecules such as perforin and granzyme, which induce cellular cytotoxicity, and by cell surface molecules such as lymphotoxin (TNF β) and Fas ligand, which interact with receptors of the TNF receptor family on the target cell to induce apoptosis. The prognosis of lupus nephritis is poorer, when CD8⁺ T cells are detectable in periglomerular infiltrates (*Couser et al., 1994*).

1.3.1.4.4 Regulatory T cells

Regulatory T cells (Treg) are subsets of CD4⁺ (and rarely CD8⁺) T cells involved in the induction and maintenance of peripheral tolerance. Several types of Treg have been described, including Tr1 cells, characterized by production of high levels of IL-10 and TGF β , and CD4⁺CD25⁺Treg, characterized by constitutive expression of CD25 and Foxp3 and using cell-contact dependent mechanisms to suppress other T cells. Impairment of Treg function has the potential to contribute to the development of autoimmune forms of glomerulonephritis. Autoimmunity can arise from failure of Treg in controlling harmful T cell activity, in addition to the classical hypersensitivity reactions.

Transfer of CD4⁺CD25⁺Treg cells into mice with passive anti-GBM glomerulonephritis significantly attenuated the development of proteinuria and reduced renal damage with a marked decrease in renal infiltration by CD4⁺, CD8⁺T cells and macrophages. Similar results achieved were in mouse adrimycin nephropathy (*Wolf et al., 2005; Mahajan et al., 2006*). Furthermore, IL-

10 producing regulatory T cells seems to have a protective role in the nephrotoxic nephritis model (*Scholz et al., 2008*).

1.3.1.5 B cells

B cells are lymphocytes that are derived from the fetal liver in the early embryonal stages of development and from the bone marrow thereafter. B cells play a pivotal role in the immune response being able to differentiate into antibody-producing plasma cells upon binding to antigens, which serve as an essential component of the humoral immune response and in presenting antigen to T cells (*Constant et al., 1995; Harris et al., 2000*).

Relatively little attention has been paid so far to renal infiltration of B cells as modulators of inflammatory kidney disease, although they were the first component of the immune system to be recognized in the pathogenesis of glomerulonephritis through the detection of antibody deposits in the glomeruli by immunofluorescence. B cells play an important role in many immune-mediated renal diseases (*Steinmetz et al., 2008*).

Immunostaining labeled 8% of the interstitial leukocytes in IgA nephropathy and 12% in interstitial nephritis as B cells by using antibody PHM14 and correlated with renal function (*Hooke et al., 1987*). In addition, using CD20 as a B cell marker, a prominent accumulation of B cells was identified in primary interstitial diseases as well as in the secondary interstitial involvement of IgA and membranous nephropathy. In about 30% of cases, B cells formed tertiary

lymphoid organs (TLOs) together with T cells. The B cells were located in the center of the aggregates and T cells distributed around as a paracortex. These intrarenal TLOs may be a result of chronic local inflammation and are ideally situated for surveillance in the tubulointerstitium (*Cohen et al., 2005; Heller et al., 2007*).

Rituximab is a monoclonal antibody that binds to the CD20 molecule expressed on immature and mature B cells, but not on plasma cells. B cells depletion treatment by infusion of rituximab has been used clinically in a variety of renal diseases and in renal transplantation (*Salama et al., 2006; Remuzzi et al., 2002*).

1.3.1.6 Mast cells

Mast cells derive from hematopoietic progenitor cells. They migrate through vascularised tissue to complete their maturation. Mast cells are tissue-specific multifunctional cells, with diverse phenotypes in different anatomic sites. Their anatomic distribution and structural relationships allow mast cells to modulate innate immune and adaptive effector responses (*Kitamura et al., 1989*). This role involves mast cell activation. The classical pathway of mast cell activation is through IgE-Fc ϵ receptor cross-linking. More recent studies have recognized alternative activation pathways including complement receptors and signaling through microbial pattern recognition receptors, such as Toll-like receptors (TLR) (*Beaven et al., 1993*).

Traditionally, mast cells are associated with allergy and host defense against parasites. But there is increasing evidence that mast cells function beyond this and they may have a role in a wide range of kidney diseases. Mast cells are only rarely present in normal kidney tissue. Their numbers increase significantly in the setting of renal disease, including most primary and secondary forms of glomerulonephritis, diabetic nephropathy, and allograft rejection. Mast cell presence is correlated with fibrosis, progressive decline in glomerular filtration, and poor prognosis. (*Ehara et al., 1998; Toth et al., 1999; Otsubo et al., 2003; Ruger et al., 1996; Jones et al., 2004; Yamada et al., 2001*).

In vivo studies in mast cell-deficient mice suggest a protective role for mast cells in renal fibrosis. In puromycin aminonucleoside-induced nephrosis, mast cell-deficient mice had enhanced fibrosis. These *KitW-sh/KitW-sh* null mice surprisingly had increased levels of mRNA encoding TGF- β , suggesting an unexpected role for mast cells in modulating TGF- β expression in this model (*Miyazama et al., 2004*). Ligation of unilateral ureter in mast cell-deficient mice also suggested that mast cells protect against fibrosis (*Kim et al., 2009*).

A number of animal studies have also analyzed the pathogenic role of mast cells in anti-GBM nephritis. One study found that mast cells augment renal injury by promoting DTH effector leukocytes (*Timoshanko et al., 2006*).

However, two other studies demonstrated a potential protective role for mast cells in this model (*Hochegger et al., 2005; Kanamaru et al., 2006*). Further works in experimental inflammatory renal disease are required to define the

pathogenic role of mast cells.

1.3.2 Renal fibrosis

Renal fibrosis, characterized by glomerulosclerosis and tubulointerstitial fibrosis, is the consequence of an excessive accumulation of extracellular matrix that occurs in progressive forms of chronic kidney disease. Irrespective of the initial insult, progressive chronic kidney disease results in widespread tissue scarring with complete destruction of kidney parenchyma and end-stage renal failure. The cellular events leading to these histologic presentations are complex, involving the participation and interaction of resident kidney cells and infiltrated cells.

1.3.2.1 Mesangial cell

The mesangium represents the core of the glomerulus from a structural point of view and is an important site of injury in glomerular disorders. The glomerular mesangium consists of resident mesangial cells and extracellular matrix. The functions of mesangial cells are many and include regulation of capillary flow, and maintenance of the glomerular extracellular matrix.

Upon activation, mesangial cells can synthesize an array of substances such as cytokines, which induce cellular proliferation, cell shape changes, and recruitment of inflammatory cells. Both resident and non-resident cells, including inflammatory cells, secrete factors such as angiotensin II that stimulate mesangial cell proliferation and matrix production and regulate blood flow.

The activation and proliferation of mesangial cells is an early event in a variety of glomerulonephritis. Mesangial cell proliferation and matrix accumulation are also considered to contribute to the development of glomerulosclerosis. Platelet derived growth factor (PDGF) is a potent mitogen for mesangial cells. Both human and rat mesangial cells are capable of synthesizing and releasing PDGF. It has been demonstrated that the binding of PDGF to human mesangial cells stimulates proliferation (*Shultz et al., 1988*). Administering neutralizing anti-PDGF IgG prior to induction of anti-Thy-1 mesangioproliferative nephritis results in a significant reduction in mesangial cell proliferation and extracellular matrix deposition (*Floege et al., 1992*). Inhibition of PDGF receptor tyrosine kinase, using STI 571, has also been shown to inhibit mesangial cell proliferation in this disease (*Gilbert et al., 2001*).

The mesangial matrix is altered in pathologic states by the deposition of increasing quantities of ECM components, some of which are not normally present in the mesangium. If this pathologic process is not controlled, glomerulosclerosis can develop. Mesangial cells become activated in response to injury. For example, they show *de novo* expression of α -SMA, which is thought to be involved in cell migration and cell contraction. The activated myofibroblastic mesangial cells acquire a prominent rough endoplasmic reticulum, ribosomes, and polysomes, indicating their increased ability to engage in active protein synthesis. These mesangial cells with myofibroblastic phenotype synthesize an array of different extracellular matrix proteins not normally present in the mesangium, including collagens I and III. This switch by

mesangial cells from the production of collagen IV to interstitial fibrillary type collagens is thought to be a major factor in progression to glomerulosclerosis (*Jefferson et al., 1999*). Mesangial cell proliferation and increased mesangial matrix are particularly prominent in IgA nephropathy and diabetic nephropathy.

1.3.2.2 Podocytes

Podocytes are highly specialized, terminally differentiated epithelial cells, with a quiescent phenotype. The podocytes line the outer aspect of the capillary loop. Podocytes are tethered to the underlying glomerular basement membrane via an intricate network of foot processes.

The slit diaphragm bridging the gap between neighbouring foot processes is thought to be a major determinant of the size permselectivity of the glomerular filtration barrier and prevents the passage of large molecular weight proteins from the vascular space into the ultrafiltrate. Podocytes act to maintain the capillary loop shape and the glomerular basement membrane (GBM), to counteract the intraglomerular pressure and produce vascular endothelial growth factor required for glomerular endothelial integrity (*Haraldsson et al., 2008*).

Podocyte dysfunction is linked to proteinuria and progressive glomerulosclerosis. The mechanism underlying proteinuria might be simply due to a lack of charge and size selectivity in areas of podocyte loss (*Shankland, 2006*). Recent studies have also linked podocyte loss with the onset and

magnitude of glomerulosclerosis. Podocyte loss leads to areas of “bare or denuded” GBM where podocytes are reduced. Because one of the functions of podocytes is to maintain capillary loop shape by opposing the outward forces of glomerular pressure (which are increased in many renal diseases), podocyte loss leads to outward bulging of the GBM in the denuded areas. An attachment forms upon contact of the denuded GBM with the parietal epithelial cells and Bowman’s capsule. This is the first “committed step” for the formation of FSGS. Recent podocyte depletion studies have demonstrated that podocyte loss could be a major mechanism driving glomerulosclerosis and progressive loss of renal function in glomerular diseases (*Matsusaka et al., 2005; Wharram et al., 2005; Wiggins et al., 2005*).

1.3.2.3 Myofibroblasts

Myofibroblasts are a type of activated fibroblast which express α -smooth muscle actin. Myofibroblasts make large quantities of ECM and are involved in wound repair. Myofibroblasts in the kidney have been considered to represent an activated population of resident fibroblasts (*Rodemann et al., 1991*).

Myofibroblasts are large cells with long processes resembling fibroblasts and vascular smooth muscle cells. They are characterized by bundled microfilaments, a well-developed rough endoplasmic reticulum, hemidesmosomes, and other intercellular attachments (*Qi et al., 2006*).

In renal fibrosis, myofibroblasts are mainly responsible for ECM deposition in tubulointerstitial fibrosis and in the fibrous organization of cellular crescents.

Renal myofibroblasts may be derived from resident renal fibroblasts, resident renal pericytes, the circulating fibrocyte population, haematopoietic progenitor or stromal cells derived from the bone marrow. They also can derive from tubular cells undergoing epithelial to mesenchymal transformation (EMT) in response to renal injury (*Kaissling et al., 2008*).

Various stimuli have been found to induce fibroblast activation. In general, fibroblasts respond to stimuli associated with tissue injury by acquiring an activated phenotype. For example, infiltration of inflammatory cells can promote the activation and proliferation of resident fibroblasts. These resident fibroblasts become activated by stimulation with cytokines including TGF- β , PDGF and FGF-2. Additional activation mechanisms include direct cell-cell contact (leukocytes and macrophages), ECM-integrin interaction (mainly α 1 and β 1), as well as environmental stimuli such as hypoxia and hyperglycemia.

Renal cortical fibroblasts play a role in the maintenance and turnover of ECM but under pathological conditions may participate in the fibrotic response in the setting of renal injury. They are responsible for production of the extracellular material, fiber and ground substance, such as collagen I, III, IV and various laminins which include fibronectin. They also secrete the matrix metalloproteases (MMPs), tissue inhibitor of MMPs (TIMP-1,-2, -3) and plasminogen activator inhibitors-1 (PAI-1) (*Hinz, 2007; Hinz et al., 2007*).

1.3.3 Cell proliferation – a feature of progressive renal disease

Renal cell proliferation is a key pathological feature in progressive kidney disease. The term proliferative glomerulonephritis refers to cell accumulation in the inflamed kidney as much as local cell proliferation. Aberrant proliferation of mesangial cells (MCs) is a common finding in a number of diseases that lead to end-stage renal failure, (e.g. IgA nephropathy and diabetic nephropathy). A variety of initial insults, which may be metabolic as in diabetic nephropathy, or immunological, can cause uncontrolled MC proliferation. In turn, this causes an increase in extracellular matrix (ECM) deposition and ultimately leads to glomerulosclerosis, with subsequent reduction in glomerular filtration rate due to loss of functioning nephrons. However, cell proliferation is also an important mechanism of renal repair.

1.3.4 Apoptosis

1.3.4.1 Introduction

Apoptosis is an active mode of cell death under molecular control and requires energy to proceed (*Riedl et al., 2007*). Apoptosis of renal cells may be beneficial and help modify renal cell number during recovery from proliferative forms of renal injury (*Nikolic-Paterson., 2003*). Apoptosis is differentiated from another type of cell death, which is necrosis, by morphologic and functional features and also by whether energy is required to proceed. The relative contribution of apoptosis and necrosis to injury is variable and depends on the severity of the insults. More severe insults or depleted cell energy will result in necrosis, e.g. acute tubular necrosis.

1.3.4.2 Apoptosis cascades

Cell survival is a consequence of the interplay between the presence of survival factors that activate intracellular survival pathways and keep the lethal pathways latent (*Sanz et al., 2008*). Two main intracellular pathways for apoptosis have been documented: one is ligation of plasma membrane death receptors called the extrinsic pathway; another is perturbation of intracellular homeostasis called the intrinsic pathway. In the extrinsic pathway ligation of death receptors leads to the assembly of multi-molecular complexes that include adaptor proteins such as FADD and the activator caspase-8 and -10. These caspases are activated upon oligomerization and then cleave protein substrates to activate downstream effector caspases (*Thorburn, 2004*).

The intrinsic pathway involves intracellular organelles, the most important of which is mitochondria. Sentinel activator BH3-only proteins trigger the activation of Bax and/or Bak, which oligomerize at the mitochondria, inducing permeabilization of the outer mitochondrial membrane and releasing proapoptotic factors such as cytochrome c, SMAC/DIABLO, and apoptosis-inducing factor (AIF), which promote caspase-dependent and –independent apoptosis. Cytochrome c facilitates the oligomerization of Apaf-1 and caspase-9 in the apoptosome, resulting in activation of caspase 9. Caspase-9 cleaves and activates effector caspases such as caspase-3 and -7, resulting in widespread proteolysis and commitment to cell death (*Green et al., 2004; Riedl et al., 2007*). It has been proposed that c-Jun N-terminal kinase (JNK) activation triggers the mitochondria-dependent apoptosis in response to many types of stress,

including UV-irradiation. The various roles of JNK activation in apoptosis depend on the individual cell type and the specific conditions observed (*Liu et al., 2005*).

1.3.4.3 Apoptosis in kidney disease

Human glomerular and tubulointerstitial diseases are associated with apoptosis. Apoptosis is evident in human glomerulonephritis though the rate of apoptosis in normal human kidneys is very low (*Hughes et al., 2004*). There is a marked induction of tubular cell apoptosis in ischemic/reperfusion injury. Apoptosis of glomerular cells is evident in human lupus nephritis and IgA nephropathy (*Baker et al., 1994*). In lupus nephritis, proliferative disease and higher activity indices are associated with higher levels of glomerular cell apoptosis. Whilst apoptosis is seen as detrimental in progressive renal injury in some human kidney diseases, yet in other diseases it is a mechanism through which disease resolution occurs (*Badillo-Almaraz et al., 2001*). For example, in acute post-infectious glomerulonephritis the incidence of apoptosis increases more than 250-fold, however, this increased apoptosis likely reflects the intense glomerular neutrophil infiltration in this condition, with short-lived neutrophils destined to die by apoptosis. In addition, apoptosis is well described in other forms of renal injury, such as acute tubular necrosis, obstructive nephropathy and toxic nephropathies, and progressive renal fibrosis and cystic renal disease (*Makino et al., 2003; Hughes et al., 2004*).

1.4 M-CSF/c-fms kinase signaling pathway

1.4.1 M-CSF and the monocyte/macrophage lineage

Macrophages are continuously derived from blood monocytes which, in turn, are derived from pluripotent hematopoietic progenitor cells under the influence of several haematopoietic growth factors. Macrophage-colony stimulating factor (M-CSF) is the most important macrophage growth factor, which can stimulate the survival, proliferation and differentiation of mononuclear phagocytes, as well as increase the motility and migration of macrophages (*Pixley et al., 2004*).

1.4.2 M-CSF and its receptor

There are functionally separable M-CSF (also known as CSF-1) isoforms, namely, a secreted glycoprotein and a secreted proteoglycan, both of which circulate; and a membrane-spanning, cell-surface glycoprotein (*Ryan et al., 2001; Dai et al., 2004*). The circulating proteoglycan and glycoprotein isoforms are synthesized by endothelial cells and can function at a distance. The cell-surface isoform is involved in local regulation, whereas the secreted proteoglycan isoform is localized to specific extracellular matrices. Many different types of cell including endothelial, mesangial, tubular epithelial cells and fibroblast synthesize M-CSF, and its synthesis is increased by a variety of stimuli, including cytokines, steroid hormones and bacterial products. The M-CSF/c-fms signaling pathway is shown in Figure 1.1.

1.4.3 Functions of M-CSF

Studies on M-CSF deficient mice indicate that M-CSF regulates the survival, proliferation and differentiation of blood monocytes and tissue macrophages

(Cecchini *et al.*, 1996; Dai *et al.*, 2002). Concentrations of M-CSF that are sufficient for the survival of primary macrophages are not sufficient to stimulate significant proliferation. Motility is an essential aspect of macrophage function. Tissue macrophages are derived from recruited circulating monocytes and by local macrophages proliferation. Thus, normal tissue development and immune responses are, in part, dependent upon the ability of macrophages to migrate into specific sites on demand. Activation of the M-CSF-R with M-CSF results in rapid stimulation of quiescent macrophages leading to increased motility and chemotaxis towards the source of M-CSF (Webb *et al.*, 1996; Allen *et al.*, 1997).

1.4.4 M-CSF in human kidney diseases

Immunohistochemistry shows that there is a significant increase in glomerular M-CSF expression in proliferative forms of human glomerulonephritis, particularly in systemic lupus erythematosus (SLE) class IV. By comparison, little change in glomerular M-CSF expression is seen in non-proliferative forms of glomerulonephritis, such as minimal change disease, membranous glomerulonephritis and primary focal glomerulosclerosis. In proliferative diseases, glomerular M-CSF staining was evident in podocytes, infiltrating macrophages and some mesangial cells and correlates with local macrophage proliferation. There is a marked increase in M-CSF expression in tubular cells in both non-proliferative and proliferative forms of glomerulonephritis (Isbel *et al.*, 2001a). In situ hybridization has shown M-CSF mRNA expression to be increased in IgA nephropathy and lupus nephritis, demonstrating that the tubular M-CSF immunostaining largely reflects local synthesis rather than

absorption of filtered serum M-CSF. The number of Ki67-positive proliferating cells, HLA-DR positive cells and alpha-smooth muscle actin-positive area in the glomerulus are increased in cases with enhanced M-CSF expression (*Matsuda et al., 1996*). In addition, serum levels of M-CSF are elevated in patients with lupus nephritis and acute kidney rejection (*Yang et al., 2008; Le Meur et al., 2004*).

1.4.5 M-CSF in experimental kidney disease

Fas-deficient lupus-prone MRL mice (MRL-Fas^{lpr}) develop a progressive inflammatory kidney disease in association with deposition of immune complexes and elevated renal M-CSF expression. MRL-Fas^{lpr} mice die of kidney disease by 5–6 months of age. Cross breeding of M-CSF deficient mice with MRL-Fas^{lpr} mice results in a reduction in systemic inflammation, renal injury and circulating autoantibodies with enhanced B cell apoptosis compared with M-CSF intact MRL-Fas^{lpr} mice (*Lenda et al., 2003; Lenda et al., 2004*). These studies also demonstrated that up-regulation of M-CSF expression precedes renal injury and is responsible for macrophage recruitment, proliferation and activation in the kidney as well as for macrophage-induced apoptosis of kidney tubular epithelial cells. Furthermore, ureteral obstruction-induced renal inflammation is reduced in M-CSF-deficient mice owing to decreased recruitment, proliferation and production of apoptotic mediators by M-CSF-independent macrophages (*Lenda et al., 2003*). These findings are consistent with earlier studies in which a neutralizing antibody against c-fms was shown to reduce macrophage recruitment and proliferation in mouse models of acute allograft rejection and

unilateral ureteral obstruction (*Jose et al., 2003; Le Meur et al., 2002*). Recently, a selective inhibitor of the tyrosine kinase activity of c-fms was used to block M-CSF in mouse UUO. Renal macrophage infiltrates and tubular cell apoptosis were significantly reduced (*Ma et al., 2009a*). Together, these results demonstrate an important role for M-CSF in the initiation and propagation of renal inflammation.

1.5 Extracellular signal-regulated kinase (ERK)

1.5.1 Introduction

The mitogen activated protein kinases (MAPK) are a family of intracellular signaling pathways. Cells can respond to many different mitogens and extracellular stresses via MAPK signaling. Through different intracellular mechanisms, including modifying gene transcription, MAPK signaling control cell responses such as survival, proliferation and apoptosis (*Bokemeyer et al., 1996*). Extracellular signal-regulated kinases (ERK) are the best described members of the MAP kinase family. There are 3 different ERK genes, named *erk1*, *2* and *5*, which encode enzymes of 42 or 44 kDa. The pathway leading to ERK activation is shown in Figure 1.2.

1.5.2 ERK in human and experimental kidney disease

In vitro studies have identified an important role for the ERK pathway in the proliferation of cultured mesangial cells, tubular epithelial cells, and fibroblasts. Also, ERK signaling contributes to TGF- β 1 stimulated fibronectin and collagen production by glomerular mesangial cells and renal fibroblasts (*Inoki et al.,*

2000; Suzuki *et al.*, 2004). To relate these *in vitro* data to normal and diseased kidneys, a time-course study of the obstructed rat kidney identified an association between ERK activation and proliferation of tubular epithelial cells and interstitial myofibroblasts (Masaki *et al.*, 2003). Also, glomerular ERK activation occurs in the rat Thy-1 model of mesangioproliferative nephritis and blockade of the ERK pathway results in a significant reduction in mesangial cell proliferation in this disease model (Bokemeyer *et al.*, 2002). In normal human kidney, activation of ERK is largely restricted to the cytoplasm of cells of the collecting duct. In glomerulopathies, glomerular ERK activation co-localizes with cell proliferation in the glomerular tuft and in crescents. Moreover, ERK activation is prominent in tubules and interstitial cells in areas of tubulointerstitial damage (Masaki *et al.*, 2004).

1.6 c-Jun N-terminal kinase signaling pathway

1.6.1 Introduction

c-Jun N-terminal kinases (JNKs) are a group of stress activated serine/threonine protein kinases, which are part of the MAPK family. The JNK signaling pathway is an important regulator of multiple cell functions and is activated by many different stimuli. These include cytokines, growth factors and multiple environmental factors such as UV irradiation, mechanical stress and osmotic stress. There are three genes encoding JNK namely *Jnk1*, 2 and 3 which share 85% homology at the amino acid level. These three genes give rise to ten different protein isoforms by alternative mRNA splicing, which have molecular weights around 46 to 54 kDa. JNK is activated by dual phosphorylation

at threonine 183 and tyrosine 185 in a threonine-proline-tyrosine activation loop. JNK1 and 2 are ubiquitously expressed while JNK 3 is limited to the nervous system, testes and heart (*Weston et al., 2007*). The JNK signaling pathway is shown in Figure 1.3.

1.6.2 JNK signaling pathway involved in apoptosis and cell proliferation

Abundant *in vitro* and *in vivo* evidence demonstrates that JNK signaling plays a proapoptotic role under most circumstances. Apoptosis induced by nerve growth factor (NGF) withdrawal in rat PC-12 pheochromocytoma cells was suppressed by inhibiting the JNK pathway, whereas activation of the JNK pathway by expressing a constitutively active MEKK1 induced apoptosis in PC-12 cells (*Minden et al., 1994; Xia et al., 1995; Le-Niculescu et al., 1999*). *In vivo* studies, using a specific JNK inhibitor reduced hepatocyte apoptosis in liver ischemia/reperfusion injury, and genetic deletion of JNK1 resulted in a significant reduction in tubular cell apoptosis in the mouse obstructed kidney (*Uehara et al., 2004; Uehara et al., 2005; Ma et al., 2007*).

A role for JNKs in regulating cellular proliferation has been shown in fibroblasts lacking both JNK1 and JNK2 (*Tournier et al., 2000; Sabapathy et al., 2004*). The *Jnk1^{-/-}Jnk2^{-/-}* fibroblasts were found to exhibit a proliferation defect and were also defective in c-Jun phosphorylation, which has been shown to be essential for cellular proliferation. *In vivo* studies using cells from knockout and transgenic mice have indicated that c-Jun is essential for efficient transition of the G1-S phase of the cell cycle, and cells lacking c-Jun have a severe

proliferation defect. In addition, it was demonstrated that c-Jun N-terminal phosphorylation is important for efficient cellular proliferation. Fibroblasts from mice carrying a mutant c-jun allele having the JNK phosphoacceptor serines 63 and 73 changed to alanines (junAA) proliferate more slowly than wild-type cells, though this defect was not as severe as found with c-jun^{-/-} fibroblasts (*Behrens et al., 1999*). It was also shown that c-Jun is required for efficient hepatocyte proliferation after partial hepatectomy (*Behrens et al., 2002*).

1.6.3 JNK in human and experimental kidney disease

Activation of JNK signaling is restricted to the collecting duct and occasional parietal epithelial cells in normal kidney (*Flanc et al., 2007*). JNK signaling has been examined in human kidney disease. Immunostaining for phosphorylated-c-Jun, a well-defined marker of JNK signaling, identified a remarkable increase in JNK activation in kidney diseases including various types of glomerulonephritis, hypertensive glomerulosclerosis and diabetic nephropathy. Phosphorylated c-Jun staining was evident in many glomerular and tubular cells. Indeed, the number of p-c-Jun⁺ glomerular cells correlated with the degree of glomerulosclerosis, while tubulointerstitial p-c-Jun staining correlated with interstitial fibrosis and renal dysfunction, implicating JNK signaling in the pathogenesis of different forms of human kidney disease (*De Borst et al., 2007*).

There is also a marked increased in JNK activity in rat anti-GBM glomerulonephritis, with immunostaining for p-JNK and p-c-Jun showing JNK activation in glomerular macrophages, podocytes, tubular epithelial cells and

myofibroblasts (*Flanc et al., 2007*). A highly selective JNK inhibitor (CC- 401) was used in a rat model of anti-GBM disease. Proteinuria and the severity of glomerular and tubulointerstitial lesions were reduced by JNK inhibition. Up-regulation of iNOS and TNF- α , which are markers of macrophage activation, were suppressed by JNK blockade, whereas the T cell and humoral immune response were unaltered, leading to the conclusion that the beneficial effects of JNK blockade were due to inhibition of the macrophage pro-inflammatory response (*Flanc et al., 2007*). These findings are supported by a recent study in which the genetic susceptibility of WKY rats to anti-GBM disease was attributed, in part, to up-regulation of JunD leading to increased AP-1 activity and a macrophage pro-inflammatory phenotype (*Behmoaras et al., 2008*).

1.7 Hypotheses and Aims

The studies in Chapter 3 of this thesis address the hypothesis that activation of the ERK pathway contributes to both renal cell proliferation and renal fibrosis in response to injury. To test this hypothesis, I administered a specific ERK inhibitor in a mouse model of fibrosis – unilateral ureteric obstruction (UUO model).

The studies in Chapter 4 of this thesis address the hypothesis that the JNK signaling pathway plays an important role in mesangial proliferative nephritis. To test this hypothesis, I used a specific pharmacological JNK inhibitor in a rat model of mesangial proliferative nephritis (Thy-1 model).

The studies in Chapters 5 and 6 in this thesis address the hypothesis that the M-CSF/c-fms signaling pathway plays a crucial role in the induction and progression of macrophage-mediated renal injury in crescentic glomerulonephritis. To test this hypothesis, I used a selective inhibitor of the c-fms kinase in a rat model of crescentic anti-GBM glomerulonephritis.

Chapter 2. Materials and Methods

2.1 Animals

Male C57BL/6 mice used for unilateral ureteric obstruction and female Wistar rats used for the anti-Thy-1 glomerulonephritis model were obtained from Monash Animal Services (Monash University, Clayton, VIC, Australia). Male Wistar-Kyoto rats used for the anti-GBM glomerulonephritis model were obtained from Animal Resources Centre (Perth, WA, Australia). Animals were housed in the conventional facility of the Monash Medical Centre Animal Service during the experimentation period. All animal studies were approved by the Monash Medical Centre Animal Experimentation Ethics Committee.

2.2 Kinase inhibitors

2.2.1 MEK1/2 kinase inhibitor

U0126 (1,4-diamino-2,3-dicyano-1,4-bis[2-aminophenylthio] butadiene, C₁₈H₁₆N₆S₂) is a highly selective and potent inhibitor of mitogen activated protein kinase kinase 1 and 2 (also known as MEK1 and MEK2). IC₅₀ values for MEK1 and MEK2 are 70 and 60 nM respectively. U0126 (MEK1/2 Inhibitor) was supplied by Bristol-Meyers Squibb (Princeton, NJ, USA) as a lyophilized white powder. Varying doses of the specific MEK1/2 inhibitor U0126 were prepared in dimethyl sulphoxide (DMSO). U0126 was administered to mice by three times daily intra-peritoneal injection (100 mg/kg U0126 in 20 µl DMSO).

2.2.2 JNK kinase inhibitor

The specific JNK inhibitor CC401 was provided and synthesized by Celgene Corporation (San Diego, CA, USA) (*Uehara et al., 2004; Uehara et al., 2005*). CC401 is a potent inhibitor of all three forms of JNK (Ki of 25-50nM), and has at least 40-fold selectivity for JNK compared to other related kinases, including p38, ERK, IKK2, PKC, Lcl and Zap70. In cell-based assays, 1 to 5µmol/L CC401 provides specific JNK inhibition (*Ma et al., 2007*). CC401 was dissolved in 50mM anhydrous citric acid (Sigma-Aldrich Corporation, St Louis, MO, USA). The pH was adjusted to pH5.0 using 1.5M NaOH. CC401 was administered to rats by twice daily oral gavage (200mg/kg in 1ml vehicle). Peak serum levels (range 0.5 to 2.0 µM) occur 3 to 5 hours after gavage. The dose of 200mg/kg bid was based upon previous studies in rat anti-GBM disease (*Flanc et al., 2007*).

2.2.3 c-fms kinase inhibitor

fms-I (4-cyano-1H-imidazole-2-carboxylic acid {2-cyclohex-1-enyl-4-[1-(2-methanesulfonyl-ethyl)-piperidin-4-yl]-phenyl} -amide) is a selective inhibitor of the tyrosine kinase activity of c-fms provided and synthesized by Johnson & Johnson Pharmaceutical Research and Development L.L.C. (Spring house, PA, USA). The selectivity of the drug has been tested using the Invitrogen SelectScreen™ Kinase Profiling Service which evaluated fms-I at 1µM for activity against 32 serine/threonine kinases and 29 tyrosine kinases in the presence of 100µM ATP. Of these, c-fms, c-kit, Flt-3, and Trk-A were inhibited by >50%. IC₅₀ values were 0.0015, 0.012, 0.058 and 0.030 µM for c-fms, c-kit, Flt-3 and Trk-A respectively using biochemical kinase assay, and 0.0031, 0.21,

0.098 and 0.50 μ M respectively using kinase-dependent cell proliferation assays (Ma *et al.*, 2009a). In our studies, fms-I was administered to rats by twice daily oral gavage (10mg/kg or 30mg/kg in 1ml 20% 2-Hydroxypropyl- β -cyclodextrin in distilled water).

2.3 Antibodies

2.3.1 Primary antibodies

2.3.1.1 Monoclonal antibodies (Table 2.1)

2.3.1.2 Polyclonal antibodies (Table 2.2)

2.3.2 Secondary antibodies (Table 2.3)

2.4 General reagents

2.4.1 Tissue fixatives

Neutral buffered formalin (10%), methyl Carnoy and paraformaldehyde-lysine-periodate (PLP) fixatives were used. Neutral buffered formalin was purchased from Australian Biostain (Traralgon, VIC). Methyl Carnoy fixative was prepared immediately before use as follow: 60% methanol (Sitecraft), 30% chloroform (AnalaR, MERCK Pty Ltd, Kilsyth, VIC), 10% glacial acetic acid. PLP fixative was prepared as follow: 2% paraformaldehyde, 0.01M sodium periodate, 0.075M lysine and 0.037M sodium phosphate buffer, adjusted to final pH of 7.4. PLP was aliquoted and stored at -20°C and thawed immediately prior to use.

2.4.2 General solutions

All chemicals used were obtained from Sigma-Aldrich unless otherwise stated. Phosphate buffered saline (PBS) was used as a general washing solution for

immunohistochemistry and flow cytometry, which consisted of 8.1mM Na₂HPO₄, 1.5mM KH₂PO₄, 2.7mM KCl and 137mM NaCl. PBS with 7% sucrose and 0.02% sodium azide was used as a preservative agent for tissue fixed in PLP prior to tissue processing. 70% ethanol (CSR Ltd, Yarraville, VIC) was used as a preservative for formalin and methylcarnoy fixed tissue. It was also used for immunohistochemistry. Xylene (AnalaR, MERCK Pty, VIC) or histo-lene (Grale Scientific, Ringwood, VIC) was used for dewaxing of paraffin sections.

2.4.3 Periodic acid – Schiff reaction reagents

Periodic acid and Schiff reagent (PAS) and haematoxylin (Amber Scientific, Midvale, WA) were used to stain formalin or methyl Carnoy fixed tissue sections.

2.4.4 Materials used in immunohistochemistry

2.4.4.1 Sera

The following sera were used as blocking agents or as diluent for primary and secondary antibodies in immunohistochemistry: normal sheep serum (NShS), foetal calf serum (FCS), normal rat serum (NRS), normal rabbit serum (NRabS), normal mouse serum (NMS) and bovine serum albumin (BSA).

2.4.4.2 Other blocking agents

Endogenous peroxide blocking solution: methanol/0.3% hydrogen peroxide (Ajax Finechem, Taren Point, NSW). Commercial Avidin/Biotin blocking kit

(Vector laboratories, USA) consisting of both avidin and biotin blocking reagents.

2.4.4.3 Avidin DH: biotinylated horseradish peroxidase H complex

The avidin DH: biotinylated horseradish peroxidase H (ABC) complex binds to biotinylated secondary antibodies to amplify the target antigen signal. 1 drop of avidin DH was mixed with 1 drop of biotinylated horseradish peroxidase H in 2 ml of PBS. These were mixed well and then left to incubate for 30 minutes prior to application to the tissue sections.

2.4.4.4 Substrates for enzyme reactions to detect antigens by immunohistochemistry

3, 3-diaminobenzidine tetrahydrochloride (DAB)

DAB was used as a substrate for horseradish peroxidase (HRP), and its brown coloured precipitate used to visualize the antibody-antigen interaction. This was prepared by dissolving 10mg DAB in 20ml of PBS, filtering the solution and adding H₂O₂ to a final concentration of 0.15% just before use.

NBT/BCIP

Alkaline phosphatase conjugated antibodies were visualized by NBT/BCIP (Roche, Mannheim, Germany). This was prepared by dissolving 1 tablet to 10ml distilled water. The composition of the staining solution (pH 9.5) after addition of distilled water was as follow: 0.4mg/ml NBT; 0.19mg/ml BCIP; 100mM Tris buffer, 50mM MgSO₄. The solution is ready to apply on tissue sections.

NBT/BCIP creates a blue/grey coloured precipitate with the alkaline phosphatase enzyme.

2.4.4.5 Mounting media for tissue sections

Eukitt medium (Ziegelhofstrade, Freiburg, Germany) was used as a standard mounting media for the slides developed using DAB. Glycerol gelatin was used for mounting of slides developed with NBT/BCIP. DABCO consisting of PBS (pH8.5), 70% Glycerin and 5% DABCO was used as mounting media for immunofluorescence staining.

2.4.4.6 Antigen Retrieval Buffer

Two different antigen retrieval buffers were used to treat tissue sections by microwaving or pressure-heating; 0.01M sodium citrate buffer pH 6.0 and Dako microwave buffer (DakoCytomation, Carpinteria, CA, USA).

2.4.5 Coomassie protein assay reagents

Coomassie protein assay reagent contains coomassie G-250 dye, methanol, phosphoric acid and solubilizing agents in water (Thermo, USA). Albumin standard ampoules contain bovine serum albumin (BSA) at a concentration of 2.0 mg/ml in a solution of 0.9% saline and 0.05% sodium azide (Pierce, Rockland, IL, USA).

2.4.6 Anaesthetic agents for animal experiments

Ketamine (Pfizer Australia Pty Ltd, West ryde, NSW) and xylazine (Troy laboratories Pty Ltd, Smithfield, NSW) were used for UUO surgery and for cardiac puncture. For other procedures the inhalational agent Isoflurane (Abbott Australiasia Pty Ltd, kurnell, NSW) was used.

2.5 Animal models

2.5.1 Unilateral Ureteric Obstruction

Male C57/BL6 mice underwent UUO surgery (see section 1.2.4). Mice were anaesthetized with ketamine and xylazine by intraperitoneal injection, a midline incision was made, the left ureter was exposed, tied at two points and then cut between these ties. The wounds were then sutured and animals kept warm until fully recovered from the anaesthesia. Three hours before being killed by cervical dislocation, mice were injected with 50mg/ml BrdU to label dividing cells.

A pilot study was conducted in which groups of two mice were given varying doses of the specific MEK1/2 inhibitor U0126, prepared in 20 μ l dimethyl sulphoxide (DMSO), by intraperitoneal injection 1 hour before undergoing UUO surgery. Animals then were killed 30 minutes after surgery and blockade of ERK signaling assessed.

The main study involved groups of eight mice that underwent UUO surgery. Starting on day 2 after surgery, mice were given 100 mg/kg U0126 in 20 μ l DMSO vehicle three times daily by intraperitoneal injection until being killed on

day 5. Control groups received either 20 μ l DMSO vehicle alone three times daily (Veh) or no treatment (NoTx).

2.5.2 Anti-Thy1 mesangioproliferative glomerulonephritis

Anti-Thy-1 disease (see section 1.2.3) was induced in female inbred Wistar (150–200 g) rats by the intravenous administration of anti-Thy-1 (OX-7, dosage 5mg/kg) mouse IgG. In a time course study, anti-Thy-1 disease was induced in groups of 2 rats without any treatment and killed at 1 hour and on day 1, 3, 4, 6, 8, 10 and 14.

Anti-Thy-1 disease was induced in groups of 4 rats which were treated with: (i) a JNK inhibitor (CC401) at 200mg/kg given twice daily by oral gavage; (ii) citrate vehicle alone, and; (iii) no treatment. In this series of experiments (from day 0 to 3), treatment began 3 hours before OX-7 administration with groups of animals killed on day 3. In a separate study, Thy-1 disease was induced in groups of 4 rats. Animals were treated with (i) a JNK inhibitor (CC401) at 200mg/kg given twice daily by oral gavage; (ii) citrate vehicle alone, and; (iii) no treatment. In this set of experiments, treatment began on day 3 after OX-7 administration (to avoid any potential effects upon mesangial lysis) with groups of animals killed on day 8 (the peak of mesangial cell proliferation).

2.5.3 Passive accelerated anti-GBM disease

2.5.3.1 Preparation of anti-GBM serum

Sheep anti-rat GBM serum was provided by Dr. David Nikolic-Paterson. It was raised by repeated immunization of a sheep with purified rat GBM particulate matter as previously described (*Isbel et al., 2001b*). The anti-GBM serum was heated at 56°C for 30 minutes to inactivate complement and absorbed overnight against an equal volume of packed rat red cells by gentle rotation at 4°C. After centrifuging, the serum was filtered by passing it through a 0.45µm filter, aliquoted and stored at -20°C until use.

2.5.3.2 Immunization with sheep IgG

Male Wistar Kyoto rats (180-200g) were immunised with sheep IgG. This was prepared by emulsification of sheep IgG in Freund's complete adjuvant (Sigma-Aldrich, St Louis, MO, USA) at a final concentration of 10mg/ml. Each rat was injected subcutaneously on both flanks with 1mg total of emulsified sheep IgG (0.5mg per site).

2.5.3.3 Passive accelerated anti-GBM glomerulonephritis

Each rat was administered 1ml/kg of sheep anti-rat GBM serum via tail vein injection (day 0), 5 days following immunization with sheep IgG. These injections were performed under isoflurane anaesthesia. Treatment with either c-fms kinase inhibitor (fms-I) at 10mg/kg, 30mg/kg or vehicle was commenced by oral gavage 2 hours prior to anti-GBM serum injection and continued twice daily until the last dose which was administered 2 hours prior to the rats being killed. There was also a no treatment (NoTx) group of anti-GBM disease rats. Three separate studies were performed in which animals were killed at day 1

(Veh, n=4: fms-I 30mg/kg, n=4), day 5 (Veh, n=4: fms-I 30mg/kg, n=4), or day 14 (No Tx, n=8, Veh, n=8: fms-I 10mg/kg,n=8; fms-I 30mg/kg, n=8) after anti-GBM serum administration.

In a separate intervention study, 3 groups of 8 rats were treated with either fms-I at 10mg/kg, 30mg/kg or vehicle which was commenced by oral gavage 14 days after anti-GBM serum injection and continued twice daily until the last dose which was administered 2 hours prior to the rats being killed at day 35.

Animals were housed in metabolic cages for 22 hours to collect urine on days 1, 5, 10, 14, 21, 28 and 35. Blood was collected at the time of killing by cardiac puncture.

2.6 Biochemistry analysis

2.6.1 White blood cell counts

White blood cell counts were performed on heparinised blood using a Cell Dyn 3500 Cell Counter (Abbott Laboratories, Abbott Park, IL, USA) in the Department of Pathology, Monash Medical Centre.

2.6.2 Serum and urinary creatinine

Collected blood was allowed to clot and then centrifuged at 3000 rpm for 10 minutes. The serum was subsequently recovered and aliquoted. Analysis of serum creatinine was performed using a Dupont ARL analyzer by the Department of Biochemistry, Monash Medical Centre. Residual serum was

stored at -20°C for later analysis. Urinary creatinine was also analysed via the Dupont ARL analyzer. CrCl (ml/min) was then calculated according to the formula:

$$\frac{\text{Urine volume (ml)} \times \text{urine creatinine } (\mu\text{mol/l})}{\text{Serum creatinine } (\mu\text{mol/l}) \times 1320 \text{ minutes}}$$

2.6.3 Serum CC401 levels

CC401 in serum was extracted by adding 160 μ l of methanol to 40 μ l of isolated serum. This was then stored at -20°C for 2 hours. The samples were subsequently centrifuged for 10 minutes. 100 μ l of supernatant was then removed and evaporated in a rotary evaporator. Samples were sealed and sent to Celgene (San Diego, CA, USA) for measurement of CC401 serum levels by HPLC. In all experiments, a serum concentration of 0.5 to 2.0 μ M CC401 was aimed for.

2.7 Periodic acid – Schiff staining

Formalin-fixed 2 μ m paraffin sections were deparaffinized and rehydrated to water. The sections were oxidized in 0.5% periodic acid solution for 10 minutes, and then rinsed in running tap water. Subsequently, the sections were placed in Schiff reagent for 10 minutes. Finally, sections were washed in tap water for 5 minutes, counterstained in hematoxylin for 1 minute, and rinsed in tap water for 10 minutes dehydrated through graded ethanol and cleared to coverslip mounting using Eukitt mounting medium.

2.8 Immunohistochemistry

2.8.1 Tissue fixation

After animals were killed, kidney and spleen were collected, cut into 2-4mm thick slices and fixed for 3 hours in 10% neutral buffered formalin, methyl Carnoy or PLP. Formalin and methyl carnoy fixed tissue was then placed into 70% ethanol. PLP fixed tissue was saturated in a PBS/7% sucrose/0.2% sodium azide solution undergoing 4 changes of solution. All tissue was stored at 4°C until being processed.

2.8.2 Tissue processing and embedding

Tissue samples fixed in formalin or methyl Carnoy were placed into tissue cassettes and stored in 70% ethanol until being processed. The cassettes were placed in a Sakura automatic tissue processor (VRX-23, Sakura Fine Technical Co., Japan). On an automated cycle over 15 hours samples were sequentially dehydrated in graded ethanol (70%, 95%, and 100%). They were subsequently saturated in histolene (Grate Scientific, Ringwood, VIC) and then paraffin embedded. The embedded paraffin sections were then placed in paraffin blocks using the paraffin dispenser (Histotap Plus, Leica, Nussloch, Germany). These tissues were then stored at room temperature until being sectioned.

After sucrose saturation, PLP-fixed kidney and spleen were placed in aluminum foil cups. They were then embedded in cryopreservative embedding media, Optimal Cutting Tissue (OCT) compound (Tissue Tek, Sakura, Finetechnical

Co. Inc., Torrance, CA, USA), which was subsequently frozen in liquid nitrogen. These frozen tissues were stored at -80°C until sectioning.

Kidney tissue collected at the time of killing was immediately embedded in OCT in aluminium foil cups and frozen in liquid nitrogen and stored at -80°C.

2.8.3 Tissue sectioning

Paraffin embedded formalin and methyl Carnoy fixed tissue were placed on a Leica RM 2035 microtome (Leica Microsystems GmbH, Wetzlar, Germany). 4µm thick sections were cut for immunohistochemistry stains, and 2µm thick sections were cut for PAS-haematoxylin staining. These sections were placed on silinated slides, air-dried and stored at room temperature.

PLP-fixed and snap frozen tissue which had been embedded in OCT compound were cut at 5µm on a Tissue Tek 2 cryostat slides (Tissue Tek) using Leica CM3000 cryostat microtome. These slides were then left to air dry for 40 minutes and either followed by immunostaining directly or stored at -20°C in sealed slide boxes with dessicant Silica Beads until being used.

2.8.4 Deparaffining of paraffin embedded tissue

Formalin and methyl Carnoy fixed tissue sections were baked at 63°C in the oven for 1 hour to melt the paraffin within and around the sections. The sections were subsequently deparaffined in xylene for 2×30 minutes. Tissue sections were then rehydrated through sequential ethanol emersion (100%, 100%, 90%

and 75%). The slides were washed in either PBS or distilled water (3×5 minutes) if antigen retrieval step was followed.

2.8.5 Antigen retrieval using microwave heating

For many nuclear and cytoplasmic antigens the cross-linking process caused by formalin or paraformaldehyde makes antigens inaccessible to immunodetection. This can be overcome by heating of tissue sections in antigen retrieval buffer in the microwave oven or a pressure cooker. The denaturation of secondary and tertiary protein structures can make the masked antigen in the sections accessible to the specific antibody for immunodetection. Microwave treatment can also be used to prevent antibody cross reactivity between rounds of immunostaining (*Lan et al., 1996*). The antibodies requiring antigen retrieval by microwave heating are documented (see Tables 2.1 and 2.2).

Following rehydration in graded ethanol, sections to be microwaved were washed in distilled water (5 minutes×3). They were subsequently placed in 400 ml of 0.01M sodium citrate buffer, pH6.0, or 400ml 1×Dako antigen retrieval buffer. The plastic container was covered in polyethylene plastic wrapping and placed in a microwave oven. The solution was microwaved for 12 minutes at 800W and 2450MHz, and then cooled for 40 minutes at room temperature. The slides were then moved into PBS (5 minutes×3) before commencing serum blocks.

2.8.6 Antigen retrieval using high pressure cooker

Sections in a metal rack were placed in the pressure cooker (TEFAL, Clipso Clipso Control 8L) filled with 2000ml of citric buffer pH 6.0. Pressure regulator valve was set to 90Kpa. The heat was placed at maximum until pressure indicator pin rose. This step took approximately 18 minutes. The procedure was continued until high-pressure steam began to escape (further 4 – 5 min), then the cooker was heated at full steam for a further 3mins. Finally, the heat was turned off and the pressure cooker put in cold water and opened after pressure had dropped to normal, then cooled for 30 minutes at room temperature.

Sections were washed in PBS for 5 minutes.

2.8.7 Peroxidase anti peroxidase method (PAP method)

Following deparaffin and rehydration, sections were washed in either PBS or distilled water if microwave treatment was to follow. Sections were subsequently blocked with 10%NShS or 10%NRabS/FCS/PBS for 30 minutes at room temperature. After tipping off the block serum, a second block of 5%BSA was also applied for 30 minutes at room temperature. The BSA block was tipped off and then the sections incubated with primary antibody in 5%NShS or 5%NRabS/3%BSA/PBS at 4°C overnight dependent upon which species the secondary antibody raised. Unbound primary antibody was removed by washing the slides with PBS (5 minutes×3). Tissue sections were then rapidly dehydrated in graded ethanol solutions (70%, 90%, 100%) and subsequently the endogenous peroxidase activity was inactivated in methanol/0.3% hydrogen peroxide block for 30 minutes avoiding light. The sections were further washed in PBS (5 minutes×3). Sections were incubated with HRP-conjugated goat anti-

mouse IgG or HRP-conjugated goat anti rabbit IgG at a 1 in 50 dilution in 5%NShS or 5%NRabS in 5%NRS/3%BSA/PBS for 40 minutes at room temperature followed by further PBS wash (5 minutes×3). Mouse or rabbit peroxidase conjugated anti-peroxidase complex (PAP) at 1 in 50 dilution in 5%NShS/5%NRS/3%BSA/PBS was then applied for 40 minutes followed by further PBS washes (5 minutes×3) to remove unbound antibodies. The horseradish peroxidase complex bound to the antigens was then detected by reaction with DAB for up to 10 minutes. Sections were dehydrated in graded ethanol (70%, 90%, 100%, and 100%) and then submersed in histolene (30 minutes×2). Slides were finally mounted using Eukitt mounting media.

2.8.8 ABC method

The same method as that described for PAP staining was used except for the following steps: Following binding with the primary antibody, washing and hydrogen peroxide/methanol blocking, sections were blocked with avidin followed by biotin blocking reagent for 30 minutes each according to the manufacturer's instructions. The sections were then incubated with biotinylated secondary antibody (1/200) for 40 minutes. The unbound antibody was washed off in PBS (5 minutes×3) and the ABC complex was subsequently applied for 30 minutes. Following a further wash in PBS, the ABC complex was detected by reaction with DAB up to 10 minutes. Slides were then dehydrated in graded ethanol, cleared in histolene and mounted.

To provide consistency of immunostaining sections from all animals in the experiments were stained at the same time. The development time was assessed using practice sections and then all sections had the same development time. This is an important control when using image analysis to measure the area of staining since this depends, in part, upon the intensity of the colour produced by the enzymatic reaction.

2.8.9 Haematoxylin and/or Periodic acid – Schiff counter staining

Some sections were counter-stained after immunohistochemistry. Before dehydration in graded alcohol immunostained sections were placed in a bath of periodic acid reagent for 10 minutes and then thoroughly washed in running tap water. The sections were incubated with Schiff reagent until adequate staining had occurred and the reaction then terminated in running tap water. Slides were submerged in a haematoxylin bath for 30 seconds. They were then again washed in running water and dipped sequentially into baths of 10% acetic acid/70% ethanol and then 2% sodium bicarbonate. The sections were washed in water, dehydrated in ethanol (70%, 90%, 100%, and 100%) and cleared in histolene. Slides were then mounted with Eukitt mounting media.

2.8.10 Direct immunofluorescence staining

Snap frozen sections (5 μ m) were cut using Leica CM3000 cryostat microtome and mounted on the Tissue Tek 2 cryostat slides, and were air-dried for 40 minutes. The sections were then rehydrated in PBS. To preserve glomerular morphology sections were fixed in 95% ethanol for 10 minutes at 4°C and

further washed in PBS. The tissue were then blocked for 30 minutes with 10%FCS in PBS, serum were tipped off and then mounted with FITC conjugated antibodies in 1%FCS in PBS and protected from light. The FITC conjugated antibodies were used in a range of 2-fold dilutions was made up from 1/4000 to 1/64000. To remove unbound antibody the slides were washed in PBS (5 minutes×3) in containers which were shielded from direct light by alumium foil. Slides were mounted with DABCO/glycerol and viewed under a fluorescence microscope.

2.9 Renal histology and quantification of immunohistochemistry

All histological analysis and quantification of immunoperoxidase and immunofluorescence staining was performed on blinded slides. All animals were scored in each experiment.

2.9.1 Renal histology

Rat anti-GBM disease model

Glomerular lesions

In the day 14 and 35 anti-GBM disease model, glomerular lesions were analysed under high magnification (×400). Each full sized glomerulus within the section (>50 glomerular cross sections) was viewed and scored individually.

Glomerular lesions of hyalinosis, fibronoid necrosis and glomerular atrophy were scored individually using a grading system based on the proportion of the glomerulus that had these lesions were used: grade 0, normal glomerulus; grade 1+, 1-10% glomerular damaged; grade 2+, 10-25% glomerular damaged;

grade 3+, 25-50% glomerular damaged; grade 4+, >50% glomerular damaged.

Crescent formation

The percentage of glomerular cross-sections with crescent formation was determined by blinded analysis of Periodic acid-Schiff haematoxylin stained formalin-fixed 2µm paraffin sections. Cellular crescents are defined as the presence of two or more layers of cells within Bowman's space (*Atkins et al., 1996*). All full sized glomerular cross-sections were analysed in each case. The percentage of glomeruli exhibiting crescent formation was scored.

Periglomerular α -SMA⁺myofibroblast accumulation

The degree of periglomerular α -SMA⁺ myofibroblast accumulation in 50 consecutive glomeruli was assessed using the following scoring method: 0, no α -SMA⁺ cells; 1+, occasional periglomerular α -SMA⁺ cells; 2+, many but discontinuous cells; 3+, a continuous layer of positive cells surrounding the glomerulus; 4+, in addition to 3+, multiple layers of positive cells.

Mouse UUO model

Tubular damage

Tubular damage was assessed at magnification ($\times 250$). The entire cortex of each section was analyzed. In each field the number of damaged tubules was expressed as a percentage of the total number of tubules. The criteria for a damaged tubule included tubular dilatation, atrophy and necrosis. The data were expressed as the mean percentage of damaged tubules.

2.9.2 Analysis of direct immunofluorescence staining

For each animal, sections were incubated with serial dilutions of anti-rat IgG and anti-rat C3 antibodies. The sections were viewed and scored according to whether or not there was a positive immunofluorescent (IF) signal on the GBM. The concentration where an IF signal was first not seen was recorded.

2.9.3 Quantification of immunostaining

Mouse UUO model

BrdU⁺ and cleaved caspase-3⁺immunostained tubular and interstitial cells

Immunostaining for BrdU and cleaved caspase-3 was quantified as follows.

Fifteen predetermined high power fields ($\times 400$) of the cortex (avoiding glomeruli) in three separate areas were scored for the number of individual tubular epithelial cells or interstitial cells positively stained for BrdU or cleaved caspase-3 and expressed as cells per high power field.

Interstitial F4/80⁺macrophage, α -SMA⁺ myofibroblast and Sirius Red stained collagen

The area of the cortex positively stained for F4/80, α -SMA and Sirius Red was scored by point counting using an eye-piece grid (11 \times 11 cross points) in 12 predetermined, medium power fields ($\times 250$) of the cortex (avoiding glomeruli and vessels).

Rat anti-GBM disease model

Glomerular ED1⁺ and R73⁺ cells

The number of positive cells per glomerular cross section was counted under high magnification ($\times 400$). All full-sized glomeruli within the sections were quantified. The results are expressed as the number of positive cells per glomerular cross section.

Interstitial ED1⁺ cells

Interstitial ED1⁺ macrophages in the renal cortex were quantified by image analysis. Medium power digital images of ED1 staining covering at least 90% of the cortex ($\times 250$) were analyzed using Image-Pro software (Media Cybernetics, Maryland, USA) to determine the area of ED1 staining as a percentage of the cortex.

Glomerular tuft WT-1⁺ cells

The number of positive cells per glomerular cross-section was counted under high magnification ($\times 400$). All full-sized glomeruli within the sections were quantified. The results are expressed as the number of positive cells per glomerular cross section.

Interstitial R73⁺ cells

The number of positive cells cross section was counted under $\times 250$ magnification in $>90\%$ of the renal cortex. The results are expressed as the number of positive cells per field ($\times 250$).

Vimentin⁺ and Osteopontin⁺ immunostained tubules

The staining pattern of vimentin and osteopontin in tubules were quite different with vimentin staining giving a highly heterogenous pattern while tubules were uniformly positive or negative for osteopontin staining. Therefore, two separate scoring methods were used.

Vimentin staining in tubular cross-section in 50 consecutive fields at magnification ($\times 250$) was assessed using the following scoring method: 0, no positive cells; 1+, few (1+ or 2+) positive tubular cells in the tubule; 2+, more than 2+ positive cells, but less than half of the cell positive in the tubule; 3+, positive cells in more than half of the tubule.

Tubular osteopontin staining was assessed at magnification ($\times 250$). The entire cortex was quantified. The positively stained tubules per field were counted and expressed as a percentage of the total number of tubules.

Interstitial α -SMA⁺ myofibroblast and collagen IV staining

The area of α -SMA and collagen IV immunostaining were scored by point counting using an eye-piece grid (11 \times 11 cross points) in 12 predetermined, medium power fields ($\times 250$) of the cortex (avoiding glomeruli and vessels).

Rat anti-Thy-1 nephritis

Total glomerular cells

The number of cells per glomerular cross section was counted under high

magnification ($\times 400$) on PAS-haematoxylin stained $2\mu\text{m}$ paraffin sections in 30 full-sized gcs in three pre-determined areas. The results are expressed as the number of cells per glomerular cross section.

Glomerular OX-7⁺ cells

The number of OX-7⁺ cells per glomerular cross section was counted under high power ($\times 400$). Thirty full-sized glomeruli in each case were quantified in three predetermined separate areas. The results are expressed as the number of positive cells per glomerular cross section.

2.10 Western Blotting

Phospho-ERK and ERK1/2

A quarter mouse kidney was homogenized in RIPA lysis buffer, left on ice for 10 min, centrifuged and the supernatant stored at -80°C . Tissue lysates were run on 12.5% sodium dodecyl sulphate polyacrylamide gel electrophoresis (SDS-PAGE) and then transferred onto PVDF membranes (Millipore, Bedford, MA, USA). Blots were blocked in 5% non-fat milk powder in Tris buffered saline with Tween (TBST) (20 mM Tris-HCl, pH 7.6, 137 mM NaCl, 0.05% Tween 20) and then washed five times in TBST. Blots then were incubated with rabbit anti-p-ERK antibody overnight at 4°C in the blocking solution plus 5% bovine serum albumin (BSA), washed, and then incubated for 1 h with peroxidase-conjugated sheep antirabbit IgG in binding buffer. After washing, bound antibody was detected using the SuperSignal[®] chemiluminescent substrate (Pierce, Rockford, IL, USA). Chemiluminescent emissions were captured on Kodak XAR

film. Blots were stripped and reprobed with the rabbit anti-ERK2 antibody as a loading control.

2.11 Flow cytometry of blood monocytes

Rat blood monocytes were isolated from heparinized peripheral blood by centrifugation on Ficoll (GE Healthcare, Uppsala, Sweden). After washing in PBS, cells were resuspended in 2% paraformaldehyde-lysine-periodate for 20 min at 4°C. These fixed cells were then incubated with either ED1 or OX42 antibodies in PBS containing 10% normal sheep serum and 10% normal rat serum for 30 min at 4°C. For ED1 detection, 0.1% saponin was also included in the antibody diluent. After washing three times, cells were then incubated with FITC-conjugated sheep anti-mouse IgG in the same antibody diluent for 30 min at 4°C. After further washing, the cells were analysed on a MoFlo flow cytometer connected to a data acquisition system (Becton Dickinson Cytomation, Fort Collins, CO). A fluorescence histogram of approximately 30,000 cells was obtained for each sample.

2.12 Coomassie protein assay

Each standard or unknown sample (5µl each) of was pipetted into the immunoplate wells (Thermo Fisher Scientific, Roskilde, Denmark), then 250µl of the coomassie reagent was added to each well and mix with plate shaker for 30 minutes. The plate was removed from shaker and incubated for 10 minutes at room temperature. The plate reader (Labsystems multiskan RC) measured the absorbance at 595nm. A standard curve prepared by plotting the average

blank-corrected 595nm measurement for each BSA standard vs. its concentration in $\mu\text{g/ml}$. A standard curve was used to determine the protein concentration of each unknown sample.

2.13 Isolation of rat glomeruli

After killing, the left kidney from each animal was dessected and placed immediately into ice-cold phosphate-buffered saline (PBS) and sieved sequentially through 250 μm , 150 μm , and 75 μm mesh. The glomerular fraction was collected from the top of the 75 μm mesh. The purity of glomerular isolation was visually determined to be greater than 95% by light microscopy. The glomerular fraction was centrifuged and resuspended in 2ml Trizol for 2 minutes, vortexed, and then store at 4°C for RNA extraction and reverse transcription.

2.14 RNA extraction and reverse transcription

At the time of animal killing, a quarter of one kidney was diced up and then snap frozen in liquid nitrogen and stored at -80°C until use. Approximately 100mg of frozen tissue fragments were added to RNAwiz, homogenized, and total cellular RNA extracted using the RiboPure Kit according to the manufacturer's protocol (Ambion Inc, Austin, TX, USA).

A total of 5 μg of total RNA from each tissue sample was reverse transcribed into cDNA using the Superscript First-Strand Synthesis kit with random primers

according to the manufacturer's protocol (Invitrogen). The RT product was either used fresh or aliquoted and stored at -20°C until use.

2.15 Probes and primers

The primers and TaqMan® MGB™ Probes (see Table 2.4) were designed by Dr Frank Ma and Dr David Nikolic-Paterson using the Qiagen Quantiprobe Design Software (Qiagen Pty Ltd, Doncaster, VIC) and purchased from Applied Biosystems Inc. The MGB (minor groove binding) moiety stabilizes the hybridized probe and effectively raises the melting temperature (T_m). The MGB probes incorporate a 5' reporter dye (FAM) and a 3' non-fluorescent quencher (NFQ).

For quantification purposes, multiplex PCR reactions were run in which 18S ribosomal RNA was also amplified using the TAqMan® Ribosomal RNA Control Reagent (Applied Biosystems, Foster City, CA, USA) in which the 18S probe is 5' labeled with the VIC dye. This enables detection of the FAM and VIC dyes at different wavelengths in different channels. The primers and probes used are as follow, see Table 2.4.

2.16 Real time RT-PCR

Real time RT-PCR was performed in a 20µl reaction volume on a Rotor-Gene 3000 system (Corbett Research, Sydney, NSW, Australia). A master-mix for each set of primers and probe was prepared using the RealMaster Probe (Eppendorf South Pacific, North Ryde, NSW) so that each 20µl reaction

contained: (1×) real MasterMix Probe, 100U/ml Uracil-DNA Glycosylase (Invitrogen, Mount Waverley, VIC), 100nM of both sets of primers (gene of interest and 18S control), 100nM probe for gene of interest, 200nM probe for 18S control, RT product and dH₂O. Thermal cycling conditions were as follows: 37°C for 10 minutes, 95°C for 5 minutes, followed by 50 cycles of 95°C for 15 seconds, 60°C for 20 seconds, and 68°C for 20 seconds. Data were examined using the Rotor-Gene analysis Software V6.0 (Corbett Research) to obtain the Ct value (the value where the threshold line crosses the amplification curve). The relative amount of mRNA compared to the 18S control was calculated using comparative ($2^{-\Delta\Delta Ct}$) method (*Ingham et al., 2001*). Three types of controls were run to validate the primer/probe combinations. First, an essentially constant ratio of the gene of interest to 18S was confirmed over a 100-fold dilution range of the RT product. Second, the PCR product was analysed by gel electrophoresis to confirm a DNA band of the predicted size. Third, it was confirmed that no differences were seen in Ct values for the gene of interest or 18S when they were amplified individually or together.

2.17 Statistical analysis

In all analyses, all animals are included unless otherwise stated. All data were analysed in Graphpad Prism 4.0 or 5.0a (Graphpad Software, USA). Data are expressed as mean±SD. Comparisons between groups were performed by one-way analysis of variance (ANOVA) using Tukey multiple comparisons test for parametric data and Kruskal-Wallis test for nonparametric data. The Pearson's rank coefficient of parametric data was used for single correlation analysis of

parametric data. A p value of less than 0.05 was considered to be statistically significant.

Chapter 3. Extracellular signal-regulated kinase-dependent interstitial cell proliferation in the obstructed mouse kidney

3.1 Introduction

Proliferation of intrinsic renal cell types is thought to contribute to progressive kidney disease (*Cybulsky et al., 2000*). Proliferation of mesangial cells leads to mesangial expansion and promotes glomerulosclerosis (*Gomez-Guerrero et al., 2005*), while proliferation of parietal epithelial cells can contribute to the development of glomerulosclerosis and crescent formation (*Smeets et al., 2006*). In addition, local proliferation of infiltrating macrophages can exacerbate macrophage-mediated renal injury (*Nikolic-Paterson et al., 2001*). However, cell proliferation is also an important mechanism for the replacement of damaged tubular and endothelial cells in the injured kidney.

A number of growth factors have been shown to induce cell proliferation in animal models of glomerular or interstitial damage. While a number of mechanisms have been identified by which such factors induce proliferation of renal cells *in vitro*, few studies have provided direct evidence that such mechanisms play a functional role in renal cell proliferation *in vivo*.

One important mechanism by which growth factors induces cell proliferation is activation of the extracellular signal-regulated kinases (ERK) pathway (*Ammitt et al., 2001*), although activation of this pathway can also regulate other cellular functions including differentiation (*Kyriakis et al., 2001*). The binding of growth

factors, such as platelet-derived growth factor (PDGF), to their respective receptors induces receptor tyrosine kinase activity that can then induce a cascade of phosphorylation events leading to phosphorylation and activation of mitogen activated protein kinase 1 and 2 (MEK1 and MEK2), and the MEK1 and MEK2 phosphorylate and activate the ERK1 and ERK2 phosphorylate and activate the ERK1 and ERK2 isoforms. The active phospho-ERK (p-ERK) can then phosphorylate transcription factors such as cyclin D1, which plays a key role in the induction of the cell cycle (*Ammitt et al., 2001*).

Analysis of the pattern of ERK activation in human glomerulonephritis identified p-ERK immunostaining in areas of glomerular and tubular cell proliferation. Indeed, p-ERK staining correlated with cell proliferation, histologic lesions and renal dysfunction (*Masaki et al., 2004*). In addition, functional blockade studies have identified a role MEK-ERK signaling in PDGF-induced mesangial cell proliferation in rat Thy-1 nephritis (*Bokemeyer et al., 2002*). However, the functional role of MEK-ERK signaling in proliferation of tubular epithelial cells and interstitial cells has not been established.

The aim of the current study was to determine the role of MEK-ERK signaling in the proliferative response to tubulointerstitial injury. We administered a highly selective MEK1/2 inhibitor in the mouse obstructed kidney. The unilateral ureteric obstruction (UUO) model was selected because there is a rapid induction of proliferation of tubular epithelial cells and interstitial cells, making it readily amenable to short-term MEK1/2 inhibition. In addition, tubulointerstitial damage is

induced by an irreversible surgical insult, and is not dependent upon T or B lymphocytes. Furthermore, we have previously performed a detailed time course study in the rat UUO model in which tubular ERK activation was found to precede tubular cell proliferation, suggesting that ERK blockade would be effective in suppressing cell proliferation (*Masaki et al., 2003*).

3.2 U0126 inhibits ERK activation *in vivo*

A pilot study was performed to assess the dose of U0126 required to inhibit ERK phosphorylation in the obstructed kidney. Groups of mice were given an intraperitoneal injection of U0126 in 20 μ l DMSO vehicle 1 hour before undergoing UUO surgery and then killed 30 minutes after surgery. Western blotting showed the presence of p-ERK in normal mouse kidney, which was increased 30 minutes after UUO (*Fig 3.1a*). Administration of 50 or 100mg/kg U0126 was effective in blocking ERK phosphorylation, whereas 12.5 or 25mg/kg was ineffective. Therefore, a dose of 100mg/kg U0126 was selected for subsequent studies.

To examine the role of ERK signaling in the UUO model, groups of eight mice underwent UUO surgery and were randomly assigned to 100mg/kg U0126 three times daily (t.i.d.), vehicle alone (20 μ l DMSO t.i.d.) or no treatment beginning on day 2 after surgery, and continued until mice were killed on day 5. This time frame was selected since substantial proliferation of tubular epithelial cells and interstitial myofibroblasts and macrophages occurs over days 2-5. The frequency of drug administration was based on the short half-life of U0126

(Bokemeyer et al., 2002), and short duration of the drug treatment period minimise the potential irritability of the DMSO vehicle.

Administration of the DMSO vehicle alone had no effect upon the increase in ERK phosphorylation seen on day 5 of UUO. However, U0126 treatment inhibited MEK1/2 activity as demonstrated by the almost complete absence of ERK phosphorylation in the obstructed kidney as shown by Western blotting (Fig. 3.1b) and immunohistochemistry (Fig. 3.2).

3.3 Effect of U0126 treatment on cell proliferation and apoptosis in the obstructed kidney

Periodic acid-Schiff stained sections of untreated obstructive nephropathy showed dilation, flattening and atrophy of tubules (Fig 3.3a,b). Cell proliferation is a prominent feature in the obstructed kidney. Cells in the S-phase of the cell cycle were labeled by injection of BrdU 3 hours before animals were killed. Significant cortical tubular and interstitial cell proliferation was evident in the no-treatment UUO group (Figs 3.3d, 3.4a, b). Administration of the DMSO vehicle had no effect upon the proliferation of interstitial cells, but the vehicle treatment did cause a significant reduction in tubular cell proliferation on day 5 (Figs 3.3e, 3.4a,b). U0126 treatment caused a significant reduction in the proliferation of interstitial cells (Figs 3.3f, 3.4b). In contrast, tubular proliferation in the U0126-treated group was not different to that in the vehicle-treated group (Fig 3.4a).

The accumulation of interstitial cells was analysed by immunostaining. There was significant interstitial accumulation of α -SMA⁺ myofibroblasts and F4/80⁺ macrophages in the no-treatment UUO group on day 5 of UUO (Fig 3.4c,d). Neither U0126 nor vehicle treatment had any effect upon interstitial accumulation of α -SMA⁺ myofibroblasts (Fig 3.4c). In contrast, U0126 caused a significant reduction in interstitial accumulation of F4/80⁺ macrophages compared with both the vehicle and no-treatment groups (Fig 3.4d).

Apoptosis was assessed by immunostaining for cleaved caspase -3. Significant apoptosis of tubular and interstitial cells was observed in the no-treatment UUO group (Fig 3.5a, b). However, neither U0126 nor vehicle treatment had any effect upon the number of tubular or interstitial apoptotic cells in the obstructed kidney (Fig 3.5a, b). The degree of tubular damage, assessed on PAS-stained sections, was not different between the vehicle, U0126 and no-treatment groups (Figs 3.3, 3.5c).

3.4 Effect of ERK blockade on fibrosis in the obstructed kidney

Interstitial fibrosis was evident on day 5 of UUO in the no-treatment group as shown by the increase in interstitial collagen identified by Sirius Red staining (Fig 3.6). Neither U0126 nor vehicle treatment affected this increase in collagen deposition in the renal interstitium (Fig 3.6).

3.5 Effect of ERK blockade on JNK activation in the obstructed kidney

Activation of JNK was assessed by immunostaining for p-c-Jun (Ser63) and p-c-Jun (Ser73), considered JNK-specific downstream targets. c-Jun is not expressed in normal kidney; however, it is rapidly induced following unilateral ureteric obstruction (*Ma et al., 2007*). JNK activation was marked on day 5 of UUU in the untreated group as shown the presence of many tubular cells with nuclear staining for p-c-Jun (Ser63) and p-c-Jun (Ser73) (*Fig 3.7a,b*). Neither U0126 nor vehicle treatment had any effect on the staining pattern for p-c-Jun (Ser63) or p-c-Jun (Ser 73) in the obstructed kidney (*Fig 3.7c,d*).

3.6 Discussion

Summary

In this chapter the main findings were as follows:

1. U0126 treatment was effective in blocking MEK1/2 activity in the mouse UUU model as demonstrated by the almost complete absence of ERK phosphorylation in U0126 treated obstructed kidney.
2. U0126 treatment caused a significant reduction in the proliferation of interstitial cells.
3. U0126 treatment had no effect upon interstitial accumulation of α -SMA⁺ myofibroblast. In contrast, U0126 caused a significant reduction in interstitial accumulation of F4/80⁺ macrophages compared to both the no-treatment and vehicle treated groups.

4. U0126 treatment had no effect upon tubular or interstitial apoptosis in the obstructed kidney.

5. U0126 treatment had no effect on collagen deposition in the renal interstitium on day 5 of UUO

These 5 issues are discussed in detail in Chapter 7

The specificity and effectiveness of U0126 for MEK-ERK signaling pathway

The specificity of U0126 for the ERK signaling pathway has been addressed by *in vitro* cell-based assays. U0126 directly inhibits the mitogen-activated protein kinase kinase family members, MEK-1 and MEK-2 with an IC₅₀ of 1μM. U0126 inhibition is selective for MEK-1 and -2, and shows little effect on the kinase activities of protein kinase C, Abl, Raf, MEKK, ERK, JNK, MKK-3, MKK-4/SEK, MKK-6, Cdk2, or Cdk4 (*Favata et al., 1998*). In this study, we have been able to inhibit ERK signaling demonstrated by Western blotting and immunostaining for p-ERK. In addition, we assessed JNK activation by immunostaining for p-c-Jun (Ser63) and p-c-Jun (Ser73), considered JNK downstream targets and specific read-out for JNK activation (*Flanc et al., 2007*). We found that U0126 inhibited ERK but not JNK signaling *in vivo*.

The vehicle DMSO affects on tubular cell proliferation

While blockade of ERK signaling reduced tubular cell proliferation, this was also apparent in the vehicle treatment group, thereby preventing any conclusion to be drawn. Oxidant stress is induced in the obstructed kidney and studies in various epithelia have shown that high levels of H₂O₂ induce cell cycle arrest and apoptosis, whereas low doses of H₂O₂ can induce epithelial cell proliferation via ERK and p38 MAPK pathways (*Sigaud et al., 2005*). DMSO is an antioxidant and this may explain the reduction in tubular cell proliferation seen with vehicle treatment, although this effect was independent of ERK signaling which was not altered by vehicle treatment.

Acknowledgements

Drs Takao Masaki and Yohei Ikezumi performed the UUO surgery and administered the drug and vehicle. Ms Lynette Hurst performed the Western blot studies.

Chapter 4. JNK signaling in mesangial proliferative nephritis

4.1 Introduction

Mesangial cell proliferation and apoptosis are key events in the development of glomerular expansion and matrix deposition resulting in glomerulosclerosis, which is a hallmark of progressive forms of kidney disease. Sclerosis of the glomerulus leads to a reduction in glomerular filtration until the nephron ceases to function, leading to progressive renal dysfunction and ultimately to end-stage renal failure.

The development of glomerulosclerosis is often associated with antibody and complement deposition and local production of growth factors (i.e. PDGF and TGF- β 1) and pro-inflammatory cytokines (i.e. IL-1 and TNF- α) (Couser *et al.*, 1994). The c-Jun amino terminal kinase (JNK) pathway is activated by extracellular stresses such as endotoxin, cytokines, growth factors, reactive oxygen species and osmotic stress (Ma *et al.*, 2009a). Signaling via the JNK pathway induces changes in gene transcription, cell proliferation and apoptosis. *In vitro* studies have shown that JNK signaling is critical for PDGF and angiotensin II-stimulated mesangial cell proliferation, caspase-3 dependent apoptosis of liver myofibroblasts, and TGF- β 1 induced collagen I and III production by myofibroblasts (Kawano *et al.*, 2003; Naito *et al.*, 2004; Park *et al.*, 2007). These findings suggest that JNK signaling may play an important role in the development of glomerulosclerosis and in particular PDGF-driven mesangial proliferation. The aim of this study is to determine the role of JNK signaling in the development of mesangial proliferative nephritis.

4.2 JNK activation in rat anti-Thy-1 mesangioproliferative nephritis

Anti-Thy-1 mesangioproliferative glomerulonephritis (Thy-1 nephritis) was induced by a bolus tail vein injection of anti-Thy-1 mouse IgG (OX-7, dosage 5mg/kg) in inbred female Wistar rats. Glomerular mesangial cell loss was examined in a pilot time-course study. PAS stained sections showed a dramatic reduction in total glomerular cellularity (*Figs 4.1 and 4.2*). OX-7 immunostaining identified a specific loss of mesangial cells (*Fig 4.3a, b, c*). Mesangial cell loss started as soon as at 1 hour post OX-7 IgG injection as shown by appearance of apoptotic cells in the mesangium (*Fig 4.2b*). The maximal reduction was seen on day 4, and then mesangial cells underwent a proliferative response leading to glomerular hypercellularity (*Fig 4.1*) and a change in phenotype with α -SMA expression by mesangial cells on day 8 accompanied by mesangial matrix expansion (*Fig 4.3d.e.f*). By day 14, cell number in most glomeruli had decreased to that of normal glomeruli (*Fig 4.1*), with most of the excess extracellular matrix (ECM) removed, and normal glomerular architecture largely restored.

An anti-phospho-JNK antibody was used to detect the activated form of JNK. Little JNK activation was observed in the normal rat glomeruli in terms of p-JNK immunostaining (*Fig 4.4a*), although nuclear and cytoplasmic immunostaining of collecting ducts within the cortex and the medulla, and in some parietal epithelial cells of Bowman's capsule were positive for p-JNK (data not shown). There was no detection of c-Jun in normal rat kidney, other than in occasional parietal epithelial cells (*Fig 4.5a*).

Immunostaining for p-JNK demonstrated induction of JNK signaling in mesangial-like cells on day 3, 6 and 8 of anti-Thy-1 nephritis (*Fig 4.4b,c,d*). c-Jun is induced, in part, through JNK signaling. Nuclear c-Jun expression was seen in many glomerular cells on day 3, 6 and 8 of anti-Thy-1 nephritis (*Fig 4.5b, c, d*).

4.3 The JNK inhibitor, CC401, did not prevent mesangial cell loss on day 3 of anti-Thy-1 nephritis

Figures 4.1 and 4.2 showed a dramatic reduction of glomerular mesangial cells on day 3 of anti-Thy-1 nephritis. This significant mesangial cell loss was thought to be due, at least in part, to apoptosis which was evident as early as 1 hour after injection of the anti-Thy-1 antibody (*Fig4.2b*). To investigate whether JNK signaling contributes to this mesangial cell loss, we treated the rats with anti-Thy-1 nephritis from day 0 to 3 with CC401.

In this series of experiments, CC401 treatment started 3 hours before OX-7 administration and continued twice daily till the animals (n=4) were killed on day 3. CC401, a specific JNK inhibitor, acts by blocking the ability of p-JNK to phosphorylate and activate its specific target c-Jun at Serine 63 and Serine 73 (*Flanc et al., 2007*), providing a read-out for inhibition of JNK activity. We used immunostaining for p-c-Jun Ser63 and Ser 73 to examine JNK signaling. Unfortunately, we had difficulty in obtaining reliable immunostaining of p-c-Jun Ser 63. Therefore, we used p-c-Jun Ser 73 as the marker for JNK activation.

Consistent with the results for p-JNK immunostaining, cells with a mesangial-like appearance showed p-c-Jun Ser 73 staining on day 3 in the vehicle treated group. CC401 treatment of anti-Thy-1 nephritis from day 0 to 3 resulted in a significant reduction of p-c-Jun (Ser73) stained cells on day 3 (*Fig 4.6a, b*). Unexpectedly, CC401 treatment did not affect the loss of OX-7⁺ mesangial cells or the change in mesangial cell phenotype shown by α -SMA immunostaining, although total glomerular cells were reduced slightly (*Figs 4.8 and 4.10a*).

4.4 CC401 treatment over day 3 to 8 did not affect mesangial cell accumulation and activation on day 8 of anti-Thy-1 nephritis

Significant glomerular JNK activation paralleled the development of glomerular mesangial cell proliferation and increased glomerular matrix deposition from day 3 to day 8 of anti-Thy-1 nephritis. Therefore, to probe JNK's role in mesangial cell proliferation and matrix production, rats with anti-Thy-1 nephritis were treated with CC401 from day 3 to 8.

In this experiment, CC401 treatment began on day 3 after OX-7 administration (to avoid any potential effects upon mesangial lysis), and treatment continued twice daily until animals were killed on day 8.

Immunostaining for p-c-Jun (Ser 73) of CC401 treated rats on day 8 of anti-Thy-1 nephritis was reduced significantly (*Fig 4.7*). However, total glomerular cell number was not altered by CC401 treatment. Moreover, Immunostaining for OX-7 antibody did not reveal any significant reduction of mesangial cell number

by CC401 treatment over day 3 to 8. In addition, the alteration of mesangial cell phenotype in terms of α -SMA expression from day 3 to 8 of anti-Thy-1 nephritis was not affected by CC401 treatment (*Figs 4.9 and 4.10b*).

4.5 Serum level of CC401 in treated rat anti-Thy-1 nephritis

The peak serum CC401 levels were determined on serum samples collected by cardiac puncture at termination. This was performed 2 hours following CC401 oral administration. The average peak serum level in drug treated rats of day 0-3 study was 1.25 ± 0.51 μ M, and the average peak serum level in CC401 treated rats of day 3-8 was 1.36 ± 0.50 μ M. This was within the target range of 0.5 to 2.0 μ M where drug specificity has been demonstrated in cell-based assays.

Due to the lack of effect of CC401 treatment on JNK activation and main endpoint parameters in this rat Thy-1 model, this study was not pursued further.

4.6 Discussion

Summary

In this chapter the main findings were as follows:

1. JNK activation was detected in mesangial-like cells in rat anti-Thy-1 nephritis.
2. JNK activation demonstrated by immunostaining for p-c-Jun (Ser63) was reduced by CC401 treatment in the rat anti-Thy-1 nephritis.
3. The initial mesangial cell loss and subsequent rebound in mesangial cell numbers which results in glomerulosclerosis in this model did not appear to be affected by JNK blockade with CC401.

Overall, results of this study suggest a role for JNK signaling in mesangial proliferative nephritis based upon immunostaining for p-JNK and p-c-Jun Ser 73. *In vitro* studies also indicate such a role for JNK signaling in mesangial cell proliferation (Kawano *et al.*, 2003). However, using CC401 which is a well characterized JNK inhibitor, we failed to modify the Thy-1 disease model although a significant reduction in p-c-Jun Ser 73 staining was seen and the target serum CC401 levels were achieved.

It appeared that we did achieve significant blockade of JNK signaling. However, we cannot distinguish between the possibilities that JNK signaling plays no role in this disease model versus a failure to achieve a sufficient degree of JNK inhibition. One further possibility is that the limited sample size (n=4) in the day 0-3 and day 3-8 studies may have caused a type II statistical error, being underpowered to disprove the null hypothesis that the two groups (CC401 and vehicle treatments) are not different.

Specificity and selected dosage of CC401 for the JNK signaling pathway

CC401 is a relatively selective inhibitor of the JNK signaling pathway. The specificity of CC401 for the JNK signaling pathway has been addressed by *in vitro* kinase assays and cell culture studies performed by Celgene (San Diego). Within the target range of 0.5-2.0 μ M, CC401 has 40-fold selectivity for JNK compared to an extensive panel of closely related kinases. In this study, the

average peak serum level in drug treated rats of day 0-3 study was 1.25 ± 0.51 μM , and the average peak serum level in CC401 treated rats of day 3-8 was 1.36 ± 0.50 μM . Both results were within the target range of 0.5 to $2.0\mu\text{M}$ where drug specificity has been demonstrated in cell-based assays.

The drug doses used in these experiments were selected on the basis that they would not exceed the target peak serum levels of $2\mu\text{M}$. These doses have been used to suppress JNK activation and inhibit aggressive forms of renal injury in the anti-GBM disease and obstructed kidney models (*Ma et al., 2007; Flanc et al., 2007*). The twice daily gavage prevents a significant drop in drug levels in the blood, although this was not measured in this study; thus, it remains a possibility that the lack of effect of CC-401 in this Thy-1 model was due to a lack of adequate drug levels over periods of time in the disease process, rather than failure to reach adequate peak drug levels in the blood.

Immunostaining for phosphorylated c-Jun closely corresponds to immunostaining for p-JNK and the staining patterns of p-c-Jun (Ser 63) and p-c-Jun (Ser 73) consistently showed that these are subsets of total cells stained for c-Jun itself (*Ma et al., 2007; Flanc et al., 2007*). Therefore, detection of phosphorylation of c-Jun at serine 63 and serine 73 residues by immunostaining can be used as primary read-outs of JNK activity. In addition, other closely related kinases, ERK and p38, are not inhibited by CC401 *in vivo* or *in vitro* (*Ma et al., 2007; Flanc et al., 2007*).

Unfortunately, in this anti-Thy-1 nephritis study we had difficulty in obtaining reliable immunostaining for p-c-Jun (Ser63). Western blotting of isolated glomeruli for p-c-Jun (Ser 63) and p-c-Jun (Ser 73) was also attempted as a third way of demonstrating drug specificity. This was repeated several times, but due to technical difficulties, no data was obtained as well. As a result, I used immunostaining for p-c-Jun (Ser 73) as main read-out for JNK activity in this study.

Immunostaining for p-c-Jun (Ser 73)

Basically, two patterns of immunostaining for p-c-Jun (Ser 73) were observed in normal and diseased kidney. They are luminal cytoplasmic and nuclear staining. This antibody is known to recognize p-JunD Ser 100 due to both phosphorylation sites sharing the same amino acid sequence. The cytoplasmic, luminal p-c-Jun (Ser73) staining seen in normal rat kidney is probably phosphorylated JunD (Ser100) on the basis that little or no c-Jun is expressed in normal kidney. The cytoplasmic pattern of p-c-Jun (Ser 73) observed in diseased kidney is the same as that seen in the normal rat kidney, making it highly likely that this cytoplasmic staining is phosphorylated JunD (Ser 100) as well.

In the rat anti-Thy-1 nephritis, there was strong p-c-Jun (Ser 73) staining in the nucleus indicating phosphorylation of c-Jun. With CC-401 treatment, the nuclear staining for p-c-Jun (Ser73) disappeared and only the luminal stain for p-c-Jun (Ser73) remained. This is presumably ERK mediated phosphorylation of JunD

(Ser 100), given that ERK is known to phosphorylate JunD at serine 100, and ERK activation was not affected by CC401 treatment.

Chapter 5. Inhibition of c-fms kinase activity reverses glomerular macrophage infiltration and halts development of crescentic anti-GBM glomerulonephritis in the rat

5.1 Introduction

Macrophages have been implicated as important effector cells in studies of rapidly progressive glomerulonephritis based upon their localization within lesions and activated pro-inflammatory phenotype, a tight correlation between the macrophage infiltrate and the degree of renal dysfunction and histologic damage at the time of biopsy and their prognostic significance for disease progression (*Nikolic-Paterson et al., 2001*). However, current non-selective immunosuppressive drugs do not target this population of immune cells, and this is a major limitation of current treatment for this group of diseases (*Little et al., 2005*). It is desirable to seek a selective and clinically applicable approach targeting monocytes/macrophages.

Animal studies have shown that experimental approaches to delete macrophages can prevent the development of crescentic glomerulonephritis, and that replacement of this macrophage population can recapitulate acute glomerular injury in these models (*Holdsworth et al., 1981; Ikezumi et al., 2003; Ison et al., 2004; Lenda et al., 2004; Duffield et al., 2005*). However, few experimental strategies have been shown to selectively reverse a pro-inflammatory macrophage infiltrate, and such strategies are not clinically applicable. To address this important issue, we have investigated selective

inhibition of the receptor for macrophage colony-stimulating factor (M-CSF), termed c-fms. While M-CSF (also known as CSF-1) is expressed widely in tissues, being up-regulated in many types of tissue injury, c-fms expression is restricted to cells of the monocyte/macrophage lineage in the adult.

It is well established that M-CSF plays a critical role in monocyte production in the bone marrow, and M-CSF plays an important anti-apoptotic role to maintain macrophage populations (*Pixley et al., 2004*). M-CSF production is markedly up-regulated in the glomerulus and tubulointerstitium in human and experimental RPGN. Indeed, there is substantial local proliferation of infiltrating macrophages in human and experimental RPGN, which occurs in association with local up-regulation of M-CSF expression (*Isbel et al., 2001a*). These data identify the M-CSF/c-fms interaction as a potential therapeutic target given the central role of M-CSF in macrophage function and the restricted distribution of its receptor, c-fms.

fms-I is a recently described small molecule inhibitor of the tyrosine kinase activity of the c-fms receptor. It has been recently shown that administration of fms-I selectively inhibited interstitial macrophage proliferation and accumulation in the obstructed kidney (*Ma et al., 2009a*).

In this study, we started treating the animals an hour before administration of anti-GBM serum to see whether blockade of c-fms could reverse the early glomerular macrophage infiltrate, rather than to prevent macrophage infiltration

altogether prior to induction of disease. Two dosages of fms-I, low dose (10mg/kg, b.i.d) and high dose (30mg/kg b.i.d), were selected for this study of rat anti-GBM disease based upon data collected in the rat UUO model in which high dose fms-I completely prevented macrophage infiltration and depleted circulating blood monocytes, while low dose fms-I treatment significantly reduced local macrophage proliferation and accumulation without affecting blood monocyte levels (see 2.5.3) (*Ma et al., 2009a*).

The aim of the current study was to determine whether blockade of c-fms could reverse the early glomerular macrophage infiltrate in a model of crescentic glomerulonephritis and thereby halt disease progression.

5.2 fms-I reverses glomerular macrophage infiltration

The fms-I treatment was well tolerated. Vehicle and no treatment groups lost body weight over days 7 to 14, and this was prevented by fms-I treatment. Over days 0 to 14, the vehicle and no treatment groups gained 13% body weight, compared to a 22% weight gain in the two fms-I treated groups (*Fig 5.1*).

Prominent glomerular and interstitial ED1⁺ macrophage infiltrates were evident on day 14 of untreated and vehicle treated rat anti-GBM disease demonstrated by immunostaining for the CD68 (ED1) antibody (*Figs 5.2a, b, c and 5.3a, b*).

Treatment with low dose of fms-I resulted in a 30% reduction in glomerular macrophages and a 50% reduction in interstitial macrophages on day 14 of anti-

GBM disease, respectively, while treatment with high dose of fms-I abrogated glomerular and interstitial macrophage accumulation (*Figs 5.2d,e and 5.3a,b*).

Next, we examined earlier time points in the disease course to determine whether high dose fms-I prevented macrophage infiltration, or reversed an early infiltrate in a separate series of studies. Glomerular macrophage infiltration was prominent in high dose fms-I treated animals on day 1 of anti-GBM disease, and this was only partially reduced compared to the vehicle treated group (*Fig 5.4a, c, e*). However, by day 5, glomerular macrophage accumulation in the high dose of fms-I treated group was reduced by 60% compared to vehicle treated anti-GBM disease. Thus, the day 1 and day 5 studies demonstrate that the abrogation of macrophage infiltration seen on day 14 with high dose fms-I treatment was the result of reversal of substantial glomerular macrophage infiltrate seen at an early stage in the disease process (*Fig 5.4b, d, e*).

Examination of circulating leukocytes showed that low dose fms-I treatment had no effect upon total white blood cell counts or individual leukocyte populations. In contrast, high dose fms-I significantly reduced total white blood cells on days 1, 5 and 14 (*Fig 5.5a*). Analysis of individual cell types showed that high dose fms-I markedly reduced blood monocytes at all time points, and significantly reduced blood neutrophil counts on days 1 and 5, whereas lymphocyte numbers were only partially reduced on day 14 (*Fig 5.5a,b,c,d*). The blood monocyte population was further analyzed on day 14 of anti-GBM disease by flow cytometry using CD68 (ED1) and CD11b (OX-42) antibodies, which

confirmed that high dose of fms-I produced a dramatic reduction in blood monocyte counts. This analysis showed that low dose fms-I prevented the increase in blood monocyte number seen in anti-GBM disease, but didn't reduce monocyte numbers compared to normal rats (*Fig 5.6a, b*). In addition, blood monocytes were significantly reduced with high dose of fms-I treatment for 5 days, but not by 1 day high dose fms-I treatment in spite of marked reduction of white blood cells and neutrophil both in day 1 and day 5 studies (*Fig 5.5b, c*).

Local macrophage proliferation is a feature of macrophage accumulation in the rat anti-GBM disease (*Lan et al., 1997a*). Dual-colour immunostaining for CD68 (ED1) and proliferating cell nuclear antigen (PCNA) antibodies showed that local macrophage proliferation within the glomerulus was evident at day 14 in vehicle treated anti-GBM disease (7.37 ± 1.27 vs 0.09 ± 0.11 ED1⁺PCNA⁺ cells/gcs in normal rats; $P < 0.001$), and the number of proliferating macrophages was significantly reduced in low dose fms-I treated day 14 disease (3.45 ± 0.93 ED1⁺PCNA⁺ cells/gcs; $P < 0.001$ vs vehicle treated) (*Fig 5.7a,b,c,d*). The percentage of glomerular macrophage infiltrate undergoing proliferation at day 14 in anti-GBM disease was also reduced by low dose fms-I treatment ($32.7 \pm 5.7\%$ in vehicle vs $21.2 \pm 4.6\%$ in low dose fms-I treated; $P < 0.01$). Since few macrophages were evident in glomeruli of high dose fms-I treated anti-GBM disease, we examined the day 5 time point and found that high dose fms-I caused a marked reduction in both the number of proliferating macrophages (7.65 ± 0.99 in vehicle vs 2.19 ± 1.42 ED1⁺PCNA⁺ cells/gcs in high dose fms-I;

P<0.001) and the percentage of glomerular macrophages undergoing proliferation (47.3 ± 2.7 in vehicle vs $23.4\pm 6.7\%$ in high dose fms-I; P<0.001) at day 5 of anti-GBM disease (*Fig 5.7a,b,c,d*).

We also examined apoptosis in day 5 anti-GBM disease by TUNEL staining. Only very occasional apoptotic cells were seen in the glomerulus in both vehicle and high dose fms-I treated anti-GBM disease groups at this time indicating no significant induction of glomerular macrophage apoptosis.

5.3 fms-I ameliorates renal pathology and renal dysfunction

Untreated and vehicle treated rats with anti-GBM disease developed severe glomerular lesions on day 14, featuring atrophy, hyalinosis, focal and segmental adhesions and sclerosis and fibrinoid necrosis. Crescent formation was observed in up to 50% of glomeruli and most of these crescents associated with Bowman's capsule rupture. By day 14 of anti-GBM disease, 90% of crescents were of the fibro-cellular type, comprised of a large cellular component with a significant amount of PAS-stained fibroid elements within the crescents. The development of fibrocellular crescents were associated with severe glomerular damage and extensive disruption of Bowman's capsule (*Figs 5.8a,b and 5.9a,b,c*). Fibrin deposition in crescents and within Bowman's space was prominent in these rats (*Fig 5.8e*). Immunostaining showed deposition of collagen IV in crescents, the glomerular tuft, the periglomerular area and in the interstitium which was associated with accumulation of α -SMA⁺ myofibroblasts (*Fig 5.14 a,b,c & 5.15 a, b,c*). Consistent with the development of interstitial

fibrosis, a significant increase in interstitial volume was evident (*Fig 5.16*). Secondary to glomerular damage, all animals in the untreated and vehicle treated anti-GBM disease groups also developed marked tubulointerstitial damage on day 14, featuring tubular dilation and atrophy, cast formation and mononuclear cell infiltration (*Fig 5.10a,b,c*). Tubular damage was also shown on day 14 of anti-GBM disease by the induction of tubular vimentin and osteopontin expression (*Fig. 5.11a,b, 5.12a,b & Fig 5.13*). This severe tissue damage was associated with the development of renal dysfunction (*Fig 5.17a, b*).

High dose fms-I treatment had a profound inhibitory effect upon the development of glomerular injury, with most glomeruli showing only mild changes, while Bowman's capsule rupture, crescent formation and fibrin deposition in Bowman's space were largely prevented (*Figs 5.8d,f and 5.9b,c*). In addition, high dose fms-I treatment significantly reduced periglomerular accumulation of α -SMA⁺ myofibroblasts (*Fig. 5.9d*). Moreover, high dose fms-I treatment prevented significant secondary tubulointerstitial injury as seen on PAS stained sections (*Fig 5.10*) and blunted the induction of markers of tubular injury – expression of vimentin and osteopontin (*Figs 5.11, 5.12 and 5.13*). High dose of fms-I treatment prevented the development of interstitial fibrosis on day 14 of anti-GBM disease showed by reduced immunostaining for collagen IV and α -SMA and normalized interstitial volume (*Figs. 5.14e, 5.15e and 5.16*). High dose fms-I prevented renal dysfunction (*Fig 5.17a, b*).

Despite only reducing glomerular macrophage accumulation by 30%, low dose of fms-I treatment significantly reduced lesions of the glomerular tuft and the degree of crescent formation (*Figs 5.8c and 5.9a, b*). Low dose fms-I also substantially reduced periglomerular α -SMA⁺ myofibroblast accumulation and the development of tubulointerstitial damage in terms of tubular vimentin and osteopontin expression (*Figs 5.9d, 5.11c, 5.12c and 5.13a, b*). Low dose of fms-I treatment significantly reduced the deposition of collagen IV, accumulation of α -SMA⁺ myofibroblast and interstitial volume (*Figs. 5.14d, 5.15d and 5.16*). Low dose fms-I treatment also prevented a reduction in the glomerular filtration rate (*Fig 5.17a,b*).

5.4 fms-I does not modulate proteinuria

Rats with untreated and vehicle treated anti-GBM disease developed heavy proteinuria between day 1 and day 5, and this was sustained to day 14, which was associated with a significant reduction in the number of glomerular WT-1 stained podocytes on days 1, 5 and 14 (*Fig 5.17c, d*). Neither high nor low dose fms-I treatment prevented the development of heavy proteinuria (*Fig 5.17c*). fms-I treatment provided a minor protection against podocyte loss between days 5 and 14, although untreated, vehicle and even fms-I treated groups still exhibited a significant reduction in podocyte numbers at day 1, 5 and 14, compared to normal kidney (*Fig 5.14c,d*).

5.5 fms-I suppresses renal inflammation

RT-PCR analysis of isolated glomeruli on day 1 and 5 of vehicle treated anti-GBM disease identified up-regulation of mRNA levels of a number of pro-inflammatory molecules which are closely associated with the M1-type macrophage response (TNF- α , CCL2/MCP-1, NOS2, MMP-12 and IL-12). (*Fig 5.18a*). Increased mRNA levels of M2-type markers of alternatively activated macrophages (Arginase-1, CD206, CD163) was also evident (*Fig 5.18e,f,g,h*). At day 14 of anti-GBM disease, analysis of whole kidney tissue showed ongoing high mRNA levels for the pro-inflammatory molecules TNF- α , MCP-1/CCL2, NOS2 and MMP-12 (*Fig 5.19a-d*).

Depletion of macrophages with high dose fms-I on day 14 of anti-GBM disease kidney suppressed these pro-inflammatory molecules and abrogated the up-regulation of mRNA levels for the pro-inflammatory molecules (*Fig 5.19a-e*). Examination of these pro-inflammatory molecules at the earlier time points showed that high dose fms-I significantly reduced up-regulation of mRNA levels for all of the M1-type markers (TNF- α , MCP-1/CCL2, iNOS, MMP-12 and IL-12), while there was a relative increase in expression of the M2-type markers arginase-1 and CD206 (but not CD163) when considering the reduction in total macrophage numbers with this treatment (*Fig 5.18f-h*). Low dose fms-I had no significant effect upon up-regulation of mRNA levels of pro-inflammatory molecule at day 14 (*Fig 5.19a,b,c,d*).

5.6 fms-I suppresses T cell and dendritic cell infiltration

Immunostained cells for $\alpha\beta$ T cell receptor (R73) antibody were scored as infiltrating T cells in the kidneys at day 1, 5 and 14 of anti-GBM disease. There was a significant glomerular T cell infiltrate on day 1 of vehicle treated anti-GBM disease compared to the occasional glomerular T cells present in normal rat kidneys. This infiltrate was diminished on day 5, but was again evident on day 14 where T cells were distributed in the glomerulus, periglomerular area and the interstitium (*Fig. 5.20a, b*). The development of glomerular and tubulointerstitial lesions on day 14 of anti-GBM disease in untreated and vehicle treated animals was associated glomerular and interstitial T cell infiltration (*Fig. 5.20a, b*).

High dose fms-I treatment resulted in a 60% reduction in glomerular T cells and a 95% reduction in interstitial T cells on day 14 of anti-GBM disease. Low dose fms-I did not affect the glomerular T cell infiltrate, but it caused an 85% reduction in interstitial T cell accumulation (*Fig. 5.20a, b*).

To determine whether high dose fms-I prevented T cell infiltration, or reversed an early infiltrate as it did to macrophages, we examined glomerular T cells on day 1 and day 5. A glomerular T cell infiltrate was evident in high dose fms-I treated animals on day 1 and day 5 of anti-GBM disease, which was not different compared to the vehicle treated group (*Fig 5.20a*). This demonstrated that fms-I treatment did not prevent glomerular T cell infiltration at day 1 and day 5 of anti-GBM disease.

We used three monoclonal antibodies to label renal dendritic cells in normal and

anti-GBM diseased kidneys. The three antibodies were OX-6, OX-62 and CD11c. OX-6 antibody recognizes a monomorphic determinant of the rat MHC class II (I-A also known as RT1B) antigen present on dendritic cells, as well as, B cells, some macrophages and some epithelial cells. OX-62 monoclonal antibody recognizes the rat α E2 integrin expressed by subsets of rat dendritic cells and by gamma--delta T cells (*Mu et al., 2005*). CD11c a 150/90kD member of the β 2 integrin family, which is expressed by dendritic cells and some myeloid cells in rats. Thus, we choose to use a panel of these three monoclonal antibodies to determine the distribution of dendritic cells in kidneys with anti-GBM disease with or without fms-I treatment.

A network of interstitial, dendritic-like cells are stained using OX-62, OX-6 and CD11c antibodies in normal rat kidney, while only occasional stained cells are seen in glomeruli (Fig 5.22). A marked glomerular infiltrate of CD11c⁺ and OX-62⁺ cells, and to a lesser extent, OX-6⁺ cells was seen in day 1 of vehicle and no treatment anti-GBM disease (Fig 5.22). As the disease developed to day 14, an increase in the interstitial populations of cells stained for CD11c, OX-62 and CD11c was evident, particularly in the periglomerular area and in focal areas of tubulointerstitial damage (Fig 5.22). Glomerular OX-6⁺ and CD11c⁺ cells also increased at day 14 of anti-GBM disease, being seen in both the tuft and in crescents. In contrast, few OX-62⁺ cells were seen in glomeruli on day 14. High dose fms-I treatment had little effect upon the glomerular infiltrate of cells stained with OX-6, OX-62 or CD11c antibodies on day 1. However, by day 14 of anti-GBM disease, high dose fms-I treatment substantially reduced

glomerular and interstitial cell populations of OX-6⁺, OX-62⁺ and CD11c⁺ cell populations (Fig 5.22).

5.7 fms-I does not modify glomerular deposition of rat IgG and C3

The deposition of rat C3 and the binding of rat IgG to sheep IgG along the GBM were assessed by immunofluorescence using a semi-quantitative method. The result showed that this was not affected by low or high dose of fms-I treatment (Fig. 5.21).

5.8 Discussion

Summary

The main findings in this chapter include:

1. fms-I, a specific c-fms inhibitor, can reverse glomerular macrophage infiltration, and over 14 days, treatment of fms-I depletes the intrarenal macrophage accumulation in the kidneys with anti-GBM disease.
2. The development of glomerular lesions including glomerular tuft damage and crescent formation largely depends on glomerular and periglomerular macrophage infiltration. Macrophage depletion suppresses the pro-inflammatory response as shown by reduction of TNF- α , MCP-1, iNOS and MMP-12 mRNA levels in the anti-GBM diseased kidney.
3. Deterioration of renal function in rat anti-GBM disease is prevented with depletion of the macrophage infiltrate by low dose and high dose of fms-I treatment which is consistent with much improved renal pathology. However,

heavy proteinuria is not affected by reversal of glomerular macrophage infiltrate.

4. Despite heavy proteinuria from day 1 to 14, tubular damage is prevented by depletion of macrophages. This argues that macrophages rather proteinuria cause significant tubular damage in this model.
5. Blockade of M-CSF/*c-fms* signaling through *c-fms* inhibition by *fms-I* is considered as a selective and clinically applicable therapeutic approach to treat rapidly progressive glomerulonephritis.

Specificity of *fms-I* for M-CSF/*c-fms* signaling pathway

Specificity of *fms-I* for the M-CSF/*c-fms* signaling pathway was demonstrated by the reduction of CD68 (ED-1) immunostaining labeled macrophages in this study. This reduction in macrophage accumulation was confirmed by using the other two different macrophage antigens including OX-42 and MHC class II in rat obstructed kidney. The immunostaining demonstrated that *c-fms* inhibition had not simply altered monocyte differentiation or modified expression of a single antigen (*Ma et al., 2009a*).

In current studies, the complete downregulation of TNF- α , MCP-1, iNOS and MMP-12 levels in rat anti-GBM disease is another indicator that *fms-I* treatment was effective in preventing macrophage accumulation. The specificity of *fms-I* was also supported by the finding that *fms-I* treatment did not substantially affect WBCs other than monocytes, except for a small reduction in lymphocyte counts, and *fms-I* had no effect on the glomerular T cell infiltrate on day 1 in the

anti-GBM disease. In addition, *in vitro* kinase assays performed by Johnson & Johnson Pharmaceutical Research and Development addressed the specificity of fms-I for c-fms tyrosine kinase (see Chapter 2).

Chapter 6. c-fms kinase inhibition in the established rat crescentic glomerulonephritis

6.1 Introduction

In the previous chapter, we selectively inhibited c-fms, the receptor for macrophage colony-stimulating factor (M-CSF) using a specific inhibitor named fms-I in a day 14 model of rat crescentic glomerulonephritis. Administration of fms-I from day 0 to 14 successfully reversed the glomerular macrophage infiltrate and prevented interstitial macrophage accumulation. The depletion of intrarenal macrophage accumulation ameliorated renal pathology and renal dysfunction on day 14 of anti-GBM disease.

In this study, we sought to model the clinical scenario when patients with crescentic glomerulonephritis present at the clinic. Therefore, we tested whether a delayed fms-I intervention treatment would affect progressive glomerular and tubulointerstitial damage in a model of established rat crescent glomerulonephritis from day 14 to day 35. The disease is well established on day 14 after anti-GBM serum injection as characterized by prominent crescent formation associated with Bowman's capsule rupture, progressive tubulointerstitial injury with deteriorated renal function and heavy proteinuria.

It was established in the Chapter 5 that high dose fms-I results in complete blood monocyte and renal macrophage depletion, while low dose fms-I can reduce renal macrophage without affecting white blood cell counts. The same fms-I dosing regime was used in this study. We used the day 14 vehicle treated

group from Chapter 5 as the control in this Chapter for disease severity at the time when fms-I treatment began.

6.2 fms-I treatment starting on day 14 depletes the renal macrophage infiltration

fms-I was well tolerated over 21 days treatment starting 14 days after administration of anti-GBM serum, with a trend towards increased body weight gain, although this was not statistically significant (*Fig 6.1*). Substantial glomerular and interstitial CD68⁺ (ED1) macrophage infiltration was evident on day 35 of vehicle treated rat anti-GBM disease as demonstrated by immunostaining for ED1 antibody, although the number of macrophages was reduced by approximately 60% compared to day 14 (*Figs 6.2 and 6.3a,b*).

Treatment with low dose of fms-I (10mg/kg) resulted in a significant reduction in glomerular and interstitial macrophages on day 35 anti-GBM disease, while treatment with high dose of fms-I (30mg/kg) fms-I achieved an 85% glomerular macrophage reduction and 82% reduction of interstitial macrophage accumulation (*Fig 6.3a,b*). The number of glomerular and interstitial macrophages in low dose and high dose of fms-I treated animals with anti-GBM disease were close to that seen in normal rat kidney.

High dose of fms-I significantly reduced total white blood cell counts, whereas low dose of fms-I treatment had no effect on white blood cell counts.

Examination of individual blood leukocyte populations showed that both low and

high dose of fms-I treatments depleted blood monocytes, while lymphocyte and neutrophil populations were unaffected compared to vehicle treated anti-GBM disease on day 35 of anti-GBM disease (*Fig. 6.4a,b,c,d*).

6.3 Effect of fms-I on renal pathology and renal dysfunction

When anti-GBM disease developed to day 14, diseased rats already developed severe glomerular lesions featuring hyalinosis, fibrinoid necrosis and focal and segmental adhesions, fibrin deposition in Bowman's space, and crescents associated with Bowman's capsule rupture (*Figs 6.5 and 6.6*). Tubulointerstitial damage involving tubular dilation and atrophy, cast formation and interstitial leukocyte infiltration were also substantial at the time (*Fig 6.7*).

When disease advanced to day 35, glomerular crescents became more fibrous with less cellular component and increased fibrous tissue. Moreover, crescent formation affected more glomeruli, crescentic glomeruli increased to 53% of total glomeruli. Among those crescentic glomeruli, around 80% of crescentic glomeruli were accompanied by Bowman's capsule rupture that is 5% increase from day 14 (*Figs 6.5 and 6.6a,b*). Meantime, tubulointerstitial damage spread and worsened at day 35 of anti-GBM disease featuring enlarged tubular dilation and severe tubular atrophy, more cast formation and interstitial leukocyte accumulation (*Fig 6.7b,c*). The induction in tubular expression of vimentin and osteopontin (*Figs 6.8a,b and 6.9a,b*) and interstitial fibrosis with increased deposition of collagen IV and α -SMA⁺ myofibroblast accumulation were also

significantly elevated (*Figs 6.12b,c and 6.13b,c*). This severe renal damage was associated with renal dysfunction (*Fig 6.11c*).

High dose fms-I treatment over 21 days from day 14 to day 35 of anti-GBM disease significantly reduced number and average size of crescents. Meantime, Bowman's capsule rupture among these crescents was reduced by 10% with high dose of fms-I, yet the difference did not achieve statistic significance. In addition, high dose of fms-I treatment significantly reduced periglomerular accumulation of α -SMA⁺ myofibroblasts (*Fig 6.6a,b,c,d*). PAS-haematoxylin staining showed high dose fms-I treatment did not halt the development of tubulointerstitial damage (*Fig 6.7*) and this result was further confirmed by the induction of tubular injury markers including vimentin and osteopontin by immunostaining and semi-quantification of tubular lumen space (*Figs 6.8, 6.9 and 6.10a,b,c*).

fms-I treatment halted the deterioration of renal dysfunction, and high dose fms-I significantly improved the renal function. Glomerular filtration rate rised to 74% of normal glomerular filter rate with high dose fms-I treatment (*Fig 6.11c*). However, high dose of fms-I treatment did not alter the ongoing proteinuria over day 14 to day 35, which was consistent with significantly reduced podocyte number in vehicle and fms-I treated animals (*Fig 6.11a,b*).

6.4 Effect of fms-I on interstitial fibrosis

Marked interstitial fibrosis at day 35 of anti-GBM disease is characterized by increased interstitial volume, interstitial deposition of collagen IV and α -SMA⁺ myofibroblast accumulation, which were evident in vehicle treated anti-GBM disease at day 35 and significantly higher than at day 14 (*Figs 6.12a,b,c, 6.13a,b,c and 6.14*). Low dose and high dose of fms-I treatment resulted in a small minor, but significant, reduction in collagen IV deposition, and high dose of fms-I treatment reduced interstitial volume on day 35 of anti-GBM disease (*Figs 6.12 and 6.14a, c*). However, neither low nor high dose of fms-I treatment caused a significant reduction in interstitial α -SMA⁺ myofibroblast accumulation on day 35 of anti-GBM disease (*Figs 6.13 and 6.14b*).

6.5 Effect of fms-I on renal inflammation and glomerular T cells

Real time RT-PCR identified a profound pro-inflammatory response on day 35 of vehicle treated anti-GBM disease on the basis of increased expression of TNF- α , iNOS and MMP-12. Both low and high dose fms-I treatment did not impact on this pro-inflammatory response (*Fig 6.15*). The development of glomerular and tubulointerstitial lesions on day 35 of anti-GBM disease in vehicle treated rats were associated with a significant interstitial T-cell infiltrate, whereas glomerular T cell numbers were close to normal by this time point. Low and high dose fms-I treatment did not caused a significant reduction in interstitial T-cell accumulation consistent with the overall tubulointerstitial injury seen with drug treatment (*Fig 6.16a, b*).

6.6 Discussion

Summary

The main findings in this chapter include:

1. Fms-I treatment starting on day 14 reverses the renal macrophage infiltrate by day 35.
2. Ablation of glomerular and interstitial macrophage infiltrate improves renal function despite failure to modulate proteinuria.
3. Depletion of the macrophage infiltrate resulted in a minor reduction in the severity of glomerular lesions by reducing crescent size and periglomerular α -SMA⁺ myofibroblast accumulation. In addition, removal of the macrophage infiltrate caused a small reduction in interstitial collagen IV deposition and the interstitial volume.

Chapter 7. Discussion

7.1 ERK blockade in mouse obstructed kidney

While many *in vitro* studies have shown an important role for MEK-ERK signaling in the proliferation of cultured cells (*Ammitt et al., 2001*), this has been difficult to translate into disease models because ERK gene knockout mice die during foetal development and the various MEK1/2 inhibitors available have poor solubility (*Favata et al., 1998*). However, short-term administration of U0126, a potent MEK1/2 inhibitor with an IC₅₀ of 1 μ M in cell-base assays was shown to be able to effectively inhibit ERK activation in the mouse-obstructed kidney as demonstrated by preventing ERK phosphorylation.

Administration of U0126 caused a significant reduction in the proliferation of interstitial cells in the obstructed kidney. This was associated with a reduction in interstitial accumulation of macrophages, but not of α -SMA⁺ myofibroblasts. This reduction in macrophage accumulation may be due to one or more ERK-dependent mechanisms. First, it is known that macrophage accumulation in the obstructed mouse kidney is dependent upon local proliferation driven by the growth factor, macrophage colony-stimulating factor (M-CSF, also called CSF-1) binding to the c-fms receptor on macrophages (*Le Meur et al., 2002*). It is known that M-CSF-induced macrophage proliferation is dependent, in part, upon MEK-ERK signaling (*Jaworrowski et al., 1999*). Therefore, the reduction in interstitial cell proliferation seen with U0126 treatment in the mouse UUO model would be consistent with inhibition of an M-CSF-ERK pathway of macrophage proliferation. Second, M-CSF is also an important survival and antiapoptotic

factor for macrophages (*Chitu et al., 2006*). However, ERK activation does not appear to be involved in the antiapoptotic actions of M-CSF *in vitro* (*Jaworrowski et al., 1999*), a finding supported in the current study by the lack of effect of U0126 treatment on interstitial cell apoptosis. Third, the reduction in interstitial macrophage accumulation could also reflect inhibition of monocyte migration. The role of MEK-ERK signaling in monocytes migration in response to monocyte chemoattractant protein-1 is controversial (*Yen et al., 1997; Cambien et al., 2001*), although this pathway is involved in macrophage migration in response to the chemokine, midkine, and in oxidant induced macrophage proliferation; thereby providing a mechanism to explain U0126 mediated inhibition of interstitial macrophage accumulation in the obstructed kidney. However, cell tracking studies are needed to answer this question in a definite fashion.

It was surprising that U0126 treatment did not affect interstitial accumulation of α -SMA⁺ myofibroblasts in the UUO model. The growth factor PDGF is well described to induce cell proliferation via the MEK-ERK signaling pathway, and treatment with an inhibitor of PDGF receptor kinase activity has been shown to inhibit interstitial accumulation of α -SMA⁺ cells in the UUO model (*Ludewig et al., 2000*). Work from this lab has previously identified ERK activation in interstitial α -SMA⁺ myofibroblasts in the rat-obstructed kidney (*Masaki et al., 2003*), while U0126 administration in the rat Thy-1 nephritis model was shown to inhibit proliferation of α -SMA⁺ mesangial cells (*Bokemeyer et al., 2002*). The inability of U0126 treatment to affect myofibroblast accumulation in the current

study presumably indicates redundancy in signaling pathways involved in interstitial myofibroblast accumulation in the obstructed kidney, providing a contrast to the ERK dependency of mesangial cell proliferation.

TGF β 1 is the primary factor inducing collagen production in most types of renal fibrosis, including the obstructed kidney. While most studies have focus on the role of Smad, JNK and p38 signaling pathways in renal fibrosis, it has been reported that ERK signaling contributes to TGF β 1-induced collagen production in cultured mesangial cells (*Hayashida et al., 1999; Hayashida et al., 2003*). However, we found no effect of U0126 treatment on collagen deposition in the UUO model suggesting that ERK signaling does not play an important role in the development of interstitial fibrosis *in vivo*.

A close association between ERK activation and tubular cell proliferation has been described in the obstructed rat kidney (*Masaki et al., 2003; Pat et al., 2005*). However, the current study was unable to define a role for MEK-ERK signaling in tubular cell proliferation in the UUO model. While blockade of ERK signaling reduced tubular cell proliferation, this was also apparent in the vehicle treatment group, thereby preventing any conclusion to be drawn. Oxidant stress is induced in the obstructed kidney and studies in various epithelia have shown that high levels of H₂O₂ induce cell cycle arrest and apoptosis, whereas low doses of H₂O₂ can induce epithelial cell proliferation via ERK and p38 MAPK pathways (*Sigaud et al., 2005*). DMSO is an antioxidant and this may explain the reduction in tubular cell proliferation seen with vehicle treatment, although

this effect was independent of ERK signaling which was not altered by vehicle treatment.

A number of different stimuli may be responsible for the induction of tubular cell apoptosis in the obstructed kidney, including mechanical stretch, oxidant damage, ischaemia, hypoxia, TNF- α and TGF- β 1 (*Klahr et al., 2002*). Most of these stresses induce apoptosis via the JNK and p38 pathways. In contrast, ERK activation by high levels of oxidant stress can play an antiapoptotic role in tubular cells (*Di Mari et al., 1999; Pat et al., 2003*). In the present study, blockade of MEK-ERK signaling had no effect upon apoptosis of tubular epithelial cells or interstitial cells indicating that this pathway is not an important player in apoptosis in the obstructed kidney. Indeed, recent studies have shown that signaling via the JNK pathway is a major mechanism inducing tubular cell apoptosis in this model (*Ma et al., 2007*).

In contrast to the current study, U0126 administration in a model of acute cisplatin-induced renal failure was found to suppress ERK activation and reduce tubular cell apoptosis. However, this reduction in tubular apoptosis may be an indirect effect because both renal leukocyte infiltration and upregulation of TNF- α were suppressed by ERK blockade of this model (*Jo et al., 2005*).

In summary, these studies show that interstitial accumulation of macrophages in the obstructed kidney is, in part, dependent upon the MEK-ERK signaling

pathway, while the development of renal fibrosis occurred independent of blockade of MEK-ERK signaling.

7.2 c-fms blockade in rat progressive crescentic glomerulonephritis

7.2.1 fms-I treatment and macrophage infiltration

We treated rat anti-GBM disease by systemic administration of fms-I, which is an inhibitor of the tyrosine kinase activity of M-CSF receptor called c-fms.

Two stages of rat anti-GBM disease were investigated: (1) development of rat progressive crescentic glomerulonephritis over day 0 to 14 and (2) established crescentic glomerulonephritis over day 14 to 35. As anti-GBM disease progresses to day 14, glomerular filtration rate is reduced by half and heavy proteinuria develops on day 5. The rats also develop severely inflamed glomerular lesions highlighted by cellular-fibrous crescent formation, Bowman's capsule rupture and hyalinosis and fibrinoid necrosis in the glomerular tuft. At day 14, tubulointerstitial damage is apparent and interstitial fibrosis is emerging. In particular, there was massive macrophage infiltration both in glomeruli and interstitium at this time point. Therefore, day 14 is considered an appropriate time point to test the effect of depletion of macrophage infiltration via c-fms blockade in rat crescentic glomerulonephritis.

Severe disease is evident on day 14 of anti-GBM glomerulonephritis based on 50% glomerular crescents and widespread interstitial damage. From a clinical perspective, patients presenting with this degree of kidney damage at the clinic

have a very poor prognosis (*Zhao et al., 2001*). Therefore, given the success of fms-I treatment over day 0-14, we investigated whether this treatment could halt or reverse the severe disease seen at day 14. Moreover, it is a crucial test of any new therapeutic strategy to treat fully established disease. Therefore, fms-I was used to treat established crescentic anti-GBM disease which treatment began on day 14 and completed on day 35.

fms-I treatment was well tolerated over 14 or 21 days. High dose of fms-I treatment entirely depleted glomerular and interstitial macrophage accumulation at day 14 of anti-GBM disease, while low dose fms-I reduced glomerular macrophage infiltrate by 30% and interstitial macrophage accumulation by 50%. In the intervention study, 21-days of low or high dose fms-I treatment markedly diminished glomerular and interstitial macrophage infiltration by day 35. In comparison to other strategies for systemic depletion of macrophages including; systemic irradiation with kidney shielding (*Schreiner et al., 1978*), liposome clodronate (*Isome et al., 2004*), cyclophosphamide (*Ikezumi et al., 2003*), and diphtheria toxin in susceptible genetically modified mice (*Duffield et al., 2005*), fms-I treatment has been shown to be a more effective and selective approach to deplete macrophages, and can be sustained over several weeks with no apparent side-effects.

In the day 14 and 35 studies, two dosing regimes of fms-I were examined: low dose (10mg/kg, b.i.d) and high dose (30mg/kg b.i.d). On day 14 of anti-GBM disease, high dose fms-I treatment completely prevented the macrophage renal

infiltrate and depleted circulating blood monocytes, whereas low dose fms-I treatment significantly reduced local macrophage proliferation and accumulation without affecting blood monocyte levels. On day 35 of anti-GBM disease, both low and high dose fms-I treatment significantly reduced glomerular and interstitial macrophage infiltration and blood circulating monocytes by day 35.

Two mechanisms may account for the inhibition of macrophage accumulation by fms-I treatment in rat anti-GBM disease. First, the low dose fms-I treatment significantly reduced local macrophage proliferation and accumulation within the inflamed kidney without affecting blood monocyte levels in the day 14 study. Dual-colour immunostaining for CD68 (ED1) and PCNA antibodies demonstrated both total macrophages and proliferating macrophages were reduced in the glomeruli of day 14 anti-GBM disease treated with low dose fms-I compared to vehicle treated. This is consistent with previous studies using c-fms blockade in the rat and mouse obstructed kidney in which there was substantially reduced local macrophage proliferation and accumulation without depleting blood monocytes (*Ma et al., 2009a; le Meur et al., 2002*). Second, high dose or prolonged fms-I treatment resulted in depletion of circulating blood monocytes, thereby severely limiting monocyte recruitment into the inflamed kidney. Presumably, this reflects increasing levels of fms-I in the bone marrow compartment to inhibit M-CSF dependent production of blood monocyte precursor cells, but this was not measured in this study.

One interesting difference between the day 14 and 35 studies was that low dose fms-I treatment over day 14 to 35 did substantially reduce blood monocyte numbers. Presumably this occurred during the last week of treatment, since it was not evident in the day 14 study, and may reflect progressive accumulation of fms-I in the bone marrow, or the consequence of inhibiting proliferation of an early precursor population. In addition, the three week period of fms-I treatment affected monocytes, but not neutrophils or lymphocyte, demonstrating the selectivity of fms-I.

In the day 14 study, high dose fms-I treatment started on the same day as the administration of anti-GBM serum depleted both circulating monocytes and macrophage accumulation in the kidney. An interesting and rather critical question is whether high dose fms-I prevented macrophage infiltration from the beginning, or reversed an early infiltrate over the course of treatment. We examined earlier time points in the disease course and found a marked glomerular macrophage infiltrate in high dose fms-I treated animals at day 1 of anti-GBM disease, which was only partially reduced compared to the vehicle treated group. However, by day 5, glomerular macrophage accumulation in the high dose of fms-I treated group was reduced by 60% compared to vehicle treated anti-GBM disease. Therefore, high dose of fms-I treatment actually reversed a substantial early glomerular macrophage infiltrate in this disease model.

7.2.2 fms-I treatment and glomerular lesions and crescent formation

Our study showed that high dose of fms-I treatment had a profound inhibitory effect upon the development of glomerular injury at day 14 of anti-GBM disease, with most glomeruli showing only mild changes, while crescent formation and Bowman's capsule rupture were largely prevented. Low dose fms-I reduced the severity of lesions of the glomerular tuft and the degree of crescent formation, despite only reducing glomerular macrophage accumulation by 30%. These findings are in sharp contrast to the study in untreated and vehicle treated anti-GBM disease rats which developed severe glomerular lesions featuring Bowman's capsule rupture in almost 80% of glomeruli and crescent formation observed in up to 57% of glomeruli on day 14. These results clearly identify a critical role for macrophages in causing and promoting crescent formation, Bowman's capsule rupture and glomerular tuft lesions.

Crescent formation and Bowman's capsule rupture are associated with a worse prognosis in crescentic glomerulonephritis (*Morel-Mroger Striker et al., 1984; Lan et al., 1992*). Although the cellular composition of crescents is still controversial, it is mostly accepted that crescents are a mixture of epithelial cells including podocytes and parietal epithelial cells, macrophages, and myofibroblasts. Several recent studies reported that podocytes form an integral cellular component of crescents in glomerular disease (*Thormer et al., 2008; Moeler et al., 2004*) and argued that podocyte bridges between the glomerular tuft and Bowman's capsule are considered a critical early event in crescent formation in anti-GBM disease (*Le Hir et al., 2001; Moeller et al., 2004*).

However, our data from fms-I treated anti-GBM disease suggested that crescent formation requires glomerular macrophage infiltration. In this study, reversing macrophage infiltration prevented significant crescent formation in spite of podocyte damage and glomerular tuft adhesions. These findings also argue that macrophages are required for the development of glomerulosclerosis, and that while podocyte damage may be required, it is not sufficient for the induction of glomerulosclerosis in this model. Our findings are consistent with the previous reports and observation in which macrophages are key effectors and modulators in crescent formation, Bowman's capsule rupture and disease progress in crescentic glomerulonephritis (*Lan et al., 1992; Duffield et al., 2005*).

An M1-type pro-inflammatory phenotype of the infiltrating macrophages is required for macrophage-mediated renal injury in anti-GBM disease (*Ma et al., 2009c; Ikezumi et al., 2003 and Ikezumi et al., 2004*). Real-time RT-PCR analysis of glomeruli on day 1 and 5 of anti-GBM disease indicated a pro-inflammatory, M1-like phenotype of the macrophage infiltrate, although expression of some M2-type markers of alternative macrophage activation was also evident. The progressive reduction in glomerular macrophages seen with high dose fms-I treatment caused a profound reduction in the expression of M1-type pro-inflammatory markers and a relative increase in the expression of some M2-type markers. Thus, while the reduction in the number of macrophages with an M1-like phenotype is likely to be a major mechanism by which fms-I treatment protected against disease progression, an augmentation

of alternative activation of the remaining macrophages may have also contributed to this protective effect.

An important clinical question is whether glomerular crescents can be reversed? It has been argued that not all cellular crescents become fibrotic. In a rabbit model of anti-GBM glomerulonephritis, Downer and colleagues observed that while 90% of glomeruli showed cellular crescents or exudate material within Bowman's space shortly after the induction of disease, only 50% of glomeruli progressed to develop fibrotic crescents (*Downer et al., 1988*). This observation was also recorded in a group of patients that spontaneously recovered from rapidly progressive glomerulonephritis (*Couser et al., 1988*). These studies led Atkins *et al* to postulate that irreversible crescent formation might be due to disruption of Bowman's capsule and macrophage and myofibroblast accumulation within Bowman's space (*Atkins et al., 1996*). In this study, we tested this hypothesis by depleting renal macrophage infiltrates from day 14 of anti-GBM disease when fibro-cellular crescents with Bowman's capsule rupture had already developed in 50% of glomeruli. High dose fms-I treatment significantly reduced crescentic glomeruli to 40% of total glomeruli compared to 53% in vehicle treated group at day 35. The average size of crescent was also significantly reduced with high dose fms-I treatment. A more detailed analysis showed that the large majority of crescents on day 14 of anti-GBM disease were of a fibrocellular phenotype with Bowman's capsule rupture, although approximately 10% were of a cellular phenotype thought to represent an earlier stage in crescent development. The small reduction in the number of crescents

seen on day 35 with high dose fms-I treatment may represent a reversal of these cellular crescents seen on day 14. However, fms-I treatment did not prevent progression of a small number of crescents to a fibrous phenotype. This is the first *in vivo* study to investigate whether depletion of macrophage infiltrates can reverse the development of crescent and Bowman's capsule rupture in late-stage of a rat crescentic glomerulonephritis.

Overall, our data reveal that macrophages are crucial to the initiation of crescent formation in experimental anti-GBM disease and indicate a role in the progression of cellular to fibrocellar stage of crescent development

7.2.3 fms-I treatment and renal function and proteinuria

A key finding of current studies is that macrophage-depleted rats with anti-GBM disease maintained normal renal function in the induction phase (Day 0-14), and showed an improvement in renal function in established phase (Day 14-35). These outcomes demonstrate that infiltrating macrophages cause renal dysfunction in rat anti-GBM disease.

A striking result in current studies was that macrophage depletion by c-fms inhibition did not prevent the induction of proteinuria, and this also failed to reverse the heavy proteinuria sustained between day 5 and day 14 of disease. The small dose of anti-GBM serum used in the WKY rat model does not induce significant heterologous injury in the first 24 hours, but proteinuria develops rapidly thereafter. Time-course studies demonstrated that there was a marked

glomerular macrophage infiltrate on day 1 of anti-GBM disease even with high dose of fms-I treatment, and by day 5, number of glomerular infiltrated macrophages was reduced, but still considerably above normal levels. Proteinuria in rat models of anti-GBM disease is macrophage-dependent (*Ikezumi et al., 2003; Isome et al., 2004; Isbel et al., 2001b*), the early glomerular macrophage infiltrate seen in the high dose fms-I treated group was likely sufficient to induce proteinuria. Quantification of WT-1⁺ podocytes confirmed that WT-1⁺ podocytes were significantly reduced from day 1 of anti-GBM disease compared to normal kidney preceding the development of proteinuria, and were not normalized even by high dose of fms-I treatment for 14 days which may reflect an inability to replace lost podocytes or recover from podocyte damage in this short timeframe. In addition, it may be that proteinuria was partially alleviated by fms-I treatment but that this effect was masked by the substantially higher glomerular filtration rate seen in these animals compared to vehicle and no treatment groups. This may partially explain the finding that fms-I treatment cannot reverse the proteinuria.

7.2.4 fms-I treatment and tubulointerstitial damage

Secondary to glomerular damage, untreated and vehicle treated anti-GBM disease developed marked tubulointerstitial damage as shown by PAS-haematoxylin staining and immunostaining for vimentin and osteopontin on day 14 of anti-GBM disease. Low and high dose fms-I treatment significantly reduced and largely prevented secondary tubulointerstitial injury, respectively. The ability of fms-I treatment to prevent tubulointerstitial injury at day 14 is most

likely a consequence of its ability to deplete macrophage infiltrates in the glomeruli and interstitium. Reduced glomerular inflammation and cytokine production as a result of macrophage depletion is a likely reason for the reduction in tubular cell activation. Indeed, this postulate is supported by the finding that fms-I treatment prevented upregulation of renal MCP-1 mRNA levels on day 14 of anti-GBM disease when MCP-1 is predominantly expressed by tubules (*Tesch et al., 1999; Okada et al., 2000*).

It is argued that proteinuria is an important factor in progressive tubulointerstitial damage. One way in which this may operate is by high levels of albumin in the glomerular filtrate inducing activation of tubular epithelial cells to produce chemokines, such as CCL2 (MCP-1) and osteopontin, that recruit interstitial macrophages which cause progressive tubular damage (*Zoja et al., 2009*). *Abbate et al* also postulated that leaked plasma albumin from the circulation through a severely dysfunctional glomerular capillary barrier causes protein overload of tubular epithelial cells and activation of complement in the kidney that is responsible for spreading of injury to the tubulointerstitium (*Abbate et al., 2006*). *In vitro* studies using proximal tubular cells exposed to plasma proteins demonstrated protein overload stimulated expression of a variety of pro-inflammatory and pro-fibrosis mediators such as MCP-1 and ET-1, as well as, activated NF- κ B, ERK and p38 signalings in renal tubular cells (*Dixon et al., 2000; Donadelli et al., 2003; Morigi et al., 2002*). However, the concentrations of albumin used in various *in vitro* experiments remains controversial. It was reported that usually concentration over 2.5mg/ml or 5mg/ml of albumin can

activate NF- κ B signaling in cultured tubular cells (*Tang et al., 2003*). These *in vitro* data are inadequate to prove that proteinuria alone can induce tubulointerstitial damage.

The other reason that proteinuria *per se* did not cause tubulointerstitial damage in fms-I treated anti-GBM disease may be that up-regulation of tubular chemokine expression is dependent upon glomerular production of pro-inflammatory cytokines (*Yu et al., 1999*). In fact, it is difficult to separate these two possible mechanisms *in vivo*. It was surprising that heavy proteinuria did not cause tubulointerstitial injury in low dose and high dose of fms-I treated animals in current study. However, *in vivo* evidence provided by experimental animal studies supports the link between proteinuria and mononuclear cell accumulation into the interstitium via cell signaling activation and upregulation of pro-inflammatory cytokines such as CCL2. Another uncertainty arises from the possibility that normal proximal tubules might have a great capacity to handle increased amount of proteins before tubular injury develops. It is also unclear why patients with minimal change nephropathy who suffer nephrotic level of proteinuria do not develop tubulointerstitial disease (*Kikuuchi et al., 2000*). The finding that high dose fms-I treatment prevented up-regulation of CCL2 and osteopontin expression despite the presence of proteinuria, suggests that glomerular inflammation may be the dominant mechanism inducing this tubular response. The results of the current study raises the postulate that proteinuria alone is unable to cause tubulointerstitial damage unless macrophages are recruited to the tubulointerstitium and activated. However,

one potential caveat is the short timeframe of these studies, and potentially in a more chronic setting, proteinuria may gradually cause tubular inflammation.

However, we observed in the intervention study that once severe tubulointerstitial damage was present, macrophage depletion with fms-I treatment did not affect the degree of tubulointerstitial damage. Indeed, numbers of infiltrating macrophage were reduced in vehicle treated rats at day 35 compared to day 14 anti-GBM disease, indicating a change to a more chronic fibrotic process from a strongly inflammatory lesion.

We found that the interstitial population of myofibroblast was expanded in the presence of inflammatory macrophages on day 14 of anti-GBM disease, together with increased interstitial deposition of collagen IV. Various *in vitro* and *in vivo* studies provide evidence that activated macrophages are able to induce myofibroblast proliferation, abnormal synthesis and degradation of extracellular matrix through production of nitric oxide, transforming growth factor- β , tumour necrosis factor- α and up-regulation of collagenases and other metalloproteinases (Roberts *et al.*, 1997; Rodriguez-Iturbe *et al.*, 2001). Thus, in the inflamed kidneys on day 14 of anti-GBM disease abundant infiltrated macrophages may play a role in promoting myofibroblast accumulation and the consequent increase in deposition of collagen IV. However, it cannot be determined whether fms-I treatment suppressed the myofibroblast accumulation and collagen deposition due to the dramatic reduction in glomerular damage, or

if this was a direct result of a lack of macrophage induced fibrosis in the kidneys.

In contrast, both low and high dose fms-I treatment failed to significantly reduce tubular damage at day 35 of anti-GBM disease as shown by vimentin and oestropontin immunostaining, increased interstitial space, and interstitial myofibroblast accumulation. Two possible mechanisms could account for this. First, on day 35 there were still many interstitial T cells in spite of macrophage abolition which may contribute to ongoing interstitial damage and fibrosis. Second, damaged tubular may themselves release pro-fibrotic and pro-inflammatory cytokines that promote myofibroblast accumulation.

An interesting finding in day 35 study was that abrogation of macrophage accumulation by fms-I treatment resulting in a minor, but significant, reduction in interstitial deposition of collagen IV and interstitial volume. This was not accompanied by a significant reduction in , the cells considered to be the main source of type IV collagen protein, although this could be within the margin of error for these data. This minor reduction in interstitial fibrosis was also not accompanied by a significant reduction in tubular damage.

In contrast to interstitial myofibroblasts, we found that macrophage depletion reduced periglomerular myofibroblast accumulation. In the day 14 study, fms-I treatment prevented substantial periglomerular myofibroblast accumulation, while high dose fms-I treatment in established disease partially reduced

periglomerular myofibroblast accumulation. These data are consistent with a study in anti-GBM disease using CD11b-DTR transgenic mouse in which tissue macrophages can be specifically and selectively ablated by minute injections of diphtheria toxin. Depletion of renal inflammatory macrophages through day 15 and 20 reduced periglomerular myofibroblasts (*Duffield et al., 2005*).

7.2.5 fms-I treatment and pro-inflammatory factors

Upregulation of pro-inflammatory factors such as TNF- α , iNOS and MMP-12 have been implicated in causing glomerular crescent formation in anti-GBM crescentic glomerulonephritis. Glomerular production of TNF- α has been described in human and experimental crescentic glomerulonephritis (*Tipping et al., 1991; Noronha et al., 1993*). The blockade of TNF- α activity by a soluble dimeric form of the p55 chain of the Type I TNF- α receptor in rat anti-GBM crescentic glomerulonephritis model largely abolished crescent formation as a result of reduced intrarenal macrophage accumulation and glomerular cell proliferation (*Lan et al., 1996*). Suppression of TNF- α expression by depletion of macrophage infiltrate in our study may contribute to reduction of crescent formation via diminishing glomerular inflammation and cell proliferation.

Expression of iNOS was hardly detected by real time PCR in high dose of fms-I treated rats with anti-GBM disease, in which almost all intrarenal macrophage infiltrates were abolished and the kidneys displayed only very mild changes compared to normal kidneys. This result is consistent with previous reports that the expression of iNOS is induced in various types of cells, especially

macrophages, in the inflammatory lesions, whereas iNOS expression is hardly detected in the normal kidney (*Heeringa et al., 1998*). Excessive amount of nitric oxide radicals generated by iNOS may accelerate the tissue injury in inflammatory lesions. High levels of NO radicals have been reported to inactivate iron-containing enzymes in the mitochondria, resulting in cytotoxicity (*Radi et al., 2002*). It was also reported that NO and its derivatives directly inactivate glutathione peroxidase leading to an increase in intracellular peroxides that are responsible for cellular peroxides that are responsible for cellular damage (*Asahi et al., 1997*). A detrimental role for macrophage nitric oxide production in forming crescents in anti-GBM disease is generally expected, although other studies reported that iNOS does not play a part in the induction and progress of anti-GBM disease in iNOS-deficiency mice model (*Cattell et al., 1998*).

Matrix metalloproteinase-12 (MMP-12) is a member of the MMP family with the ability to degrade extracellular matrix components by degrading elastin and other basement membrane components such as fibronectin and collagen IV (*Banda et al., 1981; Gronski et al., 1997; Shipley et al., 1996*). Kaneko *et al* reported MMP-12 is one of the highly expressed genes in a rat anti-GBM crescentic glomerulonephritis model using DNA arrays and discovered MMP-12 produced by macrophage infiltrates in the glomeruli and/or crescents was a major contributor to crescent formation in rat anti-GBM crescentic glomerulonephritis (*Kaneko et al., 2003*). In our study, macrophage depletion prevented up-regulation of MMP-12 which was associated with much less

crescent formation . This supports the postulate that MMP-12 is produced by infiltrated macrophages and plays an important role in crescent formation in anti-GBM crescentic glomerulonephritis.

7.2.6 fms-I treatment and T cell and dendritic cell infiltration

It is well established that T cells play a critical role in directing immune-mediated renal injury in progressive anti-GBM disease (*Huang et al., 1994; Wu et al., 2002*). In current study, fms-I treatment did not appear to affect the T cell response in anti-GBM disease. c-fms blockade did not affect glomerular T cell recruitment on day 1 or 5. By day 14, fms-I treatment did reduce glomerular, and in particular, interstitial T cell accumulation. However, It is most likely that this significant reduction simply reflects the lack of glomerular and tubulointerstitial damage resulting from reduced pro-inflammatory cytokines production. In this study, we also found c-fms inhibition did not alter glomerular deposition of rat IgG and C3 on day 14 of anti-GBM disease. It seems that depletion of macrophages by fms-I treatment did not modulate the humoral immune response in the anti-GBM disease.

Renal dendritic cells are major constituents of the mononuclear phagocytic system within the normal kidney (*John et al., 2007; Kaissling et al., 2008*). The role of dendritic cells in immunologic kidney disease has been seen renewed interest. Several descriptive studies using specific dendritic cell markers in human renal biopsy have demonstrated accumulation of renal dendritic cells during renal inflammation (*Fiore et al., 2008; Tucci et al., 2008; Sergerer et al.,*

2008). These reports suggest dendritic cell accumulation may worsen renal injury. However, a finding from *in vivo* studies show contradicting results. After systemically abating accumulating inflammatory CD11c⁺ dendritic cells in mice with experimental nephrotoxic nephritis, tubulointerstitial and glomerular injury was aggravated rather than ameliorated (Scholz *et al.*, 2008). Data from the current studies showed that fms-I treatment had little effect on glomerular accumulation of cells expressing the dendritic cell markers, OX-62, CD11c and OX-6 on day 1 of anti-GBM disease; however, but at day 14 of disease fms-I treatment caused a profound reduction in the dendritic cell populations identified by these markers.

An important issue is the source of dendritic cells present at sites of inflammation (Leon *et al.*, 2008; Segura *et al.*, 2009); are they derived from a distinct myeloid precursor population, migratory “conventional” dendritic cells, or derived from monocytes? It is well established that blood monocytes can be differentiated into dendritic cells *in vitro*, but whether this is a major mechanism for dendritic cell production *in vivo* is controversial. The identification of dendritic cells is a difficult matter since they share expression of many antigens with macrophages (Rogers *et al.*, 2009). MHC class II antigens are strongly expressed by all dendritic cells, but they can also be expressed by macrophages and other cell types. In contrast, CD11c and OX-62 are relatively specific dendritic cell markers. Our study suggests that the renal dendritic cells seen on day 14 of anti-GBM disease, as identified by expression of MHC class II, CD11c and OX-62, are dependent upon M-CSF/c-fms signaling and thus are

most probably monocyte-derived. However, we cannot exclude the possibility that dendritic cell population drives through local differentiation of a different blood leukocyte population which is diminished when renal injury is suppressed.

Blockade of M-CSF/c-fms signaling through c-fms inhibition by fms-I treatment is potentially clinically applicable due to its selectivity and efficacy in targeting monocytes and macrophages. Conventional treatment such as cyclophosphamide and prednisolone are potent immunosuppressive agents, but their use is limited by their non-selectivity causing a range of side-effects including the risk of opportunistic infection. Liposome clodronate and diphtheria toxin strategies can only be used in animal models. Blockade of pro-inflammatory cytokines, such as IL-1 and TNF- α , can prevent renal dysfunction, proteinuria and ameliorate renal lesions in rat anti-GBM crescentic glomerulonephritis model; however, positive data from clinical trials in RPGN are still lacking. Therefore, c-fms inhibition is considered as a selective and clinically applicable therapeutic approach to treat rapidly progressive glomerulonephritis.

7.3 Further studies

There are several issues that require future investigations in immune mediated glomerulonephritis.

First, it would be instructive to investigate the heterogeneity of the macrophage population in anti-GBM disease and how this is affected by different treatments. This could be done by antibody-based methods for isolating pure macrophage populations from glomeruli and the tubulointerstitium, followed by cDNA array analysis and/or real time RT-PCR analysis. This would provide insight into which macrophage populations cause damage and which are protective/reparative.

Second, many papers claim that proteinuria directly causes tubulointerstitial damage (*Abbate et al., 2006*). Therefore, the impact of heavy proteinuria on tubules should be further studied using more sensitive markers of tubular damage (for example, KIM-1) in the day 14 study. A longer study could be used to determine whether sustained macrophage depletion can prevent tubular cell activation and tubulointerstitial damage in the face of ongoing heavy proteinuria.

Third, an intervention study with fms-I treatment starting at an earlier time (e.g. day 7 to 35 or day 10 to 35) may address the question of whether macrophages are critical for the progression of cellular to fibrocellular crescents and how this relates to rupture of Bowman's capsule. This would also be a further test for the potential clinical settings in which fms-I treatment could be effective.

Finally, combination of fms-I and angiotensin II blockade as an intervention treatment in progressive crescent glomerulonephritis should be investigated since this would determine whether any added benefit could be gained and it

also reflects the setting in which a therapy such as fms-I would be used clinically.

7.4 Conclusions

ERK signaling in mouse obstructed kidney

In the mouse unilateral ureteric obstruction model, ERK phosphorylation was inhibited by U0126 treatment, and the proliferation and accumulation of interstitial F4/80⁺ macrophages were significantly reduced. However, ERK blockade had no effect upon renal interstitial fibrosis. Thus, interstitial accumulation of macrophages but not tubulointerstitial fibrosis in the obstructed kidney is, in part, dependent upon the MEK-ERK signaling pathway.

JNK signaling in rat mesangial proliferative nephritis

Activation of the JNK signaling was identified in a rat model of mesangial proliferative nephritis (Thy-1 disease). However, administration of CC401, a well characterized JNK inhibitor, failed to modify mesangial cell apoptosis in the early phase (Day 0-3) of Thy-1 disease or to affect mesangial cell proliferation and matrix deposition in the late phase (Day 3-8) of Thy-1 disease. This was despite achieving target serum CC401 levels and having evidence of JNK blockade in glomeruli.

c-fms blockade in anti-GBM glomerulonephritis

The role of macrophages in the pathogenesis of rat crescentic glomerulonephritis was examined in a rat model of rapidly progressive

crescentic glomerulonephritis (anti-GBM disease) using a novel inhibitor of the M-CSF/c-fms signaling pathway termed fms-I. In the first experiment, fms-I treatment was given during the induction phase of disease (days 0 to 14). This treatment reversed an early glomerular macrophage infiltration, and prevented glomerular and tubulointerstitial damage and loss of renal function. This was associated with prevention of the upregulation of pro-inflammatory factors and dendritic cell infiltration. In the second experiment, fms-I treatment was given during established crescentic disease (day 14 to 35). fms-I treatment reversed the renal macrophage infiltrate, improved renal function, had a minor beneficial effect upon crescent formation and reduced interstitial fibrosis in terms of the deposition of collagen IV. Thus, while fms-I treatment was highly effective when given early in the disease process, it still had beneficial effects when given late in the disease.

Chapter 8. Bibliography

Abbate M., Zoja C., Remuzzi G. (2006). How does proteinuria cause progressive renal damage? *J Am Soc Nephrol.* 17:2974-2984.

Alexopoulos, E., Seron, D., Hartley, R.B., Nolasco, F., Cameron, J.S. (1989). Immune mechanisms in idiopathic membranous nephropathy: the role of the interstitial infiltrates. *Am J Kidney Dis.*13: 4004-4012.

Aitman, T.J., Dong, R., Vyse, T.J., Norsworthy, P.J., Johnson, M.D., Smith, J., Mangion, J., Robertson-Lowe, C., Marshall, A.J., Petretto, E. (2006). Copy number polymorphism in *Fcgr3* predisposes to glomerulonephritis in rats and humans. *Nature.* 439, 851-855.

Aliberti, J.C., Machado, F.S., Souto, J.T., Campanelli, A.P., Teixeira, M.M., Gazzinelli, R.T., Silva, J.S., (1999). Beta-Chemokines enhance parasite uptake and promote nitric oxide-dependent microbistatic activity in murine inflammatory macrophages infected with *Trypanosoma cruzi*. *Infect Immun.* 67: 4819-4826.

Allen,W.E., Jones, G.E., Pollard, J.W., Ridley A.J., (1997). Rho, Rac and Cdc42 regulate actin organization and cell adhesion in macrophages. *J Cell Sci.* 110: 707-720.

Ammit, A.J., Panettieri, R.A. Jr., (2001). Invited review: The circle of life: Cell cycle regulation in airway smooth muscle. *J Appl Physiol.* 91: 1431–1437.

Asahi M, Fujii J, Takao T, Kuzuya T, Hori M, Shimonishi Y, Taniguchi N. (1997).

The oxidation of selenocysteine is involved in the inactivation of glutathione peroxidase by nitric oxide donor. *J Biol Chem.* 272:19152-7.

Atkins RC, Holdsworth SR, Glasgow EF, Matthews FE. (1976). The macrophage in human rapidly progressive glomerulonephritis. *Lancet.* 17:830-2.

Atkins, R.C., Nikolic-Paterson, D.J., Song, Q., Lan, H.Y., (1996). Modulators of crescentic glomerulonephritis. *J Am Soc Nephrol* 7: 2271-2278.

Australia & New Zealand Dialysis and Transplant Registry (ANZDATA) annual report: 6-7, 2009

Austyn, J.M., Hankins, D.F., Larsen, C.P., Morris, P.J., Rao, A.S., Roake, J.A. (1994). Isolation and characterization of dendritic cells from mouse heart and kidney. *J Immunol* 152: 2401– 2410.

Badillo-Almaráz, I., Daza, L., Avalos-Díaz, E., Herrera-Esparza, R., (2001). Glomerular expression of Fas ligand and Bax mRNA in lupus nephritis. *Autoimmunity* 34: 283-289.

Bagchus, W.M., Hoedemaeker, P.J., Rozing, J., (1986). Glomerulonephritis induced by monoclonal anti-Thy 1.1 antibodies, A sequential histological and ultrastructural study in the rat. *Lab Invest.* 55:680–687.

Baker, A.J., Mooney, A., Hughes. J., Lombardi, D., Johnson, R.J., Savill, J. (1994). Mesangial cell apoptosis: the major mechanism for resolution of glomerular hypercellularity in experimental mesangial proliferative nephritis. *J Clin Invest* 94: 2105–2116.

Banda MJ, Werb Z. (1981). Mouse macrophage elastase. Purification and characterization as a metalloproteinase. *Biochem J.* 193:589-605.

Beaven, M.A., Metzger, H. (1993). Signal transduction by Fc receptors: The Fc epsilon RI case. *Immunol Today* 14: 222–226.

Behmoaras, J., Bhangal, G., Smith, J., McDonald, K., Mutch, B., Lai, P.C., Domin, J., Game, L., Salama, A., Foxwell, B.M., Pusey, C.D., Cook, H.T., Aitman, T.J. (2008). Jund is a determinant of macrophage activation and is associated with glomerulonephritis susceptibility. *Nat Genet.* 40: 553-559.

Behrens, A., Sibilio, M., Wagner, E.F. (1999). Amino-terminal phosphorylation of c-Jun regulates stress-induced apoptosis and cellular proliferation. *Nat Genet.* 21: 326-329.

Behrens, A., Sibilio, M., David, J.P., Möhle-Steinlein, U., Tronche, F., Schütz, G., Wagner, E.F. (2002). Impaired postnatal hepatocyte proliferation and liver regeneration in mice lacking c-jun in the liver. *EMBO J.* 21: 1782-1790.

Bloom, P.D., Florquin, R., Singer, G.G., Brennan, D.C., Kelley, V.R., (1993). Colony stimulating factor- 1 in the induction of lupus nephritis. *Kidney Int.* 43: 1000-1009.

Bokemeyer, D., Sorokin, A., Dunn, M.J. (1996). Multiple intracellular MAP kinase signaling cascades. *Kidney Int.* 49: 1187–1198.

Bokemeyer, D., Panek, D., Kramer, H.J., Lindemann, M., Kitahara, M., Boor, P., Kerjaschki, D., Trzaskos, J.M., Floege, J., Ostendorf, T. (2002). *In vivo* identification of the mitogen-activated protein kinase cascade as a central pathogenic pathway in experimental mesangioproliferative glomerulonephritis. *J Am Soc Nephrol.* 13: 1473–1480.

Bogoyevitch MA. (2006). The isoform-specific functions of the c-Jun N-terminal Kinases (JNKs): differences revealed by gene targeting. *Bioessays*. 28:923-934.

Brady, H.R. (1994). Leukocyte adhesion molecules and kidney diseases. *Kidney Int*. 45:1285–1300.

Brouwer, E., Huitema, M.G., Mulder, A.H., Heeringa, P., van Goor, H., Tervaert, J.W., Weening, J.J., Kallenberg, C.G. (1994). Neutrophil activation in vitro and in vivo in Wegener' s granulomatosis. *Kidney Int*. 45:1120–1131.

Cambien, B., Pomeranz, M., Millet, M.A., Rossi, B., Schmid-Alliana, A. (2001). Signal transduction involved in MCP-1-mediated monocytic transendothelial migration. *Blood* 97: 359-366.

Camussi, G., Cappio, F.C., Messina, M., Coppo, R., Stratta, P., Vercellone, A. (1980). The polymorphonuclear neutrophil (PMN) immunohistological technique: detection of immune complexes bound to the PMN membrane in acute poststreptococcal and lupus nephritis. *Clin Nephrol*. 14: 280–287.

Cattell V, Cook HT, Ebrahim H, Waddington SN, Wei XQ, Assmann KJ, Liew FY. (1998). Anti-GBM glomerulonephritis in mice lacking nitric oxide synthase type 2. *Kidney Int*. 53:932-936.

Cecchini, M.G., Dominguez, M.G., Mocci, S., Wetterwald, A., Felix, R., Fleisch, H., Chisholm, O., Hofstetter, W., Pollard, J.W., Stanley, E.R. (1994). Role of colony stimulating factor-1 in the establishment and regulation of tissue macrophages during postnatal development of the mouse. *Development*. 120: 1357-1372.

Chadban, S.J., Atkins, R.C., (2005). Glomerulonephritis. *Lancet* 365,1797-1806.

Chitu V, Stanley ER., (2006). Colony-stimulating factor-1 in immunity and inflammation. *Curr Opin Immunol.*18:39-48.

Coates, P.T., Duncan, F.J., Colvin, B.L., Wang, Z., Zahorchak, A.F., (2004). Shufesky, W.J., Morelli, A.E., Thomson, A.W., (2004). *In vivo*-mobilized kidney dendritic cells are functionally immature, subvert alloreactive T-cell responses, and prolong organ allograft survival. *Transplantation* 77, 1080–1089.

Cochrane, C.G., Unanue, E.R., Dixon, F.J., (1965). A role of polymorphonuclear leukocytes and complement in nephrotoxic nephritis. *J Exp Med.* 122: 99–116.

Cohen, C.D., Calvaresi, N., Armelloni, S., Schmid, H., Henger, A., Ott, U., Rastaldi, M.P., Kretzler, M., (2005). CD20-positive infiltrates in human membranous glomerulonephritis. *J Nephrol.* 18: 328-333.

Constant, S., Schweitzer, N., West, J., Ranney, P., Bottomly, K., (1995). B lymphocytes can be competent antigen-presenting cells for priming CD4+ T cells to protein antigens in vivo. *J Immunol.* 155: 3734-3741.

Couser, W.G. (1988). Rapidly progressive glomerulonephritis: Classification, pathogenetic mechanisms, and therapy. *Am J Kidney Dis* XI:449-464.

Couser, W.G., Johnson, R.J., (1994). Mechanisms of progressive renal disease in glomerulonephritis. *Am J Kidney Dis.* 23: 193-198.

Cybulsky, A.V. (2000). Growth factor pathways in proliferative glomerulonephritis. *Curr Opin Nephrol Hypertens.* 9: 217–223.

D'Amico, G., Ferrario, F., Rastaldi, M.P. (1995). Tubulointerstitial damage in glomerular diseases: its role in the progression of renal damage. *Am J Kidney*

Dis. 26:124-132.

Dai, X.M., Ryan, G.R., Hapel, A.J., Dominguez, M.G., Russell, R.G., Kapp, S., Sylvestre, V., Stanley, E.R. (2002). Targeted disruption of the mouse colony stimulating factor 1 receptor gene results in osteopetrosis, mononuclear phagocyte deficiency, increased primitive progenitor cell frequencies, and reproductive defects. *Blood* 99: 111–120.

Dai, X.M., Zong, X.H., Sylvestre, V., Stanley, E.R. (2004). Incomplete restoration of colony-stimulating factor 1 (CSF-1) function in CSF-1-deficient *Csf1op/Csf1op* mice by transgenic expression of cell surface CSF-1. *Blood* 103: 1114–1123.

De Borst, M.H, Prakash, J., Melenhorst, W.B., van den Heuvel, M.C., Kok, R.J., Navis, G., van Goor, H. (2007). Glomerular and tubular induction of the transcription factor c-Jun in human renal disease. *J Pathol.* 213: 219-228.

Di Mari, J.F., Davis, R., Safirstein, R.L. (1999). MAPK activation determines renal epithelial cell survival during oxidative injury. *Am J Physiol* 277, 195–203.

Dixon, R., Brunskill, N.J. (2000). Albumin stimulates p44/p42 extracellular-signal-regulated mitogen-activated protein kinase in opossum kidney proximal tubular cells. *Clin Sci (Lond)* 98: 295–301.

Donadelli, R., Zanchi, C., Morigi, M., Buelli, S., Batani, C., Tomasoni, S., Corna, D., Rottoli, D., Benigni, A., Abbate, M., Remuzzi, G., Zoja, C. (2003). Protein overload induces fractalkine upregulation in proximal tubular cells through nuclear factor kappaB- and p38 mitogen-activated protein kinase-dependent pathways. *J Am Soc Nephrol.* 14: 2436–2446.

Dong, X., Swaminathan, S., Bachman, L.A., Croatt, A.J., Nath, K.A., Griffin,

M.D. (2005). Antigen presentation by dendritic cells in renal lymph nodes is linked to systemic and local injury to the kidney. *Kidney Int.* 68:1096–1108.

Dong, X., Bachman, L.A., Miller, M.N., Nath, K.A., Griffin, M.D. (2008). Dendritic cells facilitate accumulation of IL-17 T cells in the kidney following acute renal obstruction. *Kidney Int.* 74: 1294–1309.

Downer, G., Phan, S.H., Wiggins, R.C. (1988). Analysis of renal fibrosis in a rabbit model of crescentic nephritis. *J Clin Invest.* 82: 998-1006.

Duffield, J.S., Tipping, P.G., Kipari, T., Cailhier, J.F., Clay, S., Lang, R., Bonventre, J.V., Hughes, J. (2005). Conditional ablation of macrophages halts progression of crescentic glomerulonephritis. *Am J Pathol.* 167:1207-1219.

Eardley, K.S., Zehnder, D., Quinkler, M., Lepenies, J., Bates, R.L., Savage, C.O., Howie, A.J., Adu, D., Cockwell, P. (2006). The relationship between albuminuria, MCP-1/CCL2, and interstitial macrophages in chronic kidney disease. *Kidney Int.* 69: 1189-1197.

Ehara, T., Shigematsu, H. (1998). Contribution of mast cells to the tubulointerstitial lesions in IgA nephritis. *Kidney Int.* 54: 1675–1683.

Erwig, L.P., Kluth, D.C., Walsh, G.M., Rees, A.J. (1998). Initial cytokine exposure determines function of macrophages and renders them unresponsive to other cytokines. *J Immunol.* 161: 1983-1988.

Favata MF, Horiuchi KY, Manos EJ, Daulerio AJ, Stradley DA, Feeser WS, Van Dyk DE, Pitts WJ, Earl RA, Hobbs F, Copeland RA, Magolda RL, Scherle PA, Trzaskos JM. (1998). Identification of a novel inhibitor of mitogen-activated protein kinase kinase. *J Biol Chem.* 273:18623-18632.

Fiorentino, D.F., Zlotnik, A., Vieira, P., Mosmann, T.R., Howard, M., Moore, K.W., O'Garra, A. (1991). IL-10 acts on the antigen-presenting cell to inhibit cytokine production by Th1 cells. *J Immunol.* 146: 3444-3451.

Flanc, R.S., Ma, F.Y., Tesch, G.H., Han, Y., Atkins, R.C., Bennett, B.L., Friedman, G.C., Fan, J.H., Nikolic-Paterson, D.J. (2007). A pathogenic role for JNK signaling in experimental anti-GBM glomerulonephritis. *Kidney Int.* 72: 698-708.

Floege, J., Johnson, R.J., Couser, W.G. (1992). Mesangial cells in the pathogenesis of progressive glomerular disease in animal models. *Clin Investig.* 70: 857-864.

Foti, M., Granucci, F., Ricciardi-Castagnoli, P. (2004). A central role for tissue-resident dendritic cells in innate responses. *Trends Immunol.* 25: 650–654.

Fiore, N., Castellano, G., Blasi, A., Capobianco, C., Loverre, A., Montinaro, V., Netti, S., Torres, D., Manno, C., Grandaliano, G., Ranieri, E., Schena, F.P., Gesualdo, L. (2008). Immature myeloid and plasmacytoid dendritic cells infiltrate renal tubulointerstitium in patients with lupus nephritis. *Mol Immunol.* 45: 259–265.

Gerber, J.S., Mosser, D. M. (2001). Reversing lipopolysaccharide toxicity by ligating the macrophage Fc c receptors. *J Immunol.* 166: 6861-6868.

Gilbert, R.E., Kelly, D.J., McKay, T., Chadban, S., Hill, P.A., Cooper, M.E., Atkins, R.C., Nikolic-Paterson, D.J. (2001). PDGF signal transduction inhibition ameliorates experimental mesangial proliferative glomerulonephritis. *Kidney Int.* 59: 1324-1332.

Goerdts, S., Politz, O., Schledzewski, K., Birk, R., Gratchev, A., Guillot, P., Hakiy, N., Klemke, C.D., Dippel, E., Kodelja, V., Orfanos, C.E. (1999). Alternative versus classical activation of macrophages. *Pathobiology* 67: 222-226.

Gomez-Guerrero, C., Hernandez-Vargas, P., Lopez-Franco, O. (2005). Mesangial cells and glomerular inflammation: From the pathogenesis to novel therapeutic approaches. *Curr Drug Targets Inflamm Allergy* 4: 341–351.

Gordon, S. (2007). The macrophage: past, present and future. *Eur J Immunol.* 37 Suppl 1: S9-17.

Green, D.R., Kroemer, G. (2004). The pathophysiology of mitochondrial cell death. *Science.* 305: 626-629.

Gronski TJ Jr, Martin RL, Kobayashi DK, Walsh BC, Holman MC, Huber M, Van Wart HE, Shapiro SD. (1997). Hydrolysis of a broad spectrum of extracellular matrix proteins by human macrophage elastase. *J Biol Chem.* 272:12189-12194.

Hamilton JA. (1997). CSF-1 signal transduction. *J Leukoc Biol.* ;62:145-155.

Hancock, W.W., Atkins, R.C. (1984). Cellular composition of crescents in human rapidly progressive glomerulonephritis identified using monoclonal antibodies. *Am J Nephrol.* 4: 177-181.

Hara, M., Batsford, S.R., Mihatsch, M.J., Bitter-Suermann, D., Vogt, A. (1991). Complement and monocytes are essential for provoking glomerular injury in passive Heymann nephritis in rats. *Lab Invest.* 65: 168-179.

Haraldsson, B., Nyström, J., Deen, W.M. (2008). Properties of the glomerular

barrier and mechanisms of proteinuria. *Physiol Rev.* 88: 451-487.

Harris, D.P., Haynes, L., Sayles, P.C., Duso, D.K., Eaton, S.M., Lepak, N.M., Johnson, L.L., Swain, S.L., Lund, F.E. (2000). Reciprocal regulation of polarized cytokine production by effector B and T cells. *Nat Immunol.* 1: 475-482.

Hart, D.N., Fabre, J.W. (1981a). Demonstration and characterization of Ia-positive dendritic cells in the interstitial connective tissues of rat heart and other tissues, but not brain. *J Exp Med.* 154: 347-361.

Hart, D.N., Fabre, J.W. (1981b). Major histocompatibility complex antigens in rat kidney, ureter, and bladder. Localization with monoclonal antibodies and demonstration of Ia-positive dendritic cells. *Transplantation* 31: 318-325.

Hayashida, T., Poncelet, A.C., Hubchak, S.C., Schnaper, H.W. (1999). TGFbeta1 activates MAP kinase in human mesangial cells: A possible role in collagen expression. *Kidney Int.* 56: 1710–1720.

Hayashida, T., Decaestecker, M., Schnaper, H.W. (2003). Cross-talk between ERK MAP kinase and Smad signaling pathways enhances TGFbeta- dependent responses in human mesangial cells. *FASEB J.* 17: 1576–1578.

Heller, F., Lindenmeyer, M.T., Cohen, C.D., Brandt, U., Draganovici, D., Fischereeder, M., Kretzler, M., Anders, H.J., Sitter, T., Mosberger, I., Kerjaschki, D., Regele, H., Schlöndorff, D., Segerer, S. (2007). The contribution of B cells to renal interstitial inflammation. *Am J Pathol.* 170: 457-468.

Henderson NC, Mackinnon AC, Farnworth SL, Kipari T, Haslett C, Iredale JP, Liu FT, Hughes J, Sethi T. (2008). Galectin-3 expression and secretion links macrophages to the promotion of renal fibrosis. *Am J Pathol.* 172: 288-298.

Henson, P.M. (1972). Pathologic mechanisms in neutrophil-mediated injury. *Am J Pathol.* 68: 593–612.

Heeringa P, van Goor H, Moshage H, Klok PA, Huitema MG, de Jager A, Schep AJ, Kallenberg CG. (1998). Expression of iNOS, eNOS, and peroxynitrite-modified proteins in experimental anti-myeloperoxidase associated crescentic glomerulonephritis. *Kidney Int.* 53: 382-393

Hill, P.A., Lan, H.Y., Nikolic-Paterson, D.J., Atkins, R.C. (1994). ICAM-1 directs migration and localization of interstitial leukocytes in experimental glomerulonephritis. *Kidney Int.* 45: 32-42.

Hill CS, Wynne J, Treisman R. (1995). The Rho family GTPases RhoA, Rac1, and CDC42Hs regulate transcriptional activation by SRF. *Cell.* 30;81:1159-1170.

Hinz, B. (2007). Formation and function of the myofibroblast during tissue repair. *J Invest Dermatol.* 127: 526-537.

Hinz, B., Phan, S.H., Thannickal, V.J., Galli, A., Bochaton-Piallat, M.L., Gabbiani, G. (2007). The myofibroblast: one function, multiple origins. *Am J Pathol.* 170: 1807-1816.

Hochegger, K., Siebenhaar, F., Vielhauer, V., Heining, D., Mayadas, T.N., Mayer, G., Maurer, M., Rosenkranz, A.R. (2005). Role of mast cells in experimental anti-glomerular basement membrane glomerulonephritis. *Eur J Immunol.* 35: 3074–3082

Holdsworth, S.R., Neale, T.J., Wilson, C.B. (1981). Abrogation of macrophage-dependent injury in experimental glomerulonephritis in the rabbit. Use of an antimacrophage serum. *J Clin Invest.* 68: 686-698.

Holdsworth, S.R., Kitching, A.R., Tipping, P.G. (1999). Th1 and Th2 T helper cell subsets affect patterns of injury and outcomes in glomerulonephritis. *Kidney Int.* 55: 1198-1216.

Hooke, D.H., Hancock, W.W., Gee, D.C., Kraft, N., Atkins, R.C. (1984). Monoclonal antibody analysis of glomerular hypercellularity in human glomerulonephritis. *Clin Nephrol.* 22:163-168.

Hooke, D.H., Gee, D.C., Atkins, R.C. (1987). Leukocyte analysis using monoclonal antibodies in human glomerulonephritis. *Kidney Int.* 31: 964-972.

Huang, X.R., Holdsworth, S.R., Tipping, P.G. (1994). Evidence for delayed-type hypersensitivity mechanisms in glomerular crescent formation. *Kidney Int.* 46: 69–78.

Huang, X.R., Tipping, P.G., Apostolopoulos, J., Oettinger, C., D'Souza, M., Milton, G., Holdsworth, S.R. (1997). Mechanisms of T cell-induced glomerular injury in anti-glomerular basement membrane (GBM) glomerulonephritis in rats. *Clin Exp Immunol.* 109: 134–142.

Hughes, J., Cailhier, J.F., Watson, S., Savill, J.S. (2004). Apoptosis in glomerulonephritis. *Rheum Dis Clin North Am.* 30: 655-676.

Ikezumi, Y., Hurst, L.A., Masaki, T., Atkins, R.C., Nikolic-Paterson, D.J. (2003). Adoptive transfer studies demonstrate that macrophages can induce proteinuria

and mesangial cell proliferation. *Kidney Int.* 63: 83-95.

Ikezumi Y, Hurst L, Atkins RC, Nikolic-Paterson DJ. (2004) . Macrophage-mediated renal injury is dependent on signaling via the JNK pathway. *J Am Soc Nephrol.* 15:1775-1784.

Ingham DJ, Beer S, Money S, Hansen G. (2001). Quantitative real-time PCR assay for determining transgene copy number in transformed plants. *Biotechniques.* 31:132-134, 136-40.

Inoki K, Haneda M, Ishida T, Mori H, Maeda S, Koya D, Sugimoto T, Kikkawa R. (2000). Role of mitogen-activated protein kinases as downstream effectors of transforming growth factor-beta in mesangial cells. *Kidney Int Suppl.* 77: S76-80.

Isbel, N.M., Nikolic-Paterson, D.J., Hill, P.A., Dowling, J., Atkins, R.C. (2001a). Local macrophage proliferation correlates with increased renal M-CSF expression in human glomerulonephritis. *Nephrol Dial Transplant* 16:1638-1647.

Isbel, N.M., Hill, P.A., Foti, R., Mu, W., Hurst, L.A., Stambe, C., Lan, H.Y., Atkins, R.C., Nikolic-Paterson, D.J. (2001b). Tubules are the major site of M-CSF production in experimental kidney disease: correlation with local macrophage proliferation. *Kidney Int.* 60: 614-625.

Isome M, Fujinaka H, Adhikary LP, Kovalenko P, El-Shemi AG, Yoshida Y, Yaoita E, Takeishi T, Takeya M, Naito M, Suzuki H, Yamamoto T. (2004). Important role for macrophages in induction of crescentic anti-GBM glomerulonephritis in WKY rats. *Nephrol Dial Transplant.* 19: 2997-3004.

Jaworowski, A., Wilson, N.J., Christy, E., Byrne, R., Hamilton, J.A. (1999).

Roles of the mitogen-activated protein kinase family in macrophage responses to colony stimulating factor-1 addition and withdrawal. *J Biol Chem.* 274: 15127-15133.

Jefferson, J.A., Johnson, R.J. (1999). Experimental mesangial proliferative glomerulonephritis (the anti-Thy-1.1 model). *J Nephrol.* 12: 297-307.

Jo SK, Cho WY, Sung SA, Kim HK, Won NH. (2005). MEK inhibitor, U0126, attenuates cisplatin-induced renal injury by decreasing inflammation and apoptosis. *Kidney Int.* 67: 458-466.

John, R., Nelson, P.J. (2007). Dendritic cells in the kidney. *J Am Soc Nephrol.* 18: 2628–2635.

Jones, S.E., Gilbert, R.E., Kelly, D.J. (2004). Tranilast reduces mesenteric vascular collagen deposition and chymase-positive mast cells in experimental diabetes. *J Diabetes Complications* 18: 309–315.

Jose, M.D., Le Meur, Y., Atkins, R.C., Chadban, S.J. (2003). Blockade of macrophage colony-stimulating factor reduces macrophage proliferation and accumulation in renal allograft rejection. *Am J Transplant.* 3: 294-300

Jun, C.D., Yoon, H.J., Kim, H.M., Chung, H.T. (1995). Fibronectin activates murine peritoneal macrophages for tumor cell destruction in the presence of IFN- γ . *Biochem. Biophys. Res. Commun.* 206: 969-974.

Kaissling, B., Le Hir, M. (1994). Characterization and distribution of interstitial cell types in the renal cortex of rats. *Kidney Int.* 45: 709-720.

Kaissling, B., Le Hir, M. (2008). The renal cortical interstitium: morphological

and functional aspects. *Histochem Cell Biol.* 130: 247-262.

Kanamaru, Y., Scandiuzzi, L., Essig, M., Brochetta, C., Guerin-Marchand, C., Tomino, Y., Monteiro, R.C., Peuchmaur, M., Blank, U. (2006). Mast cell-mediated remodeling and fibrinolytic activity protect against fatal glomerulonephritis. *J Immunol.* 176: 5607–5615.

Kaneko Y, Sakatsume M, Xie Y, Kuroda T, Igashima M, Narita I, Gejyo F. (2003). Macrophage metalloelastase as a major factor for glomerular injury in anti-glomerular basement membrane nephritis. *J Immunol.* 170:377-385.

Kawasaki, K., Yaoita, E., Yamamoto, T., Kihara, I. (1992). Depletion of CD8 positive cells in nephrotoxic serum nephritis of WKY rats. *Kidney Int.* 41: 1517-1526.

Kawano, H., Kim, S., Ohta, K., Nakao, T., Miyazaki, H., Nakatani, T., Iwao, H. (2003). Differential contribution of three mitogen-activated protein kinases to PDGF-BB-induced mesangial cell proliferation and gene expression. *J Am Soc Nephrol.* 14: 584-592.

Kurts, C., Heymann, F., Lukacs-Kornek, V., Boor, P., Floege, J. (2007). Role of T cells and dendritic cells in glomerular immunopathology. *Semin Immunopathol.* 29: 317-335.

Kerr, P.G., Lan, H., Atkins, R.C. (1996). Rapidly progressive glomerulonephritis. In: Schrier RW, Gottschalk CW, eds. *Diseases of the Kidney*, 6th ed. Boston: Little, Brown; press.

Kitamura, Y. (1989). Heterogeneity of mast cells and phenotypic change between subpopulations. *Annu Rev Immunol.* 7: 59–76.

Kikuchi, H., Kawachi, H., Ito, Y., Matsui, K., Nosaka, H., Saito, A., Orikasa, M., Arakawa, M., Shimizu, F. (2000). Severe proteinuria, sustained for 6 months, induces tubular epithelial cell injury and cell infiltration in rats but not progressive interstitial fibrosis. *Nephrol Dial Transplant.* 15: 799-810.

Kim, D.H., Moon, S.O., Jung, Y.J., Lee, A.S., Kang, K.P., Lee, T.H., Lee, S., Chai, O.H., Song, C.H., Jang, K.Y., Sung, M.J., Zhang, X., Park, S.K., Kim, W. (2009). Mast cells decrease renal fibrosis in unilateral ureteral obstruction. *Kidney Int.* 75:1031-1038.

Klahr, S., Morrissey, J. (2002). Obstructive nephropathy and renal fibrosis. *Am. J. Physiol. Renal Physiol.* 283: 861–875.

Kyriakis, J.M., Avruch, J. (2001). Mammalian mitogen-activated protein kinase signal transduction pathways activated by stress and inflammation. *Physiol. Rev.* 81: 807–869.

Lake, F.R., Noble, P.W., Henson, P.M., Riches, D.W. (1994) Functional switching of macrophage responses to tumor necrosis factor α (TNF α) by interferons. Implications for the pleiotropic activities of TNF- α . *J. Clin. Invest.* 93: 1661-1669.

Lan, H.Y., Nikolic-Paterson, D.J., Atkins, R.C. (1992). Involvement of activated periglomerular leukocytes in the rupture of Bowman's capsule and glomerular crescent progression in experimental glomerulonephritis. *Lab Invest.* 67: 743-751.

Lan, H.Y., Nikolic-Paterson, D.J., Atkins, R.C. (1993). Trafficking of inflammatory macrophages from the kidney to draining lymph nodes during experimental glomerulonephritis. *Clin Exp Immunol.* 92: 336-341.

Lan, H.Y., Mu, W., Yang, N., Meinhardt, A., Nikolic-Paterson, D.J., Ng, Y.Y., Bacher, M., Atkins, R.C., Bucala, R. (1996). De Novo renal expression of macrophage migration inhibitory factor during the development of rat crescentic glomerulonephritis. *Am J Pathol.* 149:1119-1127.

Lan, H.Y., Yang, N., Metz, C., Mu, W., Song, Q., Nikolic-Paterson, D.J., Bacher, M., Bucala, R., Atkins, R.C. (1997). TNF-alpha up-regulates renal MIF expression in rat crescentic glomerulonephritis. *Mol Med.* 3: 136-144.

Lan, H.Y., Nikolic-Paterson, D.J., Mu, W., Atkins, R.C. (1997a). Local macrophage proliferation in the pathogenesis of glomerular crescent formation in rat anti-glomerular basement membrane (GBM) glomerulonephritis. *Clin Exp Immunol.* 110: 233-240.

Lan, H.Y., Mitsuhashi, H., Ng, Y.Y., Nikolic-Paterson, D.J., Yang, N., Mu, W., Atkins, R.C., (1997b). Macrophage apoptosis in rat crescentic glomerulonephritis. *Am J Pathol.* 151: 531-538.

Lan, H.Y. (2003). Tubular epithelial-myofibroblast transdifferentiation mechanisms in proximal tubule cells. *Curr Opin Nephrol Hypertens.* 12: 25-29.

Le Hir M, Keller C, Eschmann V, Hähnel B, Hosser H, Kriz W. (2001). Podocyte bridges between the tuft and Bowman's capsule: an early event in experimental crescentic glomerulonephritis. *J Am Soc Nephrol.* 12: 2060-2071.

Le Meur, Y., Jose, M.D., Mu, W., Atkins, R.C., Chadban, S.J. (2002). Macrophage colony-stimulating factor expression and macrophage accumulation in renal allograft rejection. *Transplantation.* 73:1318-1324.

Le Meur, Y., Leprivey-Lorgeot, V., Mons, S., José, M., Dantal, J., Lemauff, B.,

Aldigier, J.C., Leroux-Robert, C., Praloran, V. (2004). Serum levels of macrophage-colony stimulating factor (M-CSF): a marker of kidney allograft rejection. *Nephrol Dial Transplant.* 19:1862-1925.

Lenda, D.M., Kikawada, E., Stanley, E.R., Kelley, V.R. (2003). Reduced macrophage recruitment, proliferation, and activation in colony-stimulating factor-1-deficient mice results in decreased tubular apoptosis during renal inflammation. *J Immunol.*170: 3254-3262.

Lenda, D.M., Stanley, E.R., Kelley, V.R. (2004). Negative role of colony-stimulating factor-1 in macrophage, T cell, and B cell mediated autoimmune disease in MRL-Fas(lpr) mice. *J Immunol.*173: 4744-4754.

Le-Niculescu, H., Bonfoco, E., Kasuya, Y., Claret, F.X., Green, D.R., Karin, M. (1999). Withdrawal of survival factors results in activation of the JNK pathway in neuronal cells leading to Fas ligand induction and cell death. *Mol Cell Biol.* 19: 751-763.

León B, Ardavín C. (2008). Monocyte-derived dendritic cells in innate and adaptive immunity. *Immunol Cell Biol.* 86: 320-324.

Lin SL, Kisseleva T, Brenner DA, Duffield JS. (2008). Pericytes and perivascular fibroblasts are the primary source of collagen-producing cells in obstructive fibrosis of the kidney. *Am J Pathol.* 173: 1617-1627.

Little MA, Pusey CD. (2005). Glomerulonephritis due to antineutrophil cytoplasm antibody-associated vasculitis: an update on approaches to management. *Nephrology (Carlton).* 10: 368-376.

Liu, J., Lin, A. (2005). Role of JNK activation in apoptosis: A double edged

sword. *Cell Res.* 15: 36–42.

Lloyd, C.M., Dorf, M.E., Proudfoot, A., Salant, D.J., Gutierrez-Ramos, J.C. (1997). Role of MCP-1 and RANTES in inflammation and progression to fibrosis during murine crescentic nephritis. *J Leukoc Biol.* 62: 676-680.

Ludewig, D., Kosmehl, H., Sommer, M., Böhmer, F.D., Stein, G. (2000). PDGF receptor kinase blocker AG1295 attenuates interstitial fibrosis in rat kidney after unilateral obstruction. *Cell Tissue Res.* 299: 97-103.

Lysaght, M.J. (2002). Maintenance dialysis population dynamics: current trends and long-term implications. *J Am Soc Nephrol.* 13 Suppl 1, S37-40.

Ma, F.Y., Flanc, R.S., Tesch, G.H., Han, Y., Atkins, R.C., Bennett, B.L., Friedman, G.C., Fan, J.H., Nikolic-Paterson, D.J. (2007). A pathogenic role for c-Jun amino-terminal kinase signaling in renal fibrosis and tubular cell apoptosis. *J Am Soc Nephrol.* 18: 472-484.

Ma, F.Y., Liu, J., Kitching, A.R., Manthey, C.L., Nikolic-Paterson, D.J. (2009a). Targeting renal macrophage accumulation via c-fms kinase reduces tubular apoptosis but fails to modify progressive fibrosis in the obstructed rat kidney. *Am J Physiol Renal Physiol.* 296: 177-185.

Ma, F.Y., Liu, J., Nikolic-Paterson, D.J. (2009b). The role of stress-activated protein kinase signaling in renal pathophysiology. *Braz J Med Biol Res.* 42: 29-37.

Ma FY, Flanc RS, Tesch GH, Bennett BL, Friedman GC, Nikolic-Paterson DJ.

(2009c)..Blockade of the c-Jun amino terminal kinase prevents crescent formation and halts established anti-GBM glomerulonephritis in the rat. *Lab Invest.* 89: 470-484.

Mahajan, D., Wang, Y., Qin, X., Wang, Y., Zheng, G., Wang, Y.M., Alexander, S.I., Harris, D.C. (2006). CD4+CD25+ regulatory T cells protect against injury in an innate murine model of chronic kidney disease. *J Am Soc Nephrol.* 17: 2731-2741.

Makino, H., Sugiyama, H., Yamasaki, Y., Maeshima, Y., Wada, J., Kashihara, N. (2003). Glomerular cell apoptosis in human lupus nephritis. *Virchows Arch.* 443, 67–77.

Masaki, T., Foti, R., Hill, P.A., Ikezumi, Y., Atkins, R.C., Nikolic-Paterson, D.J. (2003). Activation of the ERK pathway precedes tubular proliferation in the obstructed rat kidney. *Kidney Int.* 63:1256-1264.

Masaki, T., Stambe, C., Hill, P.A., Dowling, J., Atkins, R.C., Nikolic-Paterson, D.J. (2004). Activation of the extracellular-signal regulated protein kinase pathway in human glomerulopathies. *J Am Soc Nephrol.* 15: 1835-1843.

Markovic-Lipkovski, J., Müller, C.A., Rislér, T., Bohle, A., Müller, G.A. (1990). Association of glomerular and interstitial mononuclear leukocytes with different forms of glomerulonephritis. *Nephrol Dial Transplant.* 5:10-17.

Matsuda, M., Shikata, K., Makino, H., Sugimoto, H., Otam Z. (1996). Glomerular expression of macrophage colony-stimulating factor and granulocyte-macrophage colony-stimulating factor in patients with various forms of glomerulonephritis. *Lab Invest.* 75: 403-412.

Matsusaka, T., Xin, J., Niwa, S., Kobayashi, K., Akatsuka, A., Hashizume, H., Wang, Q.C., Pastan, I., Fogo, A.B., Ichikawa, I. (2005). Genetic engineering of glomerular sclerosis in the mouse via control of onset and severity of podocyte-specific injury. *J Am Soc Nephrol*. 16: 1013-1023.

Magil, A.B. (1985). Histogenesis of glomerular crescents. Immunohistochemical demonstration of cytokeratin in crescent cells. *Am J Pathol*. 120: 222-229.

Matsumoto, K. (1990). Production of interleukin-1 by glomerular macrophages in nephrotoxic serum nephritis. *Am J Nephrol*. 10: 502-506.

Minden, A., Lin, A., McMahon, M., Lange-Carter, C., Dérijard, B., Davis, R.J., Johnson, G.L., Karin, M. (1994). Differential activation of ERK and JNK mitogen-activated protein kinases by Raf-1 and MEKK. *Science* 266:1719-1723.

Miyazawa, S., Hotta, O., Doi, N., Natori, Y., Nishikawa, K., Natori, Y. (2004). Role of mast cells in the development of renal fibrosis: Use of mast cell-deficient rats. *Kidney Int* 65: 2228–2237.

Moeller, M.J., Soofi, A., Hartmann, I., Le Hir, M., Wiggins, R., Kriz, W., Holzman, L.B. (2004). Podocytes populate cellular crescents in a murine model of inflammatory glomerulonephritis. *J Am Soc Nephrol*. 15: 61-67.

Morita, T., Suzuki, Y., Churg, J. (1973). Structure and development of the glomerular crescent. *Am J Pathol*. 72: 349-368.

Morigi, M., Macconi, D., Zoja, C., Donadelli, R., Buelli, S., Zanchi, C., Ghilardi, M., Remuzzi, G. (2002). Protein overload-induced NfκB activation in proximal tubular cells requires H₂O₂ through a PKC-dependent pathway. *J Am Soc Nephrol* 13: 1179–1189.

Morel-Maroger Striker, L., Killen, P.D., Chi, E., Striker, G.E. (1984). The composition of glomerulosclerosis. I. Studies in focal sclerosis, crescentic glomerulonephritis, and membranoproliferative glomerulonephritis. *Lab Invest.* 51: 181-192.

Munz, C., Steinman, R.M., Fujii, S. (2005). Dendritic cell maturation by innate lymphocytes: Coordinated stimulation of innate and adaptive immunity. *J Exp Med.* 202: 203–207.

Mu W, Ouyang X, Agarwal A, Zhang L, Long DA, Cruz PE, Roncal CA, Glushakova OY, Chiodo VA, Atkinson MA, Hauswirth WW, Flotte TR, Rodriguez-Iturbe B, Johnson RJ. (2005) IL-10 suppresses chemokines, inflammation, and fibrosis in a model of chronic renal disease *J Am Soc Nephrol.*16: 3651-3660.

Naish, P.F., Thomson, N.M., Simpson, I.J., Peters, D.K. (1975). The role of polymorphonuclear leucocytes in the autologous phase of nephrotoxic nephritis. *Clin Exp Immunol.* 22:102–111.

Naito, T., Masaki, T., Nikolic-Paterson, D.J., Tanji, C., Yorioka, N., Kohno, N. (2004). Angiotensin II induces thrombospondin-1 production in human mesangial cells via p38 MAPK and JNK: a mechanism for activation of latent TGF-beta1. *Am J Physiol Renal Physiol.* 286: 278-287.

Nikolic-Paterson DJ, Atkins RC. (2001). The role of macrophages in glomerulonephritis. *Nephrol Dial Transplant.*16 Suppl 5:3-7.

Nikolic-Paterson, D.J. (2003). A role for macrophages in mediating tubular cell apoptosis? *Kidney Int.* 63: 1582-1583.

Nishikawa, K., Guo, Y.J., Miyasaka, M., Tamatani, T., Collins, A.B., Sy, M.S., McCluskey, R.T., Andres, G. (1993). Antibodies to intercellular adhesion molecule 1/lymphocyte function-associated antigen 1 prevent crescent formation in rat autoimmune glomerulonephritis. *J Exp Med.* 177: 667-677

Noronha, I.L., Kruger, C., Andrassy, K., Ritz, E., Waldherr, R. (1993). In situ production of TNF-alpha, IL- 1 beta and IL-2R in ANCA-positive glomerulonephritis. *Kidney Int* .43: 682-692.

Okada, H., Moriwaki, K., Kalluri, R. (2000). Inhibition of monocyte chemoattractant protein-1 expression in tubular epithelium attenuates tubulointerstitial alteration in rat Goodpasture syndrome. *Kidney Int.* 57: 927–936.

Otsubo, S., Nitta, K., Uchida, K., Yumura, W., Nihei, H. (2003). Mast cells and tubulointerstitial fibrosis in patients with ANCA-associated glomerulonephritis. *Clin Exp Nephrol.* 7: 41–47.

Park, E.J., Zhao, Y.Z., Kim, Y.C., Sohn, D.H. (2007). Bakuchiol-induced caspase-3-dependent apoptosis occurs through c-Jun NH2-terminal kinase-mediated mitochondrial translocation of Bax in rat liver myofibroblasts. *Eur J Pharmacol.* 559: 115-123.

Pat, B.K., Cuttle, L., Watters, D., Yang, T., Johnson, D.W., Gobe, G.C. (2003). Fibrogenic stresses activate different mitogen-activated protein kinase pathways in renal epithelial, endothelial or fibroblast cell populations. *Nephrology (Carlton).* 8: 196-204.

Pat, B., Yang, T., Kong, C., Watters, D., Johnson, D.W., Gobe, G.. (2005). Activation of ERK in renal fibrosis after unilateral ureteral obstruction: modulation by antioxidants. *Kidney Int.* 67: 931-943.

Payne DM, Rossomando AJ, Martino P, Erickson AK, Her JH, Shabanowitz J, Hunt DF, Weber MJ, Sturgill TW. (1991). Identification of the regulatory phosphorylation sites in pp42/mitogen-activated protein kinase (MAP kinase). *EMBO J.* 10:885-892.

Pixley, F.J., Stanley, E.R. (2004). CSF-1 regulation of the wandering macrophage: complexity in action. *Trends Cell Biol.* 14: 628-638.

Qi, W., Chen, X., Poronnik, P., Pollock, C.A. (2006). The renal cortical fibroblast in renal tubulointerstitial fibrosis. *Int J Biochem Cell Biol.* 38: 1–5.

Rastaldi, M.P., Ferrario, F., Crippa, A., Dell'Antonio, G., Casartelli, D., Grillo, C., D'Amico, G. (2000). Glomerular monocyte-macrophage features in ANCA-positive renal vasculitis and cryoglobulinemic nephritis. *J Am Soc Nephrol.* 11: 2036-2043.

Remuzzi, G., Chiurciu, C., Abbate, M., Brusegan, V., Bontempelli, M., Ruggenti, P. (2002). Rituximab for idiopathic membranous nephropathy. *Lancet* 360: 923–924.

Riedl, S.J., Salvesen, G.S. (2007). The apoptosome: Signalling platform of cell death. *Nat Rev Mol Cell Biol.* 8: 405–413.

Rodemann, H.P., Muller, G.A. (1991). Characterization of human renal fibroblasts in health and disease: II. In vitro growth, differentiation, and collagen synthesis of fibroblasts from kidneys with interstitial fibrosis. *Am J Kidney Dis.* 17: 684–686.

Roberts, I.S., Burrows, C., Shanks, J.H. (1997). Interstitial myofibroblasts: Predictors of progression in membranous nephropathy. *J Clin Pathol.* 50:123-

127.

Radi R, Cassina A, Hodara R. (2002). Nitric oxide and peroxynitrite interactions with mitochondria. *Biol Chem.* 383: 401-409

Rovin, B.H., Rumancik, M., Tan, L., Dickerson, J. (1994). Gbomerubar expression of monocyte chemoattractant protein- 1 in experimental and human gbomerubonephritis. *Lab Invest.* 71: 536-542.

Rogers NM, Matthews TJ, Kausman JY, Kitching AR, Coates PT. (2009). Review article: Kidney dendritic cells: their role in homeostasis, inflammation and transplantation. *Nephrology (Carlton).* 14: 625-35.

Rodríguez-Iturbe, B., Pons, H., Herrera-Acosta, J., Johnson, R.J. (2001). Role of immunocompetent cells in nonimmune renal diseases. *Kidney Int.* 59: 1626-1640.

Ruger, B.M., Hasan, Q., Greenhill, N.S., Davis, P.F., Dunbar, P.R., Neale, T.J. (1996). Mast cells and type VIII collagen in human diabetic nephropathy. *Diabetologia* 39: 1215–1222.

Ryan, G.R., Dai, X.M., Dominguez, M.G., Tong, W., Chuan, F., Chisholm, O., Russell, R.G., Pollard, J.W., Stanley, E.R. (2001). Rescue of the colony-stimulating factor 1 (CSF-1)-nullizygous mouse (*Csf1op/Csf1op*) phenotype with a CSF-1 transgene and identification of sites of local CSF-1 synthesis. *Blood* 98: 74–84.

Sabapathy, K., Wagner, E.F. (2004). JNK2: a negative regulator of cellular proliferation. *Cell Cycle.* 3:1520-1523.

Saeki, T., Kuroda, T., Morita, T., Suzuki, K., Arakawa, M., Kawasaki, K. (1995). Significance of myeloperoxidase in rapidly progressive glomerulonephritis. *Am J Kidney Dis.* 26:13–21.

Salama, A.D., Pusey, C.D. (2006). Drug insight: rituximab in renal disease and transplantation. *Nat Clin Pract Nephrol.* 2: 221–230.

Sanz, A.B., Santamaría, B., Ruiz-Ortega, M., Egido, J., Ortiz, A. (2008). Mechanisms of renal apoptosis in health and disease. *J Am Soc Nephrol.* 19: 1634-1642.

Scholz, J., Lukacs-Kornek, V., Engel, D.R., Specht, S., Kiss, E., Eitner, F., Floege, J., Groene, H.J., Kurts, C. (2008). Renal dendritic cells stimulate IL-10 production and attenuate nephrotoxic nephritis. *J Am Soc Nephrol.* 19: 527–537.

Schnoor M, Cullen P, Lorkowski J, Stolle K, Robenek H, Troyer D, Rauterberg J, Lorkowski S. (2008). Production of type VI collagen by human macrophages: a new dimension in macrophage functional heterogeneity. *J Immunol.* 180: 5707-5719.

Schreiner, G.F., Cotran, R.S., Pardo, V., Unanue, E.R. (1978). A mononuclear cell component in experimental immunological glomerulonephritis. *J Exp Med.* 147: 369-384.

Schreiner, G.F., Kiely, J.M., Cotran, R.S., Unanue, E.R. (1981). Characterization of resident glomerular cells in the rat expressing Ia determinants and manifesting genetically restricted interactions with lymphocytes. *J Clin Invest.* 68: 920-931.

Segerer S, Heller F, Lindenmeyer MT, Schmid H, Cohen CD, Draganovici D, Mandelbaum J, Nelson PJ, Gröne HJ, Gröne EF, Figel AM, Nössner E, Schlöndorff D. (2008). Compartment specific expression of dendritic cell markers in human glomerulonephritis. *Kidney Int.* 74: 37-46.

Segura E, Wong J, Villadangos JA. (2009). Cutting edge: B220+CCR9- dendritic cells are not plasmacytoid dendritic cells but are precursors of conventional dendritic cells. *J Immunol.* 183: 1514-1517.

Shankland, S.J. (2006). The podocyte's response to injury: role in proteinuria and glomerulosclerosis. *Kidney Int.* 69: 2131-2147.

Shiple J, Wesselschmidt RL, Kobayashi DK, Ley TJ, Shapiro SD. (1996). Metalloelastase is required for macrophage-mediated proteolysis and matrix invasion in mice. *Proc Natl Acad Sci U S A.* 93: 3942-3946.

Shultz, P.J., DiCorleto, P.E., Silver, B.J., Abboud, H.E. (1988). Mesangial cells express PDGF mRNAs and proliferate in response to PDGF. *Am J Physiol.* 255: 674-684.

Sigaud, S., Evelson, P., Gonzalez-Flecha, B. (2005). H₂O₂-induced proliferation of primary alveolar epithelial cells is mediated by MAP kinases. *Antioxid. Redox Signal.* 7: 6–13.

Smeets, B., Dijkman, H.B., Wetzels, J.F., Steenbergen, E.J. (2006). Lessons from studies on focal segmental glomerulosclerosis: An important role for parietal epithelial cells? *J. Pathol.* 210: 263–267

Soos, T.J., Sims, T.N., Barisoni, L., Lin, K., Littman, D.R., Dustin, M.L., Nelson, P.J. (2006). CX3CR1+ interstitial dendritic cells form a contiguous network

throughout the entire kidney. *Kidney Int.* 70: 591–596.

Stachura, I, S.L., Whiteside, T.L. (1984). Mononuclear-cell subsets in human idiopathic crescentic glomerulonephritis (ICGN): analysis in tissue sections with monoclonal antibodies. *J Clin Immunol.* 4: 202-208.

Stanley, E.R. (2001) The hematopoietic cytokines. In *Samter's Immunological Diseases* (Austen, K.F. et al., eds), pp. 175–193, Lippincott Williams and Wilkins

Stein, M., Keshav, S., Harris, N. Gordon, S. (1992). Interleukin 4 potently enhances murine macrophage mannose receptor activity, a marker of alternative immunologic macrophage activation. *J. Exp. Med.* 176: 287-292.

Steinmetz, O.M., Velden, J., Kneissler, U., Marx, M., Klein, A., Helmchen, U., Stahl, R.A., Panzer, U. (2008). Analysis and classification of B-cell infiltrates in lupus and ANCA-associated nephritis. *Kidney Int.* 74: 448-457.

Strom, T.B., Koulmanda, M. (2009). Recently discovered T cell subsets cannot keep their commitments. *J Am Soc Nephrol.* 20:1677-1680.

Suzuki H, Uchida K, Nitta K, Nihei H. (2004). Role of mitogen-activated protein kinase in the regulation of transforming growth factor-beta-induced fibronectin accumulation in cultured renal interstitial fibroblasts. *Clin Exp Nephrol.* 8: 188-195.

Takazoe, K., Tesch, G.H., Hill, P.A., Hurst, L.A., Jun, Z., Lan, H.Y., Atkins, R.C., Nikolic-Paterson, D.J. (2000). CD44-mediated neutrophil apoptosis in the rat. *Kidney Int.* 58: 1920-1930.

Tang, W.W., Qi, M., Warren, J.S. (1996). Monocyte chemoattractant protein 1

mediates glomerular macrophage infiltration in anti-GBM Ab GN. *Kidney Int.* 50: 665-671.

Tang, S., Leung, J.C.K., Abe, K., Wah Chan, K., Chan, L.Y.Y., Mao Chan, T., Neng Lai, K. (2003). Albumin stimulates interleukin-8 expression in proximal tubular epithelial cells in vitro and in vivo. *J Clin Invest.* 111: 515-527.

Tesch, G.H., Schwarting, A., Kinoshita, K., Lan, H.Y., Rollins, B.J., Kelley, V.R. (1999). Monocyte chemoattractant protein-1 promotes macrophage-mediated tubular injury, but not glomerular injury, in nephrotoxic serum nephritis. *J Clin Invest.* 103:73-80.

Thorner, P.S., Ho, M., Eremina, V., Sado, Y., Quaggin, S. (2008). Podocytes contribute to the formation of glomerular crescents. *J Am Soc Nephrol.* 19: 495-502.

Thorburn, A. (2004). Death receptor-induced cell killing. *Cell Signal.* 16:139-144.

Tian, W., Zhang, Z., Cohen, D.M. (2000). MAPK signaling and the kidney. *Am J Physiol Renal Physiol* 279: 593–604.

Timoshanko JR, Kitching R, Semple TJ, Tipping PG, Holdsworth SR. (2006). A pathogenetic role for mast cells in experimental crescentic glomerulonephritis. *J Am Soc Nephrol.* 17: 150–159.

Tipping, P.G., Thomson, N.M., Holdsworth, S.R. (1986). A comparison of fibrinolytic and defibrinating agents in established experimental glomerulonephritis. *Br J Exp Pathol.* 67: 481-491.

Tipping, P.G., Leong, T.W., Holdsworth, S.R. (1991). Tumor necrosis factor production by glomerular macrophages in antiglomerular basement membrane glomerulonephritis in rabbits. *Lab Invest.* 65: 272-279.

Tipping, P.G., Huang, X.R., Qi, M., Van, G.Y., Tang, W.W. (1998). Crescentic glomerulonephritis in CD4- and CD8-deficient mice. Requirement for CD4 but not CD8 cells. *Am J Pathol.* 152: 1541–1548.

Tipping, P.G., Kitching, A.R. (2005). Glomerulonephritis, Th1 and Th2: what's new? *Clin Exp Immunol.* 142: 207-215.

Toth, T., Toth-Jakatics, R., Jimi, S., Ihara, M., Urata, H., Takebayashi, S. (1999). Mast cells in rapidly progressive glomerulonephritis. *J Am Soc Nephrol* 10: 1498–1505.

Tournier, C., Hess, P., Yang, D.D., Xu, J., Turner, T.K., Nimnual, A., Bar-Sagi, D., Jones, S.N., Flavell, R.A., Davis, R.J. (2000). Requirement of JNK for stress-induced activation of the cytochrome c-mediated death pathway. *Science.* 288: 870-874.

Tucci, M., Quatraro, C., Lombardi, L., Pellegrino, C., Dammacco, F., Silvestris, F. (2008). Glomerular accumulation of plasmacytoid dendritic cells in active lupus nephritis: role of interleukin-18. *Arthritis Rheum.* 58: 251–262.

Uehara, T., Xi Peng, X., Bennett, B., Satoh, Y., Friedman, G., Currin, R., Brenner, D.A., Lemasters, J. (2004). c-Jun N-terminal kinase mediates hepatic injury after rat liver transplantation *Transplantation* 78: 324–332.

Uehara, T., Bennett, B., Sakata, S.T., Satoh, Y., Bilter, G.K., Westwick, J.K., Brenner, D.A. (2005). JNK mediates hepatic ischemia reperfusion injury. *J*

Hepatol. 42: 850–859.

Van Kooten C, Daha MR, van Es LA. (1999). Tubular epithelial cells: A critical cell type in the regulation of renal inflammatory processes. *Exp Nephrol.* 7: 429-437.

Valujskikh, A., Li, X.C. (2007). Frontiers in nephrology: T cell memory as a barrier to transplant tolerance. *J Am Soc Nephrol.* 18: 2252-2261.

Vleming, L.J., Baelde, J.J., Westendorp, R.G.J., Daha, M.R., Van Es, L.A., Bruijn, J.A. (1995). Progression of chronic renal disease in humans is associated with the deposition of basement membrane components and decorin in the interstitial extracellular matrix. *Clin Nephrol.* 44: 211–219.

Webb, S.E., Pollard, J.W., Jones, G.E. (1996). Direct observation and quantification of macrophage chemoattraction to the growth factor CSF-1. *J Cell Sci.* 109: 793-803.

Weber, C., Springer, T.A. (1998). Interaction of very late antigen-4 with VCAM-1 supports transendothelial chemotaxis of monocytes by facilitating lateral migration. *J Immunol.* 161: 6825-6834.

Westerhuis, R., van Straaten, S.C., van Dixhoorn, M.G., van Rooijen, N., Verhagen, N.A., Dijkstra, C.D., de Heer, E., Daha, M.R. (2000). Distinctive roles of neutrophils and monocytes in anti-thy-1 nephritis. *Am J Pathol.* 156: 303-310.

Weston, C.R., Davis, R.J. (2007). The JNK signal transduction pathway. *Curr Opin Cell Biol.* 19: 142-149.

Wharram, B.L., Goyal, M., Wiggins, J.E., Sanden, S.K., Hussain, S., Filipiak, W.E., Saunders, T.L., Dysko, R.C., Kohno, K., Holzman, L.B., Wiggins, R.C. (2005). Podocyte depletion causes glomerulosclerosis: diphtheria toxin-induced podocyte depletion in rats expressing human diphtheria toxin receptor transgene. *J Am Soc Nephrol.* 16: 2941-2952.

Wiggins, J.E., Goyal, M., Sanden, S.K., Wharram, B.L., Shedden, K.A., Misek, D.E., Kuick, R.D., Wiggins, R.C. (2005). Podocyte hypertrophy, "adaptation," and "decompensation" associated with glomerular enlargement and glomerulosclerosis in the aging rat: prevention by calorie restriction. *J Am Soc Nephrol.* 16: 2953-2966.

Wolf, D., Hochegger, K., Wolf, A.M., Rumpold, H.F., Gastl, G., Tilg, H., Mayer, G., Gunsilius, E., Rosenkranz, A.R. (2005). CD4+CD25+ regulatory T cells inhibit experimental anti-glomerular basement membrane glomerulonephritis in mice. *J Am Soc Nephrol.* 16: 1360-1370.

Wu, J., Hicks, J., Borillo, J., Glass, W.F., Lou, Y.H. (2002). CD4(+) T cells specific to a glomerular basement membrane antigen mediate glomerulonephritis. *J Clin Invest.* 109: 517-524.

Xia, Z., Dickens, M., Raingeaud, J., Davis, R.J., Greenberg, M.E. (1995). Opposing effects of ERK and JNK-p38 MAP kinases on apoptosis. *Science.* 270:1326-1331.

Yamada, M., Ueda, M., Naruko, T., Tanabe, S., Han, Y.S., Ikura, Y., Ogami, M., Takai, S., Miyazaki, M. (2001). Mast cell chymase expression and mast cell phenotypes in human rejected kidneys. *Kidney Int* 59: 1374–1381.

Yang, N., Isbel, N.M., Nikolic-Paterson, D.J., Li, Y., Ye, R., Atkins, R.C., Lan,

H.Y. (1998). Local macrophage proliferation in human glomerulonephritis. *Kidney Int.* 54: 143-151.

Yang, P.T., Xiao, W.G., Zhao, L.J., Lu, J., He, L.M., Kasai, H., Ito, M. (2008). Increase in the level of macrophage colony-stimulating factor in patients with systemic lupus erythematosus. *Ann Rheum Dis.* 67: 429-430.

Yen, H., Zhang, Y., Penfold, S., Rollins, B.J. (1997). MCP-1-mediated chemotaxis requires activation of non-overlapping signal transduction pathways. *J Leukoc Biol.* 61: 529-532.

Yu, X.Q., Nikolic-Paterson, D.J., Mu, W., Giachelli, C.M., Atkins, R.C., Johnson, R.J., Lan, H.Y.. (1998). A functional role for osteopontin in experimental crescentic glomerulonephritis in the rat. *Proc Assoc Am Physicians.* 110: 50-64.

Yu XQ, Fan JM, Nikolic-Paterson DJ, Yang N, Mu W, Pichler R, Johnson RJ, Atkins RC, Lan HY. (1999). IL-1 up-regulates osteopontin expression in experimental crescentic glomerulonephritis in the rat. *Am J Pathol.* 154: 833-841.

Zhao M, Ding J, Liu Y, Zou W, Wang H. (2001) A clinical and pathological analysis of 41 patients with anti-glomerular basement membrane antibody related diseases. *Zhonghua Nei Ke Za Zhi.* 40:316-320.

Zoja C, Garcia PB, Remuzzi G. (2009). The role of chemokines in progressive renal disease. *Front Biosci* 14:1815-1822.

Zurawski, G., de Vries, J.E. (1994). Interleukin 13, an interleukin 4-like cytokine that acts on monocytes and B cells, but not on T cells. *Immunol Today.* 15:19-26.

Table 1.1

Main types of chronic kidney disease by pathology

Glomerular disease

Primary glomerular diseases

- Minimal change nephrotic syndrome (MCNS)
- Focal segmental glomerulosclerosis (FSGS)
- Membranous glomerulonephritis
- Mesangial proliferative glomerulonephritis
- Membranoproliferative glomerulonephritis (MPGN)
- Crescentic glomerulonephritis (Goodpasture syndrome)

Secondary glomerular diseases

- Lupus nephritis
- Diabetic nephropathy
- IgA nephropathy
- Anti-neutrophil cytoplasmic autoantibody (ANCA) associated nephritis

Tubulointerstitial diseases

Tubulointerstitial nephritis (e.g. pyelonephritis)

Non-inflammatory tubulointerstitial diseases (e.g. obstructive nephropathy)

Table 2.1 Primary antibodies (Monoclonal) used in this Thesis

Primary Antibody	Target Antigen	Supplier	Tissue Fixation	Staining Method and antigen retrieval
Mouse anti-BrdU, Bu20a	<i>BrdU</i>	<i>Dako, Glostrup, Denmark</i>	<i>Formalin</i>	<i>PAP (Microwave)</i>
Mouse anti-α-Smooth Muscle Actin, 1A4	α -Smooth Muscle Actin	Sigma-Aldrich, Castle Hill, NSW, Australia	Formalin	PAP
Mouse anti-rat CD68, ED1	rat CD68	Serotec, Oxford, UK	Formalin, PLP	PAP
Mouse anti-rat T cell receptor, R73	rat T cell receptor	Serotec, Oxford, UK	PLP	PAP
Mouse anti-rat RP1 recognising rat neutrophils	rat neutrophils	Becton Dickinson, San Diego, CA, USA	PLP	PAP
Mouse anti-vimentin	vimentin	Dako, Glostrup, Denmark	Formalin	PAP
Mouse anti-rat OX-62	Integrin α E2	Serotec	SNAP	ABC
Mouse anti-rat CD11c	Integrin α X	Serotec	SNAP	ABC
Mouse anti-rat OX-19	CD5,67KD glycoprotein	Prof Alan F Williams, Oxford University	SNAP	ABC
Mouse anti-rat Ki-67	rat Ki-67	Dako	Formalin	PAP
Mouse anti-rat RECA-1	Reca-1	Serotec	PLP	ABC
Mouse anti-rat OX-7	CD90	Prof Alan F Williams	Methyl Carnoy	PAP
Mouse anti-rat CD11b, OX42	Integrin α M	Prof Alan F Williams	SNAP	ABC
Mouse anti-rat MHC II, OX-6	CD74, MHC class II RT1B	Prof Alan F Williams	SNAP	ABC
Mouse anti-osteopontin, MPIII-B10	Osteopontin	University of Iowa city, IA, USA	Formalin	PAP

Table 2.2 **Primary antibodies (Polyclonal) used in this Thesis**

Primary Antibody	Target Antigen	Supplier	Tissue Fixation	Staining Method and antigen retrieval
Rabbit anti-phospho-JNK (Tyr183/Tyr185)	phospho-JNK (Tyr183/Tyr185)	Cell Signaling San Diego, CA, USA	Formalin	ABC (Microwave)
Rabbit anti-phospho-ERK	phospho-ERK	Cell Signaling	Formalin	ABC (Microwave)
Rabbit anti-ERK2/ERK1	ERK2/ERK1	Santa Cruz, Santa Cruz, CA, USA	Formalin	ABC (Microwave)
Rabbit anti-cleaved caspase-3	cleaved caspase-3	Cell Signaling	Formalin	ABC (Microwave)
Rabbit anti-c-Jun	anti-c-Jun	Cell Signaling	Formalin	ABC (Microwave)
Rabbit anti-phospho-c-Jun (Serine 63)	phospho-c-Jun (Serine 63)	Cell Signaling	Formalin	ABC (Microwave)
Rabbit anti-phospho-c-Jun (Serine 73)	phospho-c-Jun (Serine 73)	Cell Signaling	Formalin	ABC (Microwave)
Rabbit anti-WT1	Wilms tumor 1 protein	Santa Cruz, CA, USA	Formalin	ABC (Microwave)
Rabbit anti-α-tubulin	α -tubulin	Rockland	SNAP frozen	Western Blotting
Rabbit anti-phospho-P38	phospho-P38	Cell Signaling	Formalin	ABC (microwave)
Rabbit anti-phospho-P44/42(T202/Y204)	phospho-P44/42(T202/Y204)	Cell Signaling	Formalin	ABC (microwave)
Goat anti-collagen IV	collagen IV	Southern Biotechnology, Birmingham, AL, USA	Methyl Carnoy	ABC
FITC conjugated rabbit anti-sheep IgG	sheep IgG	Dako	SNAP frozen	Immunofluorescence
FITC conjugated rabbit anti-rat IgG	rat IgG	Sigma-Aldrich	SNAP frozen	Immunofluorescence

Table 2.3 Secondary antibodies used in this Thesis

Secondary Antibody	Source
Horseradish peroxidase conjugated goat anti-mouse IgG	Dako
Mouse peroxide conjugated goat anti-mouse IgG	Dako
Horseradish peroxidase conjugated goat anti-rabbit IgG	Dako
Rabbit peroxidase conjugates anti-peroxidase complexes (PAP)	Dako
Biotinylated goat anti-rabbit IgG	Zymed-Invitrogen, South San Francisco, CA, USA
Biotinylated goat anti-mouse IgG	Zymed-Invitrogen
Alkaline phosphatase conjugated goat anti-mouse IgG	Dako
Alkaline phosphatase conjugated mouse anti-alkaline phosphatase complexes (APAAP)	Dako

Table 2.4 Sequences of primers and probes used in this Thesis

Rat TNF-α	<i>Forward primer: 5'GGC TGC CCC GAC TAC GT 3'</i> <i>Reverse primer: 5'TTT CTC CTG GTA TGA GAT AGC AAA TC 3'</i> <i>Probe: 5'FAM-TCA CCC ACA CCG TCA G-NFQ 3'</i>
Rat iNOS	<i>Forward: 5'TTC AGAGTC AAA TCC TAC CAA G 3'</i> <i>Reverse: 5'TGT GTT GTT GGG CTG GGA ATA 3'</i> <i>probe: 5'GAA AGA GGA AAA GGA CA 3'</i>
Rat MCP-1	<i>Forward: 5'TGA CCC ATA AAT CTG AAG CTA A 3'</i> <i>Reverse: 5'GGC ATC ACA TTC CAA ATC ACA C 3'</i> <i>Probe: 5'ACA ACC ACC TCA AGCAC 3'</i>
Rat Kim-1	<i>Forward: 5'TAAACCAGAAATTCCCACAAG</i> <i>Reverse: 5' TGTTGGAGTAGAGGTGGAGA</i> <i>Probe: 5'CAACAAGACCCACAAC</i>
Rat MMP12	<i>Forward: 5' GTCACAACAGTGGGAGATAA</i> <i>Reverse: 5' GGCCACATGGAAGAAATTGAAG</i> <i>Probe: 5' AGTCCAGCCACCAACA</i>
Rat IL-12	<i>Forward: 5' CTTCTTCATCAGGGACATCATC</i> <i>Reverse: 5' CCTCTGTCTCCTTCGTCTTTTC</i> <i>Probe: 5' CCATTCTACTTCTCC</i>
Rat Arginase-1	<i>Forward: 5' GACTGACTTTCAACAGGAT</i> <i>Reverse: 5' GGTCCAGTCCATCAACATCAAA</i> <i>Probe: 5' GGAAGGAAGAAAAGGC</i>
Rat CD206	<i>Forward: 5' GACAGATATGAACAAGCATTCC</i> <i>Reverse: 5' TGAACATCTGAGAGTCCTGTCC</i> <i>Probe: 5' GTTTGGTTGGATTGAGG</i>
Rat CD163	<i>Forward: 5' TGGTTCTTCTTGAGGTG</i> <i>Reverse: 5' CTCAGTTCCTTCTTCCTTCCTT</i> <i>Probe: 5' GGTTTCTTTGTTGTGG</i>

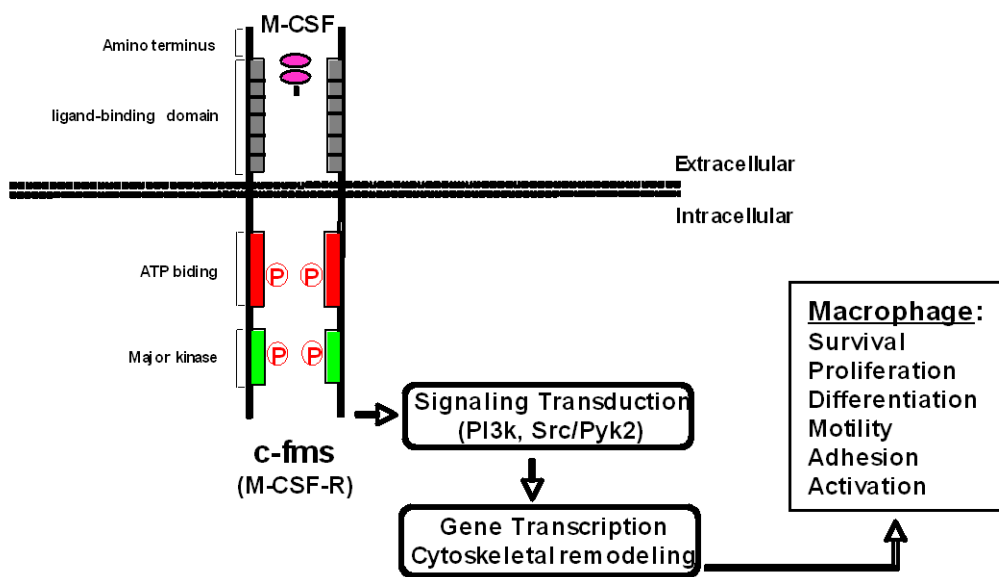


Figure 1.1. Overview of M-CSF/c-fms signaling pathway in monocyte/macrophage lineage cells. The M-CSF receptor (M-CSFR, also known as CSF-1R) is encoded by the c-fms proto-oncogene. It contains an extracellular ligand-binding domain, a transmembrane domain, and an intracellular tyrosine domain that is interrupted by a kinase insert domain. M-CSF is a disulfide-linked homodimer that, by binding M-CSF-R, stabilizes M-CSF-R dimerization to activate the receptor through autophosphorylation in trans, thereby initiating a series of membrane-proximal tyrosine phosphorylation cascades (P), leading to rapid stimulation of cytoskeletal remodeling, gene transcription and protein translation (*Hamilton, 1997*).

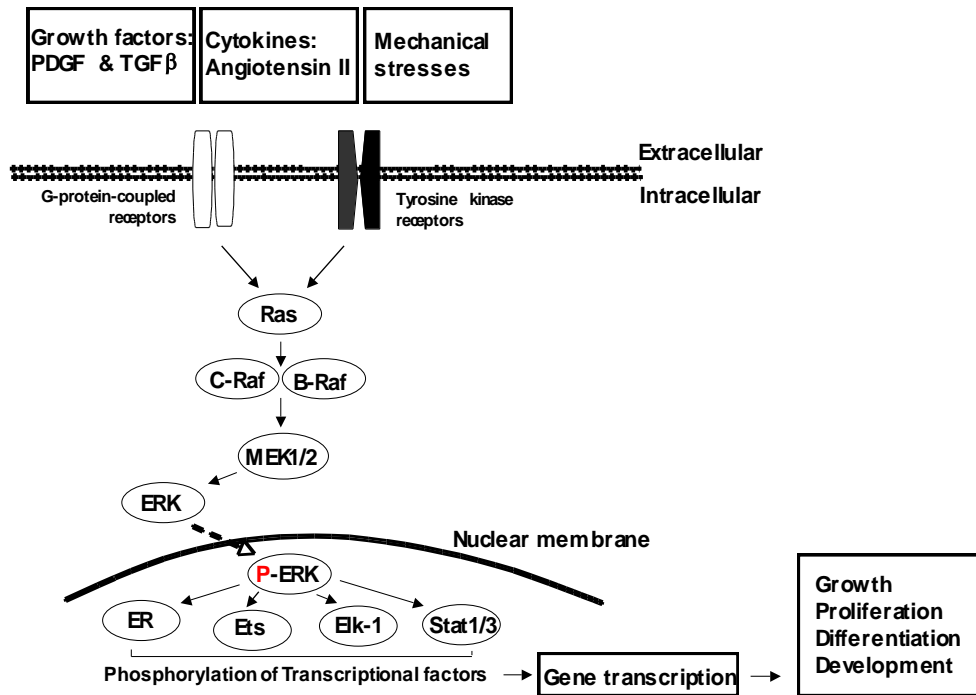


Figure 1.2 Overview of Extracellular Signal-Regulated Kinases (ERK) signaling pathways. Multiple factors including cytokines, growth factors such as PDGF, TGF- β and angiotensin II, and mechanical stresses can activate the pathway. ERK1 and ERK2 are serine/threonine kinases that regulate the transcription of many genes via the phosphorylation of several transcription factors such as ER, Ets, Elk-1 and Stat1/3. The binding of extracellular stimuli to G protein-coupled receptors or protein tyrosine kinase receptors results in the formation of GTP-Ras, which induces the sequential activation of cytoplasmic protein kinases, leading to their phosphorylation and activation (*Hill et al., 1995*). MAP kinase/ERK kinase 1 (MEK1) and MEK2 are specific activators of ERK1 and ERK2. MEK are dual-specificity protein kinases that phosphorylate both threonine and tyrosine regulatory sites in ERK (*Payne et al., 1991*). Once dual phosphorylated, ERK becomes an active kinase and can migrate to the nucleus where it phosphorylates specific transcription factors, leading to transcription of specific genes, such as cyclin D1, which plays a key role in the induction of cell cycle.

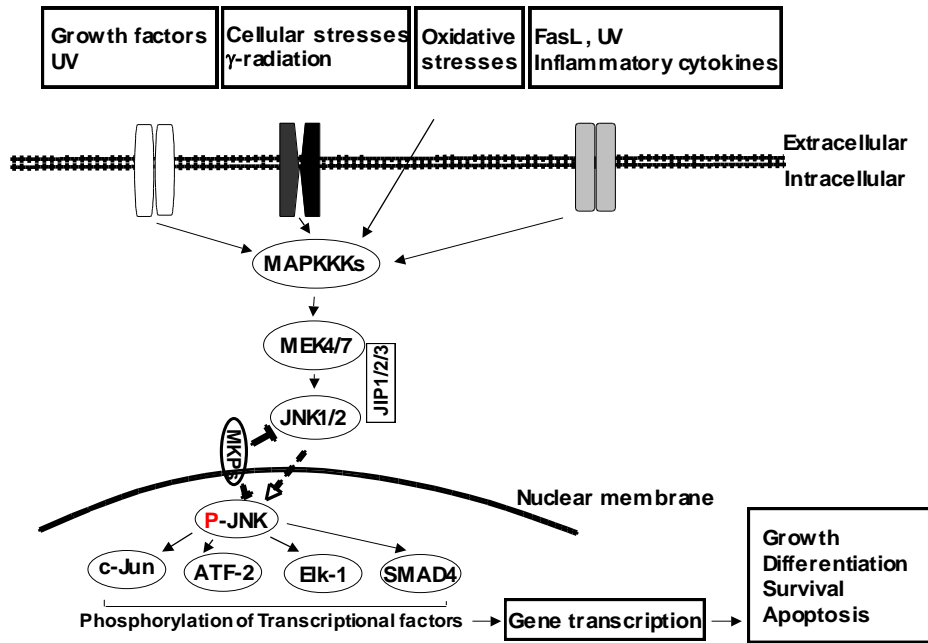


Figure 1.3 Overview of c-Jun N-terminal Kinases (JNK) signaling pathways. JNKs are activated in response to a wide range of stimuli. Ligand-based activation of cell surface receptors is linked to activation of a three-tiered MAPK cascade via the p21-activated kinase family of enzymes that bind to and are activated by small GTPases of the Cdc42 and Rac families. Phosphorylation of the activation loop in JNK operates via a cascade of a MAP kinase kinase kinase (MAP3K), and a MAP kinase kinase (MAP2K). There is a considerable redundancy in the different MAP3Ks that can lead to activation of JNK, whereas direct activation of JNK by MAP2K is restricted to MKK4 and 7. Scaffolding proteins, such as the family of JNK interacting proteins (JIP1-3), facilitate the three-tiered phosphorylation cascade by binding these kinases in close proximity. These scaffolding proteins may also be important in determining the specificity of JNK signal transduction. A further regulatory mechanism for the JNK signaling pathways is the inactivation of JNK by MAPK phosphatases (MKP). These can dephosphorylate JNK, p38 or ERK at threonine, serine or tyrosine residues. MKP-2 of the eleven members of the MKP family has been found to be specific for JNK (Bogoyevitch, 2006; Ma et al., 2009).

Figure 3.1

Figure 3.1 Western blotting of ERK phosphorylation in mouse unilateral ureteric obstruction (UUO). (a) Pilot study in which mice were treated with different doses of U0126 and then killed 30 min after UUO surgery. (b) Day 5 UUO in which groups of mice were given no treatment (NoTx), vehicle (Veh) or U0126 treatment (100 mg/kg t.i.d) over day 2-5. Blots were probed using an antibody for phosphorylated ERK1/2 (p-ERK), stripped and then probed for ERK2.

Figure 3.2

Figure 3.2 Immunostaining for phosphorylated ERK (p-ERK) in the mouse kidney cortex. (a) Normal mouse kidney showing p-ERK staining restricted to some collecting ducts. (b) Day 5 unilateral ureteric obstruction (UUO) kidney with vehicle treatment showing a marked increase in p-ERK staining in tubules, including damaged tubules, and in interstitial cells. (c) Day 5 UUO kidney with U0126 treatment showing abolition of the strong p-ERK staining seen in untreated UUO. Original magnification, $\times 250$.

Figure 3.3

Figure 3.3 Renal histology and cell proliferation in the obstructed mouse kidney. (a) Periodic acid-Schiff (PAS) staining of normal kidney. (b) PAS staining showing tubular dilation and atrophy on day 5 of vehicle-treated unilateral ureteric obstruction (UUO). (c) Day 5 UUO with U0126 treatment showing a similar degree of tubular damage to that of vehicle-treated mice. Cell proliferation was assessed by incorporation of BrdU on day 5 UUO. Immunostaining for BrdU antibody shows BrdU⁺ tubular and interstitial cells in UUO with: (d) no treatment, (e) vehicle treatment and (f) U0126 treatment. Original magnification, ×250.

Figure 3.4

Figure 3.4 Quantification of cell proliferation and interstitial macrophage and myofibroblast accumulation. Unilateral ureteric obstruction (UUO) was analyzed on day 5 in groups given no treatment (NoTx), vehicle (Veh) or U0126 treatment over days 2-5. (a) BrdU⁺ cortical tubular cells; (b) BrdU⁺ cortical interstitial cells; (c) α -SMA⁺ cortical myofibroblasts; and (d) F4/80⁺ cortical macrophages. Data are mean \pm SD with analysis by ANOVA with post-hoc analysis using Tukey's multiple comparison test.

Figure 3.5

Figure 3.5 Quantification of apoptosis using cleaved caspase-3 immunostaining and tubular damage demonstrated by PAS staining. Unilateral ureteric obstruction (UO) was analyzed on day 5 in groups given no treatment (NoTx), vehicle (Veh) or U0126 treatment over days 2-5. Graphs showed quantification of (a) cleaved caspase-3⁺ cortical tubular cells, (b) cleaved caspase-3⁺ cortical interstitial cells and (c) the percentage of damaged cortical tubules. No significant differences were detected among the different UO groups with analysis by ANOVA with post-hoc analysis using Tukey's multiple comparison test. Data are mean \pm SD.

Figure 3.6

Figure 3.6 Analysis of interstitial fibrosis. Unilateral ureteric obstruction (UUO) was analyzed on day 5 in groups given no treatment (NoTx), vehicle (Veh) or U0126 treatment over days 2-5. The area of interstitial collagen deposition in the cortex was assessed by image analysis of Sirius Red stained sections. No significant differences were detected among the different UUO groups with analysis by ANOVA with post-hoc analysis using Tukey's multiple comparison test. Data are mean \pm SD.

Figure 3.7

Figure 3.7 Immunostaining for phosphorylated c-Jun Ser 63 and 73 in the renal cortex. (a-b) Day 5 unilateral ureteric obstruction (UUO) kidney with no treatment showing nuclear staining of p-c-Jun Ser 63 and 73 in many damaged tubules and in some interstitial cells. No difference in the pattern of p-c-Jun Ser63 or Ser73 immunostaining was seen on day 5 UUO with vehicle treatment (c-d) or U0126 treatment (e-f). Original magnification, $\times 250$.

Figure 4.1

Figure 4.1 Pilot study examining glomerular cellularity over the time course of anti-Thy-1 nephritis as assessed on PAS-stained sections. The trend of reduced glomerular cell numbers were seen on day 1 after OX-7 IgG injection, reached a minimum number at day 4, and then glomerular cells increased leading to glomerular hypercellularity at day 8. By day 14, most glomeruli had normal cellularity. Data is meanonly; n=2/group.

Figure 4.2

Figure 4.2 Glomerular lesions in anti-Thy-1 nephritis in PAS stained sections. (a) normal glomeruli. (b) Apoptotic cells (arrow) are seen in the mesangium 1 hour after OX-7 IgG tail vein injection. (c) Glomerular cell loss is evident with microaneurysm (*) formation on day 3, while (d) day 8 shows glomerular hypercellularity and increased mesangial matrix. Original magnification, $\times 400$.

Figure 4.3

Figure 4.3 Immunostaining for OX-7 and α -SMA in rat anti-Thy-1 nephritis. Left panel showing a prominent glomerular OX-7⁺ mesangial cells in normal kidney (a), which are significantly reduced 3 days after OX-7 IgG injection (b) and areas of focal mesangial cell proliferation are evident on day 8 (c). Right panel shows immunostaining for α -smooth muscle actin (α -SMA). (d) Vascular staining for α -SMA is seen in normal rat kidney, but no staining in the glomerular tuft. (e) Small numbers of mesangial-like cells show immunostainning for α -SMA on day 3 of anti-Thy-1 nephritis (f) By day 8 of anti-Thy-1 nephritis, there is a dramatic increase in α -SMA expression in the glomeruli, being particularly prominent in an area of focal mesangial expansion. Original magnification, $\times 400$.

Figure 4.4

Figure 4.4 Immunostaining of phosphorylated JNK (p-JNK) in rat anti-Thy-1 nephritis. (a) Little p-JNK staining is observed in the normal rat glomeruli. Day 3 (b), Day 6 (c) and Day 8 (d) of anti-Thy-1 nephritis show a p-JNK staining in glomerular cells in a mesangial-like pattern. Original magnification, x400.

Figure 4.5

Figure 4.5 Immunostaining for c-Jun in rat anti-Thy-1 nephritis. (a) c-Jun staining was not seen in the normal rat glomeruli except in occasional parietal epithelial cells. Day 3 (b), Day 6 (c) and Day 8 (d) of anti-Thy-1 nephritis showed a marked induction of c-Jun in glomerular cells. Original magnification, ×400.

Figure 4.6

Figure 4.6 Detection of JNK activation in rat anti-Thy-1 nephritis with vehicle treatment or CC401 treatment from day 0 to day 3 by immunostaining for p-c-Jun (Ser 73). (a) Phosphorylated c-Jun (Ser 73) stained glomerular cells in anti-Thy-1 nephritis of day 3 treated by vehicle or CC401. Graph (b) quantification of p-c-Jun (Ser73)⁺ glomerular cells in anti-Thy-1 nephritis treated with vehicle or CC401. Data are mean±SD for groups of 4 rats, *P<0.05 by unpaired *t* test.

Figure 4.7

Figure 4.7 Detection of JNK activation in rat anti-Thy-1 nephritis with vehicle treatment or CC401 treatment from day 3 to day 8 by immunostaining for p-c-Jun Ser 73. (a) Phosphorylated c-Jun (Ser 73) stained glomerular cells in anti-Thy-1 nephritis of day 8 treated by vehicle or CC401. (b) Quantification of p-c-Jun (Ser73)⁺ glomerular cells in rat anti-Thy-1 nephritis treated with vehicle or CC401. Data are mean±SD for groups of 4 rats, ***P<0.001 by unpaired *t* test.

Figure 4.8

Figure 4.8 Glomerular pathology on day 3 of anti-Thy-1 nephritis in rats treated with vehicle or CC401. (a, d) PAS staining shows a similar degree of glomerular hypocellularity in both groups. (b, e) OX-7 immunostaining shows an almost complete loss of mesangial cells on day 3 of Thy-1 nephritis in both groups. (c, f) Immunostaining for α -SMA shows the appearance of a small number of myofibroblasts within the glomerular tuft in both groups. Original magnification, $\times 400$.

Figure 4.9

Figure 4.9 Glomerular pathology in anti-Thy-1 nephritis in rats treated with vehicle or CC401 from day 3 to 8. (a,d) PAS staining shows a similar degree of glomerular hypercellularity and mesangial matrix expansion in both groups on day 8 of anti-Thy-1 nephritis. (b,e) OX-7 immunostaining shows areas of focal mesangial proliferation. (c,f) Immunostaining shows α -SMA expression in areas of focal mesangial proliferation in both groups. Original magnification, $\times 400$.

Figure 4.10

Figure 4.10 Quantification of glomerular cell number in rat anti-Thy-1 nephritis on day 3 and day 8 treated with vehicle or CC401. Glomerular cells of anti-Thy-1 nephritis with vehicle or CC401 treatment on days 0 to 3 (a) and on days 3-8 (b) on basis of PAS-haematoxylin staining and immunostaining for OX-7 antibody. Data are mean \pm SD for groups of 4 rats, *P<0.05 by un-paired *t* test.

Figure 5.1

Figure 5.1 Body weight in anti-GBM disease for the no-treatment, vehicle or fms-I treatment (low and high dose) groups. Animal body weight is not affected by low dose (10mg/kg, b.i.d) and high dose (30mg/kg, b.i.d) of fms-I treatment with a trend to preventing the small drop in body weight seen in vehicle treated and no-treated groups. Data are mean \pm SD; n=8/group.

Figure 5.2

Figure 5.2 Macrophage infiltration at day 14 of anti-GBM disease.

Immunostaining for ED1⁺ (CD68) macrophages is shown for (a) there are few glomerular and interstitial residential ED1⁺ macrophages in the normal rat kidney, and at day 14 of anti-GBM disease ED1⁺ macrophages were prominent in the glomerular tuft and crescent, interstitial ED1⁺ macrophages were also evident in the (b) no-treated and (c) vehicle treated kidneys; (d) Both glomerular and interstitial ED1⁺ macrophages were significantly reduced in low dose of fms-I treatment; and (e) high dose fms-I treatment. Original magnification, x250.

Figure 5.3

Figure 5.3 Quantification of ED1⁺ macrophages. (a) Graph showing quantification of glomerular ED1⁺ macrophages infiltrate in normal kidney and in day 14 anti-GBM disease in no-treated, vehicle-treated and low (10mg/kg) and high dose (30mg/kg) fms-I treated groups. (b) Graph showing quantification of interstitial ED1⁺ macrophages infiltrate in normal kidney and in day 14 anti-GBM disease in no-treated, vehicle-treated and low (10mg/kg) and high dose (30mg/kg) of fms-I treated groups.. Data are mean±SD for groups of 8 rats, *** P<0.001 versus normal, and for specified comparisons, by one-way ANOVA with post-hoc analysis using Tukey's multiple comparison test.

Figure 5.4

Figure 5.4 Macrophage infiltrates on day 1 and 5 of anti-GBM disease. Immunostaining for ED1⁺ (CD68) macrophages on: (a) day 1 with vehicle treatment; (b) day 5 with vehicle treatment; (c) day 1 with high dose fms-I treatment; (d) day 5 with high dose fms-I treatment. Original magnification, ×250. (e) Graph showing quantification of glomerular ED1⁺ macrophages infiltrate on day 1 and day 5 of anti-GBM disease in vehicle-treated and high dose (30mg/kg) of fms-I treated groups. Data are mean±SD for groups of 4 rats with statistical analysis by one-way ANOVA with post-hoc analysis using Tukey's multiple comparison test; **P<0.01 ***P<0.001.

Figure 5.5

Figure 5.5 White blood cell counts were performed on a Cell Dyn 3500 Cell Counter. Quantification of white blood cells from anti-GBM disease of day 1, 5 and 14 (a-d). Data are mean \pm SD for groups of 8 rats, *P<0.05; **P<0.01; ***P<0.001 vs normal or for specified comparison; with analysis by one-way ANOVA with post-hoc analysis using Tukey's multiple comparison test.

Figure 5.6

Figure 5.6 Analysis of blood monocytes on day 14 of anti-GBM disease using ED1 (CD68) and OX-42 (CD11b) antibodies by flow cytometry. Low dose and high dose of fms-I treatments significantly reduce ED1⁺ circulating monocytes (a) and OX-42⁺ circulating monocytes (b). Data are mean±SD for groups of 8 rats **P<0.01; ***P<0.001 vs normal or for specified comparison; analysis by one-way ANOVA with post-hoc analysis using Tukey's multiple comparison test.

Figure 5.7

Figure 5.7 Macrophage proliferation in day 14 of anti-GBM disease. Proliferating macrophages in the kidney with anti-GBM disease of day 14 are identified by double immunostaining for ED1 and PCNA antibodies. (a) ED1⁺PCNA⁺ macrophages in the glomeruli on day 14 in vehicle treatment (arrows), compared to (b) low dose fms-I (10mg/kg) on day 14. Original magnification, x400. Graphs showing quantification of glomerular ED1⁺PCNA⁺ macrophages infiltrate (c), and the percentage of total glomerular macrophages (ED1⁺ cells) that are proliferating (ED1⁺PCNA⁺ cells) on day 5 and day 14 anti-GBM disease in vehicle-treated and high or low dose (10mg/kg) of fms-I treated groups. Data are mean±SD for groups of 4 rats (day 5) or groups of 8 rats (day 14) , *P<0.05, **P<0.01, ***P<0.001 vs normal or for specified comparison with statistical analysis by un-paired *t* test.

Figure 5.8

Figure 5.8 Effect of fms-I treatment on glomerular pathology on day 14 of anti-GBM disease. PAS-haematoxylin staining of untreated and vehicle-treated day 14 anti-GBM disease shows severe glomerular tuft lesions including hyalinosis, segmental fibrinoid necrosis and atrophy, and extensive crescent formation (*) and Bowman's capsule rupture compared to normal kidney (a-b). (c) Low dose of fms-I treatment reduced lesions of the glomerular tuft and crescent formation. (d) High dose of fms-I treated rats show only mild changes in the glomeruli, with crescent formation and Bowman's capsule rupture largely prevented. (e) PTAH staining shows fibrin deposition (intense blue stain, * marked) in glomerular crescents and Bowman's space in a vehicle treated rat, which (f) is absent in rats given high dose fms-I treatment. Original magnification: $\times 400$.

Figure 5.9

Figure 5.9 Quantification of glomerular lesions on day 14 of anti-GBM disease induced in rats that received fms-I (10mg/kg or 30mg/kg), vehicle (Veh) or no treatment (NoTx). (a) Graph showing a semi-quantitative assessment of glomerular tuft lesions defined by hyalinosis, focal and segmental adhesions, fibrinoid necrosis, and glomerular atrophy, and graded on the proportion of the glomerulus damaged (see section 2.9.3). (b) Graph of the percentage of glomeruli exhibiting crescent formation. (c) Graph of the percentage of glomeruli exhibiting Bowman's capsule rupture. (d) Graph of the semi-quantitative score of periglomerular α -SMA⁺ myofibroblast accumulation. Data (b) and (c) are mean \pm SD for groups of 8 rats, Graphs (b) and (c) **P<0.001; *** P<0.001 for specified comparison with statistical analysis by one-way ANOVA with post-hoc analysis using Tukey's multiple comparison; Graphs (a) and (d) **P<0.001; *** P<0.001 for specified comparison with statistical analysis by one-way ANOVA with Kruskal-Wallis test.

Figure 5.10

Figure 5.10 Effect of fms-I treatment on tubulointerstitial damage on day 14 anti-GBM disease. PAS-haematoxylin staining of untreated and vehicle-treated anti-GBM disease of day 14 shows marked tubulointerstitial damage featuring tubular dilation and atrophy, cast formation and mononuclear cell infiltration (b-c) compared to normal kidney (a). (d) Low dose of fms-I treatment reduce the degree of tubulointerstitial damage. (e) High dose of fms-I treated rats show only mild changes in the tubulointerstitium. Original magnification: $\times 400$.

Figure 5.11

Figure 5.11 Tubular damage and de-differentiation on day 14 of anti-GBM disease. Immunostaining for vimentin is shown in (a) normal rat kidney, (b) no treatment, (c) vehicle treated, (d) low dose (10mg/kg) fms-I treated, and (e) high dose (30mg/kg) treated day 14 of anti-GBM disease. Vimentin staining is seen in the glomeruli in the normal kidney. No treatment and vehicle treated rats on day 14 anti-GBM disease show vimentin staining in many tubules and interstitial cells, which is reduced by fms-I treatment. Original magnification, $\times 250$.

Figure 5.12

Figure 5.12 Tubular damage and de-differentiation on day 14 of anti-GBM disease. Immunostaining for osteopontin in (a) normal rat kidney, (b) no treated, (c) vehicle treated, (d) low dose (10mg/kg) fms-I treated, and (e) high dose (30mg/kg) treated day 14 of anti-GBM disease. No osteopontin staining is seen in the cortex in the normal kidney. However, on day 14 of anti-GBM disease, osteopontin immunostaining is evident in many tubules in vehicle and no treatment groups, and this is diminished with fms-I treatment. Original magnification, $\times 250$.

Figure 5.13

Figure 5.13 Quantification of tubular damage and de-differentiation. (a) Graph showing tubular vimentin expression; and (b) graph showing tubular osteopontin on day 14 anti-GBM disease. Data are mean \pm SD, *P<0.05 **P<0.01 *** P<0.001 for specified comparison with statistical analysis by one-way ANOVA with post-hoc analysis using Tukey's multiple comparison test.

Figure 5.14

Figure 5.14 Renal interstitial fibrosis on day 14 of anti-GBM disease. Immunostaining for collagen IV in (a) normal rat kidney, (b) No treatment, (c) vehicle, (d) low dose of fms-I (10mg/kg) or (e) high dose (30mg/kg) of fms-I treatment on day 14 of anti-disease. Original magnification, $\times 250$.

Figure 5.15

Figure 5.15 Renal interstitial fibrosis on day 14 of anti-GBM disease.

Immunostaining for α -SMA in (a) normal rat kidney, (b) no treatment, (c) vehicle, (d) low dose of fms-I (10mg/kg) or (e) high dose (30mg/kg) of fms-I treatment on day 14 of anti-disease. Original magnification, $\times 250$.

Figure 5.16

Figure 5.16 Quantification of interstitial volume. Graph showing interstitial volume on day 14 anti-GBM disease. Data are mean±SD, *P<0.05 **P<0.01 ***P<0.001 vs normal or for specified comparison with statistical analysis by one-way ANOVA with post-hoc analysis using Tukey's multiple comparison test.

Figure 5.17

Figure 5.17 Renal injury on day 14 of anti-GBM disease. Anti-GBM disease was induced in rats, which were given no treatment (NoTx), vehicle (Veh), or low and high dose of fms-I treatment. The effect of fms-I treatment on progressive anti-GBM disease was assessed in terms of: (a) serum creatinine levels, (b) creatinine clearance at day 14, and (c) proteinuria over the disease course. (d) Graph showing effect of fms-I treatment on the number of glomerular WT-1⁺ on day 1, 5 and 14 of anti-GBM disease. Results are shown as mean±SD, ### P<0.001 vs NoTx at day 14, *P<0.05 **P<0.01 *** P<0.001 vs normal or for specified comparison with statistical analysis by one-way ANOVA with post-hoc analysis using Tukey's multiple comparison test.

Figure 5.18

Figure 5.18 Real time RT-PCR analysis of mRNA levels at days 1, 5 of anti-GBM disease. Analysis of isolated glomeruli from days 1 and 5 of anti-GBM disease for (a) TNF- α ; (b) NOS2; (c) MMP-12; (d) CCL2; (e) IL-12; (f) Arginase-1; (g) CD206, and ; (h) CD163. Data are mean \pm SD; n=4; *P<0.05 **P<0.01 ***P<0.001 vs normal or for specified comparison with statistical analysis by one-way ANOVA with post-hoc analysis using Tukey's multiple comparison test.

Figure 5.19

Figure 5.19 Real time RT-PCR analysis of mRNA levels at day 14 of anti-GBM disease. Analysis of whole kidney tissue on day 14 of anti-GBM disease for: (a) TNF- α ; (b) NOS2; (c) MMP-12; (d) CCL2. Data are mean \pm SD. *P<0.05 **P<0.01 *** P<0.001 vs normal or for specified comparison with statistical analysis by one-way ANOVA with post-hoc analysis using Tukey's multiple comparison test.

Figure 5.20

Figure 5.20 Effect of fms-I treatment on the T-cell infiltrate on days 1, 5 and 14 of anti-GBM disease. (a) Quantification of immunostaining for R73⁺ T cells in glomeruli on days 1, 5 and 14 of anti-GBM disease; (b) Quantification of interstitial R73⁺ T cell on day 14 of anti-GBM disease. Data are mean±SD, ### P<0.001 vs NoTx at day 14, *P<0.05 **P<0.01 *** P<0.001 vs normal for specified comparison with statistical analysis by one-way ANOVA with post-hoc analysis using Tukey's multiple comparison test.

Figure 5.21

Figure 5.21 Effect of fms-I treatment on rat IgG and complement C3 deposition on day 14 of anti-GBM disease. Representative immunofluorescence staining for deposition of rat anti-sheep IgG in vehicle treated group (a) and high dose fms-I treated (30mg/kg) group (b); representative immunofluorescence staining for deposition of rat C3 in vehicle treated (c) group and high dose fms-I (30mg/kg) treated group (d). Semi-quantification of rat IgG (e) and C3 deposition (f) in the glomeruli of day 14 of anti-GBM disease. Results expressed as the antibody titre at which positive staining was lost. The deposition of rat IgG and C3 was unaffected by fms-I treatment. Original magnification, $\times 400$.

Figure 5.22

Figure 5.22 Immunostaining for dendritic cell markers MHC class II (left panel), OX-62 (middle panel) and CD11c (right panel) is shown in normal rat kidney, day 1 and day 14 anti-GBM disease with vehicle treatment (Veh), and day 1 and 14 anti-GBM disease with high dose fms-I treatment (30mg/kg fms-I). Original magnification, ×400.

Figure 6.1

Figure 6.1 Body weight in anti-GBM disease over 35 days with no-treatment, vehicle or fms-I treatment (low and high dose). Animal body weight is not affected by low dose (10mg/kg, b.i.d) or high dose (30mg/kg, b.i.d) fms-I treatment, although there was a non-significant trend towards greater weight with fms-I treatment compared to vehicle treatment . Data are mean \pm SD; n=8/group.

Figure 6.2

Figure 6.2 Macrophage infiltrates on day 35 of anti-GBM disease. Immunostaining for ED1⁺ (CD68) macrophages showing for normal rat kidney (a), vehicle treated on day 14 (b), day 35 of anti-GBM disease of with vehicle treatment (c), low dose (10mg/kg) (d) or high dose (30mg/kg) (e) of fms-I treatments. Of note, there is a decreased glomerular and interstitial ED1+ macrophages infiltrates at day 35 of vehicle treated anti-GBM disease compared to at day 14, Original magnification, x250.

Figure 6.3

Figure 6.3 Quantification of ED1⁺ (CD68) macrophages in normal rat kidney and anti-GBM disease. (a) Graph showing quantification of glomerular ED1⁺ macrophages infiltrate in normal rat kidney, vehicle treated day 14 anti-GBM disease and day 35 anti-GBM disease in vehicle-treated, low (10mg/kg) or high dose (30mg/kg) fms-I treated groups. (b) Graph showing quantification of interstitial ED1⁺ macrophages infiltrate in normal rat kidney, vehicle treated day 14 anti-GBM disease and day 35 anti-GBM disease in vehicle treated, low (10mg/kg) or high dose (30mg/kg) fms-I treated groups. Data are mean±SD for groups of 8 rats; *** P<0.001 vs normal, or for specified comparison with statistical analysis by one-way ANOVA with post-hoc analysis using Tukey's multiple comparison test. ### P<0.001 vs day 14 vehicle treatment.

Figure 6.4

Figure 6.4 White blood cell counts on day 35 anti-GBM disease with vehicle, low dose fms-I (10mg/kg) and high dose fms-I (30mg/kg). (a) White blood cells, (b) monocyte, (c) lymphocytes, and (d) neutrophils. White blood cell counts were performed on a Cell Dyn 3500 Cell Counter. Data are mean±SD for groups of 8 rats, *P<0.05, **P<0.01, ***P<0.001 vs normal or for specified comparison with statistical analysis by one-way ANOVA with post-hoc analysis using Tukey's multiple comparison test.

Figure 6.5

Figure 6.5 PAS staining of renal pathology on day 35 of anti-GBM disease.

(a) Normal rat kidney. (b) Vehicle treated day 14 anti-GBM disease. (c) Vehicle treated day 35 anti-GBM disease. Low dose fms-I (10mg/kg) (d) and high dose (30mg/kg) (e) treated day 35 anti-GBM disease showing severe glomerular tuft lesions including hyalinosis, segmental fibrinoid necrosis and atrophy, and extensive crescent formation with increased fibrous tissue compared to at day 14 of anti-GBM disease(*). Original magnification, ×400.

Figure 6.6

Figure 6.6 Quantification of glomerular lesions on PAS stained sections of anti-GBM disease. Disease was induced in rats that received fms-I (10mg/kg or 30mg/kg) or vehicle (Veh), treatment from day 14 until being killed on day 35, and were compared to vehicle treated rats killed on day 14 . (a) Crescent formation, (b) Crescent size, and (c) Bowman's capsule rupture. (d) Semi-quantitative scoring of periglomerular α -SMA⁺ myofibroblast accumulation. Data are mean \pm SD for groups of 8 rats, Graphs (a) and (c) **P<0.001; *** P<0.001 for specified comparison with statistical analysis by one-way ANOVA with post-hoc analysis using Tukey's multiple comparison; Graphs (b) and (d) **P<0.001; *** P<0.001 for specified comparison with statistical analysis by one-way ANOVA with Kruskal-Wallis test.

Figure 6.7

Figure 6.7 Effect of fms-I treatment on tubulointerstitial damage on day 35 anti-GBM disease. PAS-haematoxylin staining kidney sections. (a) Normal rat kidney. Vehicle-treated day 14 and 35 anti-GBM disease show severe tubulointerstitial damage featuring tubular dilation and atrophy, cast formation and mononuclear cell infiltration (b-c. (d) low dose and (e) high dose fms-I treated rats show a similar degree of tubulointerstitial damage. Original magnification $\times 250$.

Figure 6.8

Figure 6.8 Effect of fms-I treatment on tubulointerstitial damage on day 35 anti-GBM disease. Immunostaining for vimentin on day 35 anti-GBM disease. (a) Vimentin staining of normal rat kidney showing glomerular staining and little interstitial vimentin staining; (b) and (c) Vimentin staining of vehicle-treated days 14 and 35 anti-GBM disease and (d) low dose fms-I (10mg/kg) and (e) high dose fms-I (30mg/kg) treated day 35 anti-GBM disease showing marked induction of vimentin in tubules and interstitial cells compared to normal kidney. There is no significant difference between fms-I treated and vehicle treated kidneys of anti-GBM disease on day 35, Original magnification, $\times 250$.

Figure 6.9

Figure 6.9 Effect of fms-I treatment on tubulointerstitial damage on day 35 anti-GBM disease. Immunostaining for oestropontin on day 35 anti-GBM disease. (a) complete negative oestropontin staining in normal rat kidney ; (b) and (c) oestropontin staining of vehicle-treated days 14 and 35 anti-GBM disease and (d) low dose fms-I (10mg/kg) and (e) high dose fms-I (30mg/kg) treated day 35 anti-GBM disease showing marked induction of oestropontin in tubules and interstitial cells compared to normal kidney. However, there is no significant difference between fms-I treated and vehicle treated kidneys of anti-GBM disease on day 35, Original magnification, ×250.

Figure 6.10

Figure 6.10 Graphs showing quantification of (a) tubular vimentin expression, (b) tubular osteopontin, and (c) tubular lumen space on day 35 anti-GBM disease. Results are mean \pm SD, *P<0.05 and **P<0.01 by one-way ANOVA with post-hoc analysis using Tukey's multiple comparison test.

Figure 6.11

Figure 6.11 Renal injury on day 35 anti-GBM disease. Anti-GBM disease was induced in rats, which were given vehicle (Veh), low or high dose of fms-I treatment from day 14 to day 35 day. The effect of fms-I treatment on established anti-GBM disease was assessed in terms of: (a) proteinuria over the disease course and (b) showing effect of fms-I treatment on the number of glomerular WT-1⁺ on day 14 and 35 anti-GBM disease. Graph (c) showing serum creatinine level and (d) creatinine clearance at day 35 anti-GBM disease. Results are mean±SD, *** P<0.001 and *P<0.05 vs normal or for specified comparison with statistical analysis by one-way ANOVA with post-hoc analysis using Tukey's multiple comparison test.

Figure 6.12

Figure 6.12 Renal interstitial fibrosis on day 35 anti-GBM disease.

Immunostaining for collagen IV in (a) normal rat kidney ; (b) and (c) collagen IV staining of vehicle-treated days 14 and 35 anti-GBM disease and (d) low dose fms-I (10mg/kg) and (e) high dose fms-I (30mg/kg) treated day 35 anti-GBM disease showing marked glomerular and interstitial increase compared to normal kidney. However, there is no significant difference between fms-I treated and vehicle treated kidneys of anti-GBM disease on day 35, Original magnification, ×250.

Figure 6.13

Figure 6.13 Renal interstitial fibrosis on day 35 anti-GBM disease.

Immunostaining for α -SMA in (a) normal rat kidney showing a few stained blood vessels; (b) and (c) vehicle-treated days 14 and 35 anti-GBM disease and (d) low dose fms-I (10mg/kg) and (e) high dose fms-I (30mg/kg) treated day 35 anti-GBM disease showing marked glomerular and interstitial increase compared to normal kidney. However, there is no significant difference between fms-I treated and vehicle treated kidneys of anti-GBM disease on day 35, Original magnification, $\times 250$.

Figure 6.14

Figure 6.14 Quantification of interstitial fibrosis on day 35 anti-GBM disease. (a) the area of interstitial collagen IV, (b) the area of interstitial α -SMA immunostaining, and (c) interstitial volume on day 35 anti-GBM disease. Results are shown as mean \pm SD, *P<0.05, **P<0.01 and *** P<0.001 vs normal or for specified comparison with statistical analysis by one-way ANOVA with post-hoc analysis using Tukey's multiple comparison test. ## P<0.01 and ### P<0.001 vs day 14 vehicle treatment.

Figure 6.15

Figure 6.15 Real time RT-PCR analysis of mRNA levels at day 35 of anti-GBM disease. Analysis of whole normal rat kidney tissue and kidney tissue of day 35 of anti-GBM disease for: (a) TNF- α ; (b) NOS2; (c) MMP-12. Data are mean \pm SD. *P<0.05 **P<0.01 vs normal with statistical analysis by one-way ANOVA with post-hoc analysis using Tukey's multiple comparison test.

Figure 6.16

Figure 6.16 Effect of fms-I treatment on T-cell infiltration on day 35 of anti-GBM disease. (a) Quantification of immunostaining for R73⁺ T cell in glomeruli, and (b) quantification of interstitial R73⁺ T cell on days 14 and 35 vehicle treated anti-GBM disease and low dose fms-I (10mg/kg) and high dose fms-I (30mg/kg) treated day 35 anti-GBM disease. Data are mean±SD, *P<0.05 **P<0.01 ***P<0.001 vs normal or for specified comparison with statistical analysis by one-way ANOVA with post-hoc analysis using Tukey's multiple comparison test.

Figure 3.1

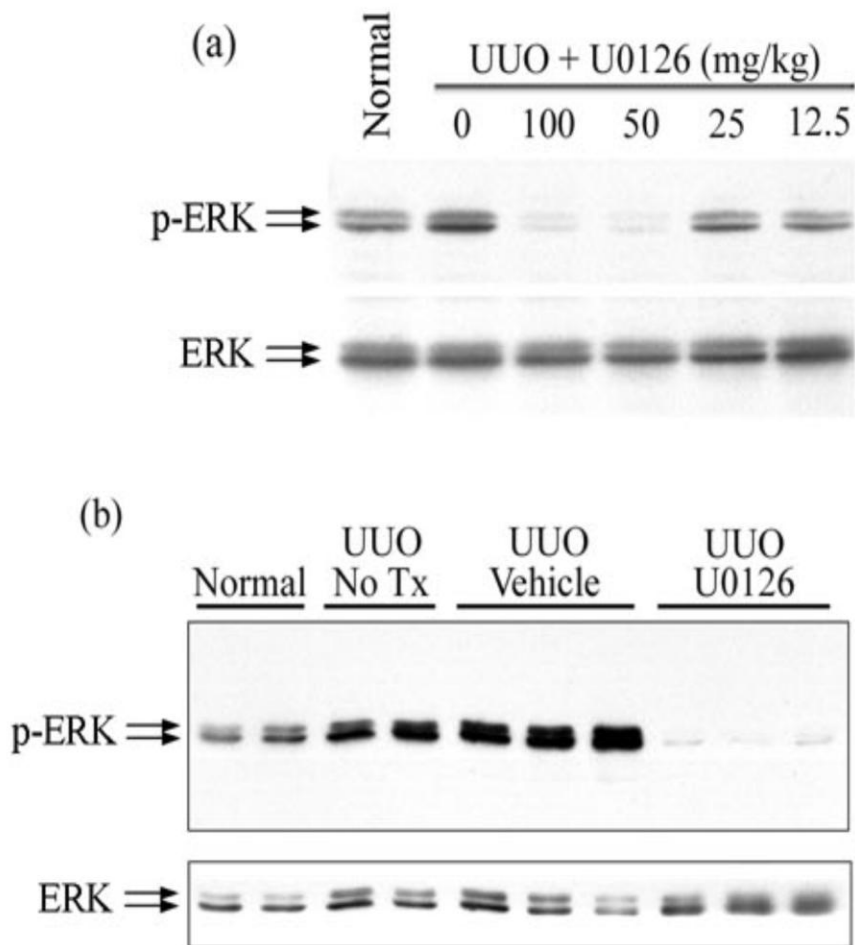
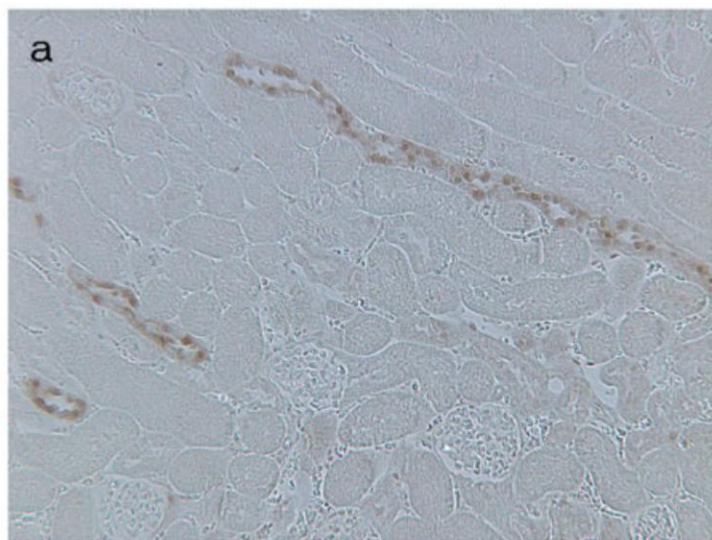
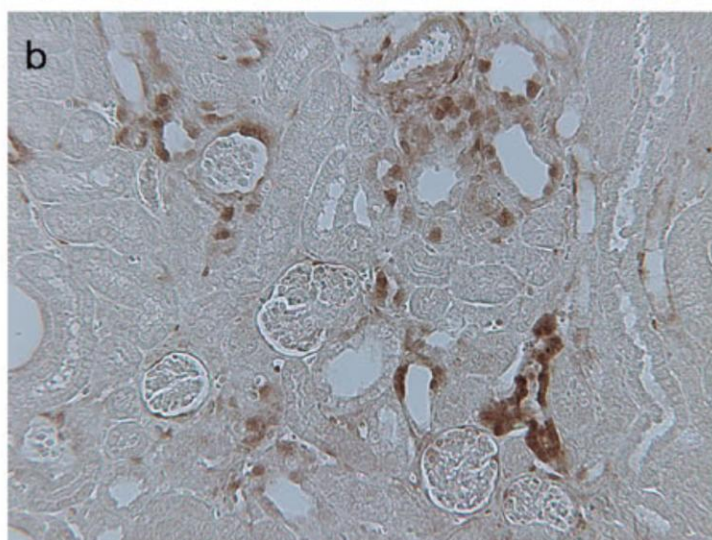


Figure 3.2

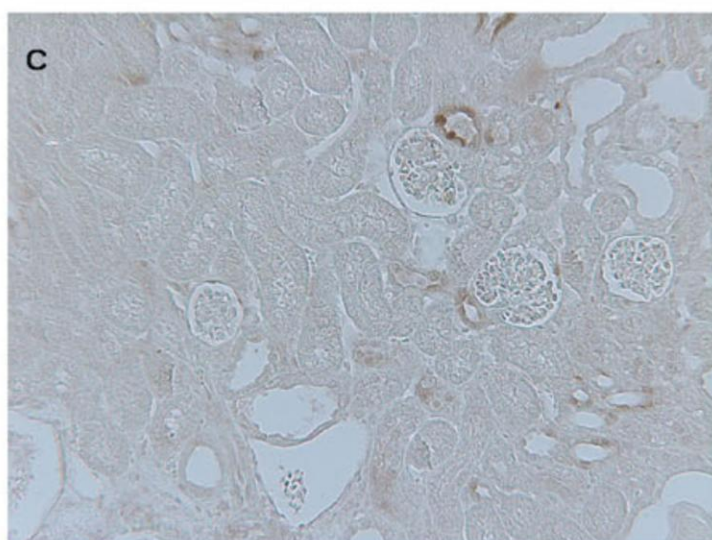
p-ERK



Normal



Day 5 UUO Veh



Day 5 UUO U0126

Figure 3.3

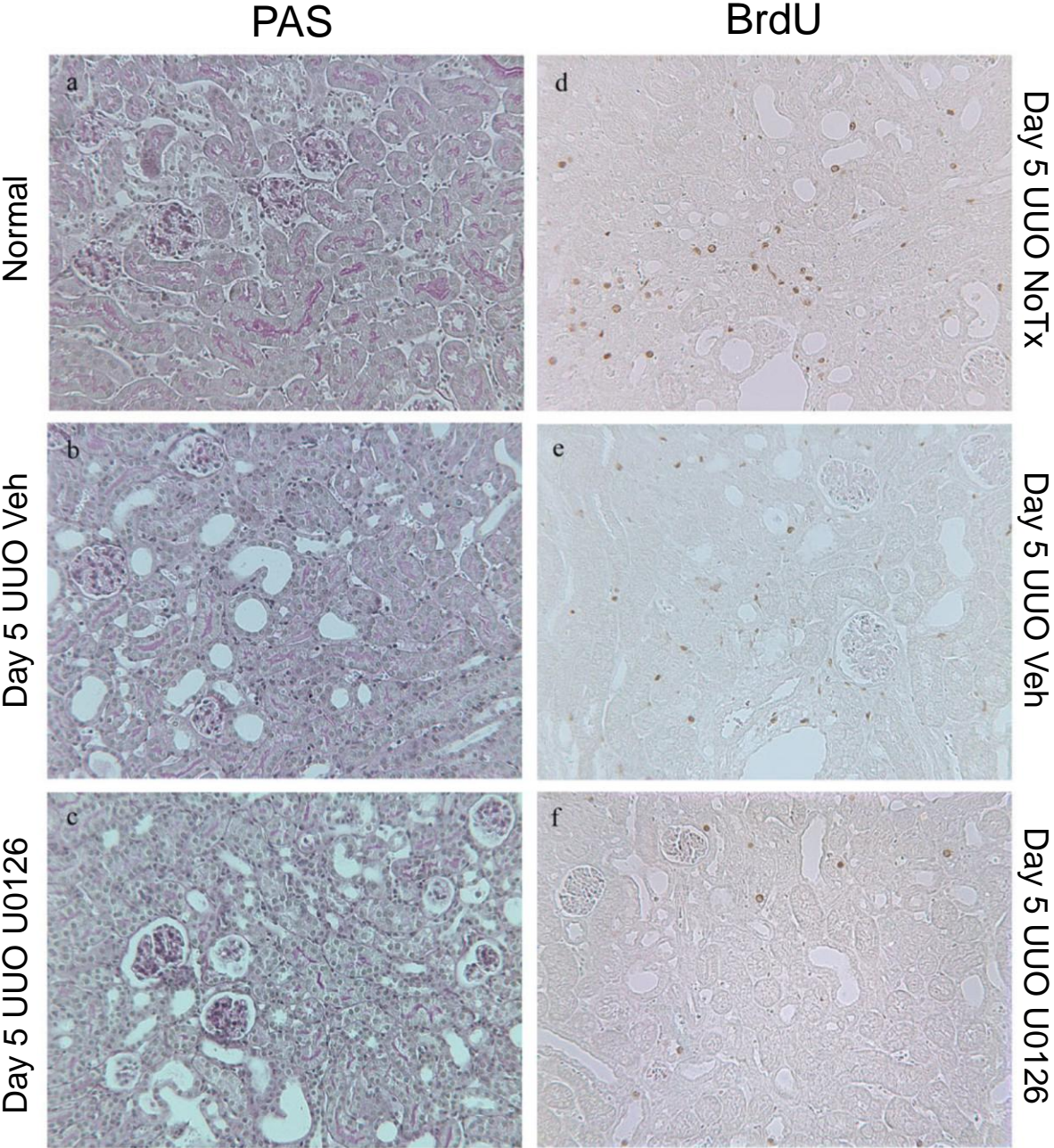


Figure 3.4

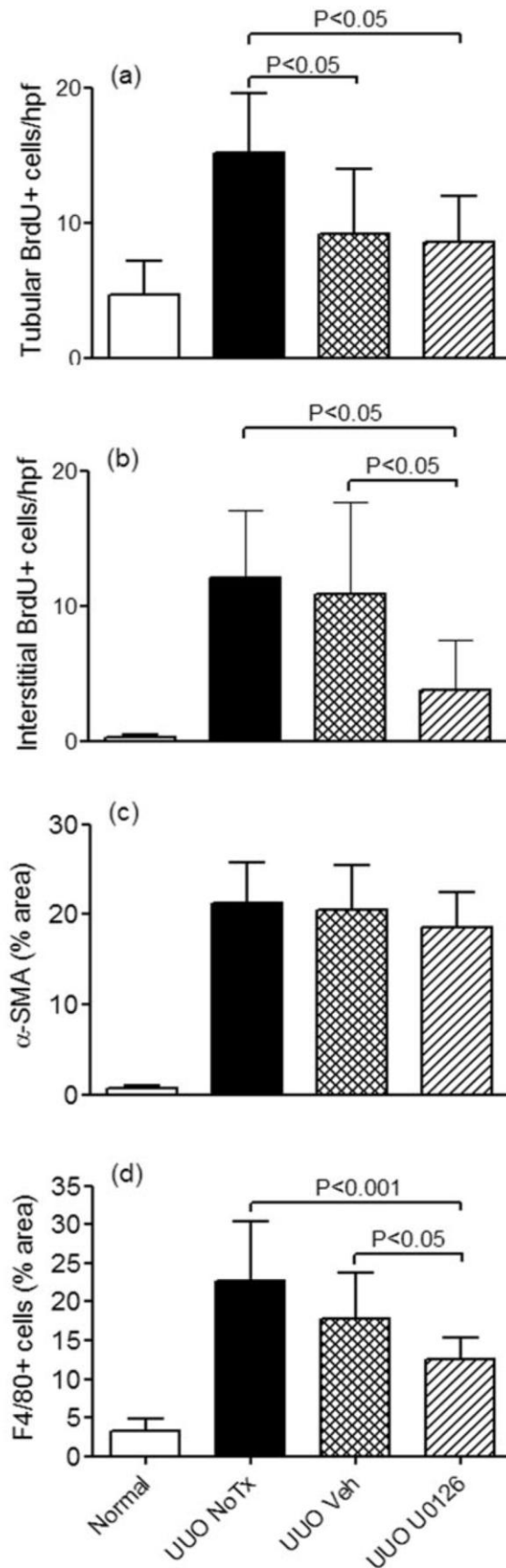


Figure 3.5

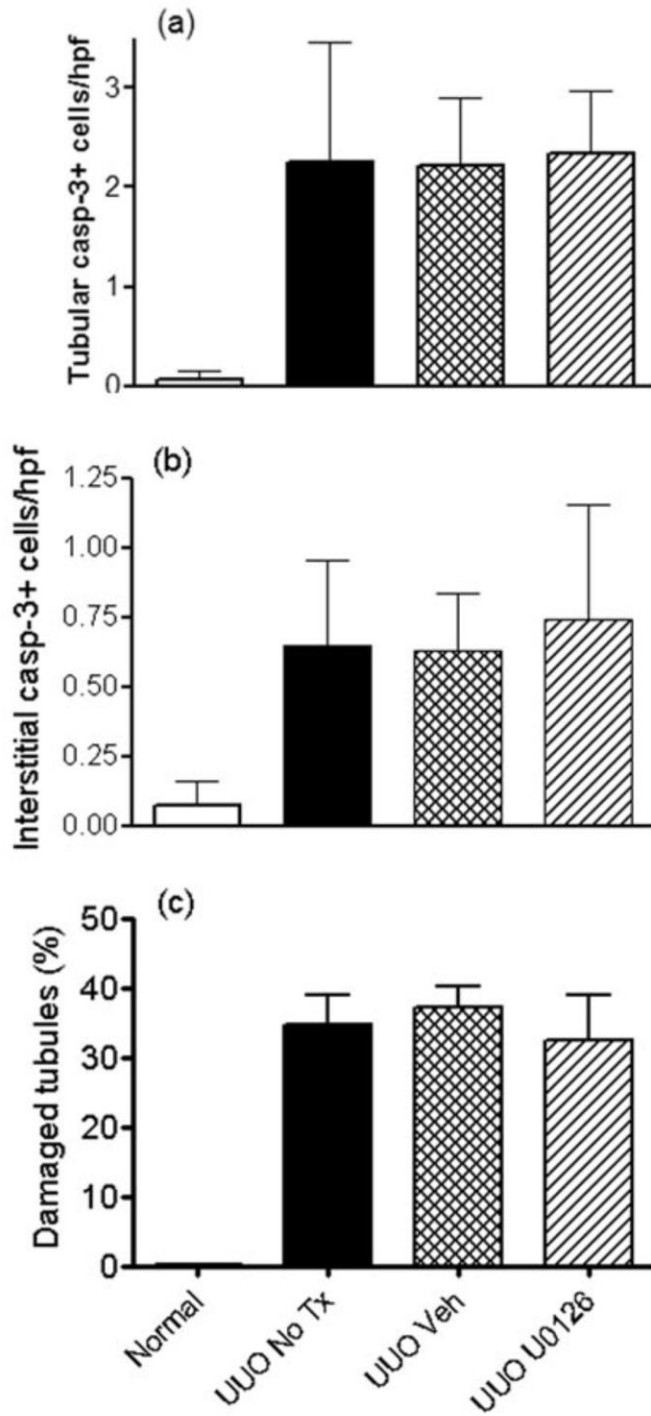


Figure 3.6

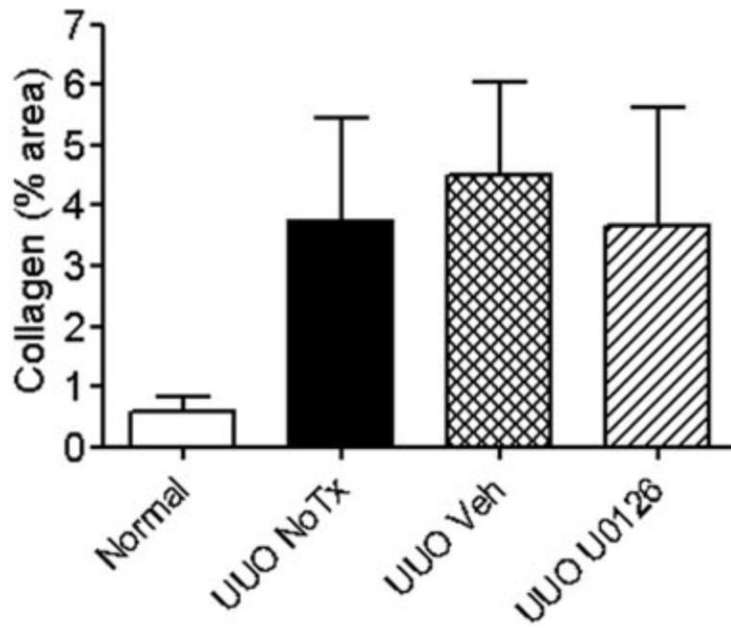


Figure 3.7

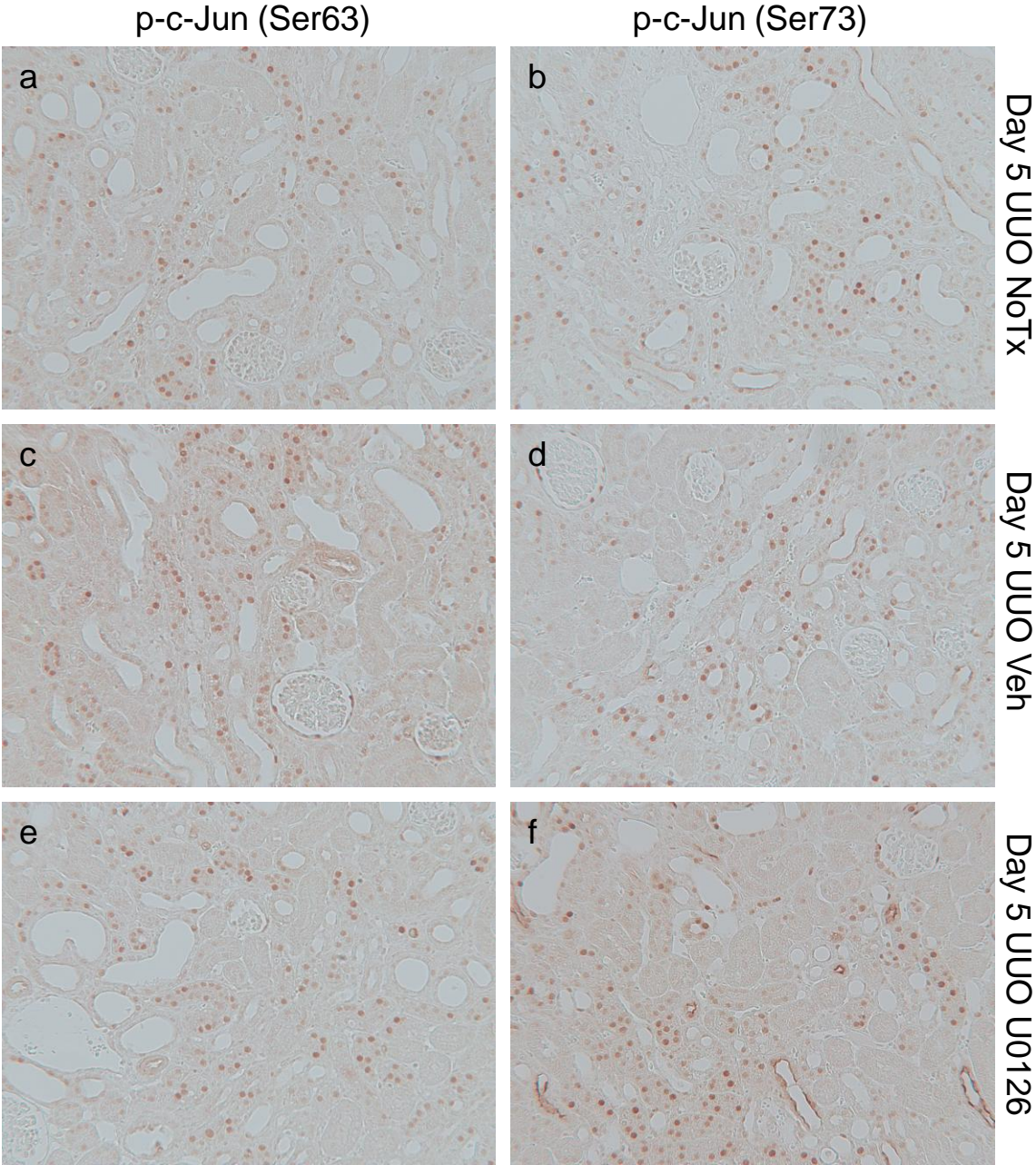


Figure. 4.1

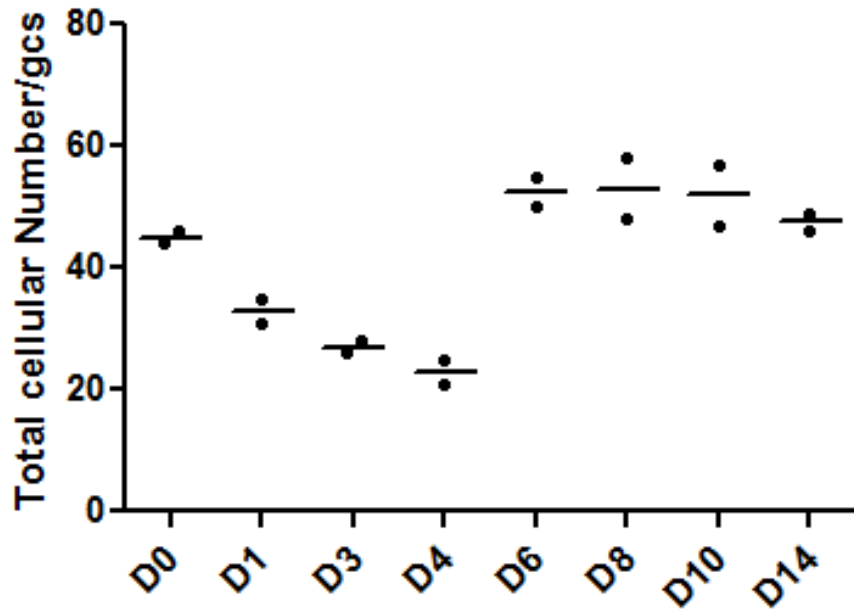


Figure 4.2

PAS staining

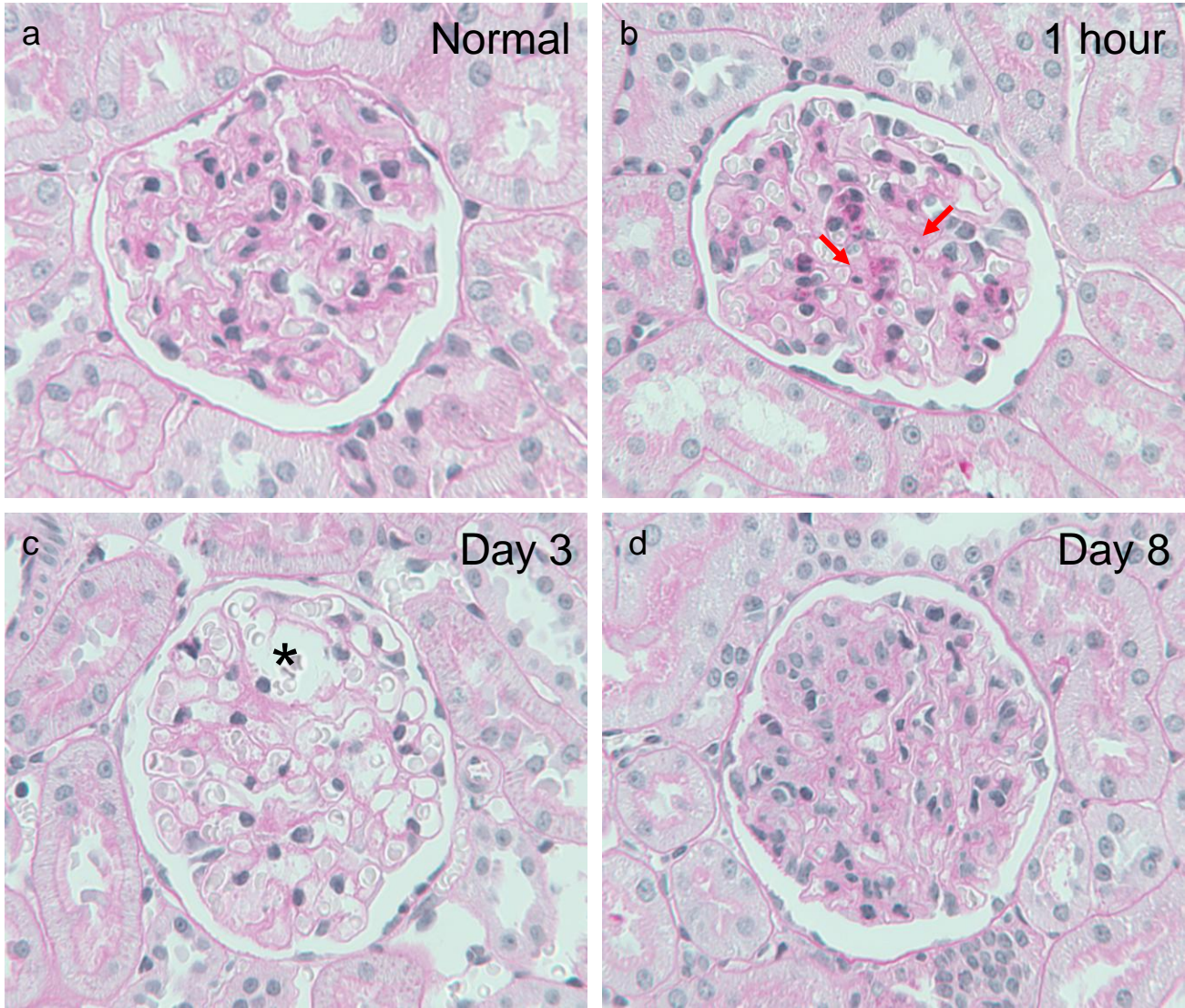


Figure 4.3

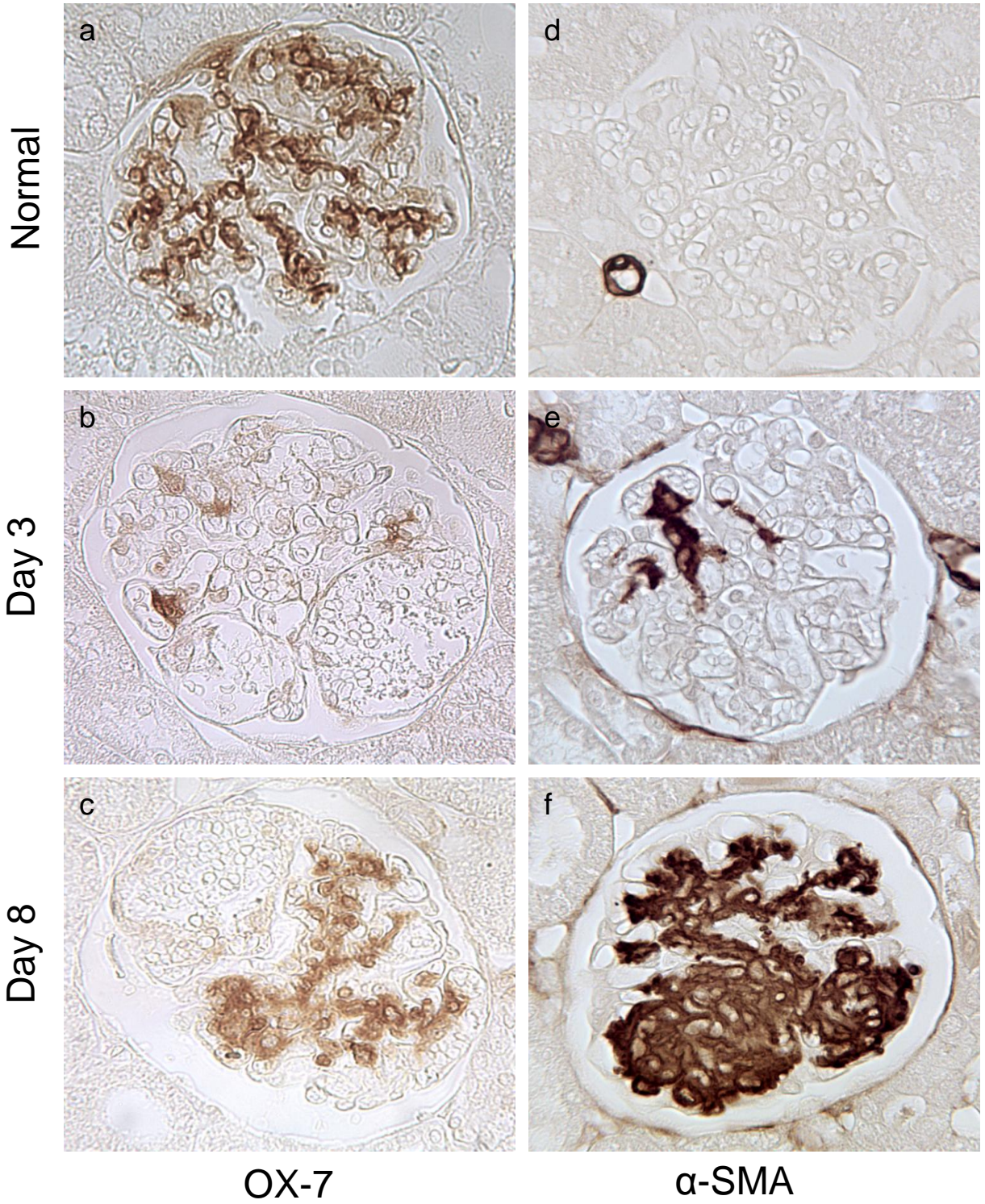


Figure 4.4

p-JNK immunostaining

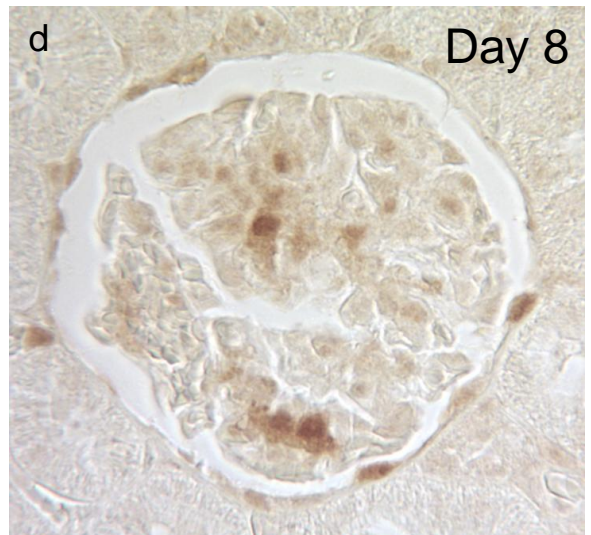
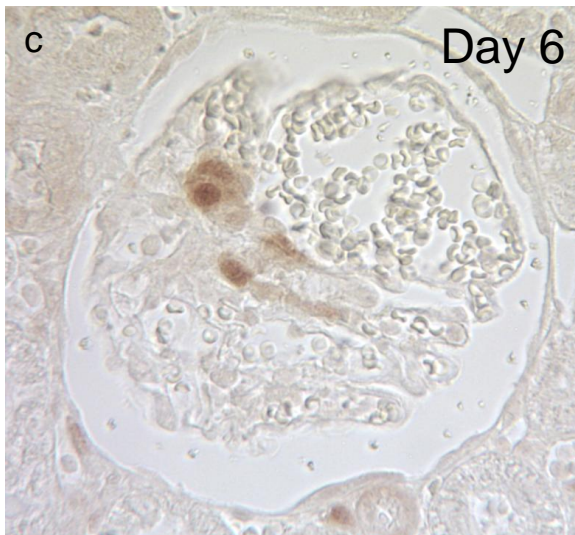
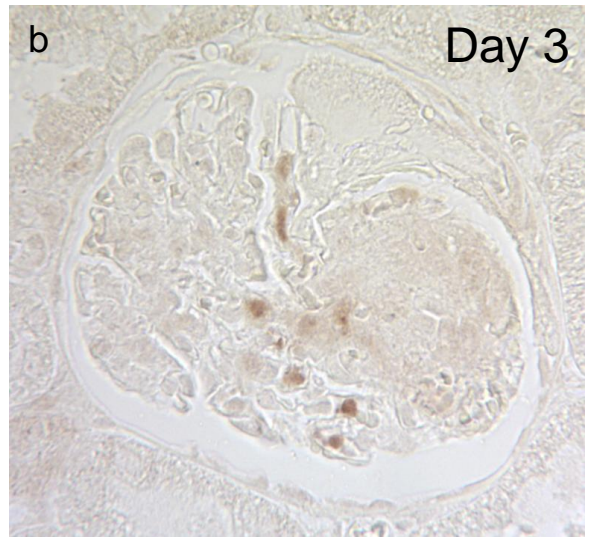
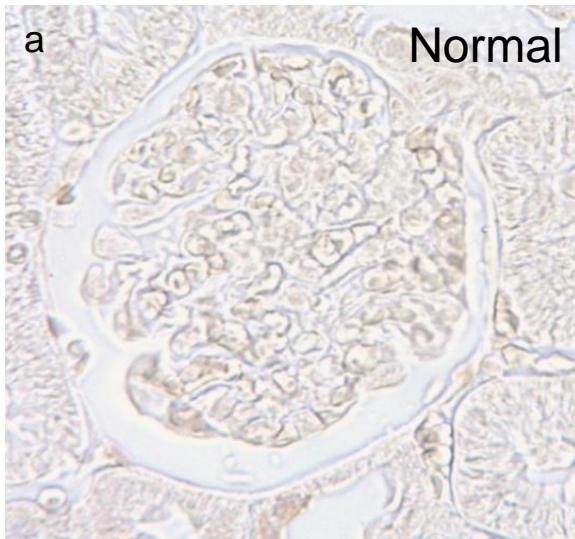


Figure 4.5

c-Jun immunostaining

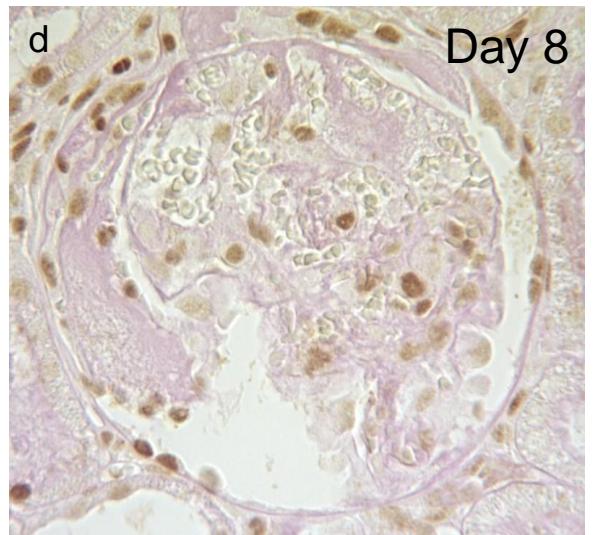
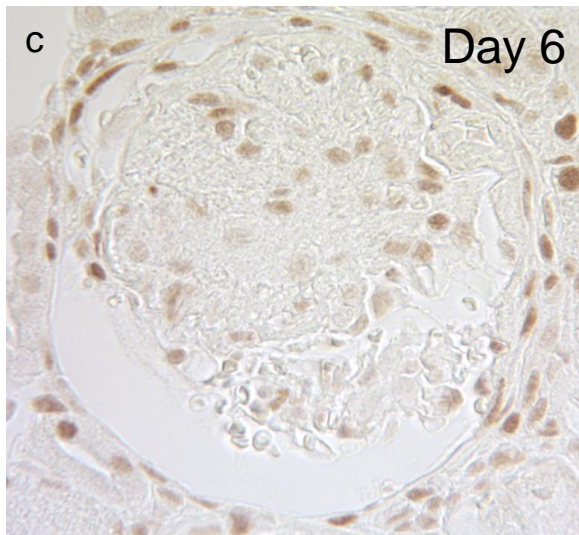
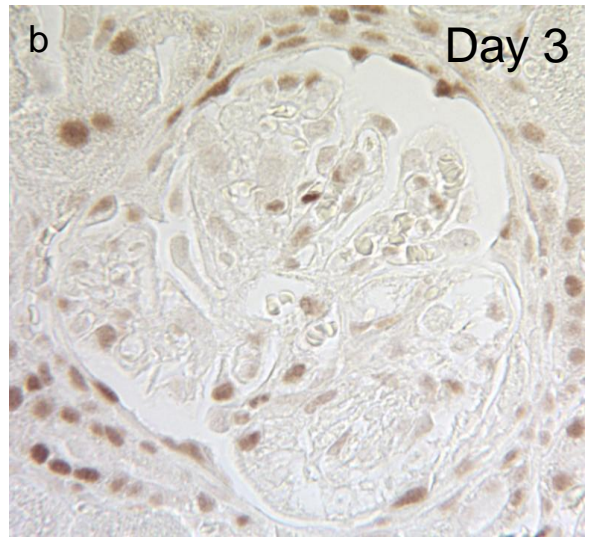
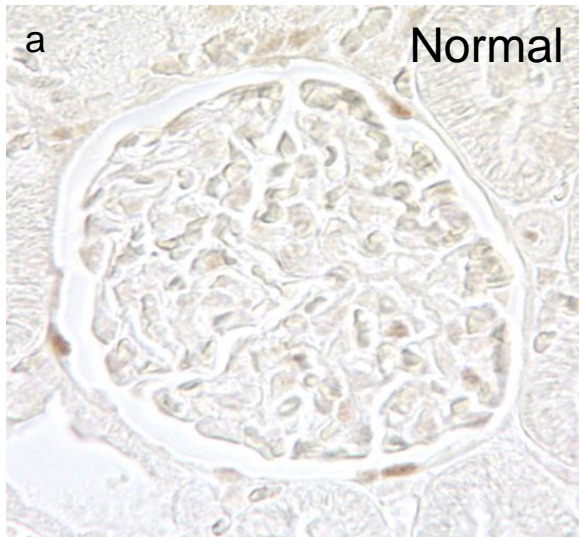
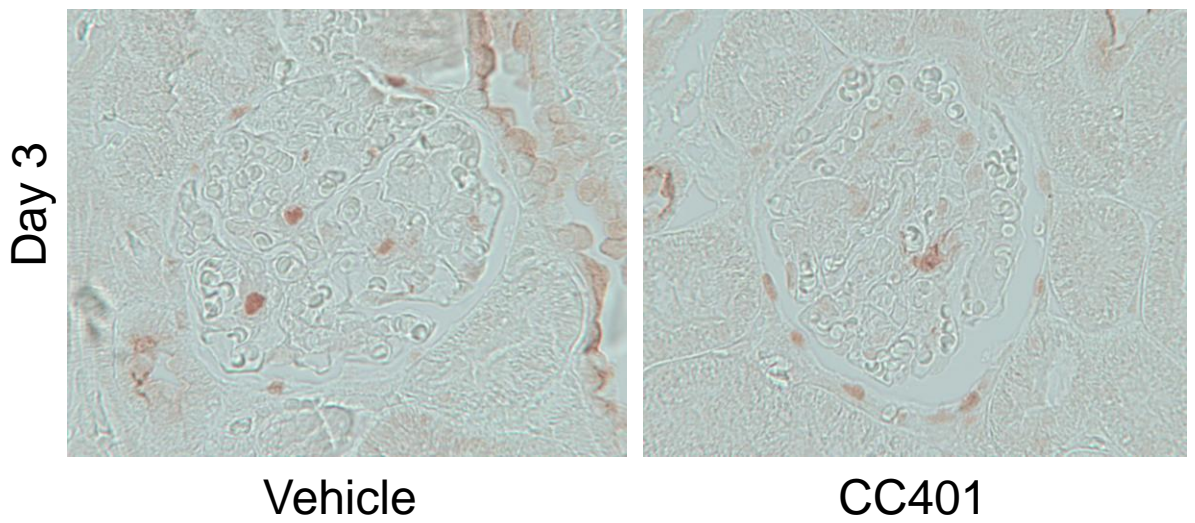


Figure 4.6

(a)

p-c-Jun Ser73 immunostaining



(b)

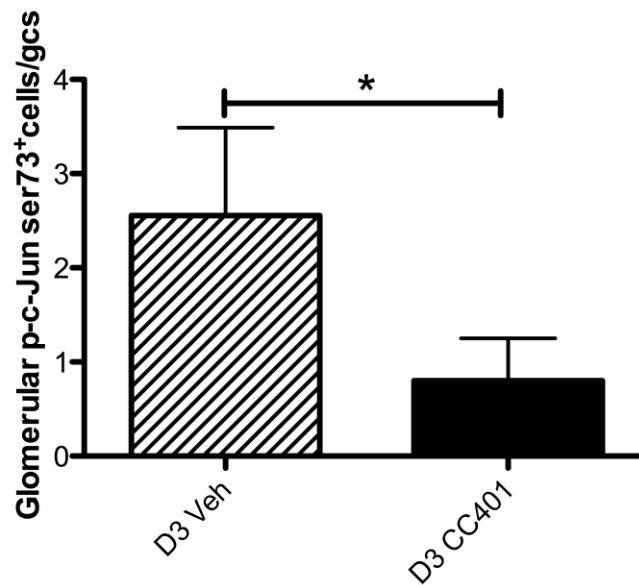
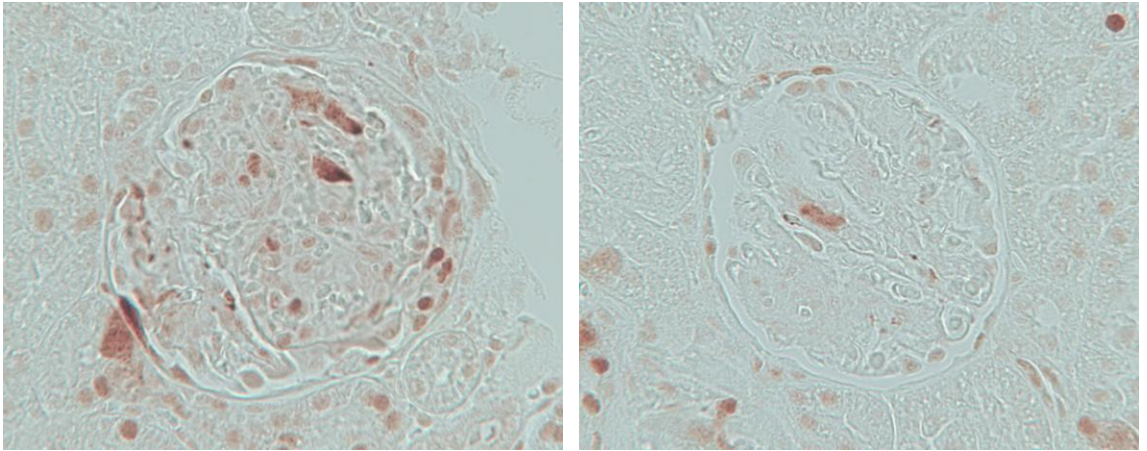


Figure 4.7

(a)

p-c-Jun Ser73 immunostaining

Day 8



Vehicle

CC401

(b)

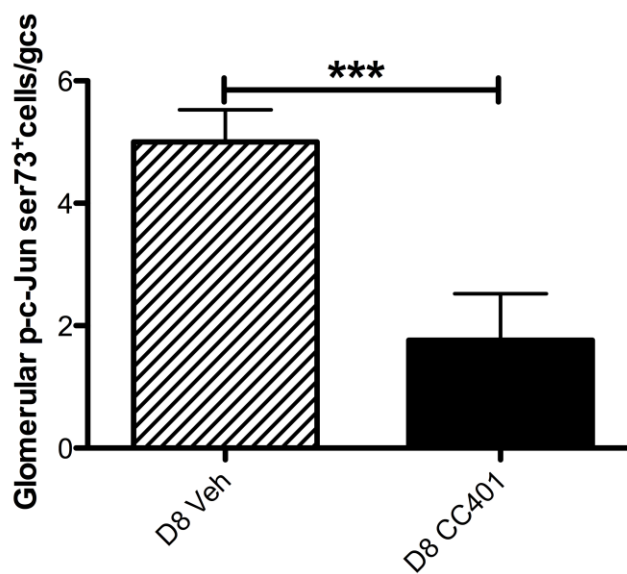


Figure 4.8

Day 3 of anti-Thy-1 nephritis

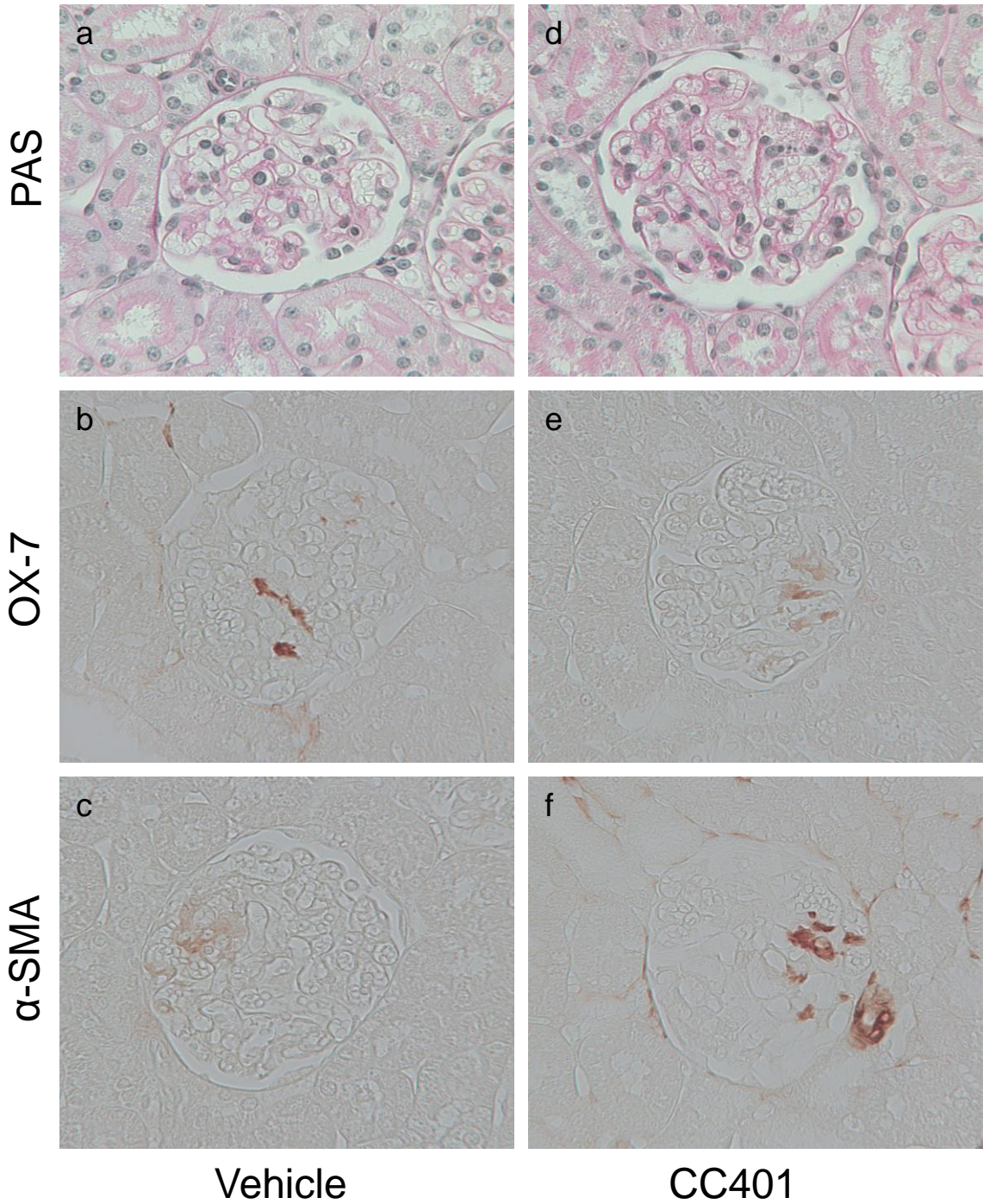


Figure. 4.9

Day 8 of anti-Thy-1 nephritis

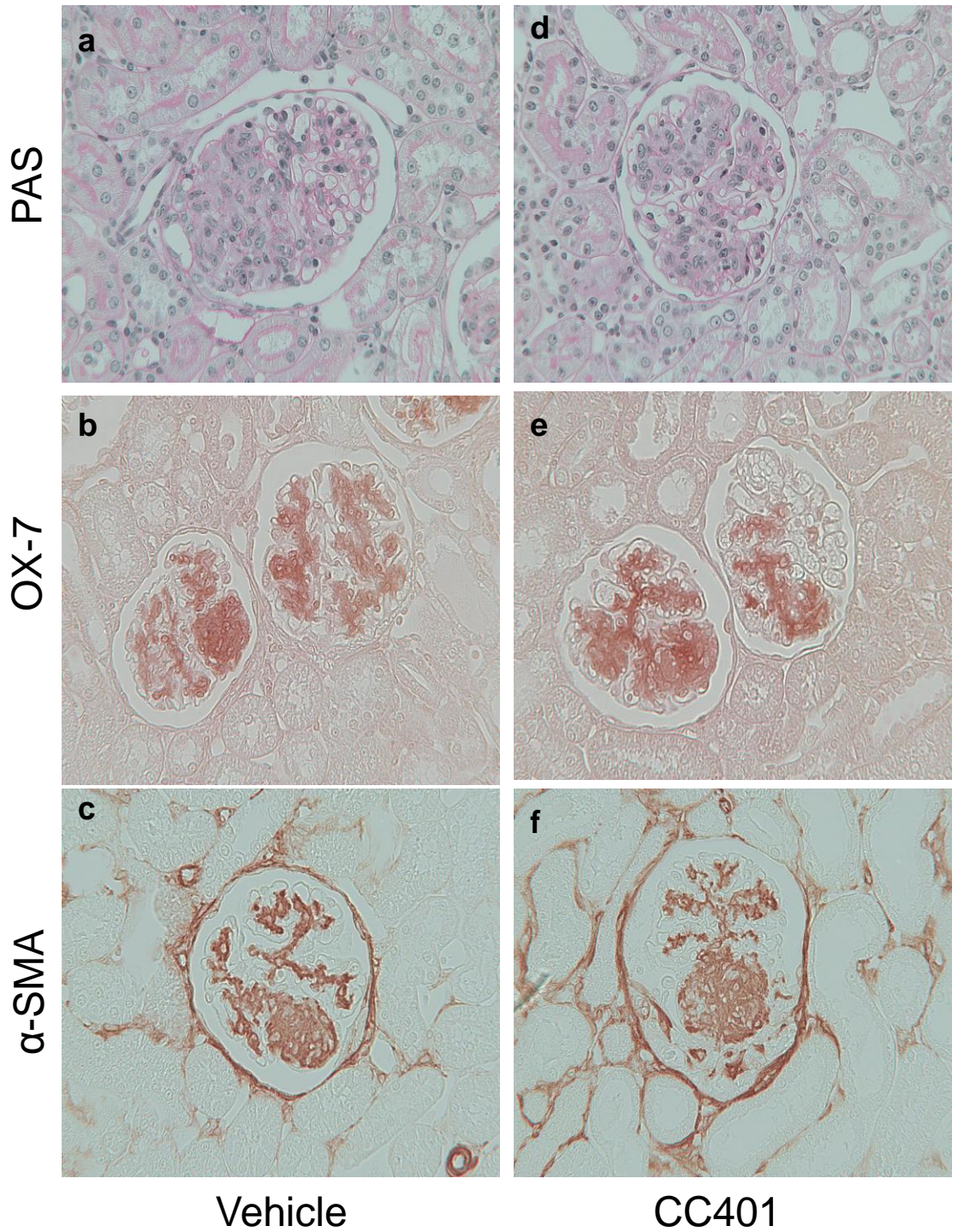


Figure 4.10

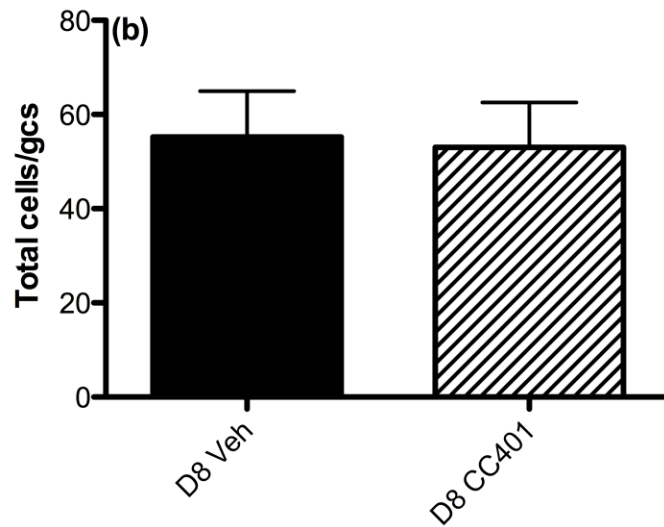
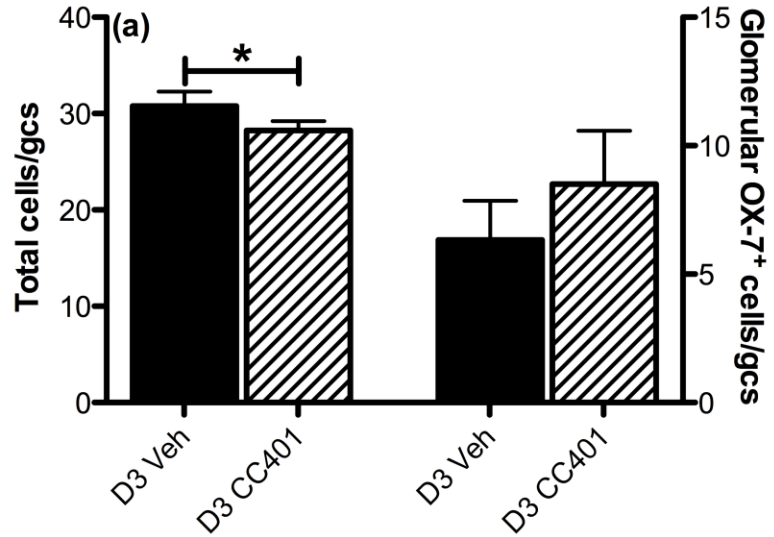


Figure 5.1

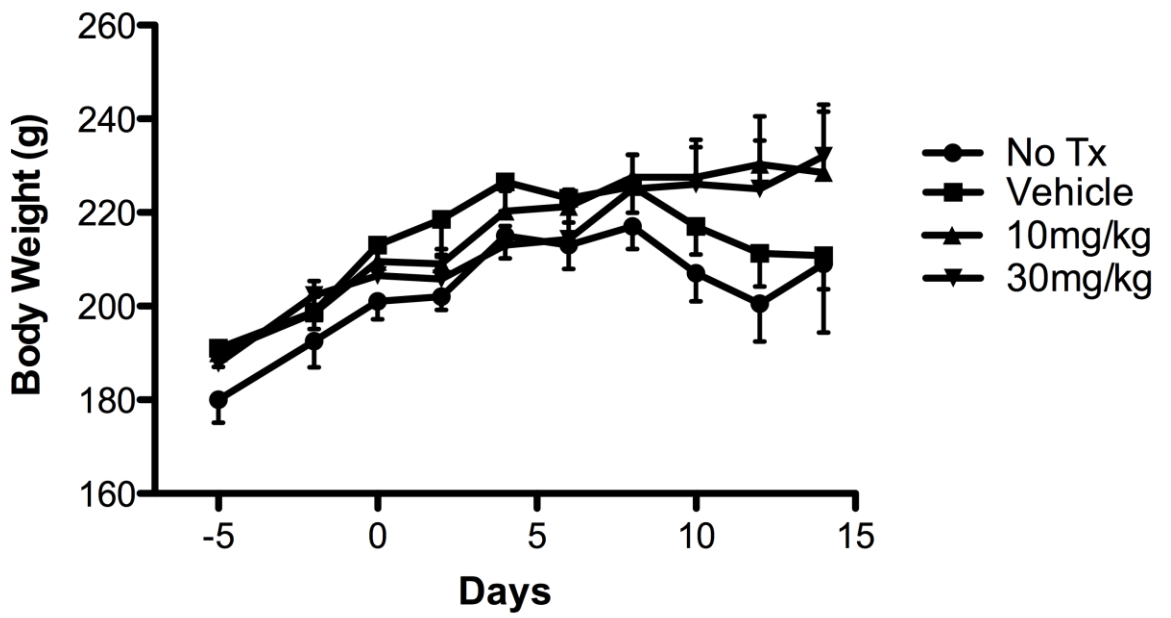


Figure 5.2

CD68 (ED1) immunostaining

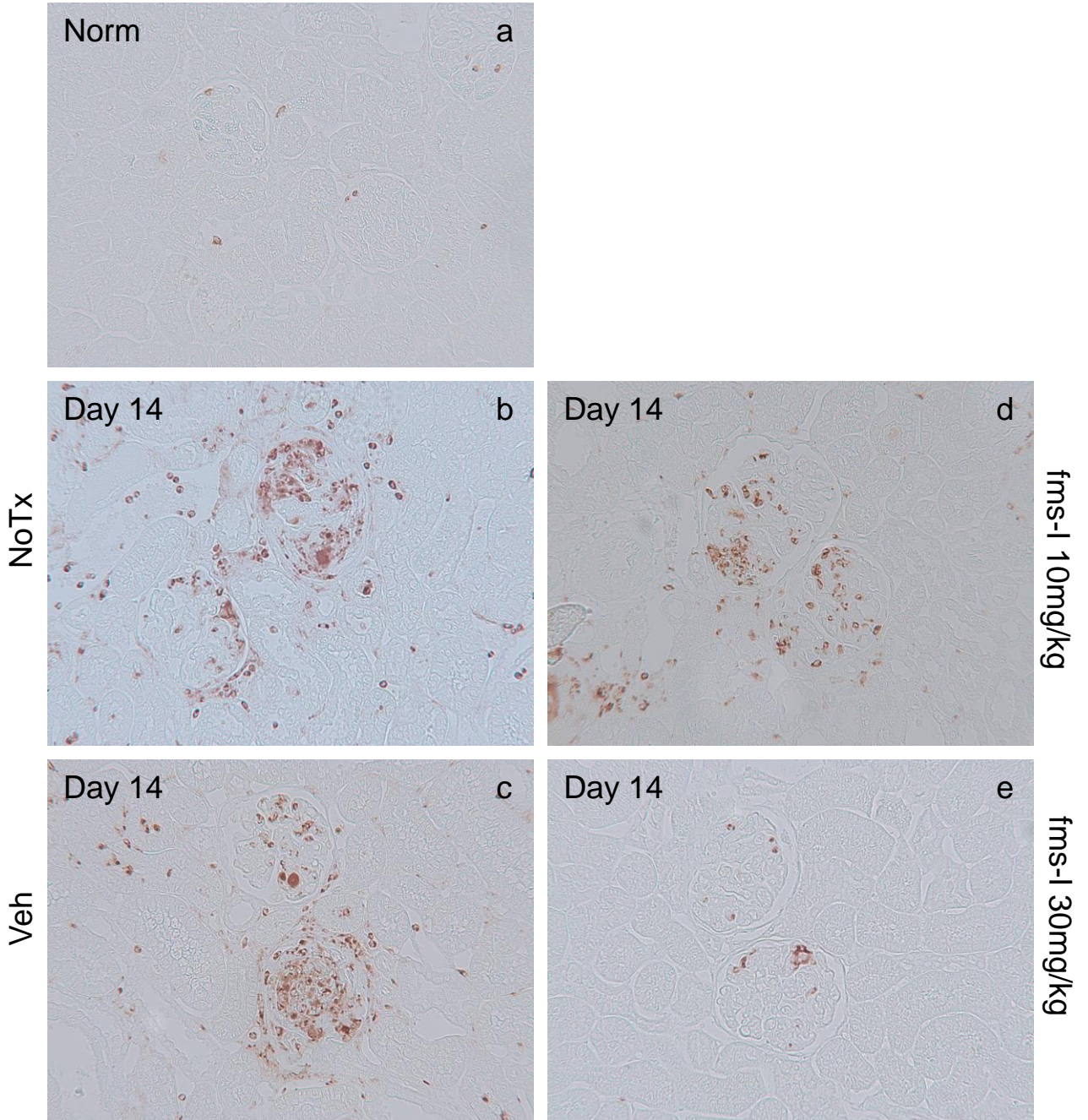


Figure 5.3

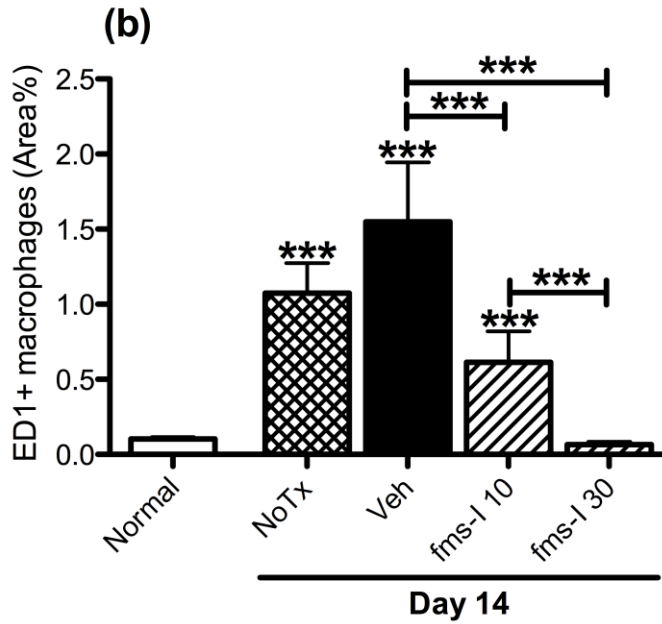
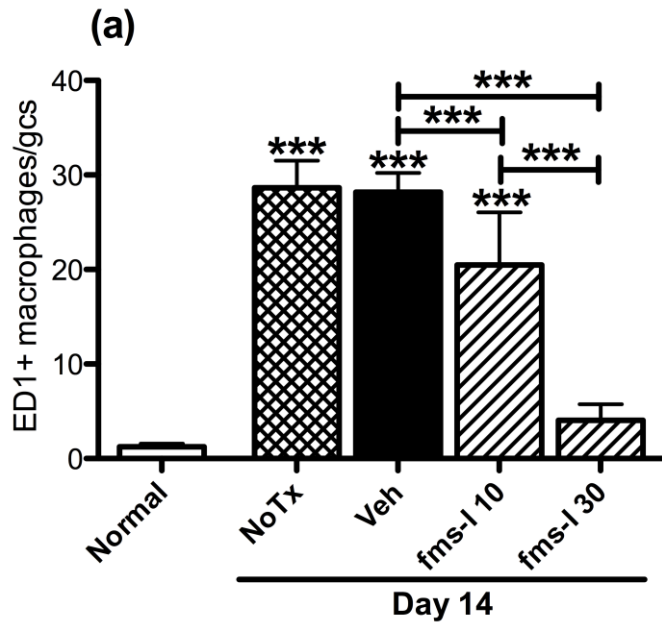


Figure 5.4

CD68 (ED1) immunostaining

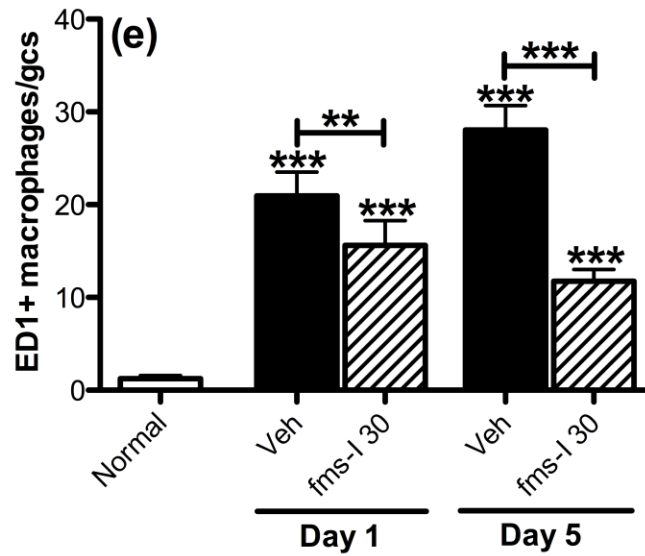
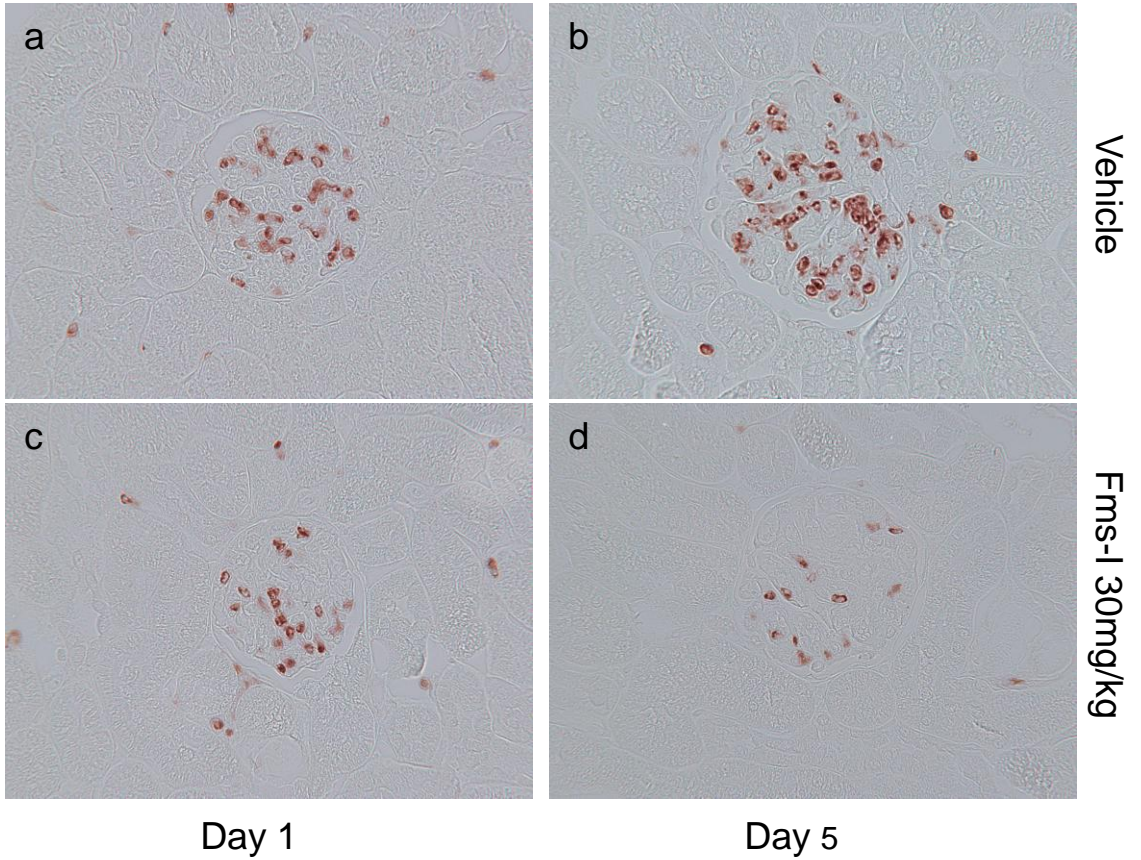


Figure 5.5

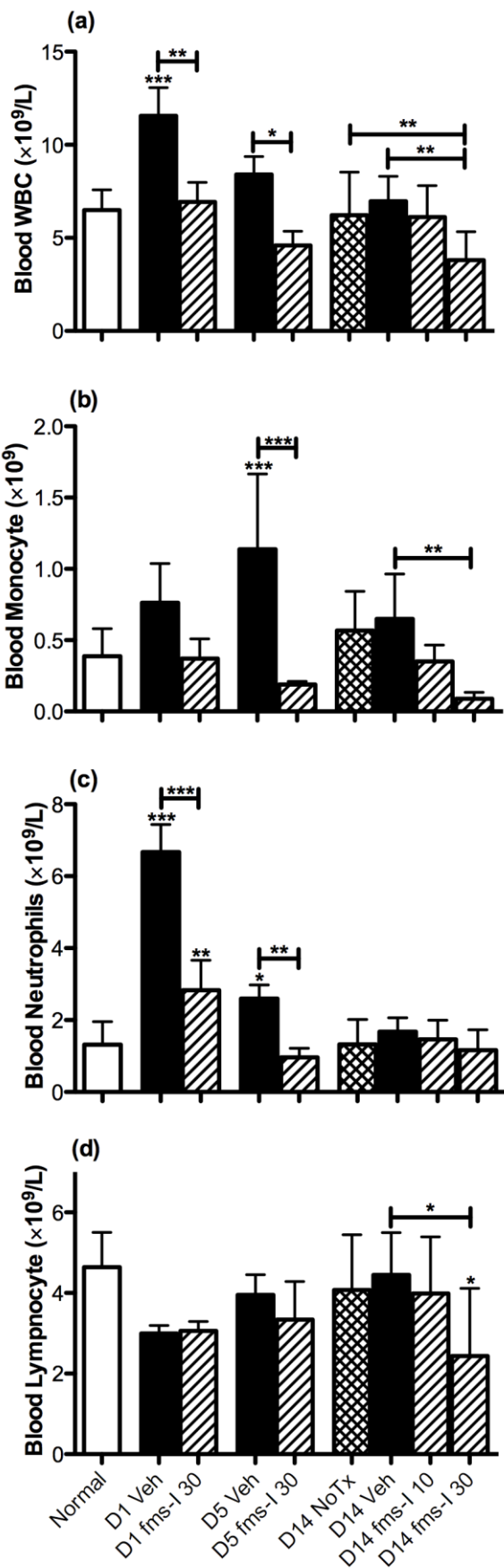


Figure 5.6

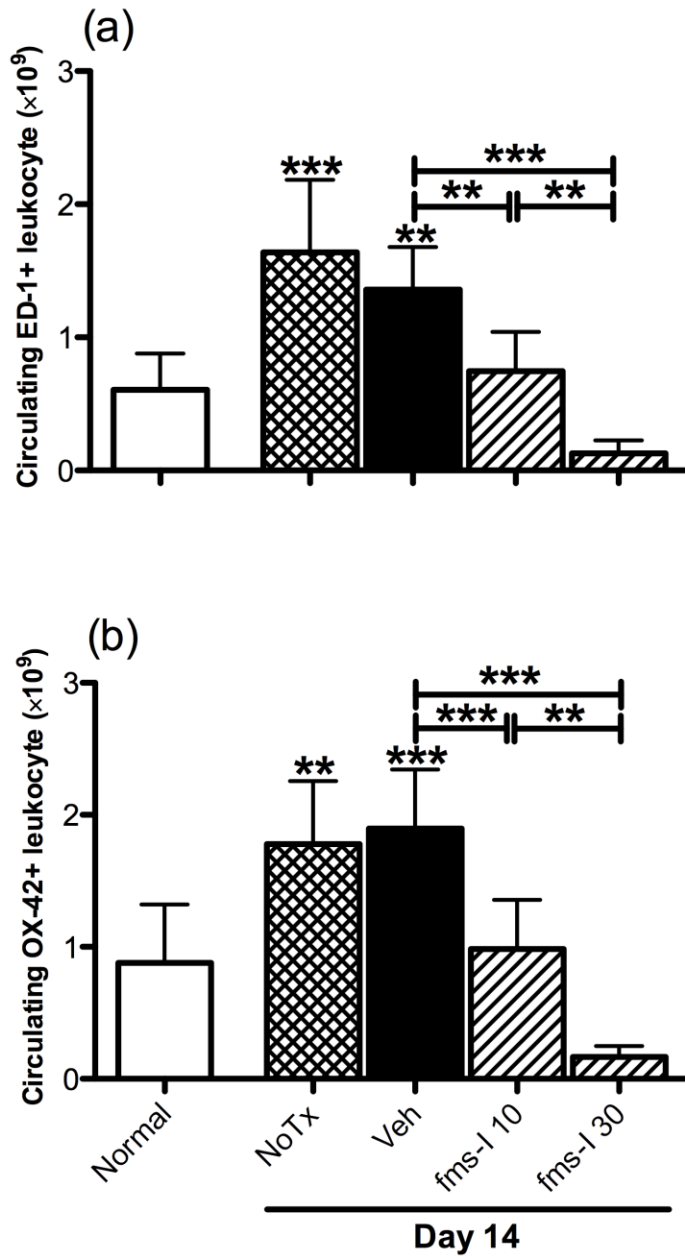


Figure 5.7

ED1(blue/grey)/PCNA(brown) double immunostaining

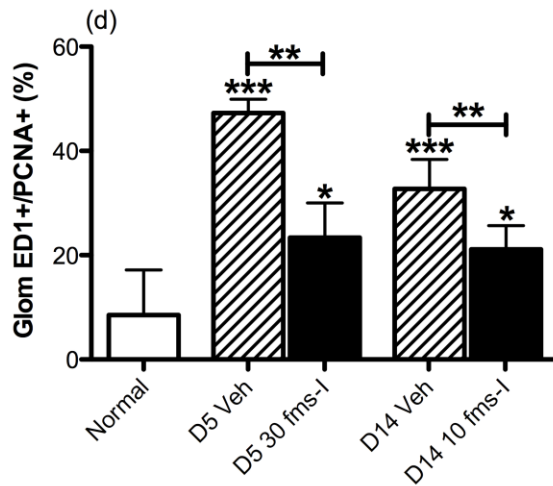
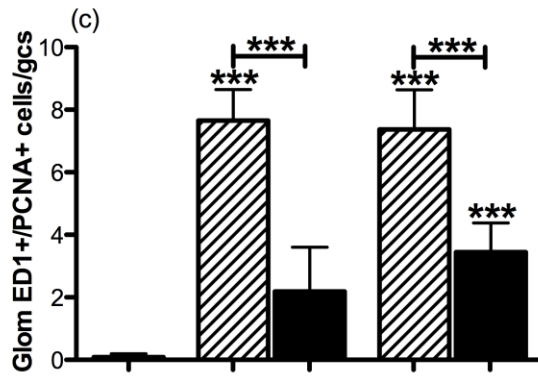
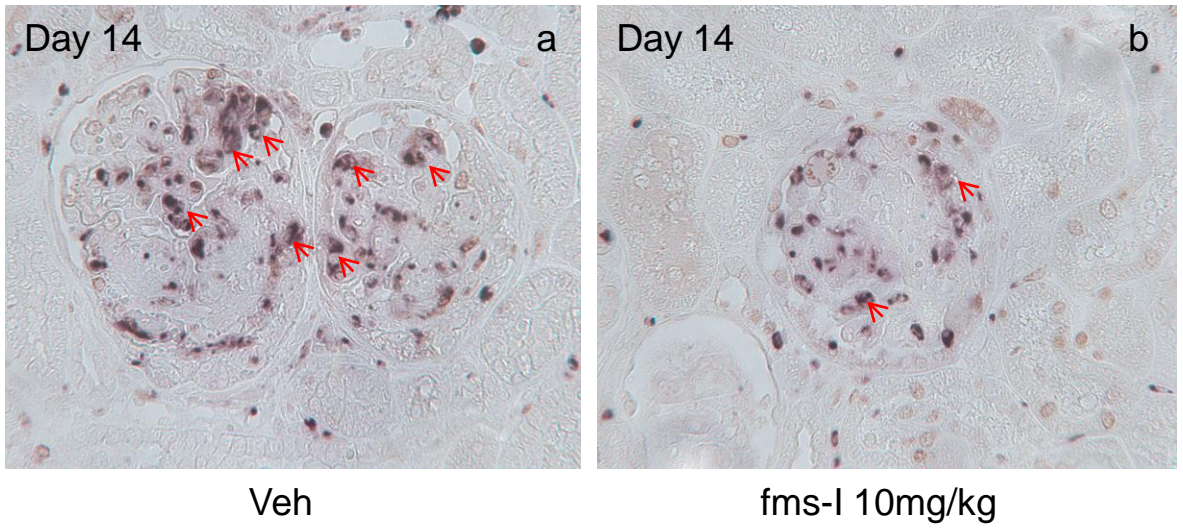
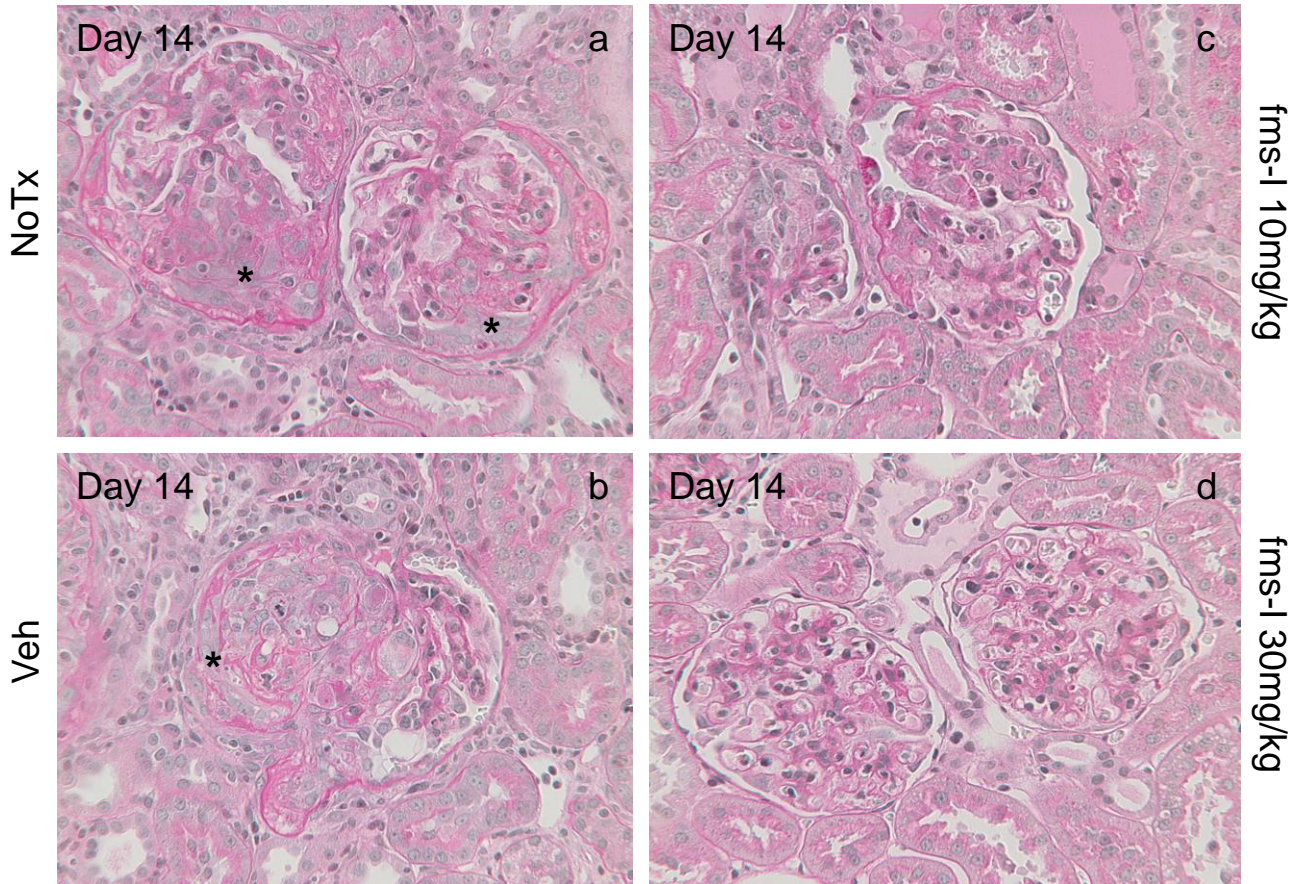


Figure. 5.8

Periodic acid-Schiff staining



PTAH staining

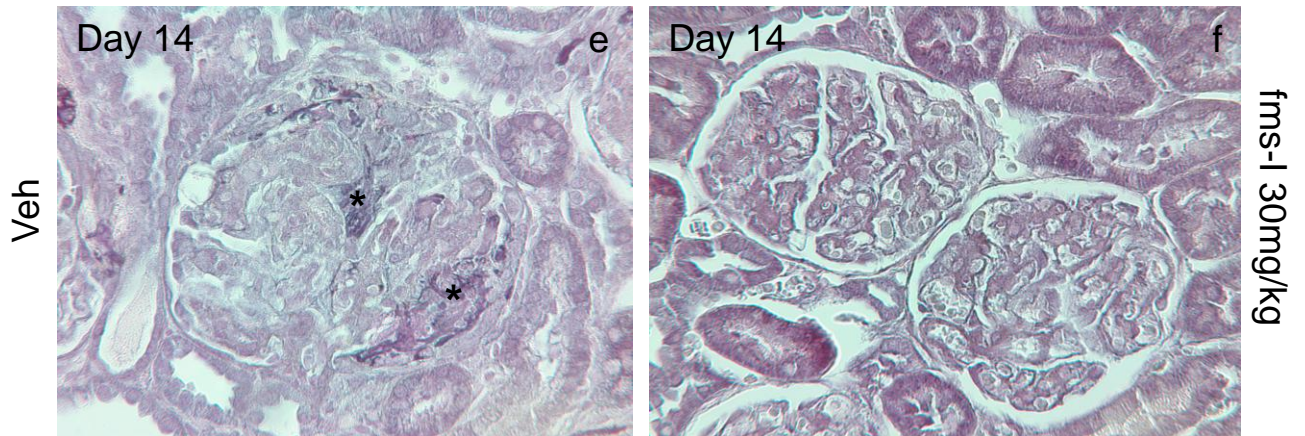


Figure 5.9

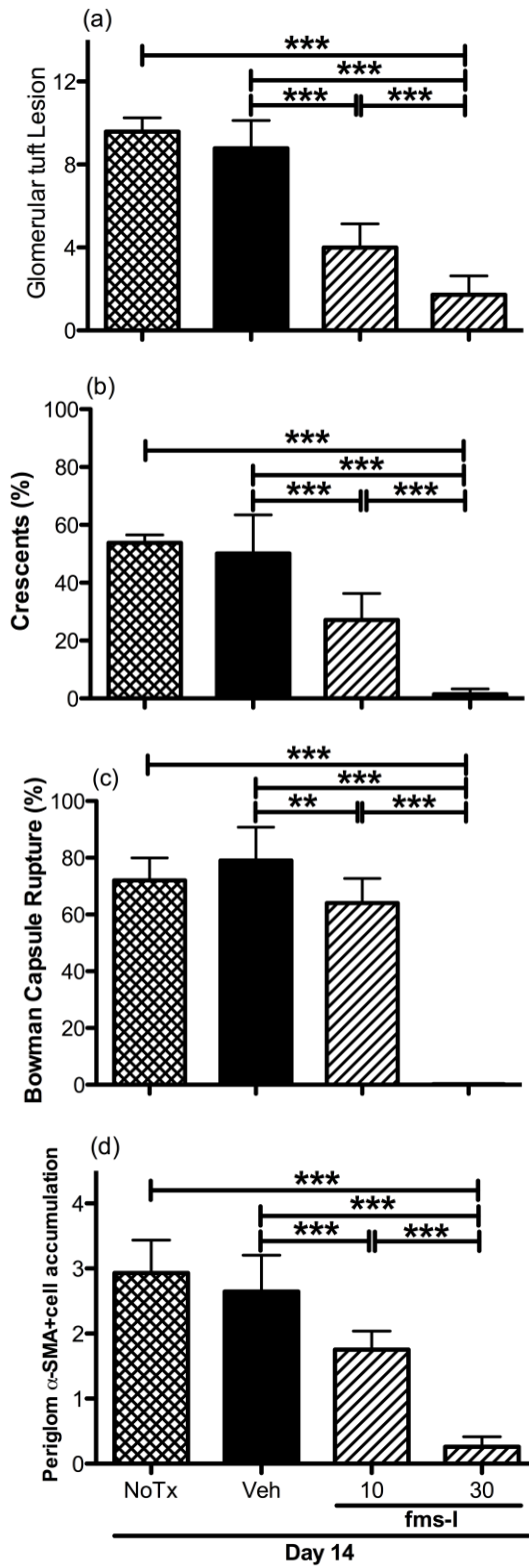


Figure 5.10

Periodic acid-Schiff staining

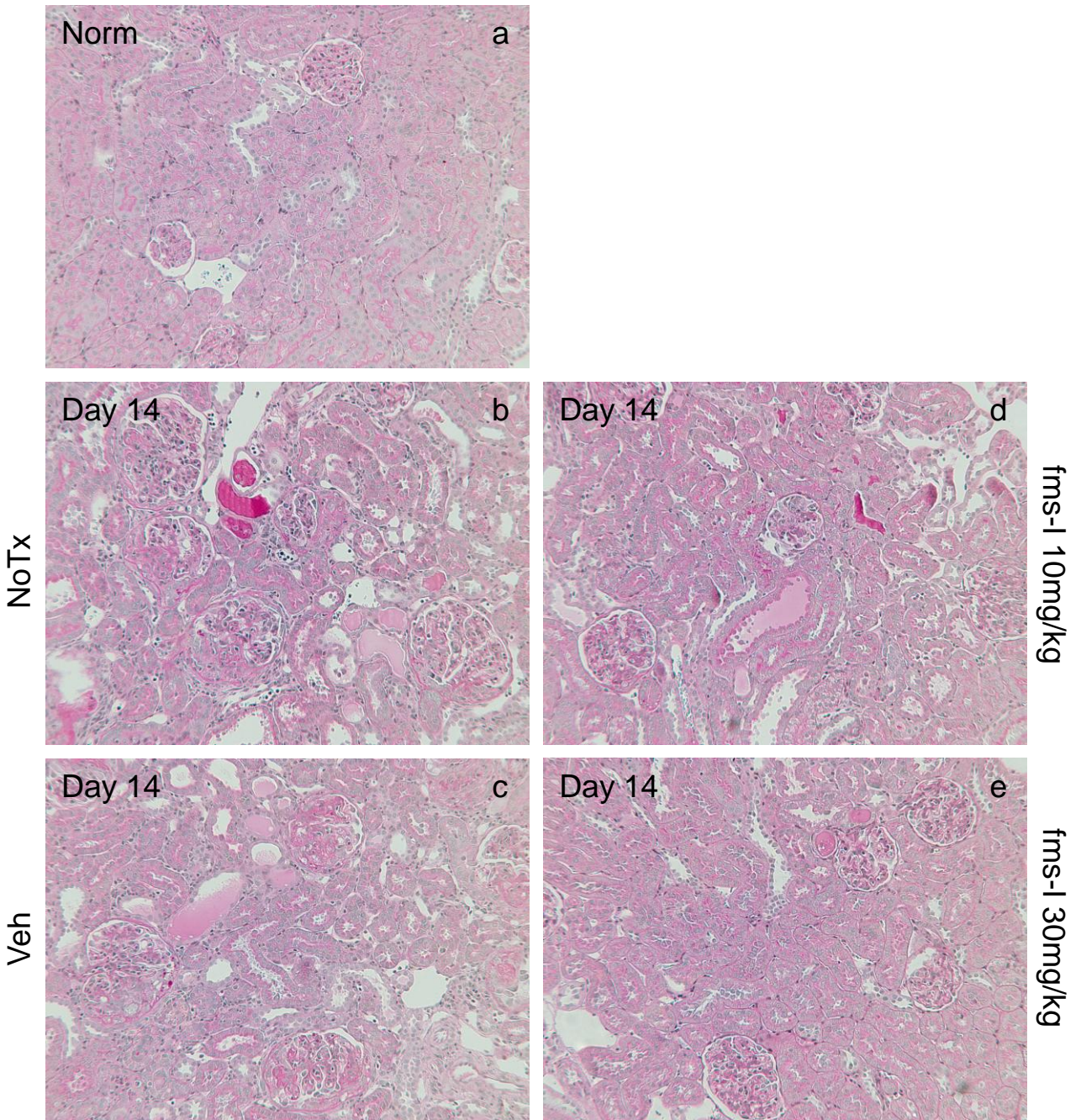


Figure 5.11

Vimentin immunostaining

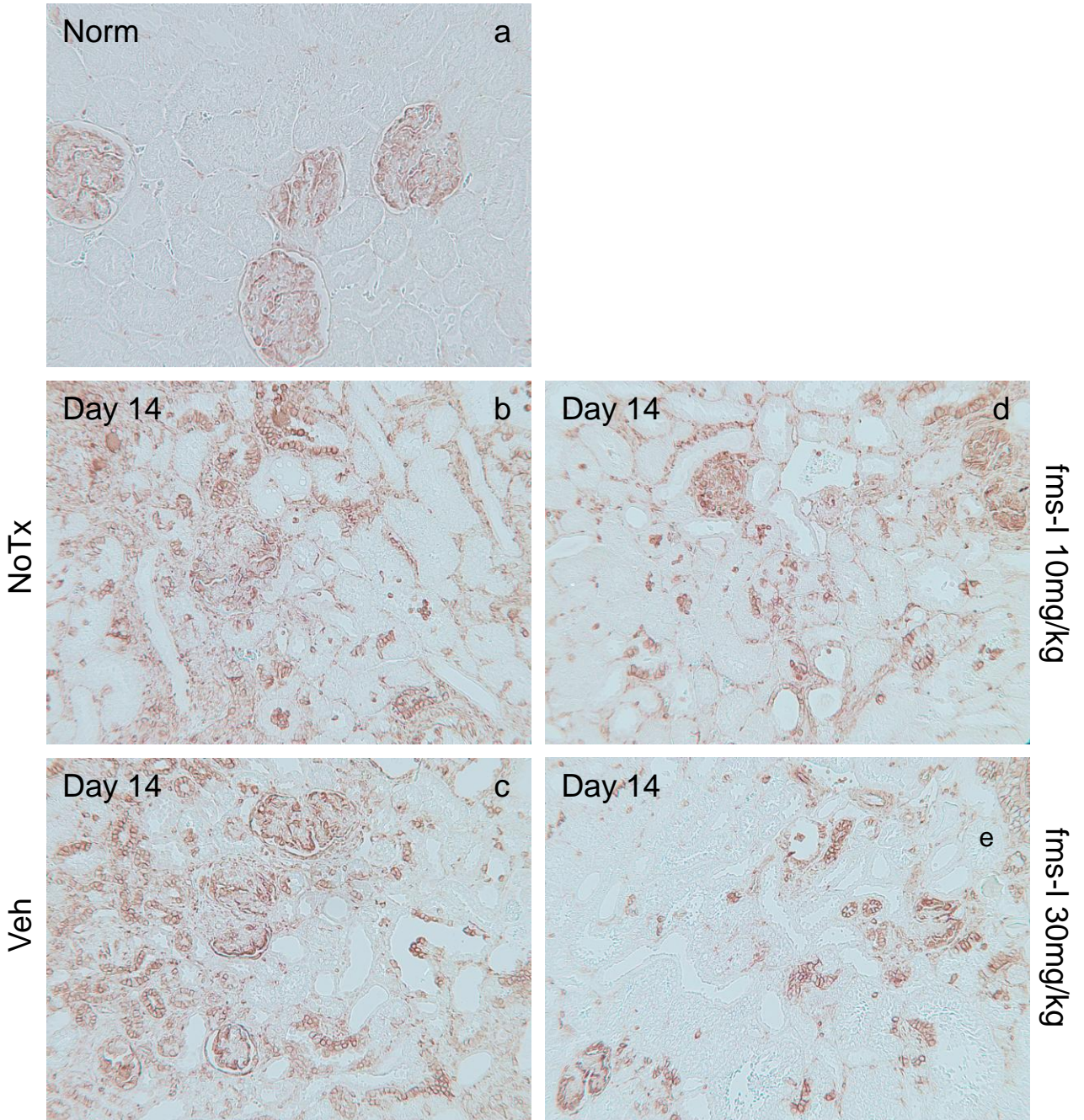


Figure 5.12

Oesteopontin immunostaining

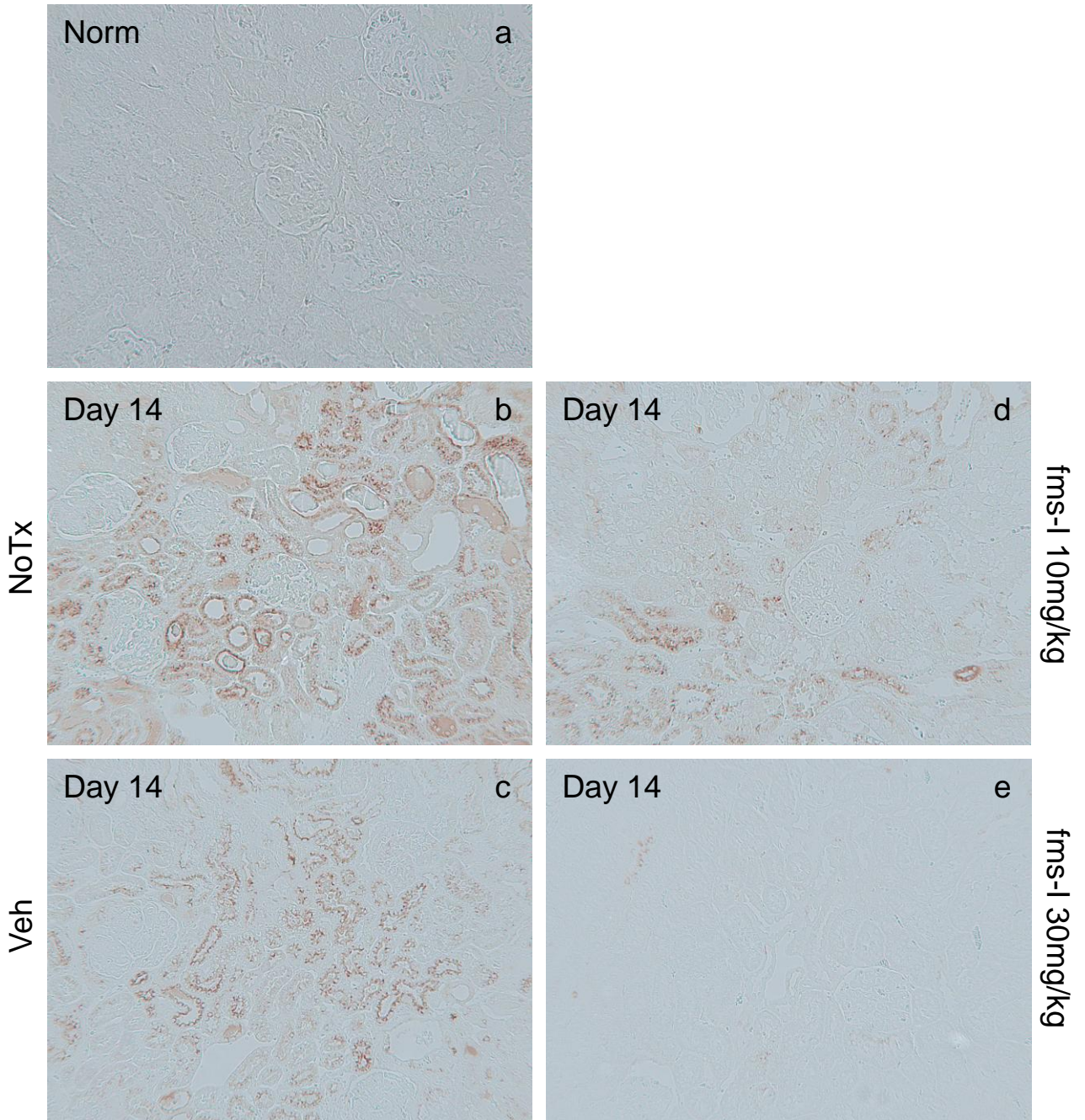


Figure 5.13

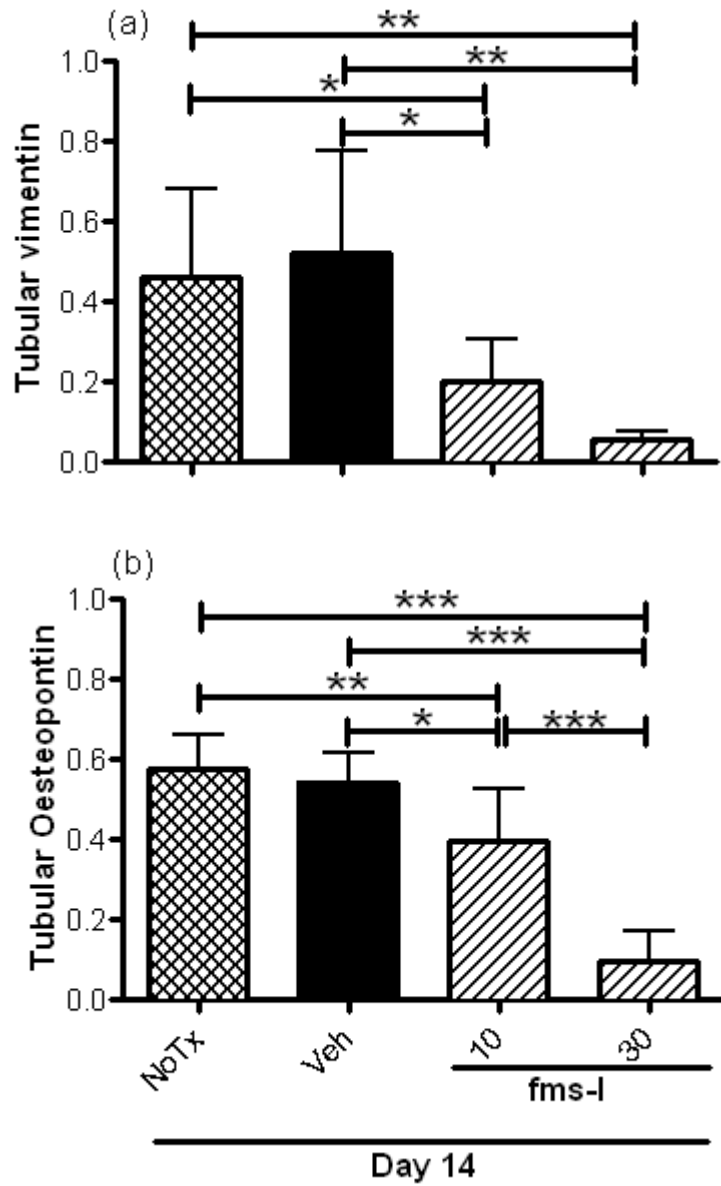


Figure 5.14

Collagen IV immunostaining

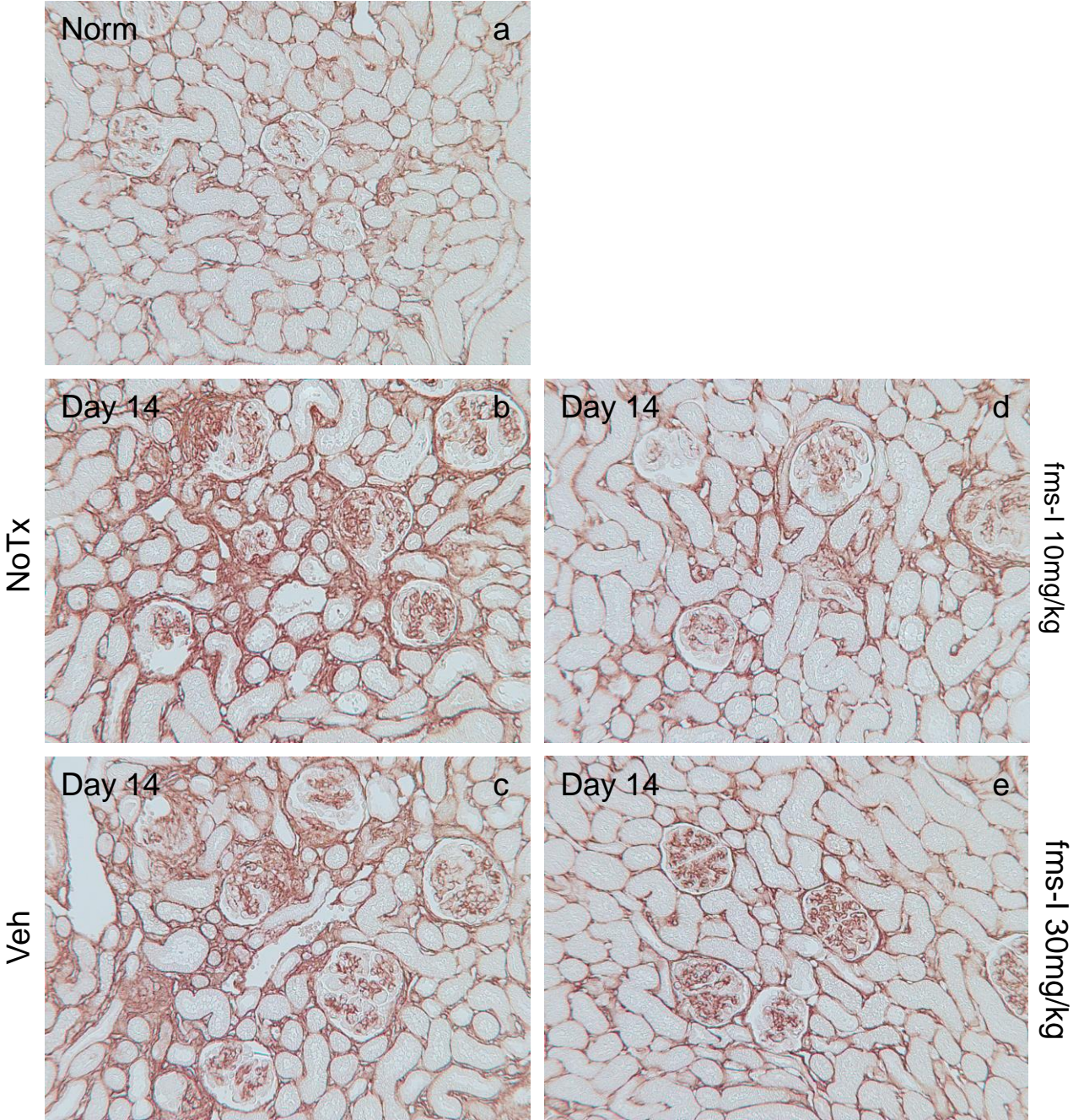


Figure 5.15

α -SMA immunostaining

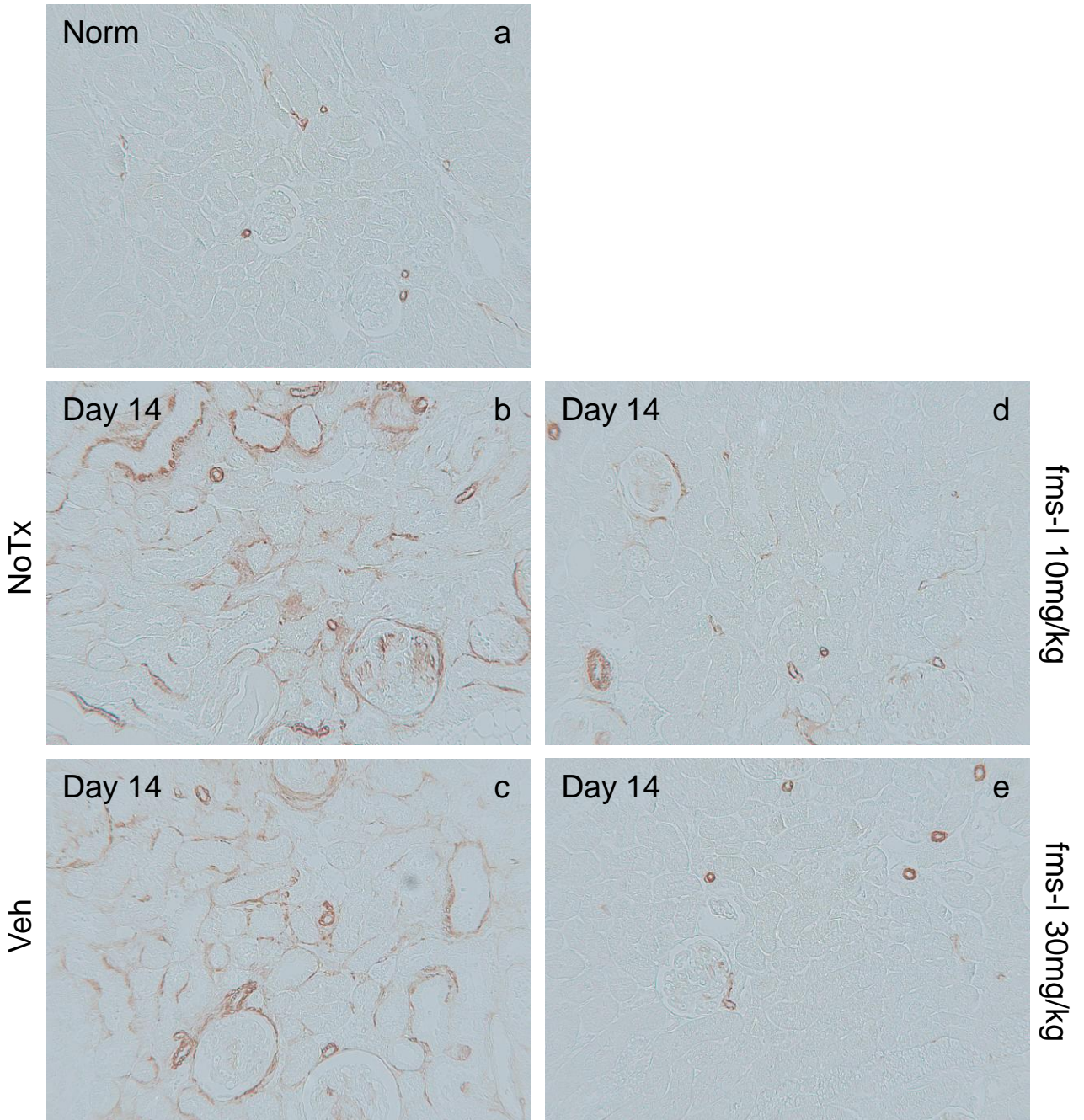


Figure 5.16

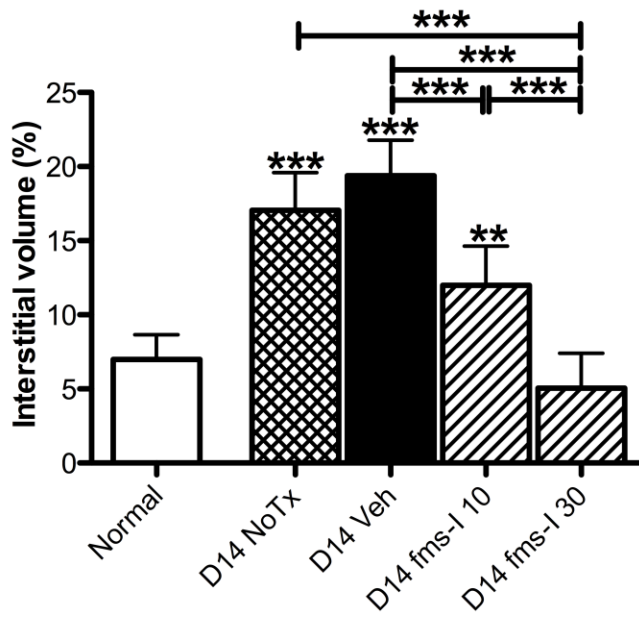


Figure 5.17

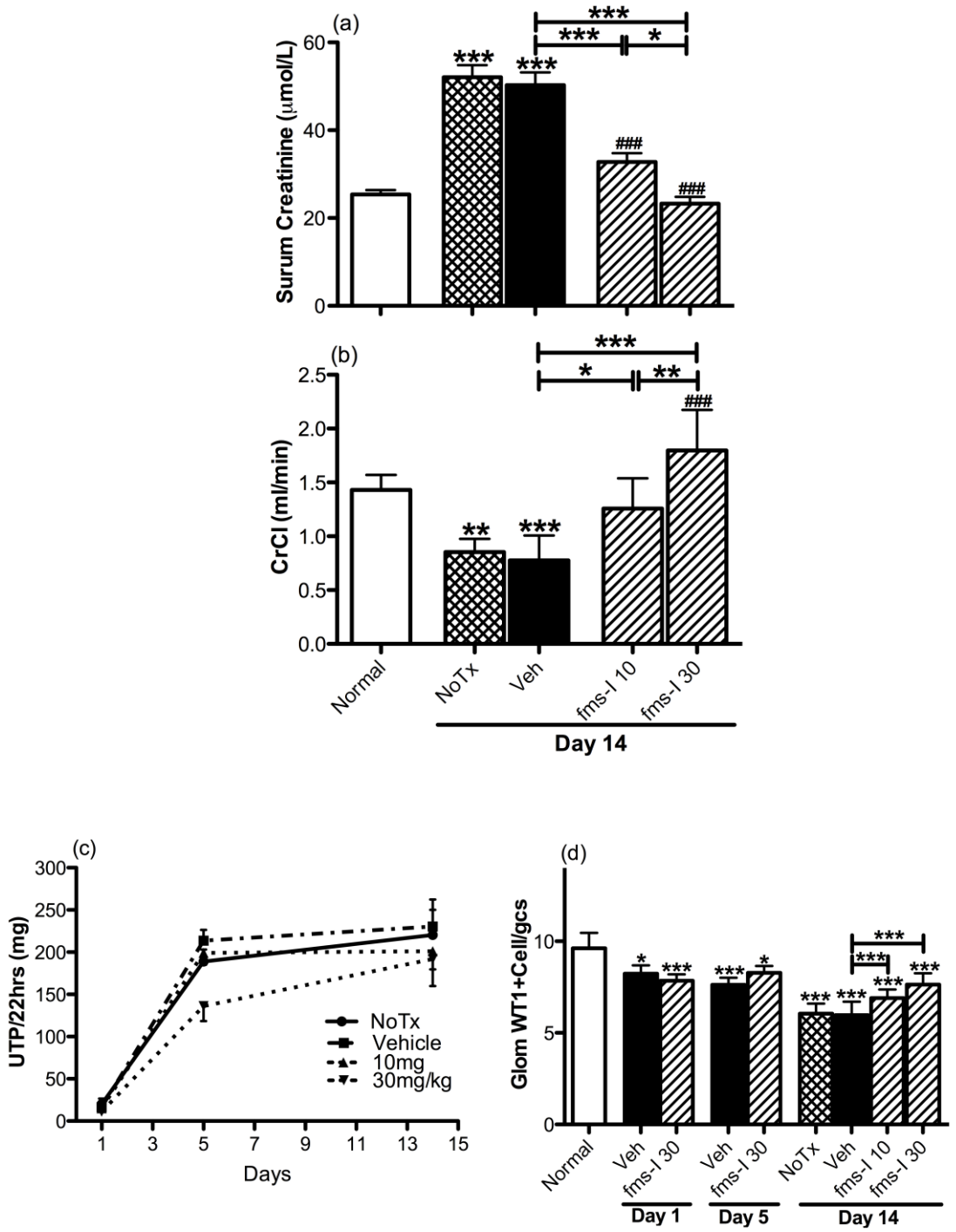


Figure 5.18

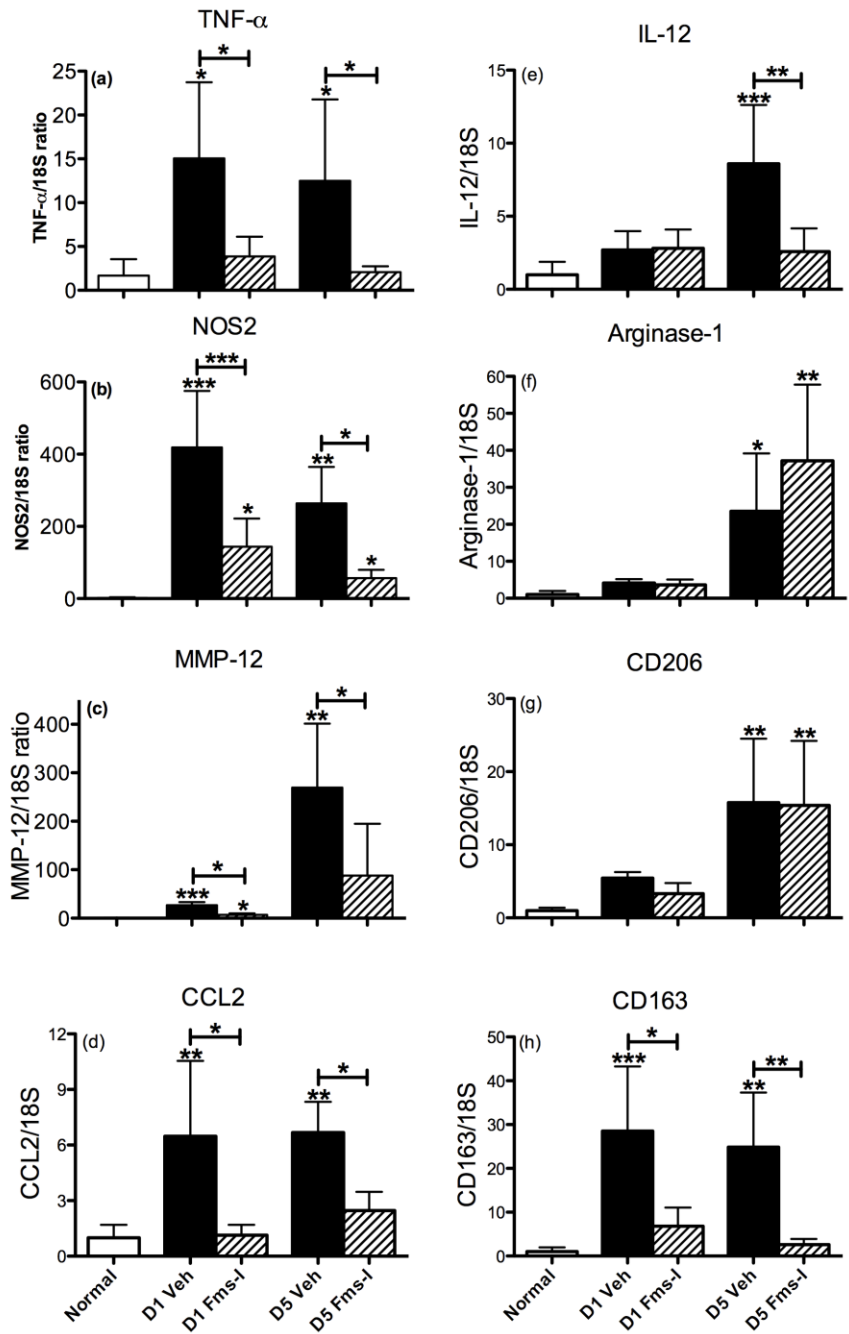


Figure 5.19

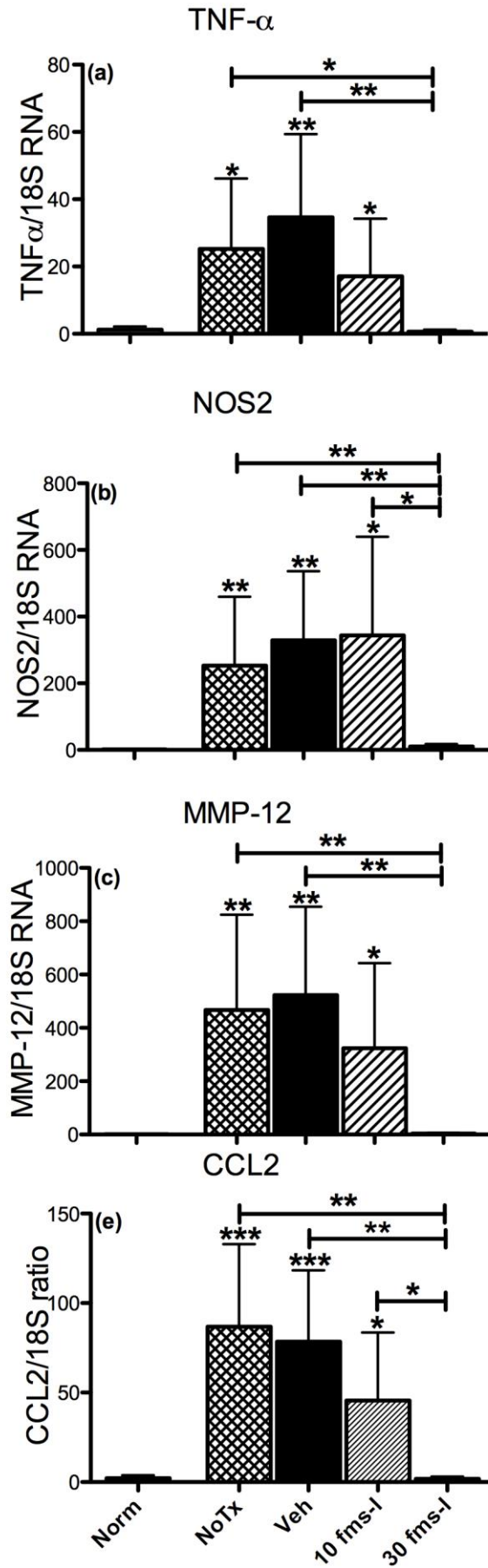


Figure 5.20

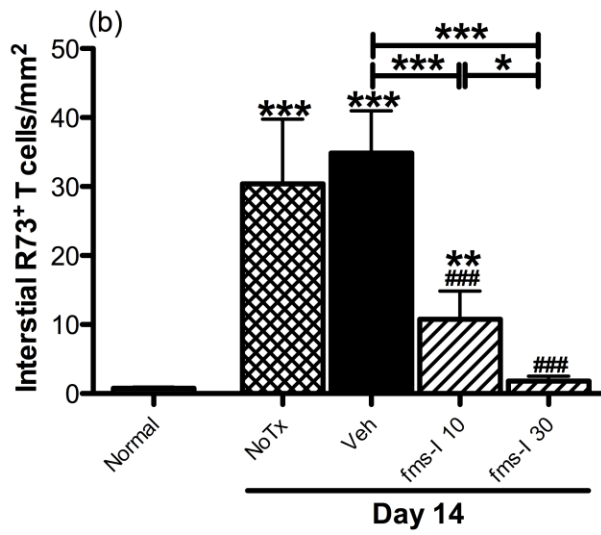
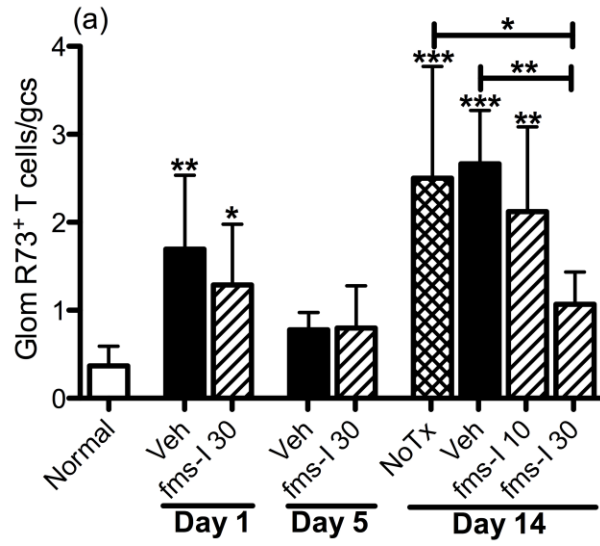


Figure 5.21

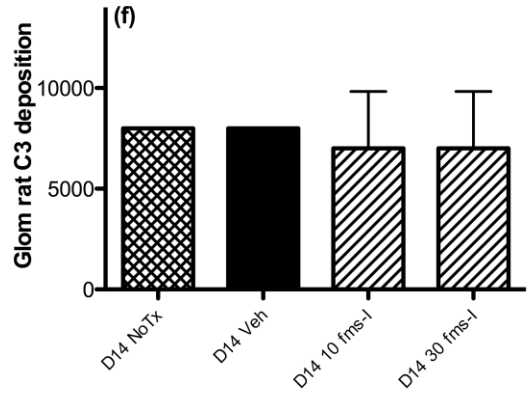
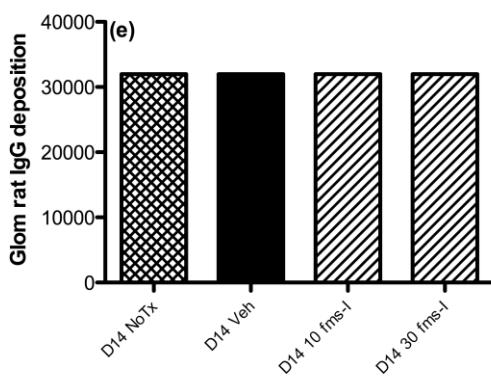
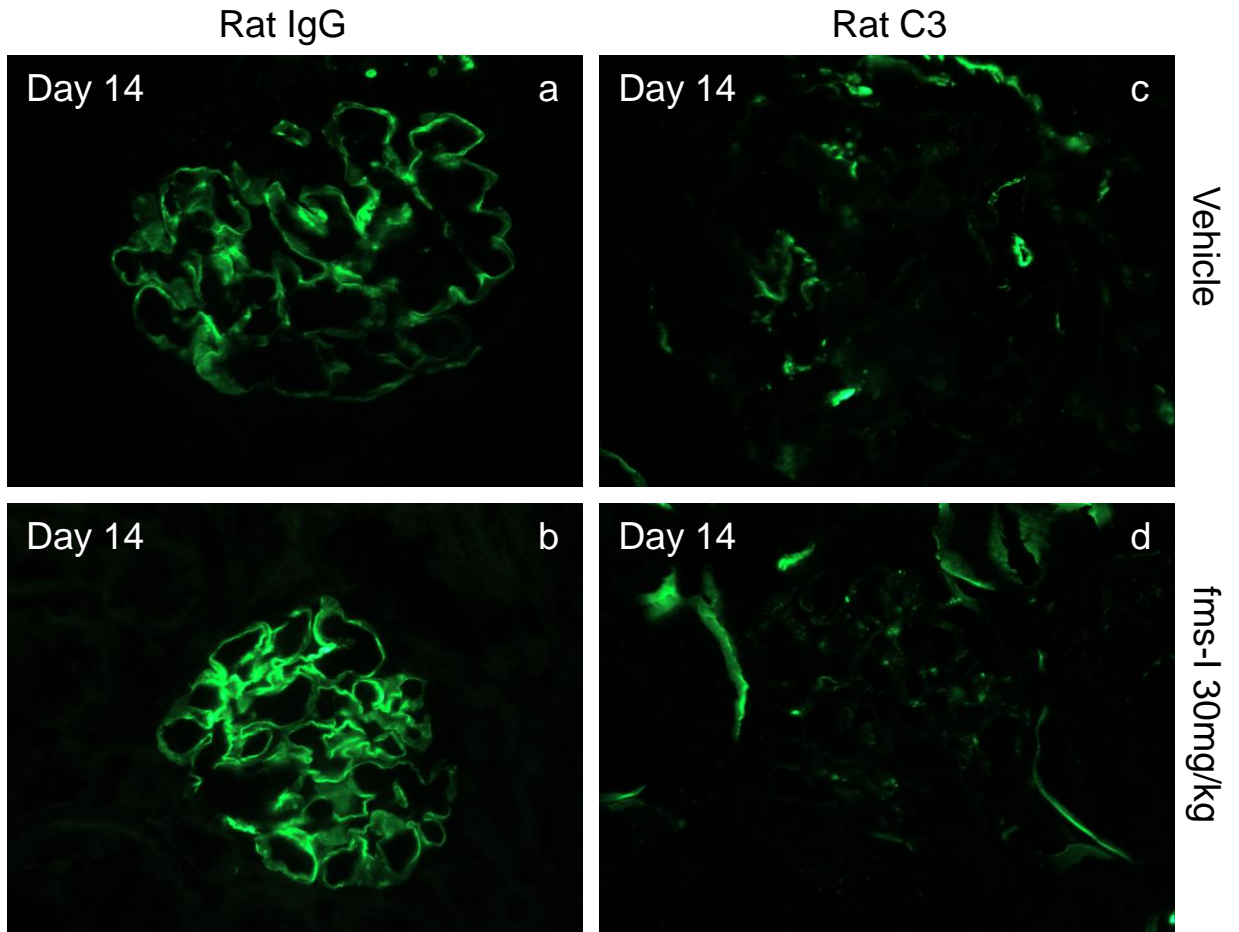


Figure 5.22

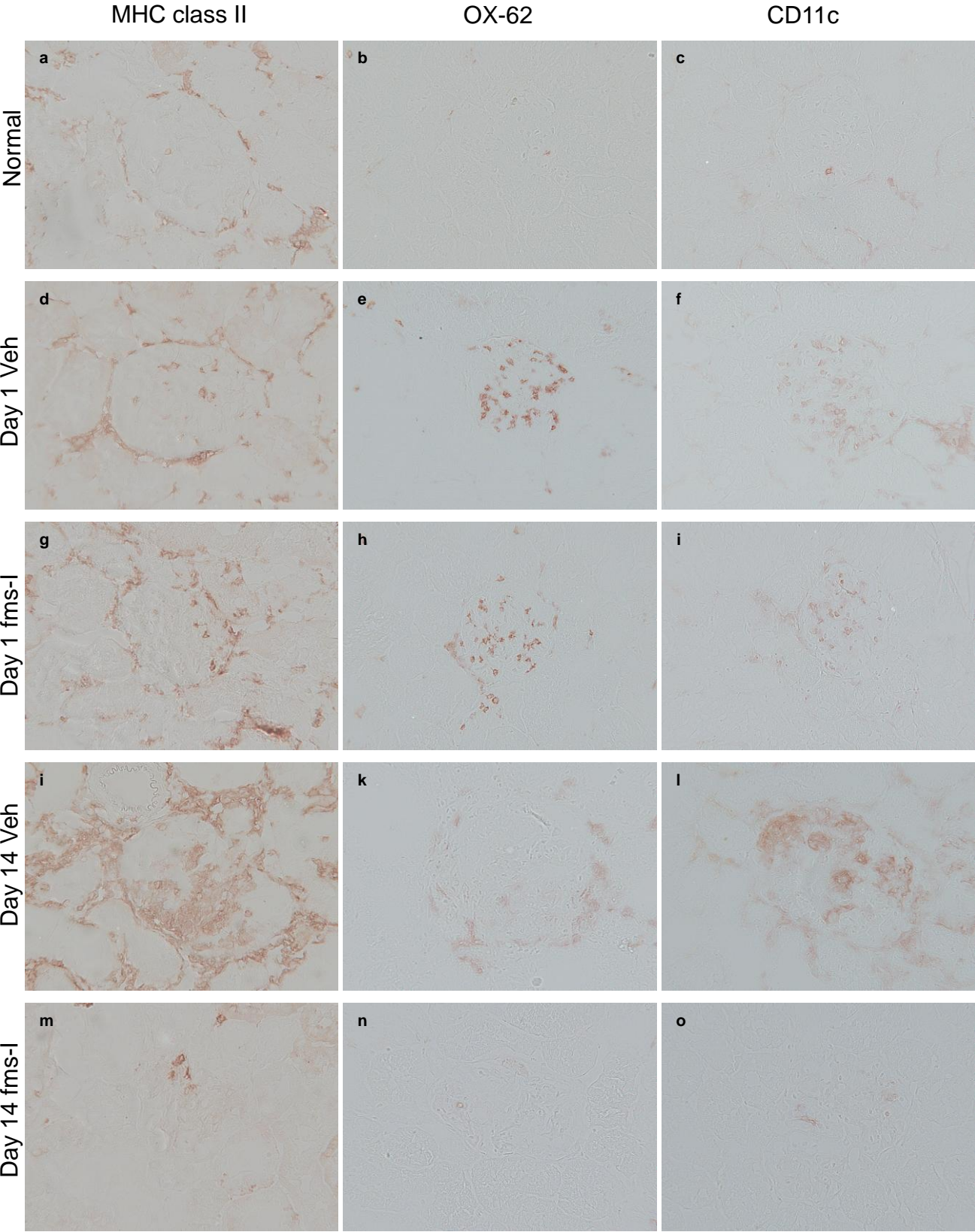


Figure 6.1

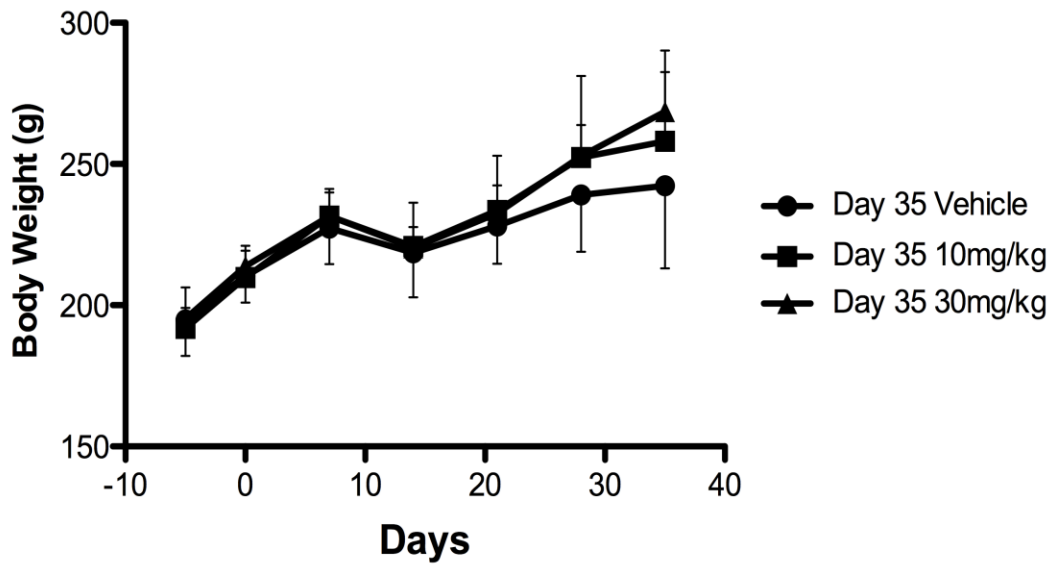


Figure 6.2

CD68 (ED1) immunostaining

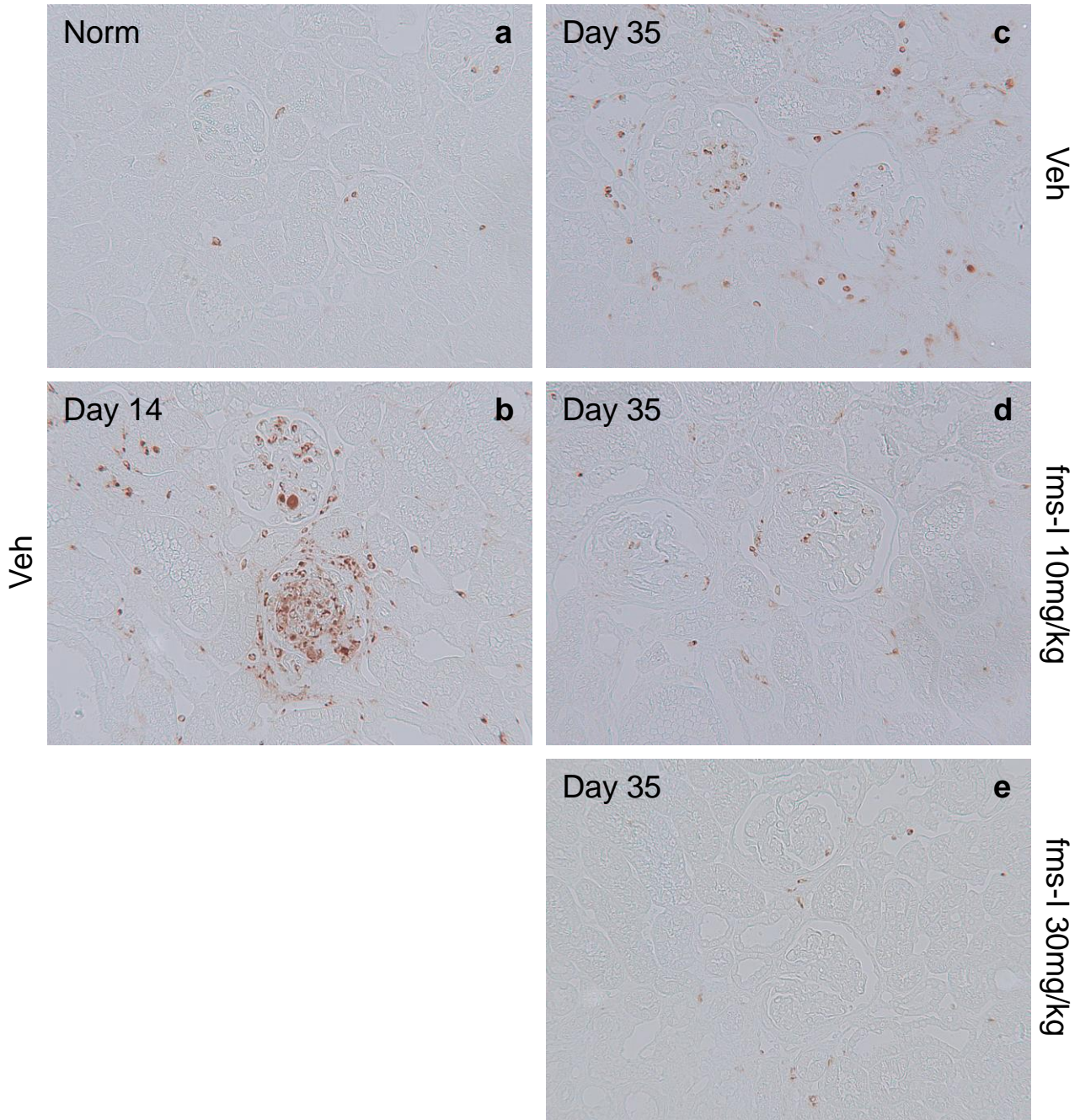


Figure 6.3

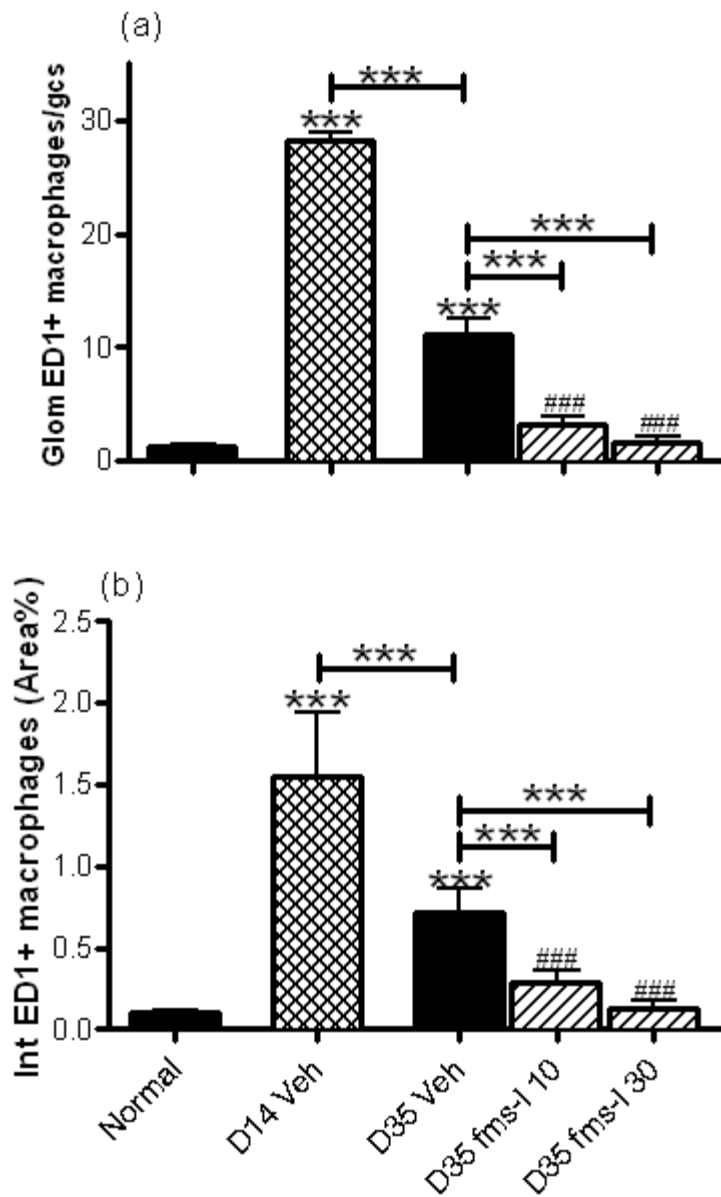


Figure 6.4

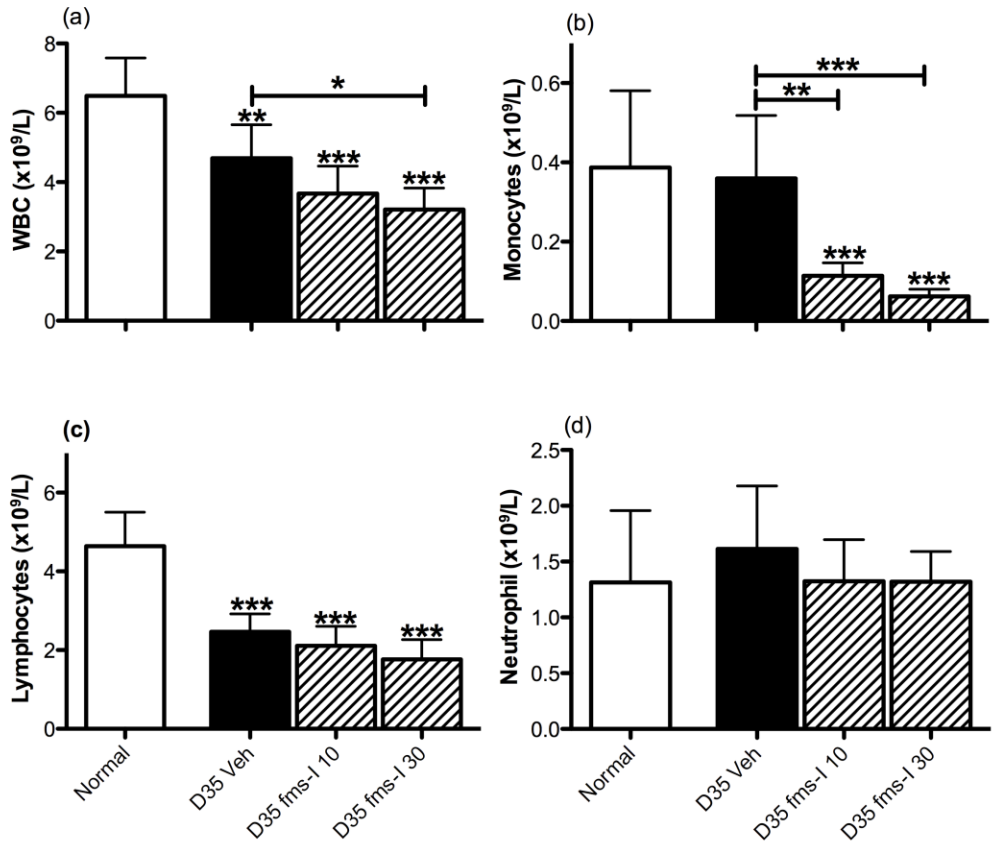


Figure 6.5

Periodic acid-Schiff staining

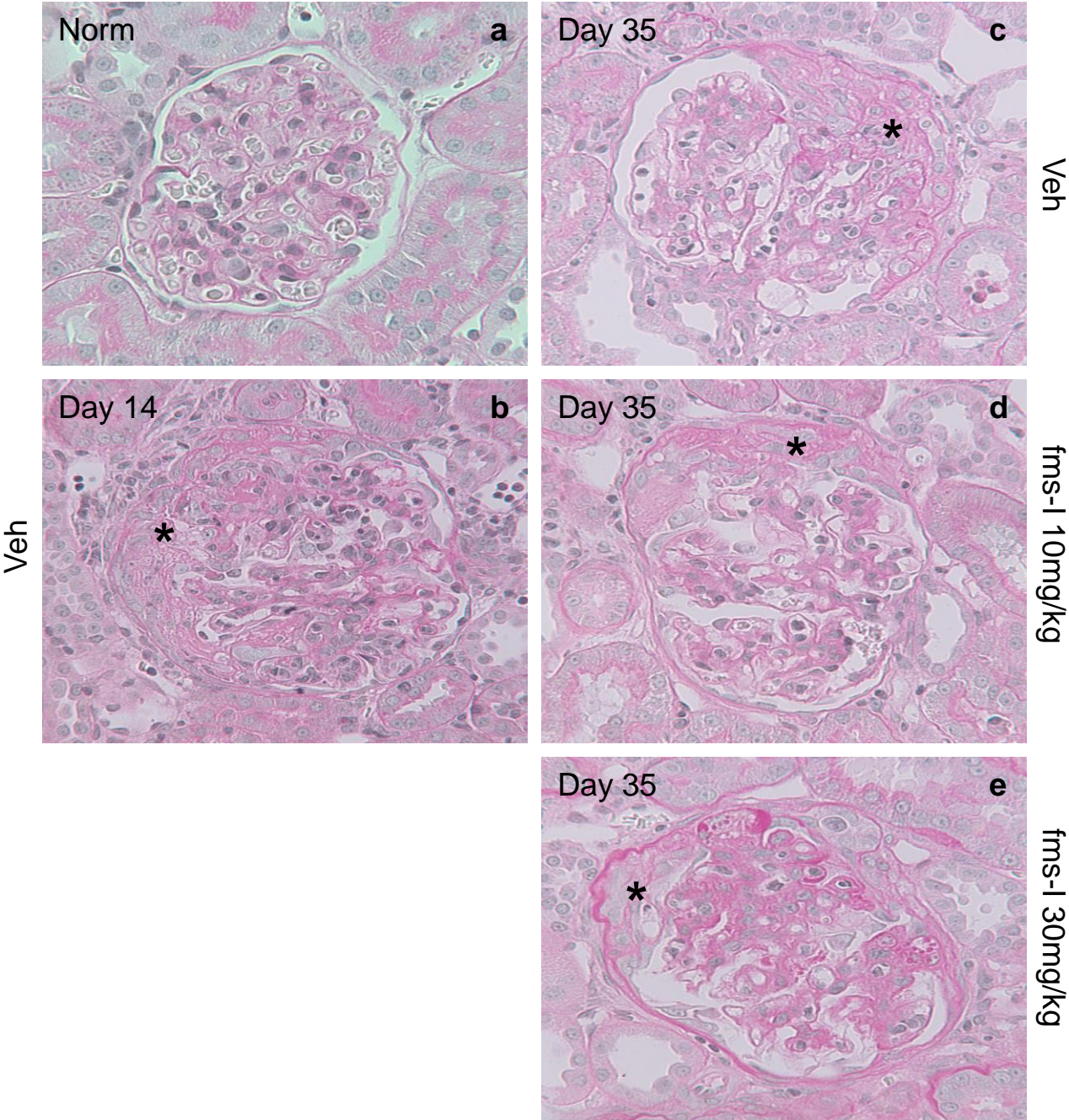


Figure 6.6

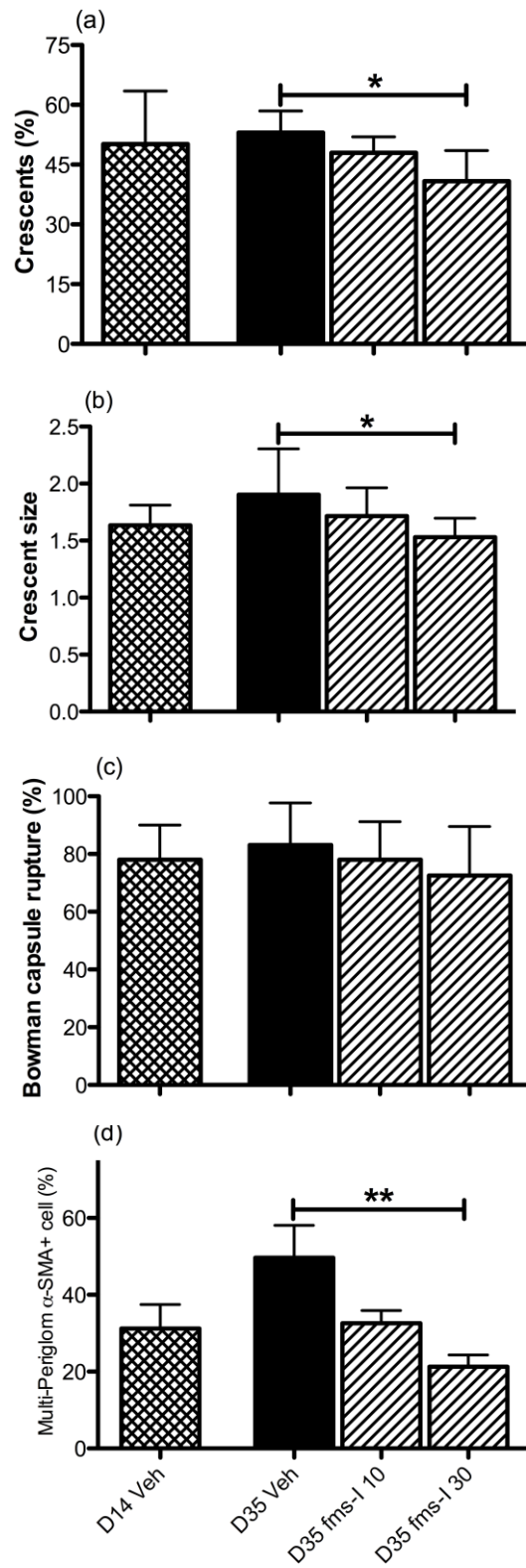


Figure 6.7

Periodic acid-Schiff staining

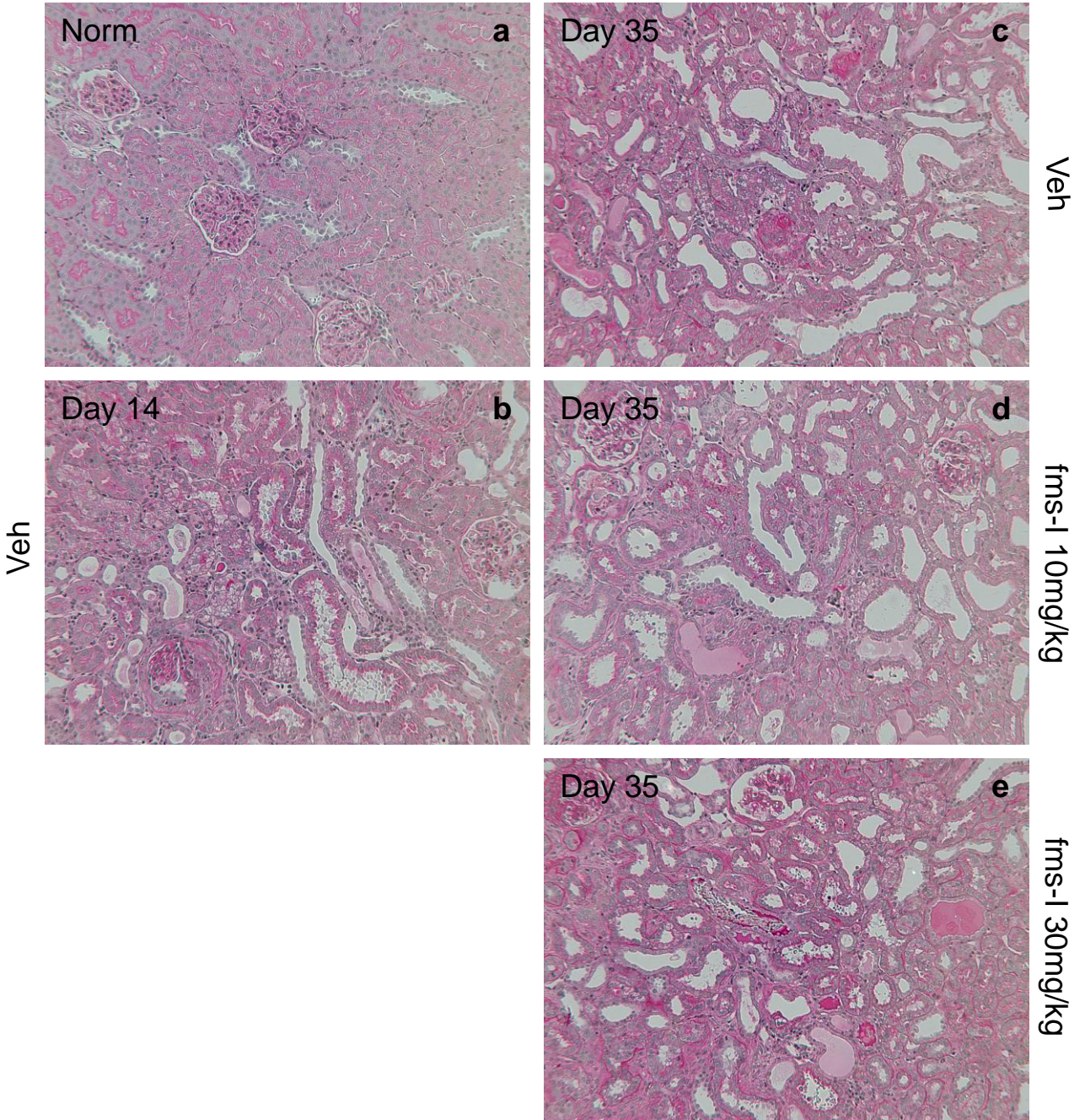


Figure 6.8

Vimentin immunostaining

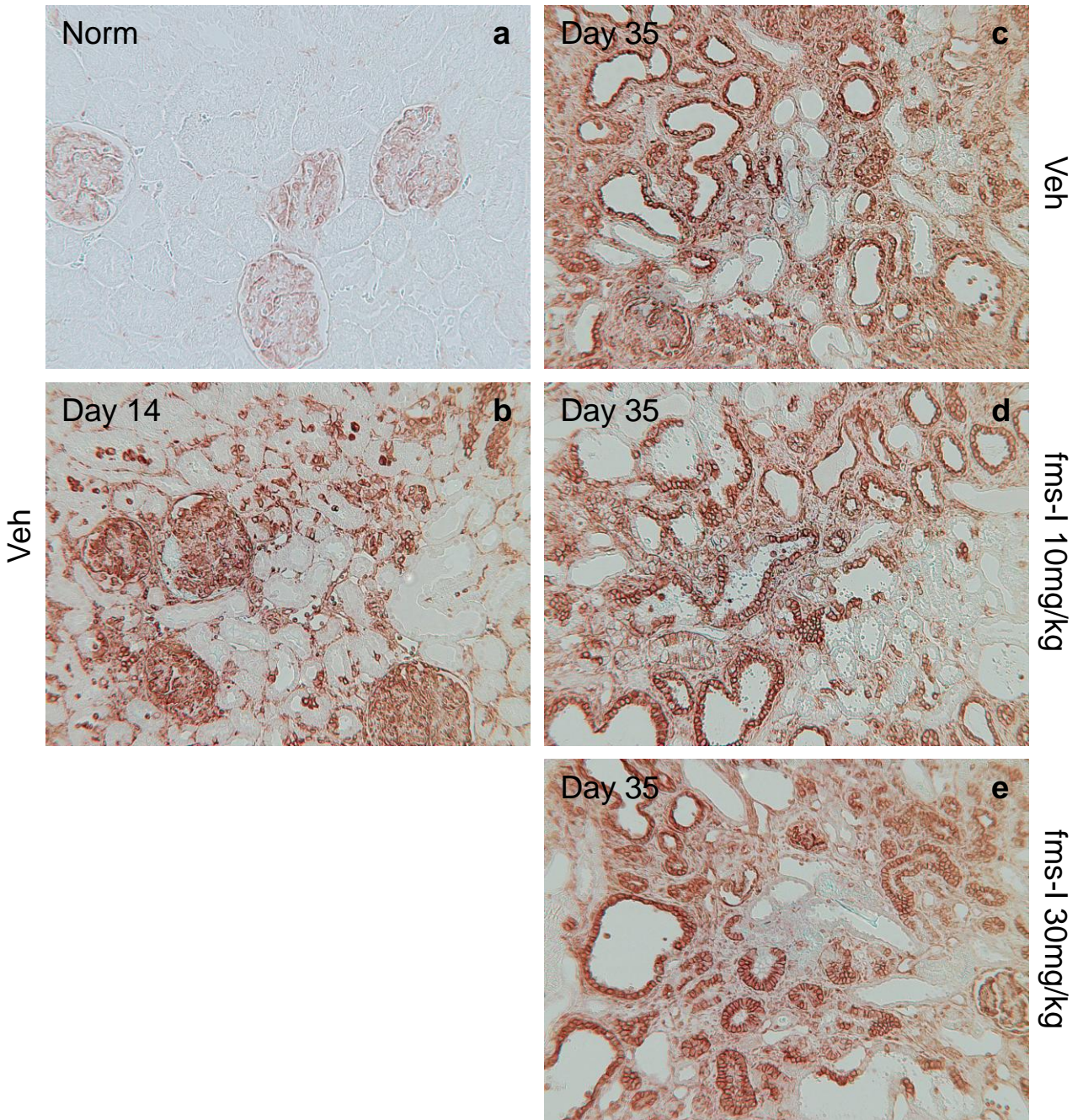


Figure 6.9

Oesteopontin immunostaining

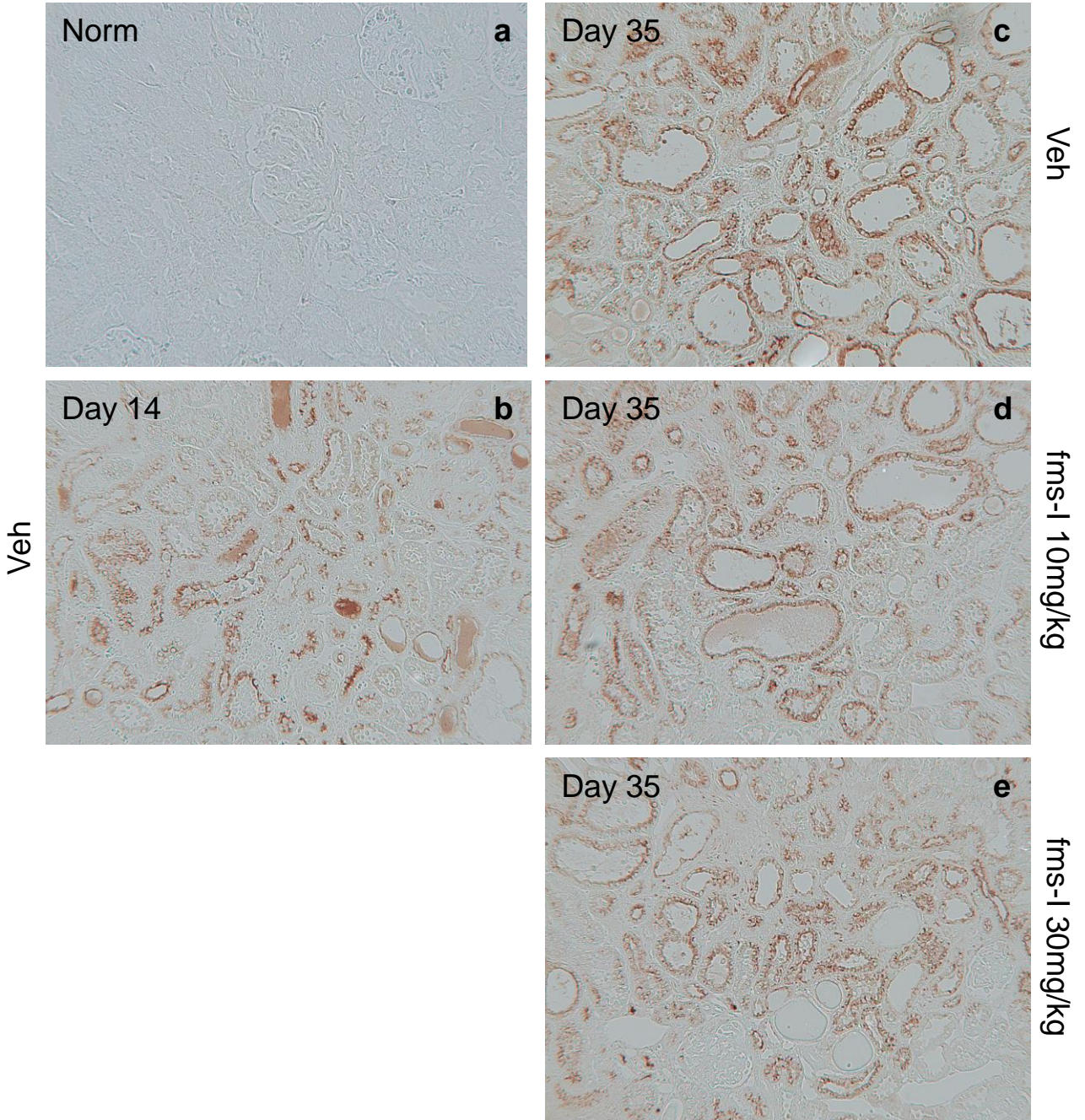


Figure 6.10

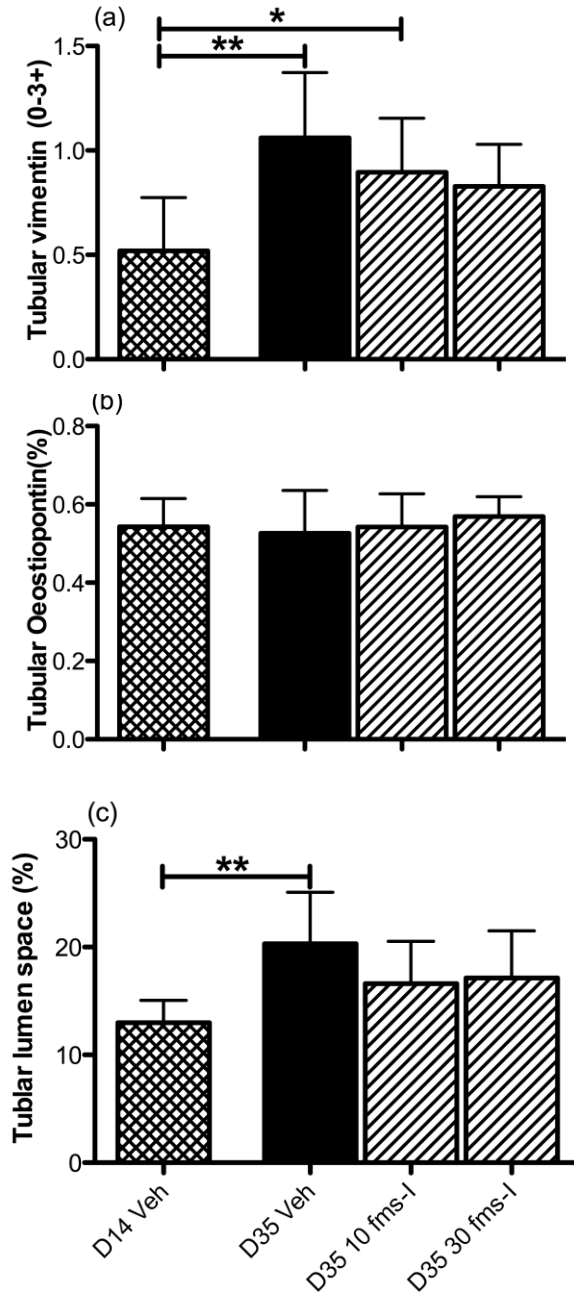


Figure 6.11

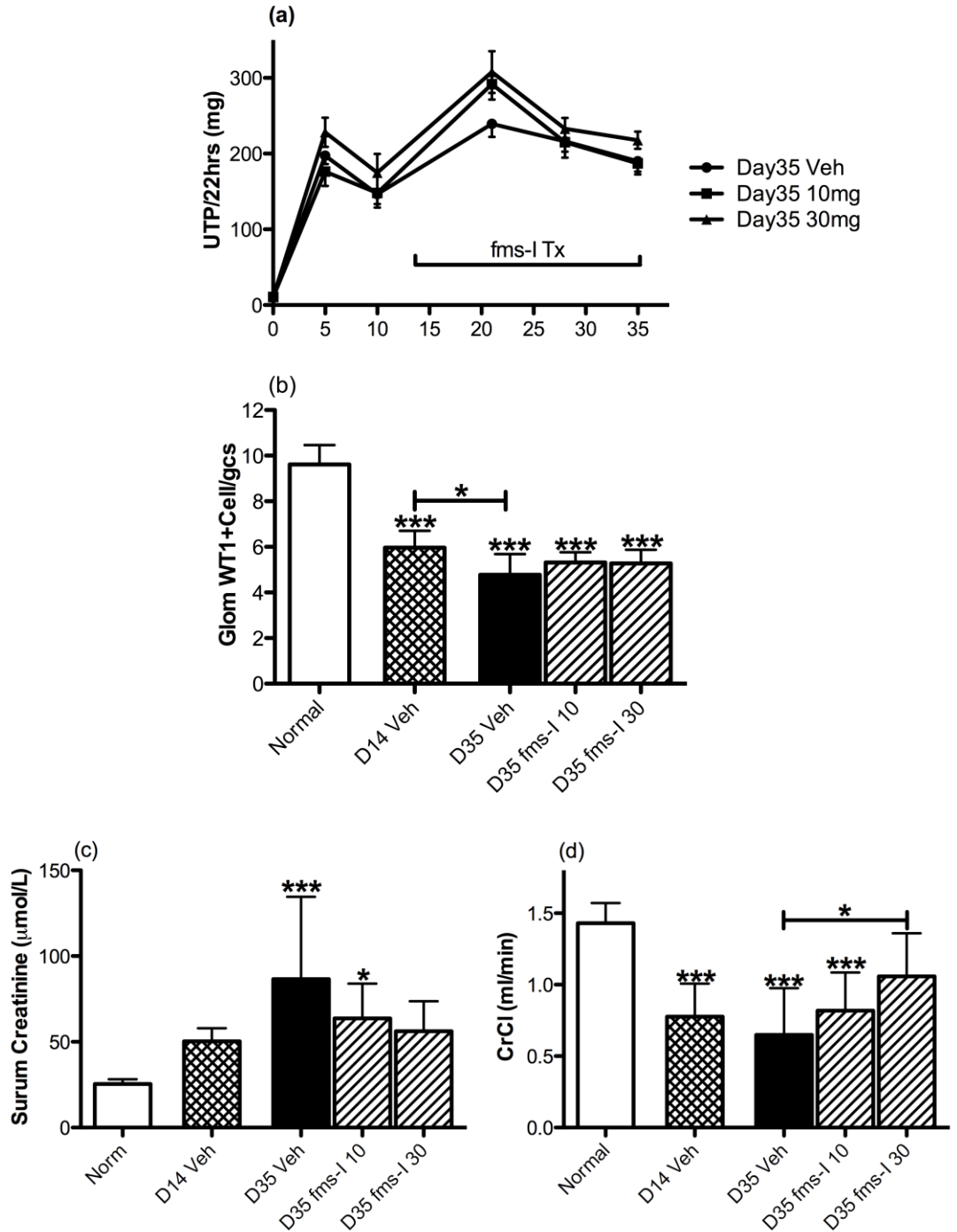


Figure 6.12

Collagen IV immunostaining

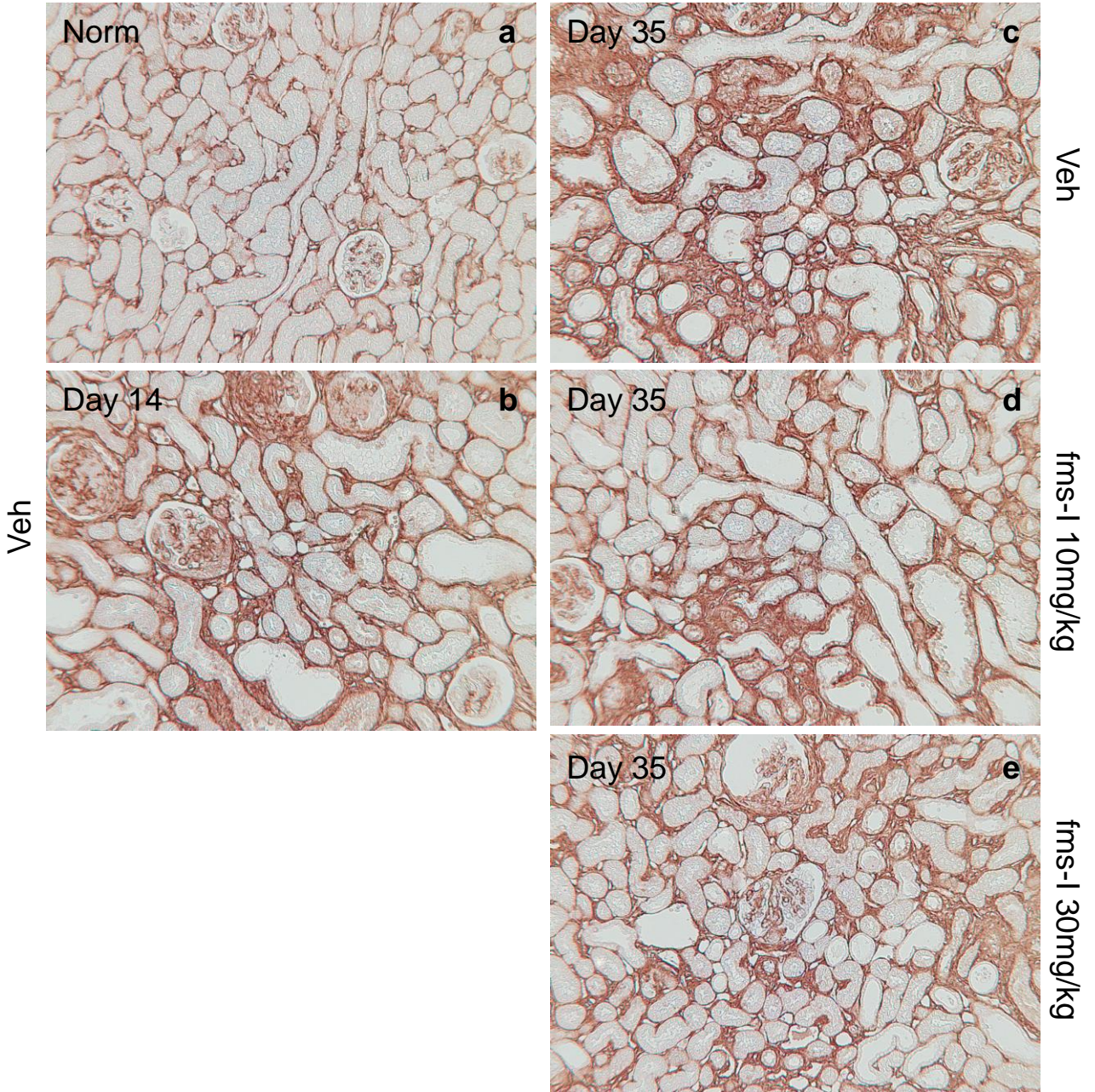


Figure 6.13

α -SMA immunostaining

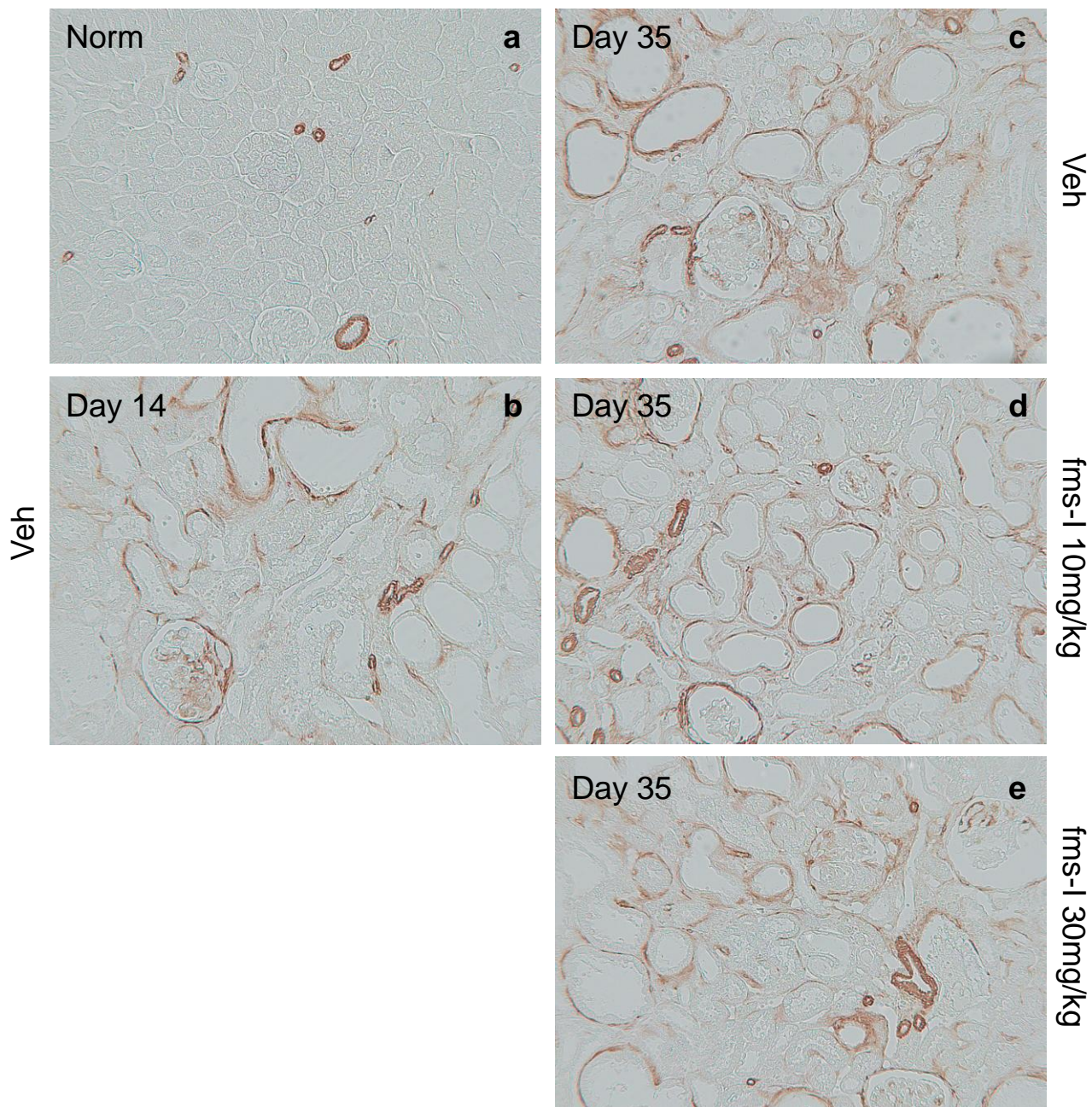


Figure 6.14

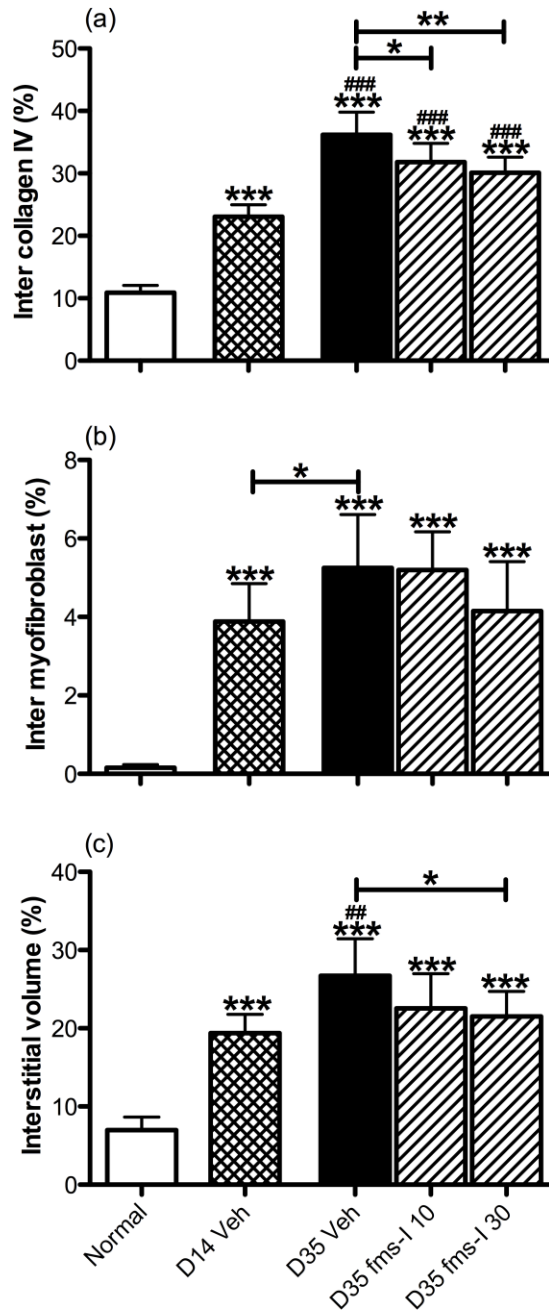


Figure 6.15

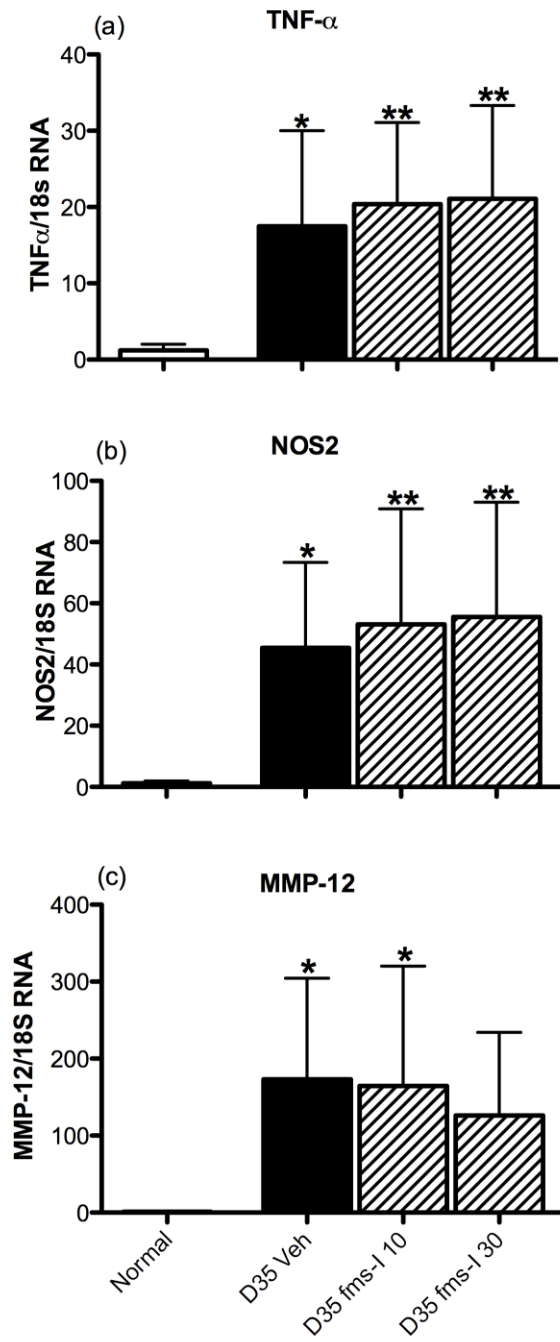


Figure 6.16

